AD-A014 742

SHOCK WAVE TURBULENT BOUNDARY LAYER INTERACTION IN HYPERSONIC FLOW

Michael S. Holden

Calspan Corporation

Prepared for:

Aerospace Research Laboratories

June 1975

DISTRIBUTED BY:

NTIS

National Technical Information Service
U. S. DEPARTMENT OF COMMERCE

Best
Available
Copy

267083

ARL TR 75-0204

AD A014742

SHOCK WAVE - TURBULENT BOUNDARY LAYER INTERACTION IN HIGH SPEED FLOW

MICHAEL S. HOLDEN
CALSPAN CORPORATION
BUFFALO, NEW YORK 14221

DDC
RECEIVED
SEP 15 1975
B

JUNE 1975

FINAL REPORT 15 MARCH 1972 — 15 MAY 1974

Approved for public release; distribution unlimited

Reproduced by
NATIONAL TECHNICAL
INFORMATION SERVICE
U.S. Department of Commerce
Springfield, VA 22151

THEORETICAL AERODYNAMICS RESEARCH LABORATORY (LH)
AEROSPACE RESEARCH LABORATORIES
Building 450 — Area B
Wright-Patterson Air Force Base, Ohio 45433

AIR FORCE SYSTEMS COMMAND

United States Air Force

185

NOTICES

When Government drawings, specifications, or other data are used for any purpose other than in connection with a definitely related Government procurement operation, the United States Government thereby incurs no responsibility nor any obligation whatsoever; and the fact that the Government may have formulated, furnished, or in any way supplied the said drawings, specifications, or other data, is not to be regarded by implication or otherwise as in any manner licensing the holder or any other person or corporation, or conveying any rights or permission to manufacture, use, or sell any patented invention that may in any way be related thereto.

Organizations or individuals receiving reports via Aerospace Research Laboratories automatic mailing lists should refer to the ARL number of the report received when corresponding about change of address or cancellation. Such changes should be directed to the specific laboratory orginating the report. Do not return this copy; retain or destroy.

Reports are not stocked by the Aerospace Research Laboratories. Copies may be obtained from:

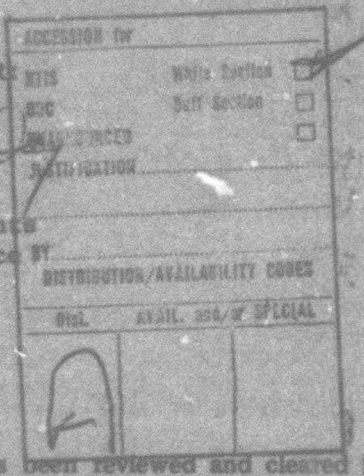
National Technical Information Services
Clearinghouse
Springfield, VA 22161

This technical report has been reviewed and is approved for publication.

FOR THE COMMANDER:

Elizabeth Day

ELIZABETH DAY
Technical Documents
and STINFO Office



This report has been reviewed and cleared for open publication and public release by the appropriate Office of Information in accordance with AFR 190-12 and DODD 5230.0. There is no objection to unlimited distribution of this report to the public at large, or by DDC to the National Technical Information Service.

Unclassified

SECURITY CLASSIFICATION OF THIS PAGE *(When Data Entered)*

REPORT DOCUMENTATION PAGE		READ INSTRUCTIONS BEFORE COMPLETING FORM
1. REPORT NUMBER ARL TR 75-0204	2. GOVT ACCESSION NO.	3. RECIPIENT'S CATALOG NUMBER AD-A014 742
4. TITLE *(and Subtitle)* SHOCK WAVE TURBULENT BOUNDARY LAYER INTERACTION IN HYPERSONIC FLOW		5. TYPE OF REPORT & PERIOD COVERED Technical - Final March 1972-May 1974 6. PERFORMING ORG. REPORT NUMBER
7. AUTHOR(s) Michael S. Holden		8. CONTRACT OR GRANT NUMBER(s) F33615-72-C-1319
9. PERFORMING ORGANIZATION NAME AND ADDRESS Calspan Corporation P. O. Box 235 Buffalo, New York 14221		10. PROGRAM ELEMENT, PROJECT, TASK AREA & WORK UNIT NUMBERS DOD Element 61102F 70640206
11. CONTROLLING OFFICE NAME AND ADDRESS Theoretical Aerodynamics Research Laboratory(LH) Aerospace Research Laboratories (AFSC) Wright-Patterson AFB, Ohio 45433		12. REPORT DATE June 1975 13. NUMBER OF PAGES 185
14. MONITORING AGENCY NAME & ADDRESS*(if different from Controlling Office)*		15. SECURITY CLASS. *(of this report)* Unclassified 15a. DECLASSIFICATION/DOWNGRADING SCHEDULE

16. DISTRIBUTION STATEMENT *(of this Report)*

Approved for public release; distribution unlimited.

17. DISTRIBUTION STATEMENT *(of the abstract entered in Block 20, if different from Report)*

18. SUPPLEMENTARY NOTES

19. KEY WORDS *(Continue on reverse side if necessary and identify by block number)*

Turbulent boundary layers
Skin friction, heat transfer and pressure
High Mach number and Reynolds number
Flap induced separation
Incipient separation
Incident shock
Plateau pressure
Shock tunnel
Hypersonic flow
Viscous interaction
Separated flow

20. ABSTRACT *(Continue on reverse side if necessary and identify by block number)*

A study is presented of the characteristics of transitional and turbulent layers, and regions of shock wave-turbulent boundary layer interaction in high Reynolds number hypersonic flow. An examination and correlation of skin friction, heat transfer and pressure measurements in laminar, transitional and turbulent boundary layers on sharp flat plates and cones are presented for the Mach range from 3 to 13 at wall-to-free stream temperature ratios from 0.1 to 0.4. The skin friction and heat transfer measurements made in turbulent boundary layers

DD FORM 1 JAN 73 1473 EDITION OF 1 NOV 65 IS OBSOLETE

Unclassified

SECURITY CLASSIFICATION OF THIS PAGE *(When Data Entered)*

AIR FORCE - 7-P-75 - 200

over flat plates and cones have been compared with the theories of Van Driest II, Spalding and Chi, and Eckert. The Van Driest II method is in best overall agreement with the measurements. From 50 to 100 boundary layer thicknesses are required downstream of transition before the turbulent boundary layer approaches an equilibrium behavior. Measurements over a wide range of Reynolds numbers have demonstrated a reversal in the trend of incipient separation with Reynolds numbers. This result can be explained in terms of characteristic changes in the character of the wall layer resulting from the non-equilibrium and subsequent equilibrium development downstream of transition. Correlations of the measurements are presented to enable the occurrence and the salient features of shock- and wedge-induced separated flows to be predicted.

PREFACE

The work described in this final report was performed by Calspan Corporation (formerly Cornell Aeronautical Laboratory, Inc.), Buffalo, New York, with the support of the U.S. Air Force under the Hypersonic Research Laboratory, Aerospace Research Laboratories (ARL), Air Force Systems Command, Wright-Patterson Air Force Base, Ohio, Contract No. F33615-72-C-1319. The contract monitor for this program, conducted during the period March 1972 to May 1974, was Dr. Herbert Law of ARL.

The author would like to acknowledge many helpful discussions on hypersonic turbulent boundary layer and shock wave-turbulent boundary layer interaction which he has had with Drs. Herbert Law, Wilbur Hankey, and Anthony Fiore of ARL during the course of the program.

TABLE OF CONTENTS

Section		Page
I	INTRODUCTION	1
II	EXPERIMENTAL FACILITIES AND MEASUREMENT TECHNIQUES.	7
	1. EXPERIMENTAL FACILITIES	7
	2. MODELS, TEST CONDITIONS, AND INSTRUMENTATION.	9
	a. Skin Friction and Heat Transfer Instrumentation . . .	9
	b. Surface Pressure Measurements	15
	3. DATA RECORDING AND PROCESSING	15
III	OBSERVATIONS ON BOUNDARY LAYER TRANSITION AND THE TRANSITIONAL REGION IN HIGH SPEED FLOWS	17
	1. INTRODUCTION.	17
	2. DISTRIBUTION OF PROPERTIES IN THE TRANSITION REGION . . .	21
	3. OBSERVATIONS ON THE OCCURRENCE OF TRANSITION	21
IV	COMPARISONS BETWEEN TURBULENT PREDICTION METHODS AND MEASURED SKIN FRICTION AND HEAT TRANSFER	31
V	EXPERIMENTAL STUDIES OF SHOCK WAVE-TURBULENT BOUNDARY LAYER INTERACTION	94
	1. INTRODUCTION	94
	2. DISTRIBUTIONS OF PROPERTIES IN WEDGE AND SHOCK-INDUCED INTERACTION REGIONS	97
	3. CHARACTERISTICS OF SEPARATED TURBULENT INTERACTION REGIONS	137
	4. INCIPIENT SEPARATION	145
	5. COMPARISON BETWEEN EXPERIMENT AND NAVIER-STOKES SOLUTIONS	156
	6. CONCLUSIONS	165
	REFERENCES.	166

LIST OF ILLUSTRATIONS

Figure		Page
1	Wave Diagram for Tailored-Interface Shock Tube	8
2	Test Time Available for Tailored Interface Operation of the Shock Tunnel	8
3	Maximum Local Reynolds Number on a 24-Inch 8° Cone in the 96-Inch Tunnel	10
4	Sharp Flat Plate Model	11
5	Cone Models	12
6	Drawing of Section Through Skin Friction Transducer	14
7	High Frequency Pressure Mounting	14
8	Typical Distribution of Heat Transfer Along the Flat Plate Model	19
9	Correlation of the Scale Length of the Transition on Flat Plates and Cones	20
10	Universal Intermittency Distribution	22
11	Heat Transfer Distribution in the Transition Region	23
12	Correlation of Transition Showing the Effects of Tunnel Size	25
13	Correlation of the Flat Plate Transition Data in Terms of the Parameters Suggested by Pate and Schueler	26
14	Correlation of Transition Measurements in the Calspan Shock Tunnels with Ballistic and Downrange Measurements	27
15	Correlation of the Eddy Reynolds Number with the Transition Measurements on the Flat Plates	29
16	Turbulent Boundary Layer Displacement and Momentum Thickness from Shock Nozzle Data	30
17	Reynolds Analogy Factors for Turbulent Hypersonic Boundary Layers	34
18	Reynolds Analogy Factors for Turbulent Hypersonic Boundary Layers	34
19a	Comparison Between the Measured Heat Transfer and the Theory of Eckert (T_A^*) on Sharp Flat Plates	38
19b	Comparison Between the Measured Heat Transfer and the Theory of Eckert (T_E^*) on Sharp Flat Plates	39
19c	Comparison Between the Measured Heat Transfer and the Theory of Van Driest on Sharp Flat Plates	40

Figure		Page
19d	Comparison Between the Measured Heat Transfer and the Spalding-Chi Theory on Sharp Flat Plates	41
20a	Comparison Between the Measured Skin Friction and the Theory of Eckert (T_A^*)	42
20b	Comparison Between the Measured Skin Friction and the Theory of Eckert (T_E^*)	43
20c	Comparison Between the Measured Skin Friction and the Theory of Van Driest	44
20d	Comparison Between the Measured Skin Friction and the Spalding-Chi Theory	45
21a	Comparison Between the Measured Heat Transfer and the Theory of Eckert ($\theta_V=\theta_B+\theta_{BE}$)	46
21b	Comparison Between the Measured Heat Transfer and the Theory of Van Driest ($\theta_V=\theta_B+\theta_{BE}$)	47
21c	Comparison Between the Measured Heat Transfer and the Spalding-Chi Theory ($\theta_V=\theta_B+\theta_{BE}$)	48
22a	Comparison Between the Measured Skin Friction and the Theory of Eckert ($\theta_V=\theta_B+\theta_{BE}$)	49
22b	Comparison Between the Measured Skin Friction and the Theory of Van Driest ($\theta_V=\theta_B+\theta_{BE}$)	50
22c	Comparison Between the Measured Skin Friction and the Spalding-Chi Theory ($\theta_V=\theta_B+\theta_{BE}$)	51
23a	Comparison Between the Measured Heat Transfer and the Theory of Eckert ($\theta_V=\theta_B+\theta_{BE/2}$)	52
23b	Comparison Between the Measured Heat Transfer and the Theory of Van Driest ($\theta_V=\theta_B+\theta_{BE/2}$)	53
23c	Comparison Between the Measured Heat Transfer and the Spalding-Chi Theory ($\theta_V=\theta_B+\theta_{BE/2}$)	54
24a	Comparison Between the Measured Skin Friction and the Theory of Eckert ($\theta_V=\theta_B+\theta_{BE/2}$)	55
24b	Comparison Between the Measured Skin Friction and the Theory of Van Driest ($\theta_V=\theta_B+\theta_{BE/2}$)	56

LIST OF ILLUSTRATIONS (cont.)

Figure		Page
24c	Comparison Between the Measured Skin Friction and the Spalding-Chi Theory ($\theta_V=\theta_B+\theta_{BE/2}$)	57
25a	Comparison Between the Measured Heat Transfer and the Theory of Eckert ($\theta_V=\theta_B+\theta_{BE\ LAMINAR}$)	58
25b	Comparison Between the Measured Heat Transfer and the Theory of Van Driest ($\theta_V=\theta_B+\theta_{BE\ LAMINAR}$)	59
25c	Comparison Between the Measured Heat Transfer and the Spalding-Chi Theory ($\theta_V=\theta_B+\theta_{BE\ LAMINAR}$)	60
26a	Comparison Between the Measured Skin Friction and the Theory of Eckert ($\theta_V=\theta_B+\theta_{BE\ LAMINAR}$)	61
26b	Comparison Between the Measured Skin Friction and the Theory of Van Driest ($\theta_V=\theta_B+\theta_{BE\ LAMINAR}$)	62
26c	Comparison Between the Measured Skin Friction and the Spalding-Chi Theory ($\theta_V=\theta_B+\theta_{BE\ LAMINAR}$)	63
27a	Comparison Between the Measured Heat Transfer and the Theory of Eckert ($\theta_V=\theta_B$)	64
27b	Comparison Between the Measured Heat Transfer and the Theory of Van Driest ($\theta_V=\theta_B$)	65
27c	Comparison Between the Measured Heat Transfer and the Spalding-Chi Theory ($\theta_V=\theta_B$)	66
28a	Comparison Between the Measured Skin Friction and the Theory of Eckert ($\theta_V=\theta_B$)	67
28b	Comparison Between the Measured Skin Friction and the Theory of Van Driest ($\theta_V=\theta_B$)	68
28c	Comparison Between the Measured Skin Friction and the Spalding-Chi Theory ($\theta_V=\theta_B$)	69
29a	Comparison Between the Measured Heat Transfer and the Theory of Eckert ($X_V=0$ at $\theta_B+\theta_{BE/2}$)	70
29b	Comparison Between the Measured Heat Transfer and the Theory on Van Driest on Sharp Flat Plates ($X_V = 0$ at $\theta_B + \theta_{BE/2}$)	71
29c	Comparison Between the Measured Heat Transfer and the Theory of Spalding-Chi ($X_V=0$ at $\theta_B+\theta_{BE/2}$)	72

LIST OF ILLUSTRATIONS (cont.)

Figure		Page
30a	Comparison Between the Measured Skin Friction and the Theory of Eckert (X_V=0 at $\theta_B+\theta_{BE/2}$)	73
30b	Comparison Between the Measured Skin Friction and the Theory of Van Driest (X_V=0 at $\theta_B+\theta_{BE/2}$)	74
30c	Comparison Between the Measured Skin Friction and the Theory of Spalding-Chi (X_V=0 at $\theta_B+\theta_{BE/2}$)	75
31a	Comparison Between the Measured Heat Transfer and the Theory of Eckert (T_A*) on Sharp Cones	76
31b	Comparison Between the Measured Heat Transfer and the Theory of Van Driest (TE*) on Sharp Cones	77
31c	Comparison Between the Measured Heat Transfer and the Theory of Spalding-Chi on Sharp Cones	78
32a	Comparison Between the Measured Heat Transfer and the Theory of Eckert on Sharp Cones ($\theta_V=\theta_B+\theta_{BE}$)	79
32b	Comparison Between the Measured Heat Transfer and the Theory of Van Driest on Sharp Cones ($\theta_V=\theta_B+\theta_{BE}$)	80
32c	Comparison Between the Measured Heat Transfer and the Spalding-Chi Theory on Sharp Cones ($\theta_V=\theta_B+\theta_{BE/2}$)	81
33a	Comparison Between the Measured Heat Transfer and the Theory of Eckert on Sharp Cones ($\theta_V=\theta_B+\theta_{BE/2}$)	82
33b	Comparison Between the Measured Heat Transfer and the Theory of Van Driest on Sharp Cones ($\theta_V=\theta_B+\theta_{BE/2}$)	83
33c	Comparison Between the Measured Heat Transfer and the Spalding-Chi Theory on Sharp Cones ($\theta_V=\theta_B+\theta_{BE/2}$)	84
34a	Comparison Between the Measured Heat Transfer and the Theory of Eckert on Sharp Cones ($\theta_V=\theta_B+\theta_{BE\ LAMINAR}$)	85
34b	Comparison Between the Measured Heat Transfer and the Theory of Van Driest on Sharp Cones ($\theta_V=\theta_B+\theta_{BE\ LAMINAR}$)	86
34c	Comparison Between the Measured Heat Transfer and the Spalding-Chi Theory on Sharp Cones ($\theta_V=\theta_B+\theta_{BE\ LAMINAR}$)	87

LIST OF ILLUSTRATIONS (cont.)

Figure		Page
35a	Comparison Between the Measured Heat Transfer and the Theory of Eckert on Sharp Cones ($\theta_V=\theta_B$)	88
35b	Comparison Between the Measured Heat Transfer and the Theory of Van Driest on Sharp Cones ($\theta_V=\theta_B$)	89
35c	Comparison Between the Measured Heat Transfer and the Spalding-Chi Theory on Sharp Cones ($\theta_V=\theta_B$)	90
36a	Comparison Between the Measured Heat Transfer and the Theory of Eckert on Sharp Cones ($X_V=0$ at $\theta_B+\theta_{BE/2}$)	91
36b	Comparison Between the Measured Heat Transfer and the Theory of Van Driest on Sharp Cones ($X_V=0$ at $\theta_B+\theta_{BE/2}$)	92
36c	Comparison Between the Measured Heat Transfer and the Theory of Spalding-Chi on Sharp Cones ($X_V=0$ at $\theta_B+\theta_{BE/2}$)	93
37	Flat Plate-Wedge Model	99
38a	Flat Plate Model Instrumentation	100
38b	Flat Plate Model-Instrumentation	101
39a	Variation of the Size of the Interaction Region with Strength of Interaction ($M_\infty = 8.6$; $Re_\delta = 1.4\times10^6$)	102
39b	Variation of Pressure Distribution with Interaction Strength.	103
40a	Variations of Size of Separated Region with Reynolds Number ($M_\infty = 8.6$ $\theta_\omega = 33°$)	104
40b	Variation of Pressure Distribution with Unit Reynolds Number.	105
40c	Distribution of Heat Transfer and Pressure in a Small Separated Region in Wedge-Induced Flow.	106
41a	Distribution of Heat Transfer and Pressure in an Attached Wedged Induced Interaction Region	107
41b	Distribution of Heat Transfer and Pressure in an Attached Wedge-Induced Interaction Region	108
41c	Distribution of Heat Transfer and Pressure in a Separated Wedge-Induced Interaction Region	109

Figure		Page
41d	Distribution of Heat Transfer and Pressure in a Well Separated Wedge-Induced Interaction Region	110
42a	Variation of the Heat Transfer and Pressure Distribution with the Strength of the Interaction	111
42b	Variation of the Heat Transfer and Pressure Distribution with the Strength of the Interaction	112
42c	Variation of the Heat Transfer and Pressure Distribution with the Strength of the Interaction	113
42d	Variation of the Heat Transfer and Pressure Distribution with the Strength of the Interaction	114
43a	Variation of Size of Separated Region with Reynolds Number ($M_\infty = 8.6$ $\theta_w = 33°$)	116
43b	Variation of Pressure Distribution with Unit Reynolds Number	117
44a	Variation of Pressure Distribution with Reynolds Number. . .	118
44b	Variation of Heat Transfer Distribution with Reynolds Number for a Wedge-Induced Interaction Region	119
45a	Variation of Heat Transfer Distribution with Reynolds Number	120
45b	Variation of Pressure Distribution with Reynolds Number . .	121
46a	Variation of Pressure Distribution with Reynolds Number. . .	122
46b	Variation of Heat Transfer Distribution with Reynolds Number	123
47	Variation of Heat Transfer with Shock Strength	125
48	Variation of Pressure Distribution with Shock Strength . . .	126
49a	Distribution of Pressure and Heat Transfer in Shock-Induced Separated Flow	127
49b	Distribution of Heat Transfer and Pressure in a Shock-Induced Separated Flow	128
50a	Variation of Plateau Pressure with Mach Number	129
50b	Variation of Plateau Pressure with Size of Separated Region.	130
51a	Reynolds Number Effect on Length of Separation $M_\infty = 8.1$, $\theta_{SG} = 17.5°$	131
51b	Reynolds Number Effect on Length of Separation	132
52a	Variation of the Pressure Distribution with Reynolds Number For Shock-Induced Separated Flow	133

Figure		Page
52b	Variation of Heat Transfer Distribution with Reynolds Number in Shock-Induced Separated Flow	134
53a	Variation of Pressure Distribution with Reynolds Number in Shock-Induced Separated Flow.	135
53b	Variation of Heat Transfer Distribution with Reynolds Number in Shock-Induced Separated Flow.	136
54	The Development of a Wedge-Induced Separated Flow (M_∞ = 8.6, Re_L=22.5 x 10^6)	138
55	Correlation of Maximum Heating Rate in Wedge- and Externally-Generated Shock-Induced Turbulent Separated Flows.	141
56a	Conditions for Incipient Separation.	143
56b	Summary of Reynolds Number Effect on Compression Corner Angle for Incipient Separation at about Mach 2.9	143
57	Correlation of Plateau Pressure Measurements in Wedge- and Shock-Induced Turbulent Separated Region	144
58	Incipient Separation at Mach 6.5 and RE_L=27x10^6.	148
59	Conditions for Incipient Separation, $2.5 \leq M_e \leq 5$	149
60	Wedge Angle to Induce Incipient Separation	151
61	Correlation of Incipient Separation Conditions for Wedge- and Shock-Induced Turbulent Interaction Regions	152
62	Variation of N with $R_{e,\theta}$ For Flat Plates, Cones, and Hollow Cylinders	154
63	VElocity Profiles Ahead and Downstream of the Interaction. .	158
64	Calculated Stream Lines with Velocity Defect (in).	159
65	Comparison between Navier-Stokes Solutions and Experiment. .	160
66	Time for Convergence to Steady State	161
67	Calculations of the Effect of Roughness on Skin Friction . .	162
68	Calculations of the Effect of Roughness on Heat Transfer . .	163

SECTION I

INTRODUCTION

The development of the space shuttle and the current interest in maneuverable re-entry vehicles has promoted renewed interest in the study of the characteristics of transitional and turbulent boundary layers,and the phenomena of shock wave-turbulent boundary interaction at large Reynolds numbers in high speed flows. These problems are, of course, interrelated through a sensitivity of the characteristics of turbulent interaction regions to the detailed structure of the boundary layer upstream of the turbulent interaction regions. In this report we address the two problem areas: (1) the development of the boundary layer downstream of the beginning of transition, its approach to "equilibrium turbulence" and the characteristics of a constant pressure turbulent boundary layers in hypersonic highly cooled flows , and (2) the structure and the characteristics of attached and separated regions of shock wave-turbulent boundary layer interaction in high Mach number highly cooled flows. Here we seek to understand the mechanics of turbulent boundary layer separation and reattachment and their dependence on Reynolds number and Mach number.

Two areas of particular interest in gaining an understanding of the structure of hypersonic turbulent boundary layers under constant pressure conditions are the transition region and the region downstream from the point of maximum heating where the turbulent boundary layer approaches an "equilibrium condition". The mean and fluctuating components of skin friction, heat transfer, and the pressure fluctuations through the transition region are of particular interest because it is in this region that theoretical models of the flow are particularly weak. The fluid physics of the beginning of the transition process as well as the structure of the transition region are not well understood and the theoretical prediction methods used to described these regions are based on convenient expressions rather than an enlightened physical insight. These models do not describe the generation of turbulence or turbulent bursts which we believe are essential elements of the fluid mechanics of these regions. There is a clear need to obtain detailed experimental measurements of the length of the transition region and the properties within it.

Close to the end of the transition process, in the neighborhood of the point of maximum heat transfer and skin friction, the local Reynolds number based on momentum thickness is generally low enough for the outer region of the turbulent boundary layer to be strongly influenced by viscosity. This "low Reynolds number effect" is far more pronounced in compressible high Mach number, highly cooled flows. While the phenomena is not well understood, it is believed that the turbulent scale size in this region of the flow is significantly larger than for an equilibrium boundary layer and thus the observed increased heat transfer and skin friction results from an increase in the turbulent diffusivity. It is clear that the region downstream of the point of maximum heating contains remnants of the transition process. Just how long the "memory" of the turbulence generated in the transition process is retained in the boundary layer is an important question which is at the heart of the development of the non-equilibrium turbulence theory. Here it is of particular importance because we would like to know at what distance downstream from the point of maximum heat transfer a valid comparison can be made between measurements in turbulent boundary layers over cones and flat plates and the methods devised to describe fully developed turbulent boundary layers under constant pressure. An equally important question is at what Reynolds number can we study regions of shock wave-turbulent boundary layer interaction to be sure that the variation of incipient separation and scale of the interaction region with Reynolds number do not simply reflect the variations of the structure and properties of the initial boundary layer with Reynolds number as the result of the non-equilibrium development of turbulence downstream of the transition region.

The detailed description of regions of shock wave-turbulent boundary layer interaction in compressible high speed high Reynolds number flows presents one of the most formidable tasks in fluid mechanics. For not only is the problem fully elliptic, we are faced with describing the non-equilibrium development of turbulence, where for flows above Mach 6 the effects of pressure fluctuations and compressibility must be incorporated. For this reason, it is essential that the experimental studies be conducted to provide insight into modelling these flows. From the modelling standpoint, there are two basic

approaches which are being employed at this time. Techniques which employ the first or second order boundary layer equations require a model for the turbulent interaction process, as well as a model for turbulence; at this time a proven model for this purpose remains to be forthcoming. Recently, solutions based on the time-dependent Navier Stokes equations have been generated at Mach numbers up to 8 and Reynolds numbers of 200×10^6. Here the uncertainties revolve about the gross approximations which are made in the numerical schemes to obtain a large mesh size so that computer solution times are within practical bounds. Again, turbulence modelling becomes of key importance.

Aside from turbulence modelling questions, the development of simple models based on the boundary layer equations to describe regions of shock wave-boundary layer interaction presents significant problems. The upstream influence in these flows was originally thought to be associated with propagation through the subsonic region of the boundary layer. Howarth,[1] Tsien[2] and Finston,[2] and Lighthill[3] developed this model of flows, but found upstream effects were far smaller than observed in experiment. This approach could not be used to explain the differences between upstream influence in laminar and turbulent boundary layers. For low Mach number flows the interaction concept first proposed by Oswatitsch and Wieghardt[4] has met with far greater success. This model, in which the boundary layer is assumed to grow in equilibrium with the pressure gradient caused by its growth, has formed the backbone of later more sophisticated theroretical approaches. Surprisingly, two of the first interaction models to successfully employ this approach, developed by Crocco and Lees[5] and Lighthill[6] take a markedly different approach. While Crocco-Lees assumes that the viscous and inertial terms are of equal importance in the interaction leading to separation, Lighthill suggests that the viscous terms are important only in the incompressible sublayer, with the flow along any streamline in the main body of the boundary layer being governed only by inertial and pressure forces. This latter work was further developed by Stewartson and Williams,[7] who demonstrated that the Lighthill model is strictly accurate only at high Reynolds number or order 10^8. It is interesting to note that while both Lighthill and Crocco-Lees predict an increase in upstream influence with increased Reynolds number for laminar flows, Lighthill's work

predicts a decrease in upstream influence with increasing Reynolds number for turbulent interactions with Crocco-Lees predicting the opposite trend. Glick,[8] using a modified form of the Crocco-Lees method, was the first person to obtain solutions describing a complete separation region induced by shock wave-laminar boundary layer interaction; however his method was highly empirical and could not be extended to describe high Mach number flows under non-adiabatic wall conditions. To eliminate some of the semi-empirical features of the Crocco-Lees method, Honda[9] introduced a fourth equation, the moment of momentum or kinetic energy equation. A fourth order polynomial profile was used to describe laminar profile in attached and separated flows. Honda found this approach was in good agreement with pressure measurements in laminar supersonic flow over adiabatic surfaces. Honda found that when an analogous approach was used to describe turbulent separation in supersonic flow above Mach 3, a mutual interaction between the viscous and inviscid flow which gives rise to an adverse pressure gradient could not be developed - the flow is termed supercritical in Crocco[10] formulation.

Later, Lees and Reeves[11] used Honda's formulation together with the compressible forms of the Falkner-Skan velocity profiles, obtained by Cohen and Reshotko,[12] as suggested earlier by Bray, Gadd and Woodger[13] and Savage[14] to describe laminar separated flows. Good agreement was obtained with measurements obtained by Chapman, Kuehn and Larson[15] in adiabatic flows. Holden[16] found this approach could not be used to describe separated flows over cooled surfaces. To describe laminar viscous interaction regions under highly cooled wall conditions, Holden introduced the integral form of the energy equation in addition to the equations for the conservation of mass, momentum and moment of momentum used earlier by Honda. The similar solutions of Cohen and Reshotko were used to describe both the velocity and enthalpy profiles in the attached and separated regions. While good agreement was found between theory and experiment for highly cooled laminar separated flows at Mach number below 12, above this value laminar boundary layers were found to exhibit a supercritical response. Similar results were obtained later by Klineberg and Lees,[17] Gautier and Ginoux,[18] Riethmuller and Ginoux,[19] and Bloy and Georgeff.[20] When an analogous approach was adopted by Holden to describe turbulent

interaction regions, he found, as did Honda for adiabatic flows, that the free interaction model could not be used to describe the separation process above Mach 2.3. In these flows the separation length is of the same magnitude as the boundary layer thickness and it is believed that a significant pressure ratio is generated across the boundary layer in these regions. For laminar interactions in high speed flows, Holden[21] found it is possible to remove the supercritical response of the boundary layer by allowing pressure to vary accross the boundary layer. The normal momentum equation in which the viscous terms were assumed small was used, in conjunction with the forementioned conservation equations, to obtain solutions where previously artifices such as the super-subcritical jump were required. Myring's[22] solutions for the development of turbulent boundary layers on compression surfaces again demonstrated the imporance of including a pressure gradient across the boundary layer. Todisco and Reeves,[23] and Hunter and Reeves[24] have attempted to use the conventional momentum integral technique, together with revised velocity profiles and scaling suggested by Alber and Lees.[25] In this formulation, a super-subcritical jump is required to link the solution ahead of the interaction region with that in the recirculation region. The analyses are strictly valid only for adiabatic flows, and as we shall see later from the experimental evidence in section 5, the flow model is an oversimplification of a region or shock wave-boundary layer interaction which can be justified only for large separated regions.

It is clear from experimental studies and Navier Stokes solutions, the pressure gradients generated across the boundary layer in the separation and reattachments of turbulent interaction regions are of the same magnitude as the streamwise gradient and must be modelled if these are to be described correctly. Here the most attractive simple approach is to divide the flow into two or more layers, treating the lower layer as viscous while incorporating the normal pressure gradient into equations for the outer layers. This approach has been used in the earlier studies by Lighthill, Honda and later by Rose.[26] However, problems of matching conditions at the boundaries between layers and modelling turbulence has thwarted attempts to obtain a successful solution which describes the properties of a complete turbulent interaction region in high speed flows.

Within recent years the increase in the speed of digital computers combined with the development of efficient numerical codes has made it possible to attempt solutions the Navier-Stokes equations for Reynolds numbers of practical interest. To avoid problems stemming from this inherently elliptic character of the separated region in these flows, these equations are solved in their time-dependent form which are parabolic in form. One of the first detailed solutions using this technique was obtained by Carter,[27] who investigated laminar flow separation induced over a flat plate-wedge compression corner. However, MacCormack[28] and Baldwin and MacCormack,[29] with the development of more efficient numerical codes, were able to obtain the first solution for regions of shock wave-turbulent boundary interactions. Subsequently, Horstmann,[30] et al, and Hankey[31] have used this approach with varying degrees of success. However, each author uses a different model for turbulences and it is clear that none of these models is completely satisfactory, when used to describe turbulence in highly cooled flow at high Mach numbers. The large mesh size (based on Reynolds number) required to obtain solutions within a practical time for turbulent interactions introduces questions on the accuracy of the computer solutions. Only by comparing these solutions to detailed experimental measurements will we be able to resolve questions on turbulence modelling and the numerical accuracy of these techniques.

In this report, we first describe the experimental facilities and measurement techniques which were used in the experimental program. A discussion of the observed characteristics of transition and the transition region on flat plates and cones is given in Section III. In Section IV, comparisons between measurements on flat plates and cones are compared with simple prediction techniques. A detailed study of the characteristics of regions of shock wave-turbulent boundary layer interaction is then presented. Here we first present the measurements made in the experimental study. These salient characteristics of the interaction regions are correlated with measurements made earlier of the results of semi-empirical prediction methods. Incipient separation and Reynolds number effects are discussed in detail. Finally, comparisons are made between measurements in shock-induced interaction regions and Navier Stokes solutions by Baldwin and MacCormack.

SECTION II

EXPERIMENTAL FACILITIES AND MEASUREMENT TECHNIQUES

1. EXPERIMENTAL FACILITIES

The experimental programs were conducted in Calspan's 48-inch and 96-inch Hypersonic Shock Tunnels. The operation of these tunnels can be shown simply with the aid of the wave diagram in Figure 1. The tunnel is started by rupturing a double diaphragm which permits the high-pressure air in the driver section to expand into the driven section, and in so doing generates a normal shock which propagates through the low-pressure air. A region of high-temperature, high-pressure air is produced between this normal shock front and the gas interface between the driver and driven gas, often referred to as the contact surface. When the primary or incident shock strikes the end of the driven section, it is reflected, leaving a region of almost stationary high-pressure heated air. This air is then expanded through a nozzle to the desired freestream conditions in the test section.

The duration of the flow in the test section is controlled by the interactions among the reflected shock, the interface, and the leading expansion wave generated by the nonstationary expansion process in the driver section. The initial conditions of the gases in the driver and driven sections are controlled so that the gas interface becomes transparent to the reflected shock, as shown in Figure 1; thus, there are no waves generated by interface-reflected shock interaction. This is known as operating under "tailored-interface" conditions. Under these conditions, the test time is controlled by the time taken for the driver-driven interface to reach the throat or the leading expansion wave to deplete the reservoir of pressure behind the reflected shock; the flow duration is said to be either driver-gas limited or expansion limited, respectively. Figure 2 shows the flow duration in the test section as a function of the Mach number of the incident shock. Here

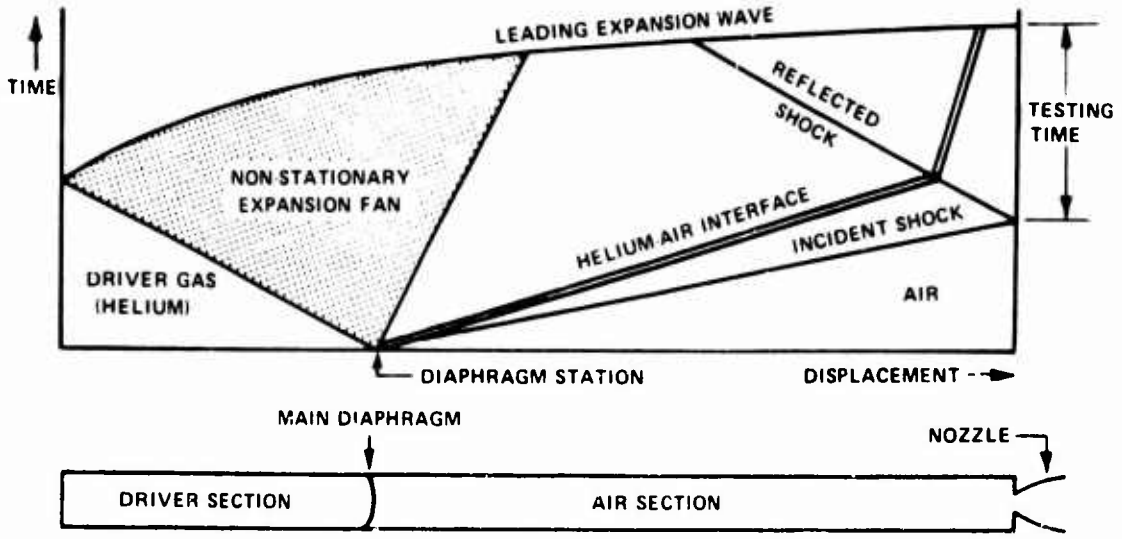


Figure 1. WAVE DIAGRAM FOR TAILORED–INTERFACE SHOCK TUBE

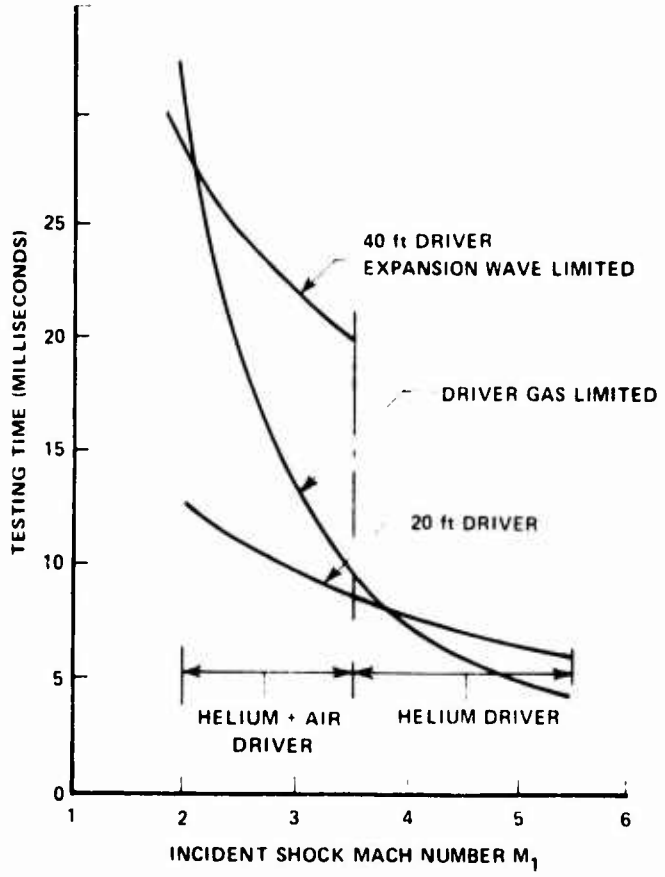


Figure 2. TEST TIME AVAILABLE FOR TAILORED INTERFACE OPERATION OF THE SHOCK TUNNEL

it can be seen that for operation at low M_i's running times of over 25 milliseconds can be obtained with a long driver section. By running the tunnels at low incident shock Mach numbers at high driver pressures, we can generate large unit Reynolds numbers at high Mach numbers as shown in Figure 3.

2. MODELS, TEST CONDITIONS, AND INSTRUMENTATION

The measurements presented in this report were taken on sharp flat plate and cone models, similar to those shown in Figures 4 and 5, over a large range of test conditions generated in the Calspan 48" and 96" Shock Tunnels. Table I lists the configurations and test conditions for the flat plate studies.

a. Skin Friction and Heat Transfer Instrumentation

A diagram of the skin friction transducer used in the present studies is shown in Figure 6. The transducer consists of a diaphragm supported flush with the model surface by two piezo-ceramic beams, which develop a charge when placed in bending by a surface shear on the diaphragm. A third beam provides acceleration compensation; the beams are connected electrically to eliminate thermal, normal, and transverse pressure effects. An FET impedance transform circuit is mounted internally to eliminate cable noise effects at low levels of skin friction. The gage, developed and refined over the past 11 years, has been used to measure very low levels of skin friction encountered in separated regions in low Reynolds number hypersonic flow and more recently, very high levels in regions of shock wave-turbulent boundary layer interactions in hypersonic flow. Because of the very severe heating conditions encountered in the latter studies, special care was taken to minimize the heat conduction through the flexures. The very large dynamic loads generated on the transducers during tunnel shutdown when run at the high dynamic pressure conditions used in our studies caused the diaphragms to be torn from the supporting beam. This problem was minimized by careful

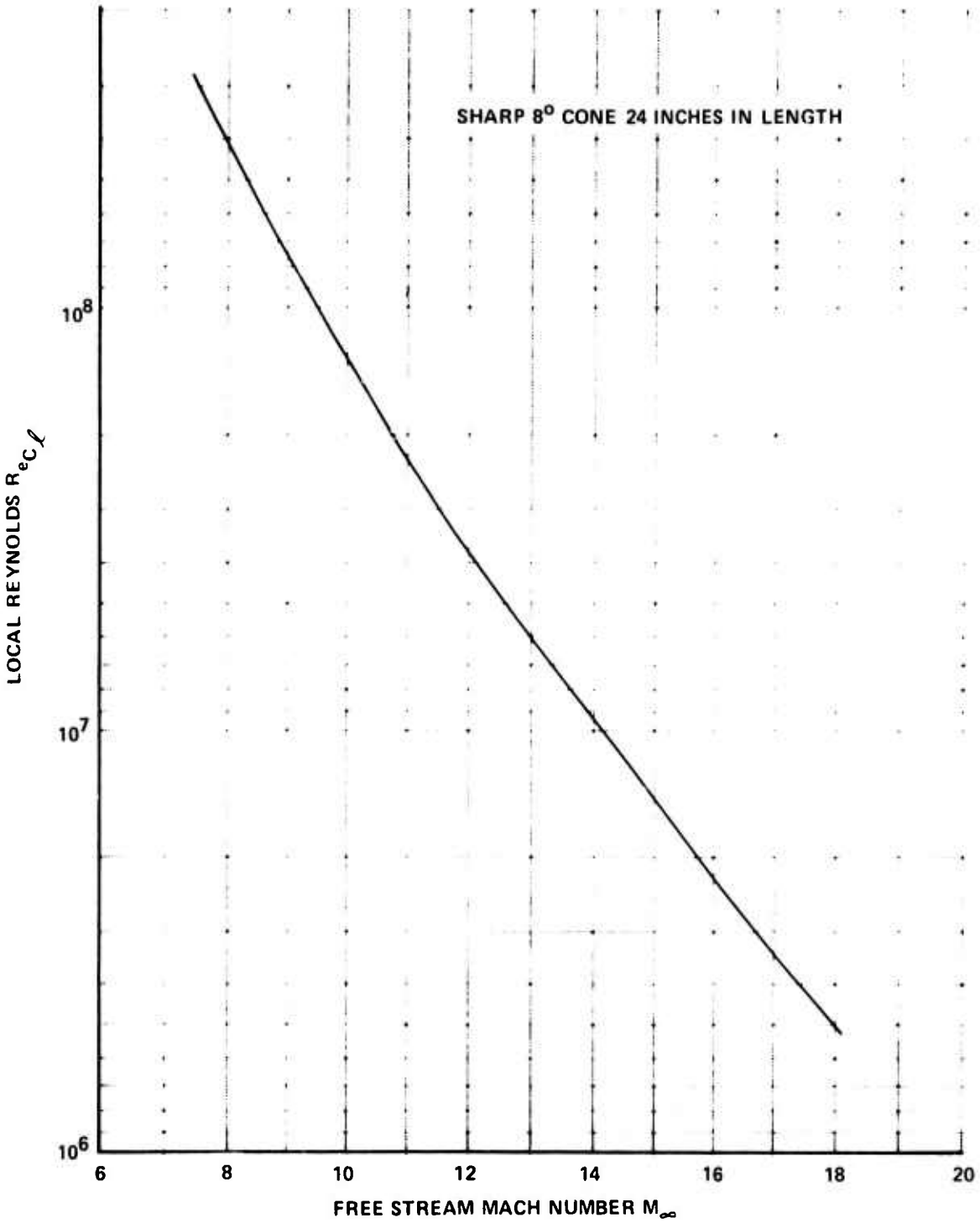


Figure 3. MAXIMUM LOCAL REYNOLDS NUMBER ON A 24 INCH 8° CONE IN THE 96-INCH TUNNEL

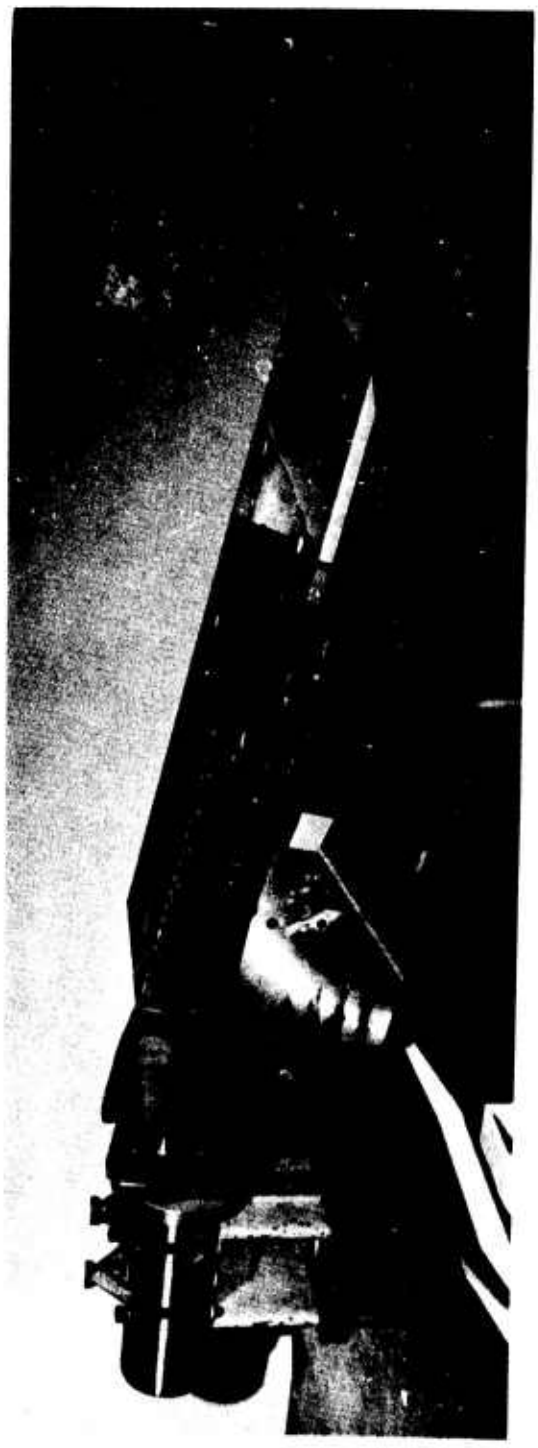


Figure 4. SHARP FLAT PLATE MODEL

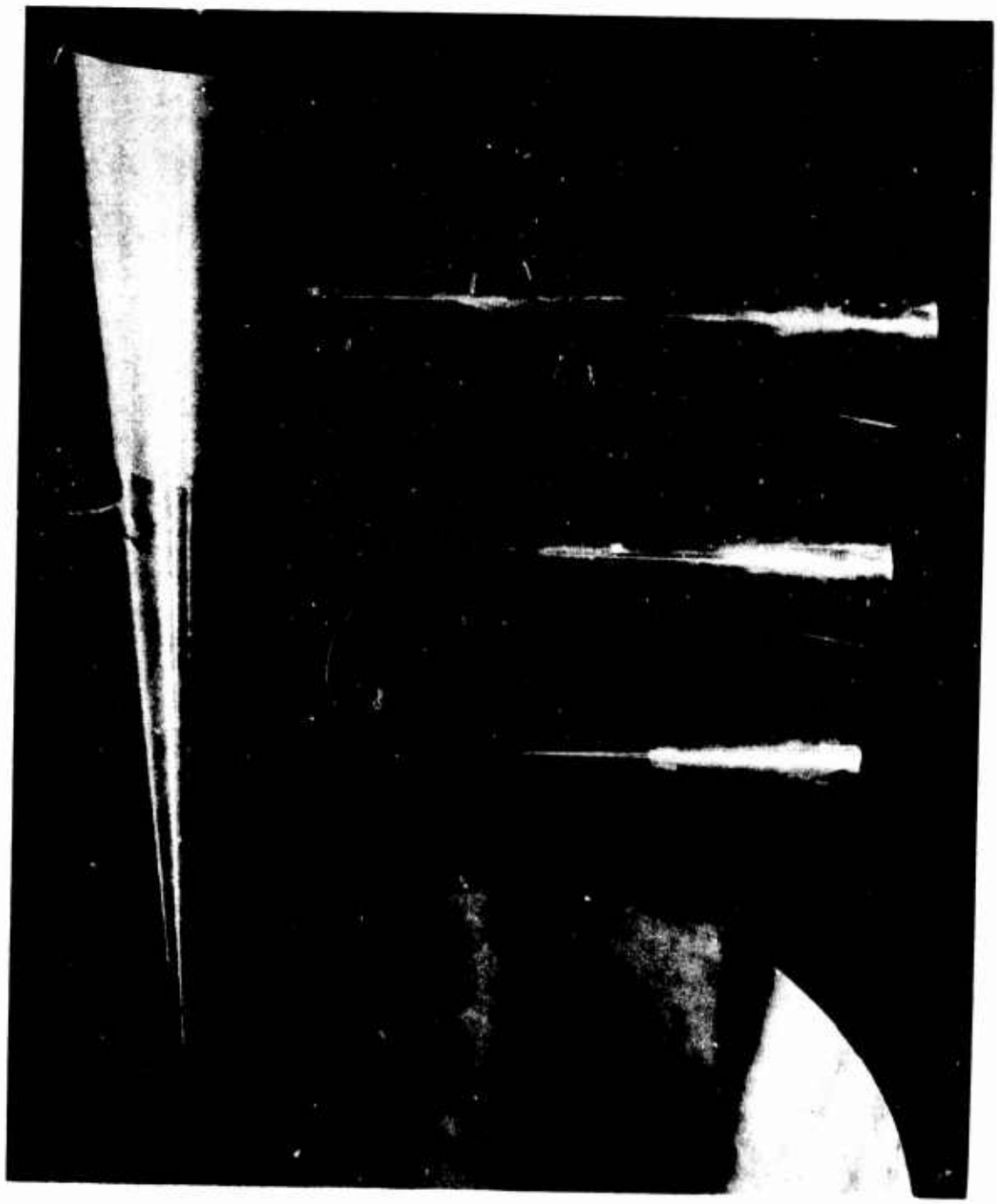


Figure 5. CONE MODELS

Table I
TEST CONDITIONS

RUN NO.	5	6	7	8	9	10	11	12
ATTACK	0.0	0.0	0.0	0.0	0.0	0.0	0.0	0.0
YAW	0.0	0.0	0.0	0.0	0.0	0.0	0.0	0.0
ROLL	0.0	0.0	0.0	0.0	0.0	0.0	0.0	0.0
M(I)	3.725E 00	3.815E 00	3.323E 00	3.136E 00	3.279E 00	3.215E 00	3.586E 00	3.280E 00
P(O)	1.149E 04	2.060E 04	1.843E 04	7.759E 03	1.935E 04	1.460E 04	9.123E 03	1.968E 04
H(O)	2.149E 07	2.225E 07	2.783E 07	1.611E 07	1.740E 07	1.681E 07	2.068E 07	1.773E 07
T(O)	3.237E 03	3.368E 03	2.759E 03	2.509E 03	2.748E 03	2.649E 03	3.135E 03	2.796E 03
M	1.040E 01	1.204E 01	1.109E 01	1.053E 01	1.072E 01	1.057E 01	1.018E 01	1.073E 01
U	6.412E 03	6.562E 03	5.856E 03	5.555E 03	5.777E 03	5.676E 03	6.285E 03	5.833E 03
T	1.580E 02	1.236E 02	1.158E 02	1.157E 02	1.208E 02	1.198E 02	1.584E 02	1.229E 02
P	2.022E-01	1.469E-01	2.534E-01	1.369E-01	3.446E-01	2.673E-01	1.839E-01	3.456E-01
Q	1.533E 01	1.491E 01	2.186E 01	1.064E 01	2.774E 01	2.094E 01	1.336E 01	2.788E 01
RHO	1.074E-04	9.975E-05	1.836E-04	9.929E-05	2.394E-04	1.872E-04	9.741E-05	2.360E-04
MU	1.324E-07	1.039E-07	9.742E-08	9.729E-08	1.015E-07	1.008E-07	1.326E-07	1.033E-07
RE/FT.	5.202E 06	6.302E 06	1.104E 07	5.669E 06	1.362E 07	1.055E 07	4.616E 06	1.333E 07
PITOT	2.849E 01	2.773E 01	4.050E 01	1.968E 01	5.138E 01	3.877E 01	2.482E 01	5.165E 01
T*	9.736E 02	9.856E 02	8.504E 02	7.962E 02	8.388E 02	8.201E 02	9.531E 02	8.524E 02
MU*	5.883E-07	5.931E-07	5.367E-07	5.126E-07	5.316E-07	5.233E-07	5.799E-07	5.375E-07
SQRT.C*	8.494E-01	8.462E-01	8.663E-01	8.750E-01	8.682E-01	8.712E-01	8.524E-01	8.661E-01
H(W)	3.177E 06	3.171E 06	3.207E 06	3.189E 06	3.207E 06	3.201E 06	3.225E 06	3.237E 06
T(W)	5.290E 02	5.280E 02	5.340E 02	5.310E 02	5.340E 02	5.330E 02	5.370E 02	5.390E 02
P(TS)	3.868E-04	4.835E-04	7.736E-04	3.868E-04	3.868E-04	4.448E-04	4.642E-04	4.448E-04
RE(STAG)	4.586E 04	4.226E 04	7.730E 04	4.266E 04	1.005E 05	7.969E 04	4.139E 04	9.905E 04

RUN NO.	13	14	15	16	17	18	19
ATTACK	0.0	0.0	0.0	0.0	0.0	0.0	0.0
YAW	0.0	0.0	0.0	0.0	0.0	0.0	0.0
ROLL	0.0	0.0	0.0	0.0	0.0	0.0	0.0
M(I)	2.488E 00	3.668E 00	3.178E 00	2.594E 00	3.599E 00	2.547E 00	3.199E 00
P(O)	5.223E 03	1.433E 04	1.048E 04	1.838E 04	1.072E 04	1.315E 04	8.771E 03
H(O)	1.069E 07	2.073E 07	1.613E 07	1.147E 07	2.031E 07	1.127E 07	1.699E 07
T(O)	1.707E 03	3.151E 03	2.529E 03	1.899E 03	3.083E 03	1.850E 03	2.642E 03
M	7.970E 00	7.738E 00	7.982E 00	8.324E 00	7.367E 00	7.712E 00	7.441E 00
U	4.447E 03	6.178E 03	5.472E 03	4.627E 03	6.102E 03	4.561E 03	5.586E 03
T	1.294E 02	2.651E 02	1.954E 02	1.285E 02	2.853E 02	1.455E 02	2.344E 02
P	6.072E-01	1.816E 00	1.194E 00	2.088E 00	1.846E 00	2.203E 00	1.501E 00
Q	2.703E 01	7.620E 01	5.329E 01	1.014E 02	7.019E 01	9.180E 01	5.822E 01
RHO	3.937E-04	5.750E-04	5.126E-04	1.364E-03	5.429E-04	1.271E-03	5.374E-04
MU	1.087E-07	2.161E-07	1.625E-07	1.080E-07	2.308E-07	1.220E-07	1.929E-07
RE/FT.	1.610E 07	1.644E 07	1.726E 07	5.846E 07	1.435E 07	4.750E 07	1.556E 07
PITOT	4.974E 01	1.415E 02	9.858E 01	1.867E 02	1.317E 02	1.690E 02	1.089E 02
T*	6.302E 02	9.809E 02	8.195E 02	6.573E 02	9.781E 02	6.580E 02	8.638E 02
MU*	4.333E-07	5.912E-07	5.231E-07	4.469E-07	5.901E-07	4.473E-07	5.425E-07
SQRT.C*	9.046E-01	8.599E-01	8.760E-01	8.996E-01	8.635E-01	9.002E-01	8.734E-01
H(W)	3.153E 06	3.165E 06	3.159E 06	3.183E 06	3.183E 06	3.201E 06	3.225E 06
T(W)	5.250E 02	5.270E 02	5.260E 02	5.300E 02	5.300E 02	5.330E 02	5.370E 02
P(TS)	5.802E-04	5.415E-04	5.802E-04	4.835E-04	4.835E-04	4.835E-04	3.868E-04
RE(STAG)	1.736E 05	2.406E 05	2.159E 05	5.674E 05	2.269E 05	5.352E 05	2.254E 05

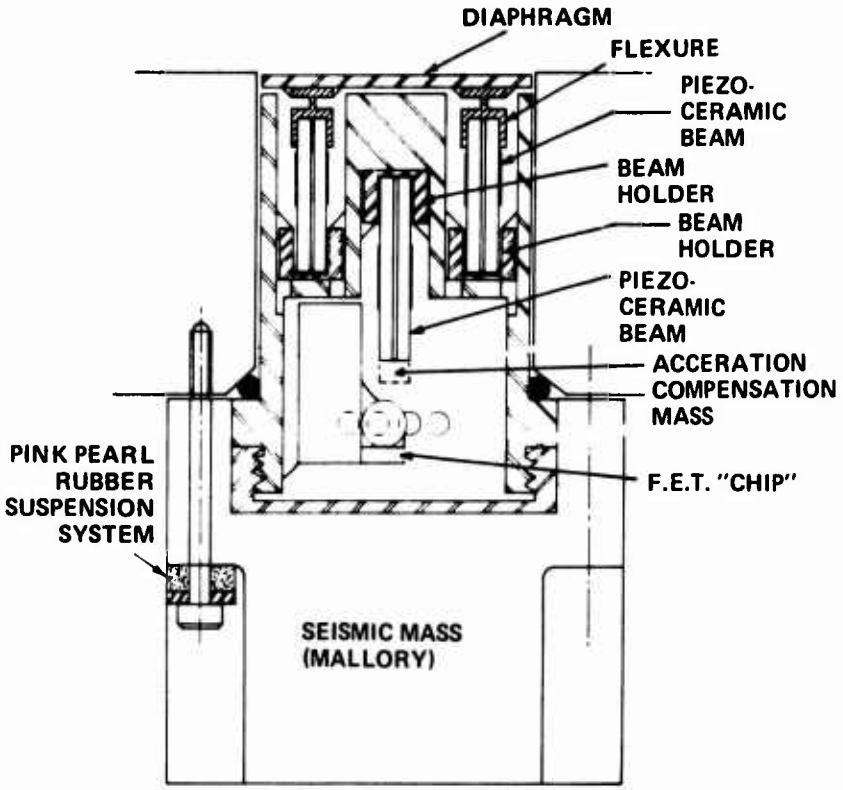
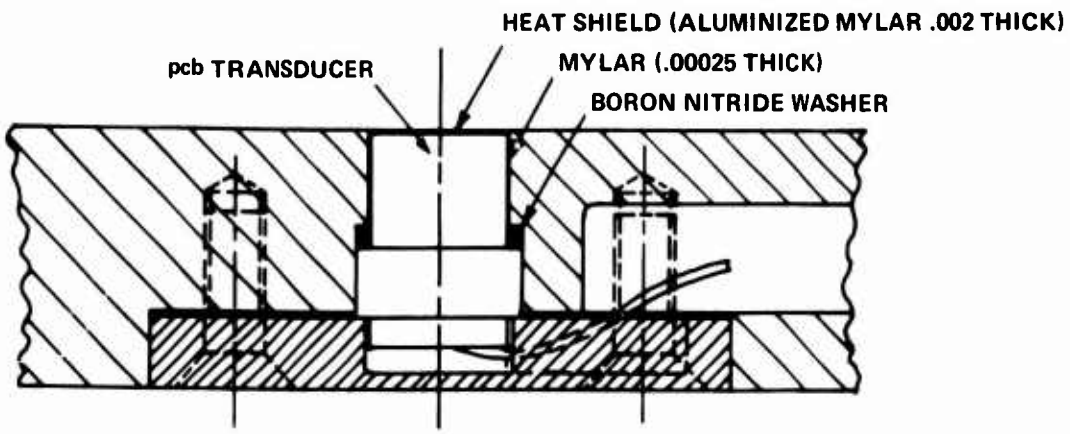


Figure 6. DRAWING OF SECTION THROUGH SKIN FRICTION TRANSDUCER



(a) TYPICAL MOUNTING TECHNIQUE USED IN MODEL

Figure 7. HIGH FREQUENCY PRESSURE MOUNTING

design of the flexure and by mounting the transducer in the seismic mass-rubber suspension system shown in Figure 6.

Thin-film heat transfer gages were used in the present study. This technique is based on sensing the transient surface temperature of a non-conducting model by means of thin-film resistance thermometers. Because the thermal capacity of the gage is negligible, the instantaneous surface temperature of the backing material is related to the heat transfer rate by the classical semi-infinite slab theory. Analog networks were used to convert the outputs of the gages, which are proportional to surface temperature, to a voltage directly proportional to heat transfer. The gages are fabricated on either small pyrex buttons or contoured inserts and mounted flush with the model surface.

b. Surface Pressure Measurements

We employed two types of surface pressure transducers in our studies of turbulent boundary layers. The Calspan-designed and -constructed lead zirconium titanate piezoelectric pressure transducers were used to obtain essentially the mean pressure distribution, although the transducer and orifice combination could follow fluctuations up to 15 kHz. A second flush-mounted transducer, especially designed for high-frequency measurements by PCB in Buffalo, was used to obtain surface pressure fluctuation measurements from 200 Hz to 120 kHz. To prevent a resonance, a special mounting system was developed (as shown in Figure 7) to lock the gage firmly into the model. A thin insulating barrier of aluminized mylar was attached to the diaphragm of the transducer to prevent thermal heating effects.

3. DATA RECORDING AND PROCESSING

The outputs from the transducers were recorded on a NAVCOR magnetic drum system and on a high frequency FM tape recorder, and also monitored on oscilloscopes. The NAVCOR system, which holds 48 channels in digital form,

is essentially a low-frequency system; whereas the 18 channel AMPEX FM recorder has a range of 0 to 1 MHz and was used to record the fluctuation data. The fluctuation measurements were recorded in analog form and subsequently processed by an analog-to-digital conversion/data storage system and digital computer program using a fast Fourier transform to yield the statistical properties of these measurements.

SECTION III

OBSERVATIONS ON BOUNDARY LAYER TRANSITION AND THE TRANSITIONAL REGION IN HIGH SPEED FLOWS

1. INTRODUCTION

Predicting the beginning of transition to turbulence is of course of fundamental importance in every branch of fluid mechanics, but of particular importance in high-speed flows where heat transfer is a prime consideration. Although recent advances have been made in understanding the mechanism of transition, the point at which a high-speed laminar boundary layer becomes unstable cannot be predicted with any accuracy from purely theoretical considerations. It is becoming increasingly evident that the level of disturbance induced within the boundary layer from roughness or mass addition at the leading edge or nose, or external to the boundary layer from pressure fluctuations in the free stream, is a factor of fundamental importance in the mechanics of transition. Thus one must incorporate the detailed response of the boundary layer to the specific initial and external environment, as well as describe the amplification of unstable modes within a laminar boundary layer, to describe the mechanics of transition.

Experimental observations of transition in hypersonic flow suggest that this process may be characterized at onset by a series of "wave-like" instabilities. These instabilities are followed by the occurrence of intermittent eddies, the intermittency increasing with downstream distance until the generation process appears continuous. Following this region of increased turbulent intensity, there is a relaxation region where both the turbulent scale size and intensity relax toward fully developed, or mature, values.

Transition is first observed in our studies as a series of "spikes" in the time-heating rate history from the thin-film heat transfer gages.

These well-defined increases in heating can be associated with the turbulent bursts created at the edge of the viscous sublayer which occur during the second phase of the transition process. These observations are supported by the reduction of records from adjacent gages which indicate that the disturbance responsible for the temporal increase in heating is convected downstream at a fraction of the freestream velocity. Just downstream of where the spikes in heat transfer are first observed, the output of the gages exhibits strong fluctuations, and the mean heating and skin friction levels increase above their equivalent values for laminar flow. In this region, the outputs from the high-frequency pressure transducers showed fluctuation levels significantly larger than those observed downstream of transition. The heat transfer and skin friction rises monotonically through the transition region to reach a maximum value close to the "end" of the transition process. The relaxation process during which the heat transfer and skin friction approach "equilibrium turbulent flat plate values" occurs downstream from the point of maximum heating. The length of this relaxation process is to some extent dependent upon the heat transfer properties chosen to define it; however, for gross prediction purposes, this length is approximately 15% of the length to the point of maximum heating. A typical heat transfer distribution through a transition region in hypersonic flow is shown in Figure 8. Similar measurements over a wide range of Mach and Reynolds numbers over both flat plates and cones, plotted in Figure 9, have indicated for untripped boundary layers that the length of the transition process is roughly equal to the preceding length of laminar run. Here for convenience we have defined the length of transition as the distance between the initial departure from a laminar behavior and the point of maximum heating. The variations shown in Figure 9 reflect the intermittent nature of the process as well as real differences between the length of transition in different transition environments.

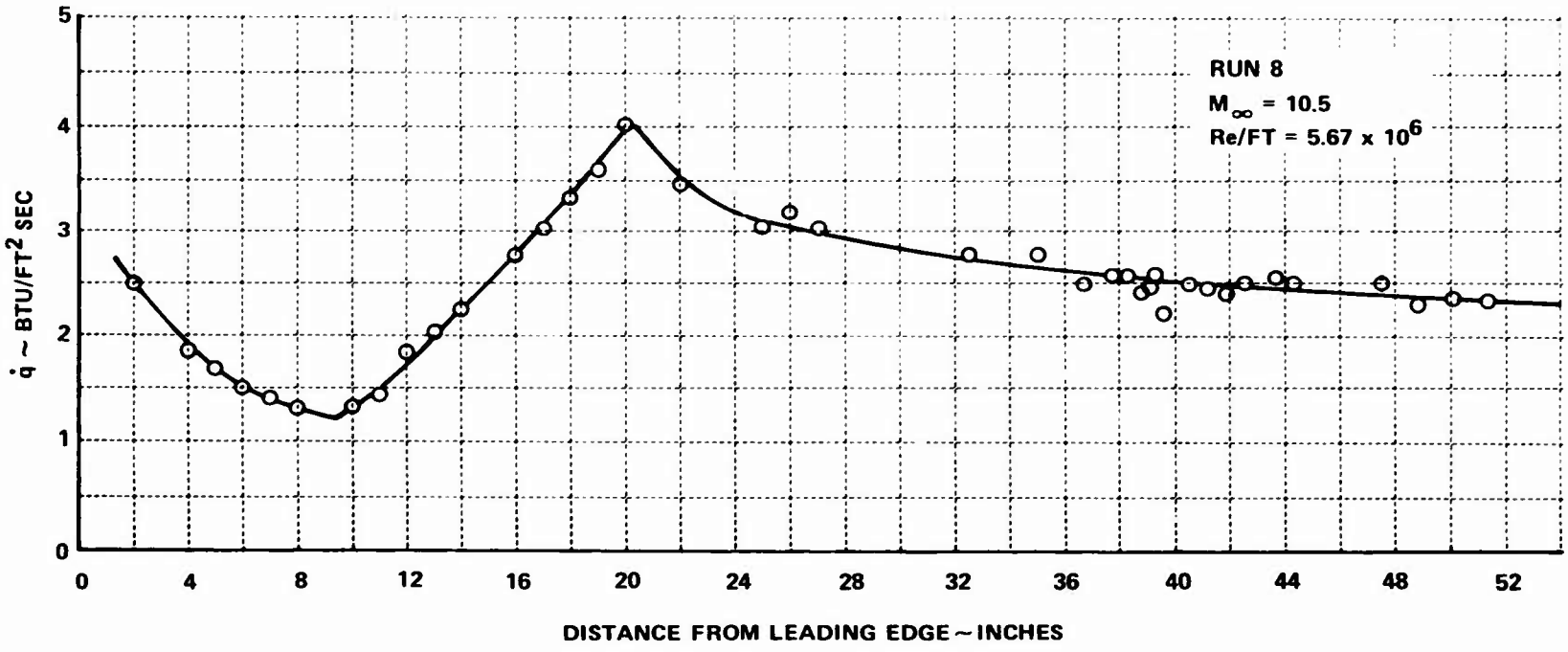


Figure 8. TYPICAL DISTRIBUTION OF HEAT TRANSFER ALONG THE FLAT PLATE MODEL

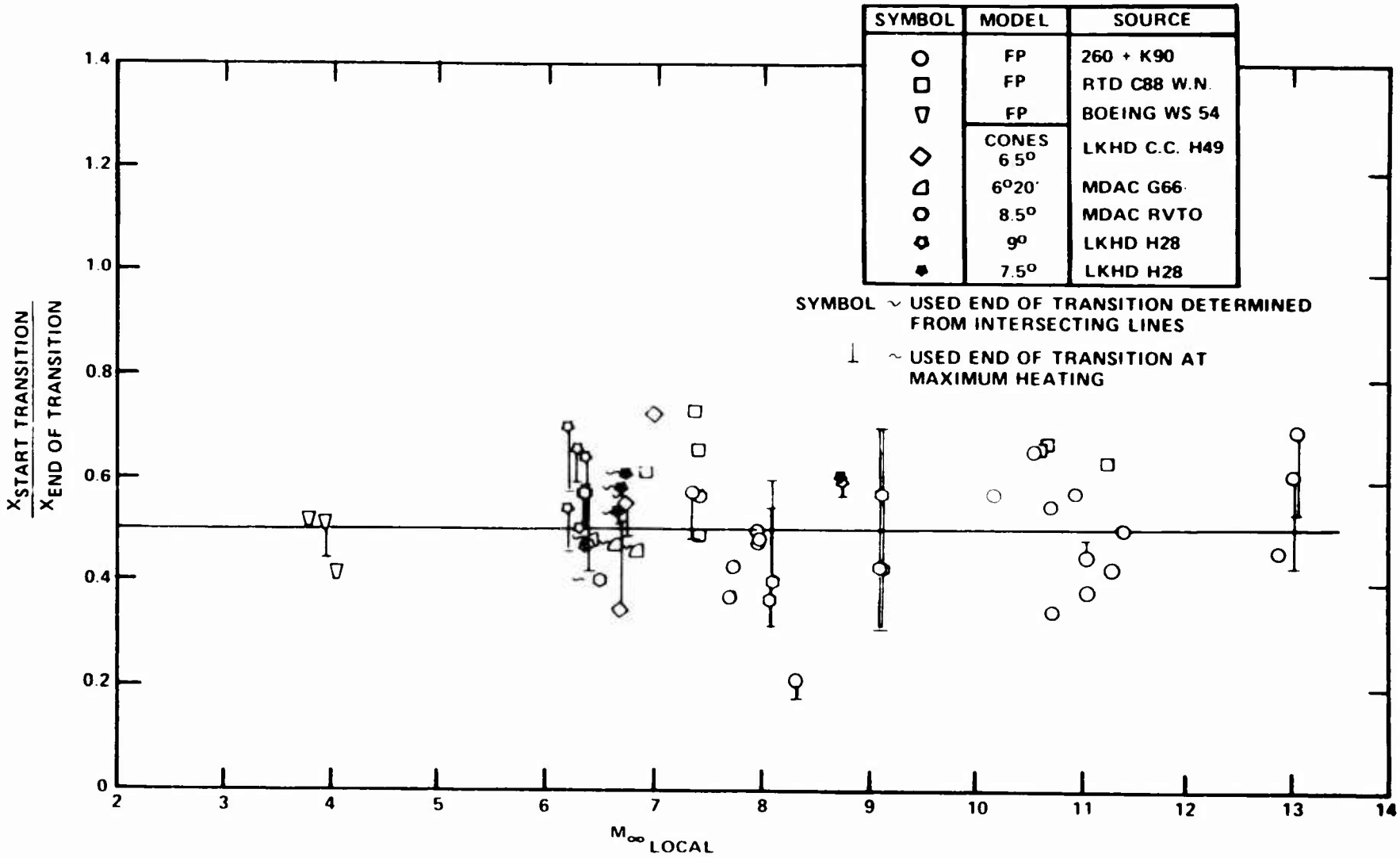


Figure 9. CORRELATION OF THE SCALE LENGTH OF THE TRANSITION ON FLAT PLATES AND CONES

2. DISTRIBUTION OF PROPERTIES IN THE TRANSITION REGION

Applying Emmons[32] theory, together with a point breakdown hypothesis, Dhawan and Narashima[33] suggest that the intermittency γ can be related to nondimensional distance in the transition region $\zeta = \frac{(x - x_B)}{x_{trans} - x_B}$, through the relationship

$$\gamma = \frac{1 - e^{-A\zeta}}{1 - e^{-A}} \qquad (1)$$

From this we can develop the equation

$$C_H = (1-\gamma)\, C_{H_{LAM}} + \gamma\, C_{H_{TURB}} \qquad (2)$$

The measurements of intermittency using hot-wire and thin-film gages (shown in Figure 10) suggest that surface thin films can be used to obtain accurate measurements of γ. Figure 11 shows the variation in the form of the heat transfer distribution through the transition region as a function of A. Our measurements suggest that $A \doteq 2$ describes the form of the distribution most accurately. This value compares with the figure of 0.412 suggested in Owens[34] for subsonic flows.

3. OBSERVATIONS ON THE OCCURRENCE OF TRANSITION

Experimental measurements of boundary transition on sharp flat plates and cones made in many different studies conducted in the Calspan 48- and 96-inch Shock Tunnels form the basis for the correlations presented herein. We have also selected measurements and observations from ballistic range and downrange shots for comparison. It is clear from the studies of Pate and Schueler[35] and extensive measurements made at NASA Langley that boundary layer transition on models in wind tunnel studies is strongly influenced by the freestream pressure environment. In general, our studies were conducted at Mach and Reynolds numbers considerably larger than those in the studies of Pate and Schueler. Thus, the magnitude of the noise radiated from the tunnel walls and the intensity on the axis should be significantly less in our studies. A direct result of Pate and Schueler's findings is that

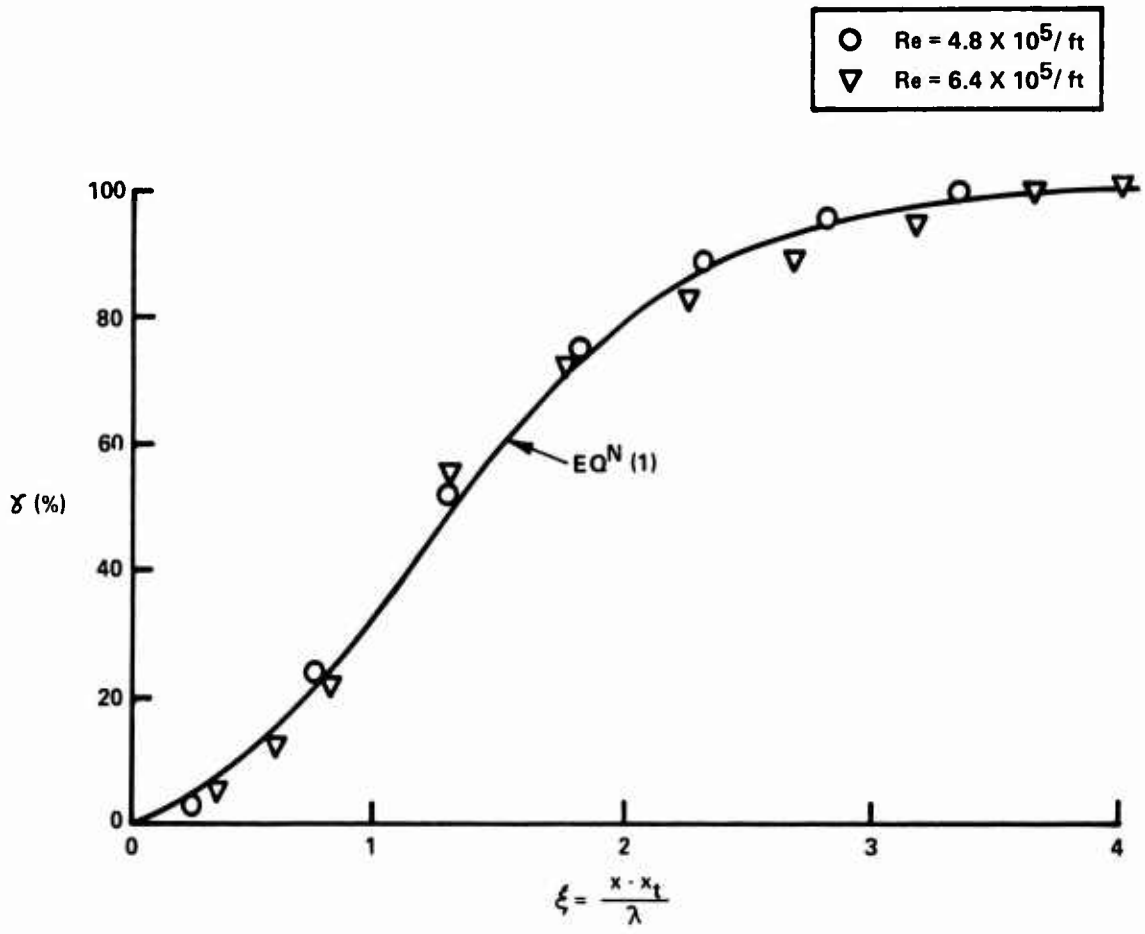


Figure 10. UNIVERSAL INTERMITTENCY DISTRIBUTION

$$C_H = \gamma' C_{H_{TURB}} + (1-\gamma') C_{H_{LAM}}$$

$$\text{WHERE } \gamma' = \frac{1 - e^{-A\xi^2}}{1 - e^{-A}}$$

$$\text{AND } \xi = \frac{x - x_{LAM}}{x_{TURB} - x_{LAM}}$$

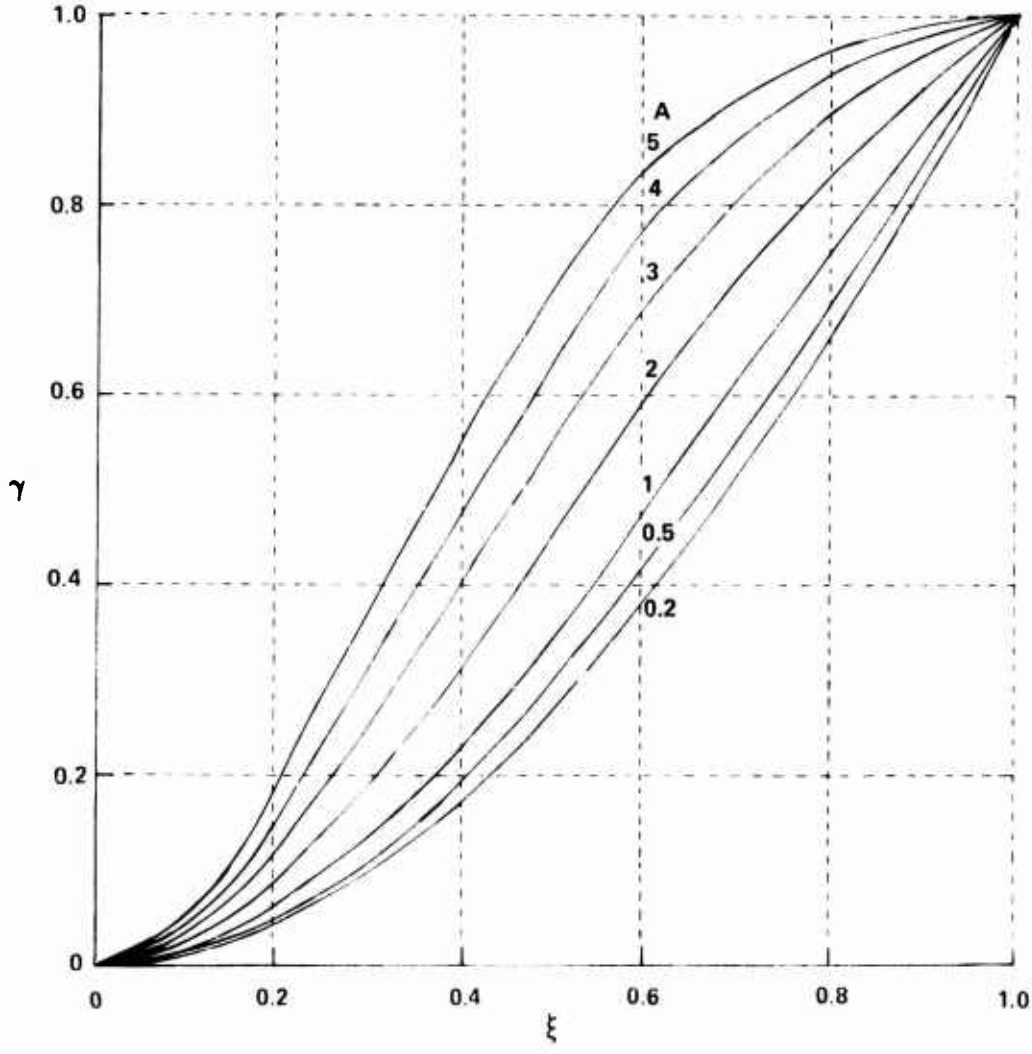


Figure 11. HEAT TRANSFER DISTRIBUTION IN THE TRANSITION REGION

a decrease in the tunnel size, for the same freestream conditions, should decrease the transition Reynolds number. However, transition measurements (shown in Figure 12) made in the A and D nozzles, which have exit diameters of 24 and 48 inches, respectively, do not exhibit this scale effect, even though a unit Reynolds number variation is evident in the correlation. Predictions based on Pate and Schueler's correlation suggest transition Reynolds numbers of over 200 million should be anticipated for our test conditions, which is clearly well in excess of physically meaningful values. Our measurements of transition plotted in terms of the parameters suggested by Pate and Schueler fall below their earlier correlation (Figure 13). Expressing transition in terms of the Reynolds number based on the momentum thickness at transition onset, we can compare our measurements with the results of earlier studies conducted in the ballistic range and on full scale flight tests, as shown on Figure 14. Here we have included measurements from cone and flat plate studies; we can see that, although our transition measurements on flat plates are consistently larger than those on cones, both sets of measurements are in essential agreement with ballistic range and flight tests. It is clear that in these tests the position of transition was influenced by factors more complex than those governing transition in the tests conducted by Pate and Schueler. Whether the fluctuating pressure level of the freestream is the principal factor influencing transition, as indicated by the measurements of Stainback, Fisher, and Wagner,[36] or whether this quantity is directly related to parameters which themselves govern transition remains to be determined.

One of the most interesting and puzzling aspects of boundary layer transition in hypersonic flows is the difficulty one finds in attempting to induce transition prematurely. Experimental studies at Calspan and Langley in which attempts were made to trip boundary layer above Mach 8 were singularly unsuccessful. To generate a de-stabilizing disturbance in a hypersonic, highly cooled, laminar boundary layer requires large trips to reach into the critical layer located in the outer region of the boundary layer. Although tripping was found to disturb the structure of the boundary layer, causing an increase in the local values of skin friction and heat

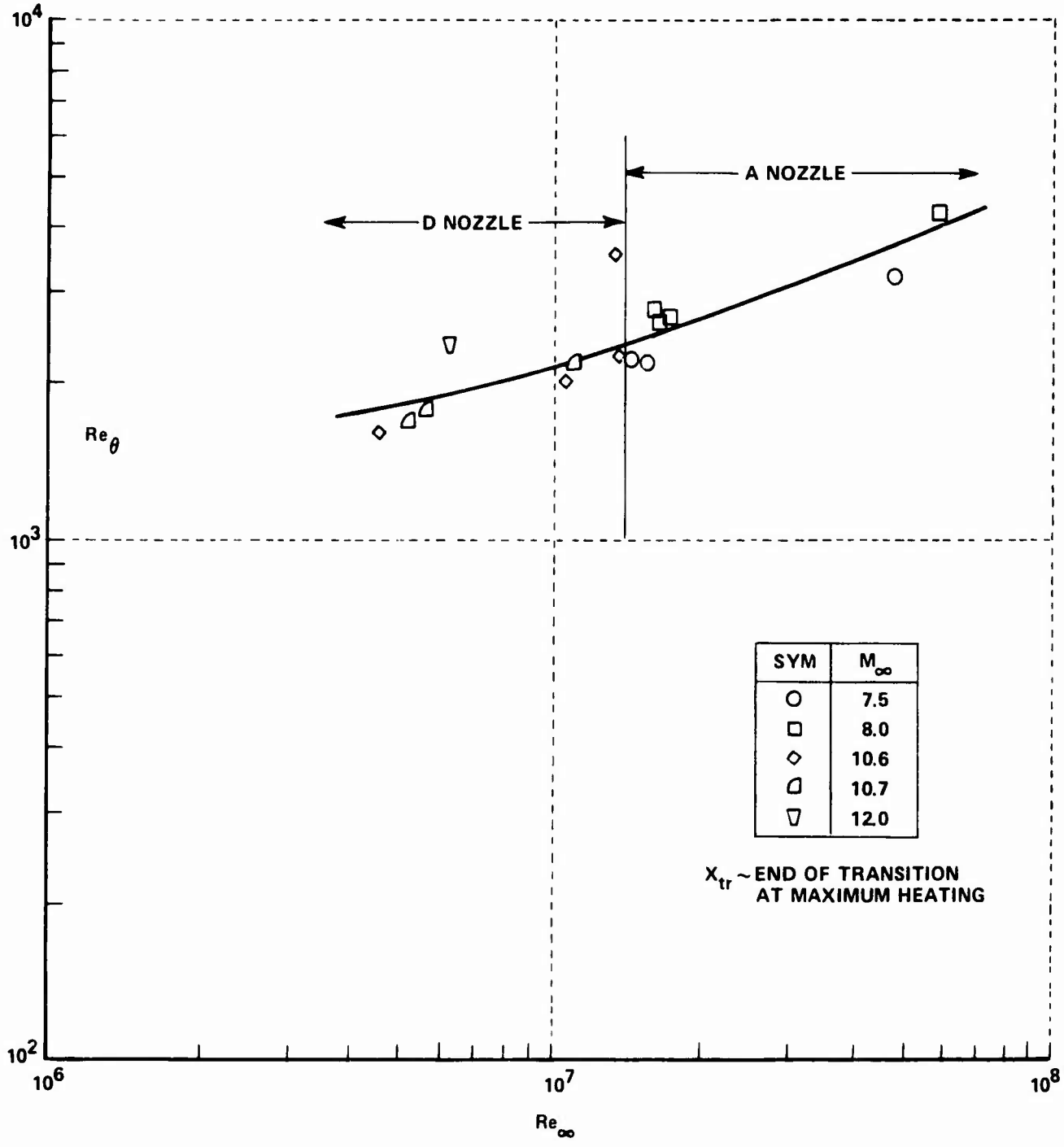


Figure 12. CORRELATION OF TRANSITION SHOWING THE EFFECTS OF TUNNEL SIZE

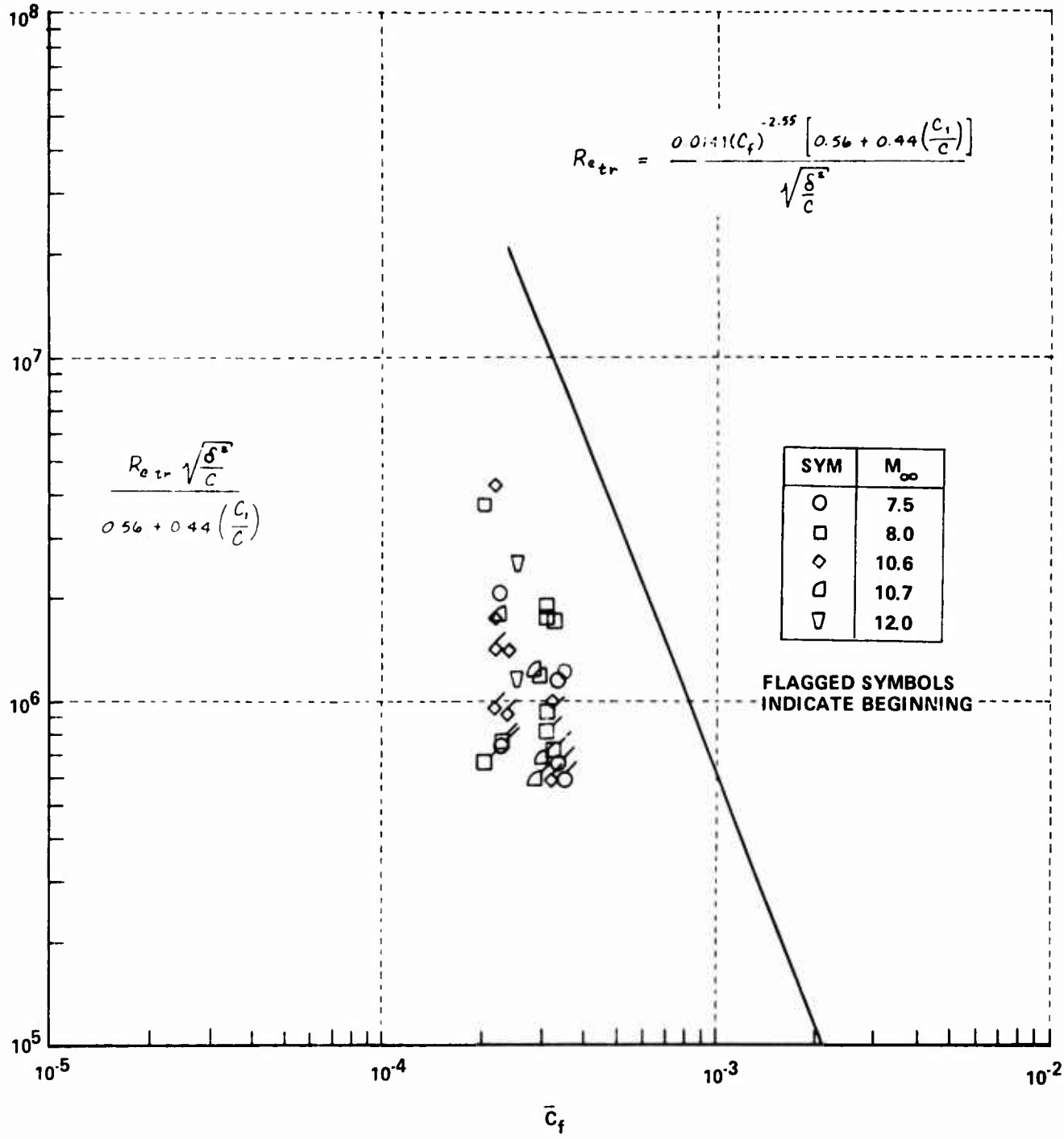


Figure 13. CORRELATION OF THE FLAT PLATE TRANSITION DATA IN TERMS OF THE PARAMETERS SUGGESTED BY PATE AND SCHUELER

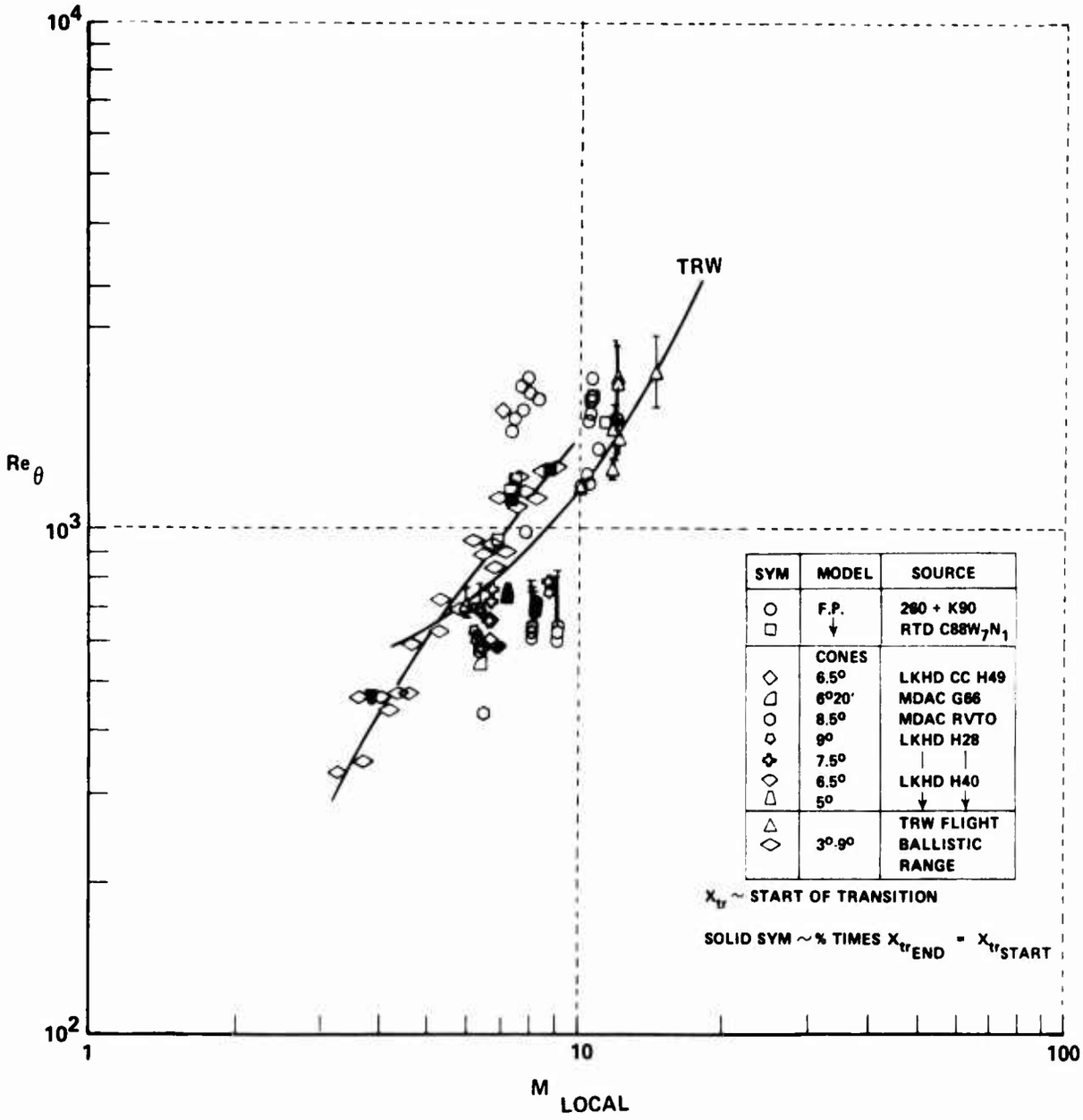


Figure 14. CORRELATION OF TRANSITION MEASUREMENTS IN THE CALSPAN SHOCK TUNNELS WITH BALLISTIC AND DOWNRANGE MEASUREMENTS

transfer, the Reynolds number (based on distance to the end of transition) at which the boundary layer exhibited the characteristics of a "fully turbulent" boundary layer was only slightly less than if "natural" transition had been allowed to occur. This finding suggests in high-speed flow one cannot develop an equilibrium turbulent boundary layer until it can become self-sustaining. Following Bradshaw [37], one can examine the lowest Reynolds number at which turbulence can exist by suggesting that self-sustaining turbulence can exist only when the energy or shear stress producing eddy size and the dissipating range of eddy scale size just overlap; i.e., where a viscosity-independent region can be established. Here production and dissipation exist in equilibrium, while a lower Reynolds number dissipation is the dominant mechanism. This criterion can be expressed in terms of an eddy Reynolds number Re_λ which is derived from comparing the scale size of the energy containing eddies $[\lambda = (\tau/\rho)^{3/2}/E]$ with the Kolmogorov scale size $[\nu^3/E^{1/4}]$, to give $Re_\lambda = \left(\frac{u'\lambda}{\nu}\right)$, which must exceed 30 for equilibrium flow. For hypersonic turbulent boundary layers, the measurements of Demetriades indicate that $u' \simeq 0.02 u_\infty$ and $\lambda \simeq 0.1\delta$. By evaluating μ at the edge of the sublayer for a turbulent boundary layer with momentum thicknesses equal to those at the beginning and end of transition, we obtained the correlation shown in Figure 15. Here we have related θ and δ from the correlations shown in Figure 16. Our measurements indicate that transition is complete by Re_x's of approximately 50, with transition beginning at Reynolds numbers of approximately half this value. It is interesting to note that plotting the measurements in this format significantly reduces the Mach number dependence although a slight Reynolds number trend is still observed.

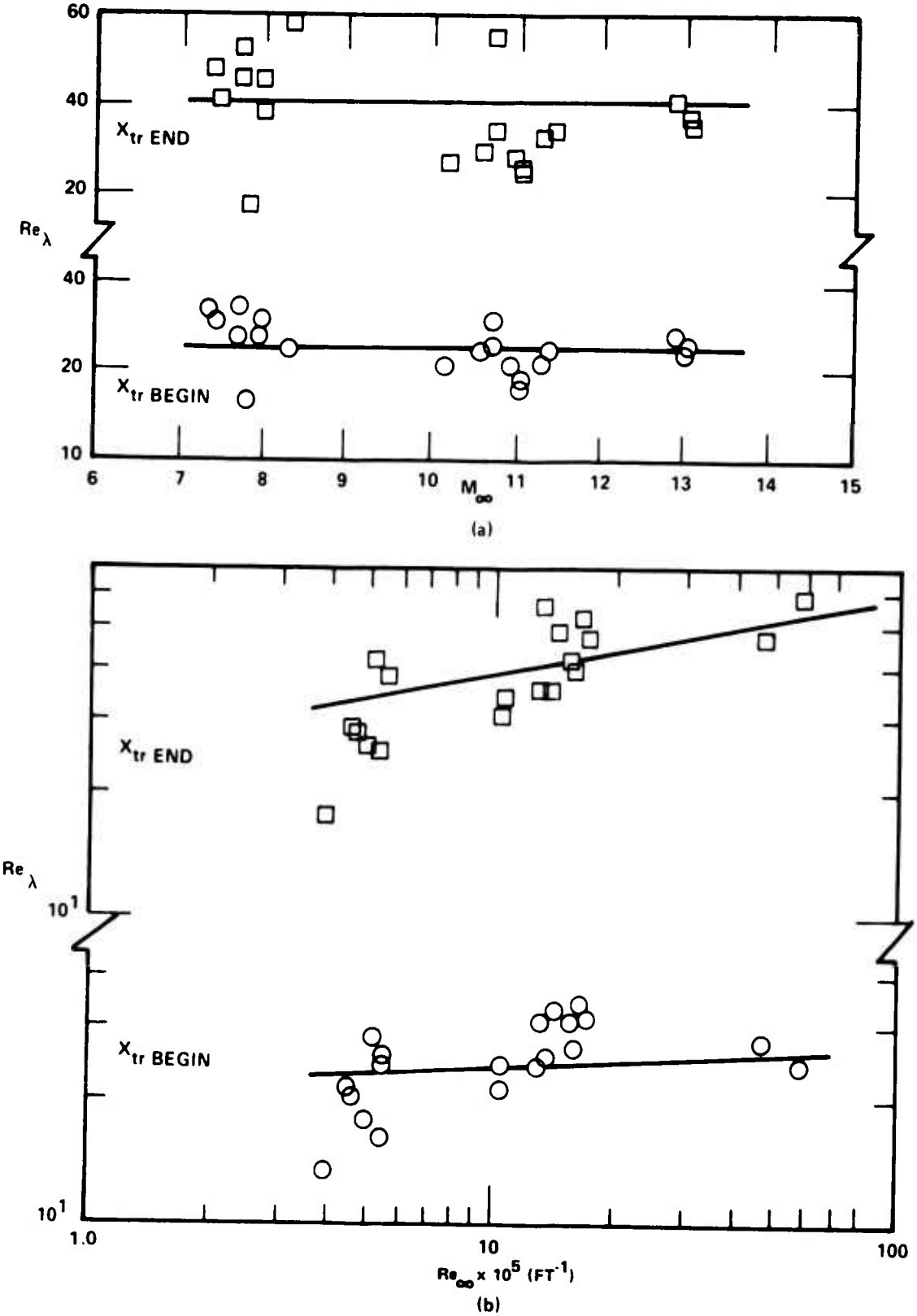


Figure 15. CORRELATION OF THE EDDY REYNOLDS NUMBER WITH TRANSITION MEASUREMENTS ON THE FLAT PLATES

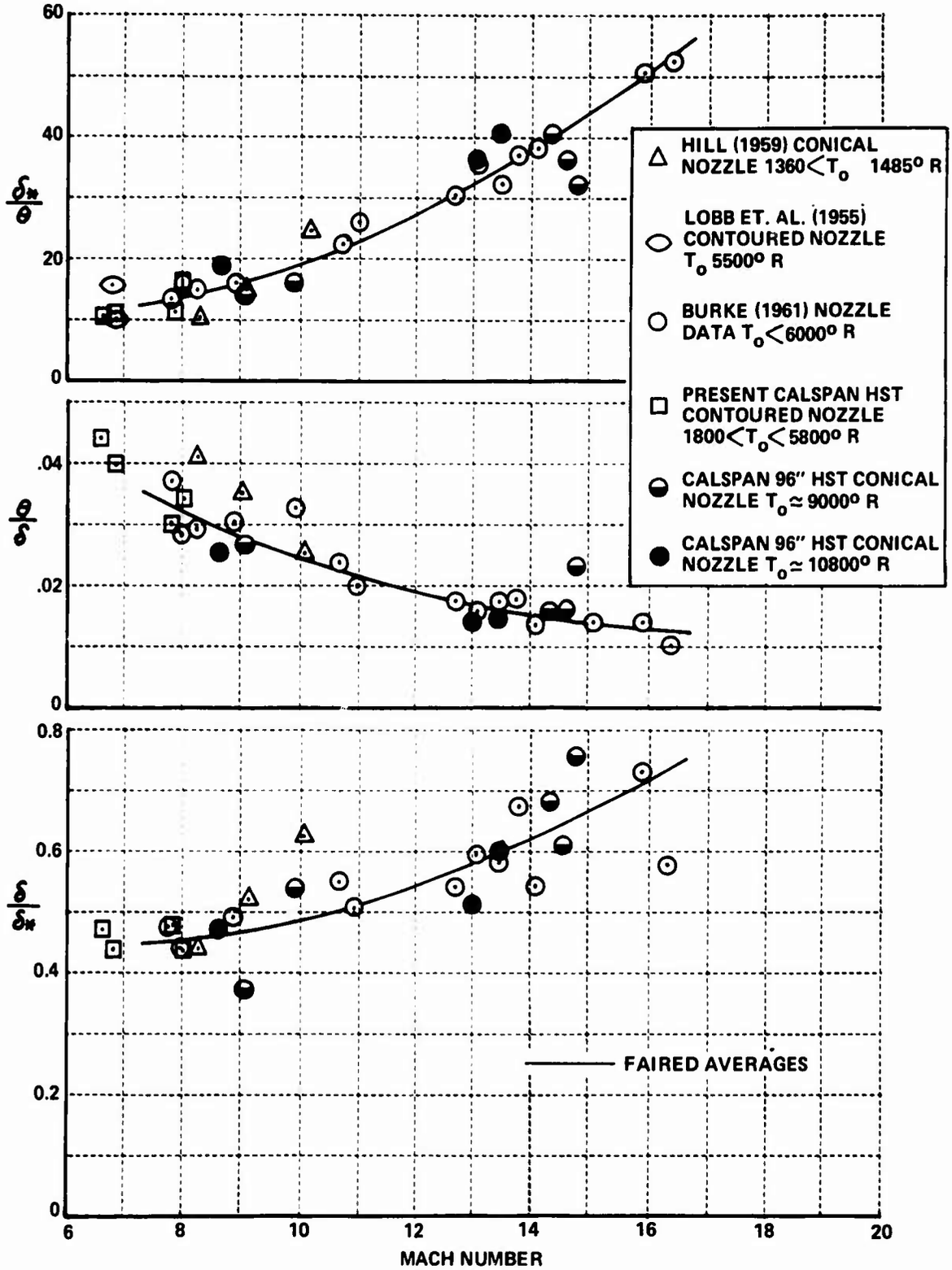


Figure 16. TURBULENT BOUNDARY LAYER DISPLACEMENT AND MOMENTUM THICKNESS FROM SHOCK TUNNEL NOZZLE DATA

SECTION IV

COMPARISONS BETWEEN TURBULENT PREDICTION METHODS AND MEASURED SKIN FRICTION AND HEAT TRANSFER

We have chosen to perform the comparison between the measurements of heat transfer and skin friction within the framework suggested by the Spalding-Chi[38] method. Here the measured coefficient of local skin friction and heat transfer (C_f and C_H) are related to an equivalent quantity in an incompressible flow (C_{f_i} and C_{H_i}) through the relationship

$$C_{f_i} = Fe(Me\ T_w/T_o)\ C_f$$
$$C_{H_i} = F_c(Me\ T_w/T_o)\ C_H$$

The local Reynolds numbers based on the momentum thickness, θ , and distance from the virtual origin X_v, Re_o and Re_x, respectively, are related to similar quantities in the incompressible plane through the relationships

$$F_c C_f = F_\theta\ Re_\theta$$
$$F_c C_f = F_x\ Re_x$$

We have assumed that the Karman-Schoenherr relationship

$$\log_{10}(Re_{x_i} C_{F_i}) = \log_{10}(2Re_\theta) = 0.242\,(C_{F_i})^{-1/2}$$

where the average skin friction C_{F_i} is related to the local skin friction C_{f_i} by

$$C_{f_i} = 0.242\ C_{F_i}\left[0.242 + 0.8686\,(C_{F_i})^{1/2}\right]^{-1}$$

accurately describes the skin friction distribution in the incompressible plane.

In the Spalding-Chi analysis, the transformation factors F_c, F_θ, and F_χ were determined from Van Driest's[39] analysis and correlations of experimental measurements. For this analysis, the transformation factors are

$$(F_c)_{SC} = r\, me \left(\sin^{-1}\alpha + \sin^{-1}\beta\right)^{-2}$$

$$(F_\theta)_{SC} = \left(T_w/T_e\right)^{-0.702}\left(T_w/T_{AW}\right)^{-0.772}$$

and

$$F_\chi = F_\theta \cdot F_c^{-2}$$

where

$$\alpha = (2A^2 - B)(4A^2 + B^2)^{-1/2} \quad \text{and} \quad \beta = B(4A^2 + B^2)^{-1/2}$$

and

$$A = \left[r\, me \left(\frac{T_w}{T_e}\right)^{-1}\right]^{1/2} \quad \text{and} \quad B = \left(1 + r\, Me - \frac{T_w}{T_e}\right)\left(\frac{T_w}{T_e}\right)^{-1}$$

where a recovery factor (r) of 0.89 was used.

Van Driest's analysis is based on the Prandtl-Karman mixing length model, together with a compressibility transformation, to describe the compressible turbulent boundary layer over a flat plate. From this analysis, the transformation or compressibility factors are

$$(F_c)_{VD} = r\, me \left(\sin^{-1}\alpha + \sin^{-1}\beta\right)^{-2}$$

$$(F_\theta)_{VD} = \mu_e/\mu_w$$

and

$$F_\chi = F_\theta\, F_c^{-1}$$

The function F_c is identical in the Van Driest and Spalding-Chi analyses.

From Eckert's[40] enthalpy method, we can deduce the transformation factors

$$(F_c)_E = T^*/T_e$$

$$(F_\theta)_E = \mu_e/\mu^*$$

and

$$F_\chi = F_\theta\, F_c^{-1}$$

where we have evaluated these expressions for two definitions of the reference temperature T^*,

$$T_E^* = 0.5\,T_w + 0.22\,T_{AW} + 0.28\,T_E$$

$$T_A = 0.5\,T_w + 0.1667\,T_{AW} + 0.333\,T_E$$

To compare the prediction methods with the experimental measurements in the $C_f F_e - F_\theta Re_\theta$ plane, the momentum thickness, θ, must be calculated. We have used the relationship from the momentum equation $\theta = \int_0^x \frac{C_f}{2}\,dx$ to calculate this quantity. For our measurements in transitional and turbulent flows, we found that the Reynolds analogy factor was close to unity, as shown in Figures 17 and 18. Thus, when only heat transfer measurements were available, we calculated the momentum thickness from the expression $\theta = \int_0^x C_H\,dx$

To compare the experimental measurements with the theories in the $F_c C_f - F_x Re_x$ plane, it is necessary to define a virtual origin from which the turbulent boundary layer is assumed to grow. We assumed that the momentum thickness of the turbulent boundary layer at the end of transition θ was given by

(1) $$\theta_V = \int_0^{x_B} C_H\,dx + \int_{x_B}^{x_B} \equiv \theta_B + \theta_{BE}$$

(2) $$\theta_V = \theta_B + \theta_{BE}/2$$

(3) $$\theta_V = \theta_B + \int_{x_B}^{x_E} C_{H_{LAM}}\,dx$$

(4) $$\theta_V = \theta_B$$

The first assumption gives a comparison in the $F_c\,C_f - F_{R_x} Re_x$ plane which is directly equivalent to the $F_c C_f - F_\theta Re_\theta$ correlation. We make the second assumption for a direct comparison with the method for determining the virtual origin suggested by Bertram and Cary[41] which is discussed as follows.

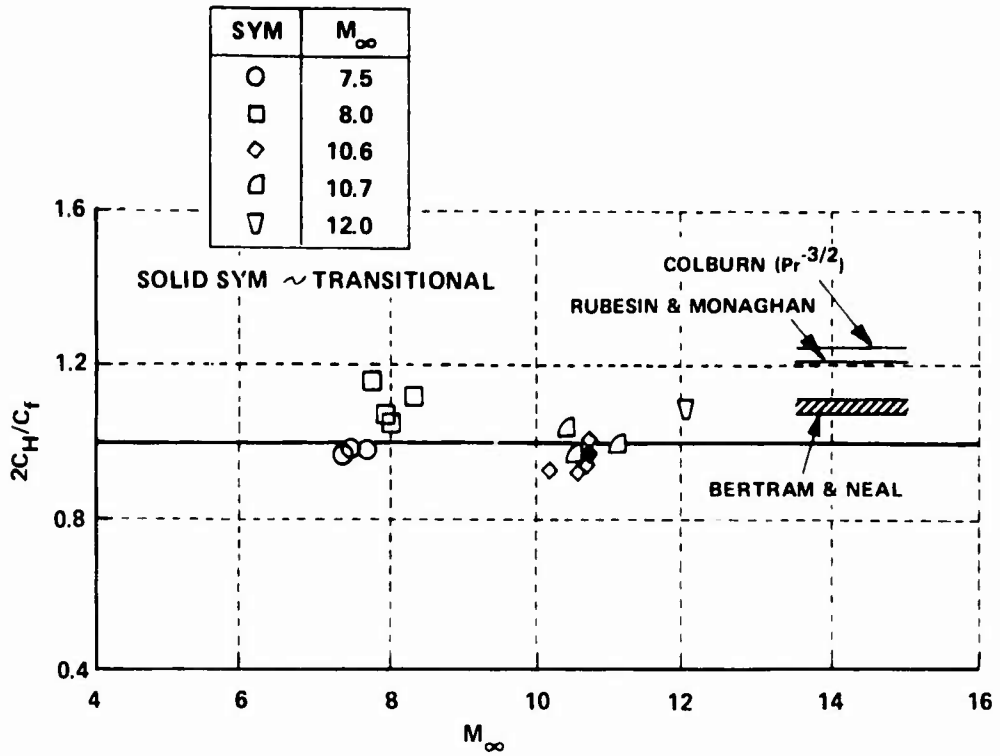


Figure 17. REYNOLDS ANALOGY FACTORS FOR TURBULENT HYPERSONIC BOUNDARY LAYERS

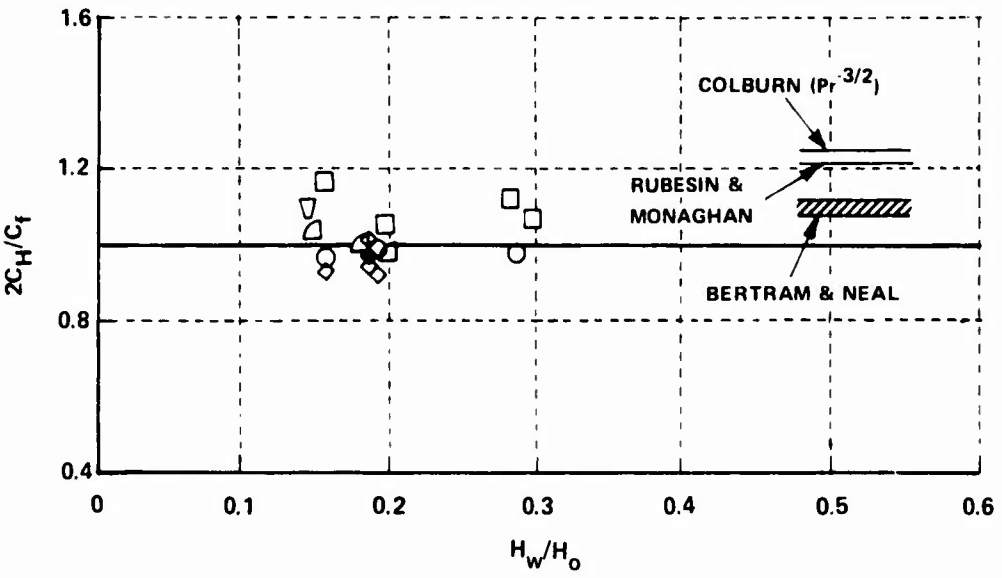


Figure 18. REYNOLDS ANALOGY FACTORS FOR TURBULENT HYPERSONIC BOUNDARY LAYERS

The third and fourth assumptions are based on pragmatic situations where no measurements of transitional heating and the momentum thickness exist. We assume that the momentum thickness is identical to that of a boundary layer which is laminar up to the assumed beginning and end of transition, respectively. In each case, once the momentum thickness is specified, the distance of the virtual origin from the point of maximum heat transfer is calculated from the respective theories.

Finally, we have used the method suggested by Bertram and Cary, who, based on the best correlation of their data with the Spalding-Chi theory, place the virtual origin at the point where $Re_\theta = R\theta_B + \frac{R\theta_{BE}}{2}$.

In correlating the measurements made on the conical models in the $F_c C_H - F_{R_x} Re_x$, we employed the Mangler transformation in the form suggested by Bertran and Neal to relate the measurements on the cones to an equivalent two-dimensional flow. For an equal distance from the virtual origin of the turbulent boundary layer on flat plates and cones, the local Stanton number on the cone would be larger than that on a flat plate by the ratio

$$\frac{(C_H)_{cone}}{(C_H)_{fp}} = \left(\frac{2n-1}{n-1}\right)^{1/n} \left[\left(\frac{1+R_{x_v}}{R_x}\right) - \frac{R_{x_v}}{R_x}\left[\frac{R_{x_v}/Re_x}{1+(R_{x_v}/R_x)}\right]^{n/n+1}\right]^{-1/n}$$

By employing the above equation, the measurements on the conical bodies were transformed into the equivalent two-dimensional compressible plane and subsequently to the incompressible plane by the transformations given above.

The measured heat transfer and skin friction over sharp flat plates are compared with the prediction methods of Van Driest, Eckert, and Spalding-Chi in Figures 19 through 30. In the $F_c C_f - F_\theta Re_\theta$ plane, the measurements can be compared with the incompressible theory without additional assumptions. However, in the $F_c C_f - F_\theta Re_\theta$ plane, each comparison is influenced at small values of Re_θ by the choice of the position of the virtual origin. A

major purpose of the present study was to examine the prediction methods under high Mach number ($M_\infty > 6$) and highly cooled wall conditions. Examining the comparison between theory and experiment in $F_c C_f - F_{R\theta} R_{e_\theta}$ plane, we see that the Van Driest theory is in best overall correspondence though it tends to overpredict the heat transfer and skin friction at the lower Mach numbers. The Spalding-Chi method, while comparing best with the low Mach number measurements, significantly underpredicts the heat transfer and skin friction at high Mach numbers. The prediction method supported by the Eckert approach falls between the Van Driest and Spalding-Chi methods on predicting heat transfer and skin friction. Defining T^* based on the average temperature T_A^* gives the best overall comparisons between the prediction method and experiment.

The comparisons between theory and experiment of course require an assumption of the position of virtual origin, as described above. Assuming $\theta_T = \theta_B + \theta_{BE}$ has its equivalent in the comparisons in the R_{e_θ} plane; thus, it is not suprising that we again find Van Driest's method compares best with experiment, followed by Eckert and Spalding-Chi. The remaining three assumptions have the effect of progressively decreasing the distance to the virtual origin, which tends to move the Spalding-Chi method into better correspondence with the experimental observations. Using the position of the virtual origin at the mid-point of the transition region as suggested by Bertram and Cary, we find that the Spalding-Chi method compares best with the measurements in the high Reynolds number (low Mach number) regions, while the Van Driest theory over-predicts the measurements. Surprisingly, Eckert's method with this definition for the virtual origin is in best overall correspondence with experiment.

The heat transfer measurements on the conical models are compared with the prediction methods in the same format as that used for the flat plate measurements in Figures 31 through 36. The comparisons in the $C_f F_c - F_{R\theta} R_{e_\theta}$ plane again show closest correspondence between the Van Driest method and the measurements. The Spalding-Chi method underpredicts the heating rates by as much as

20 percent in the high-Mach-number, low-Reynolds-number regions. The Eckert method again falls between these two methods in accuracy. In the $F_c C_H - F_x R_{e_x}$ plane, choosing $\theta_v = \theta_B + \theta_{BE}$ results in the best comparison with the Van Driest model, as shown in Figure 31b. Here Spalding-Chi underpredicts significantly. Defining $X_v = 0$ at $\theta_B + \theta_{BE}/2$ as suggested by Bertram and Cary results in the smallest length of virtual origin; however, again the Spalding-Chi predictions are low and the Van Driest theory compares best with the measurements.

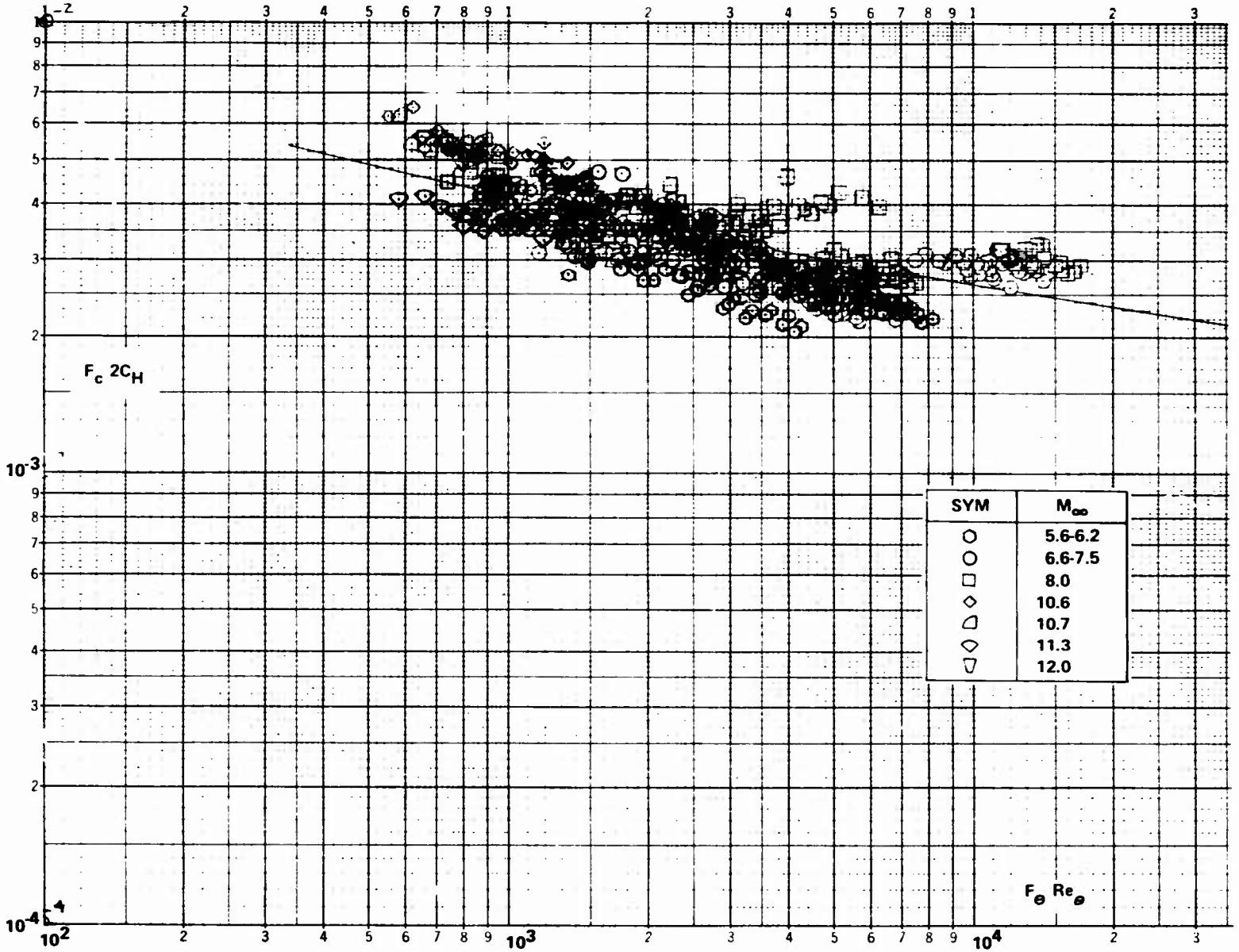


Figure 19a. COMPARISON BETWEEN THE MEASURED HEAT TRANSFER AND THE THEORY OF ECKERT (T_A*) ON SHARP FLAT PLATES

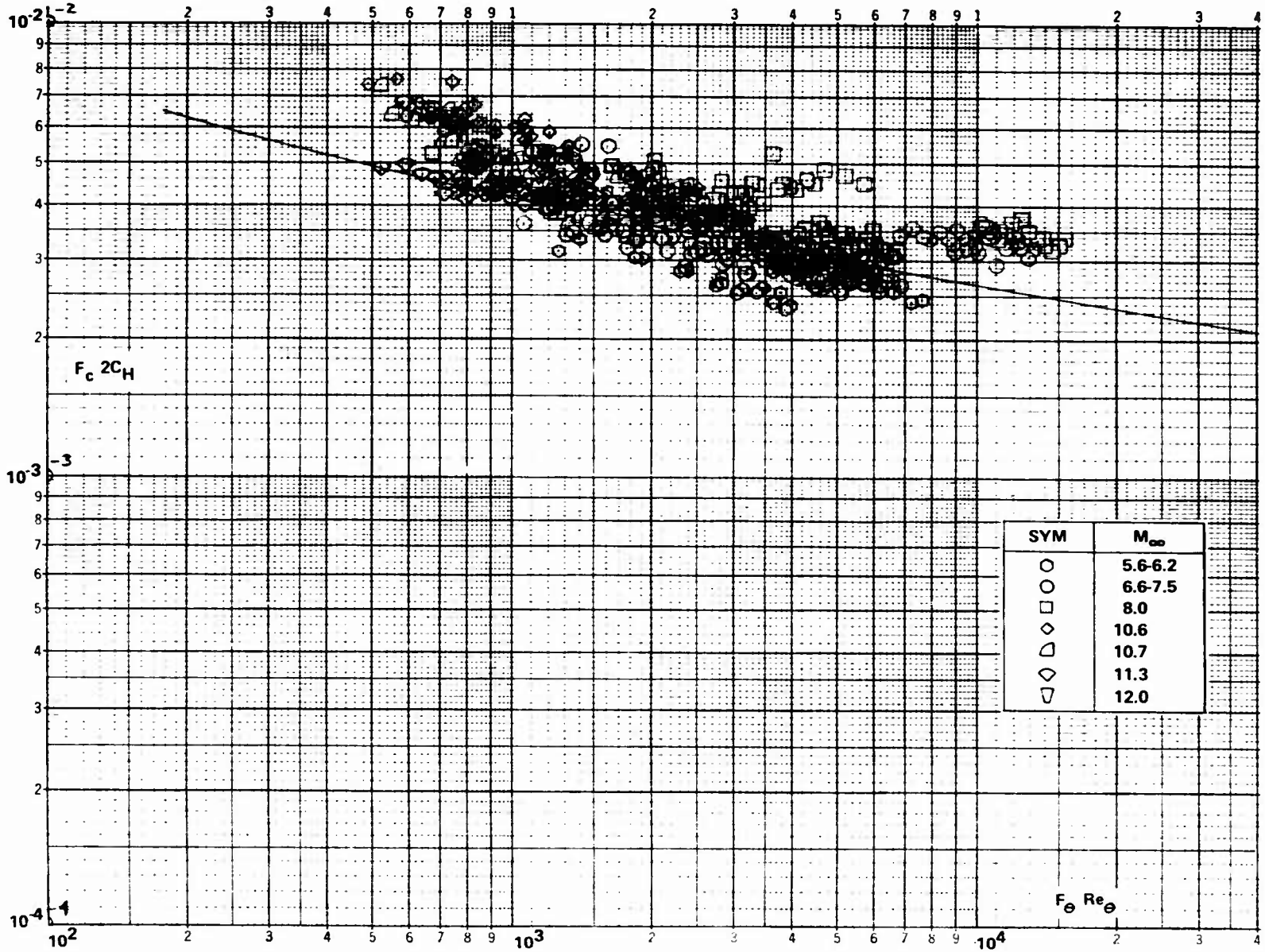


Figure 19b. COMPARISON BETWEEN THE MEASURED HEAT TRANSFER AND THE THEORY OF ECKERT (T_E*) ON SHARP FLAT PLATES

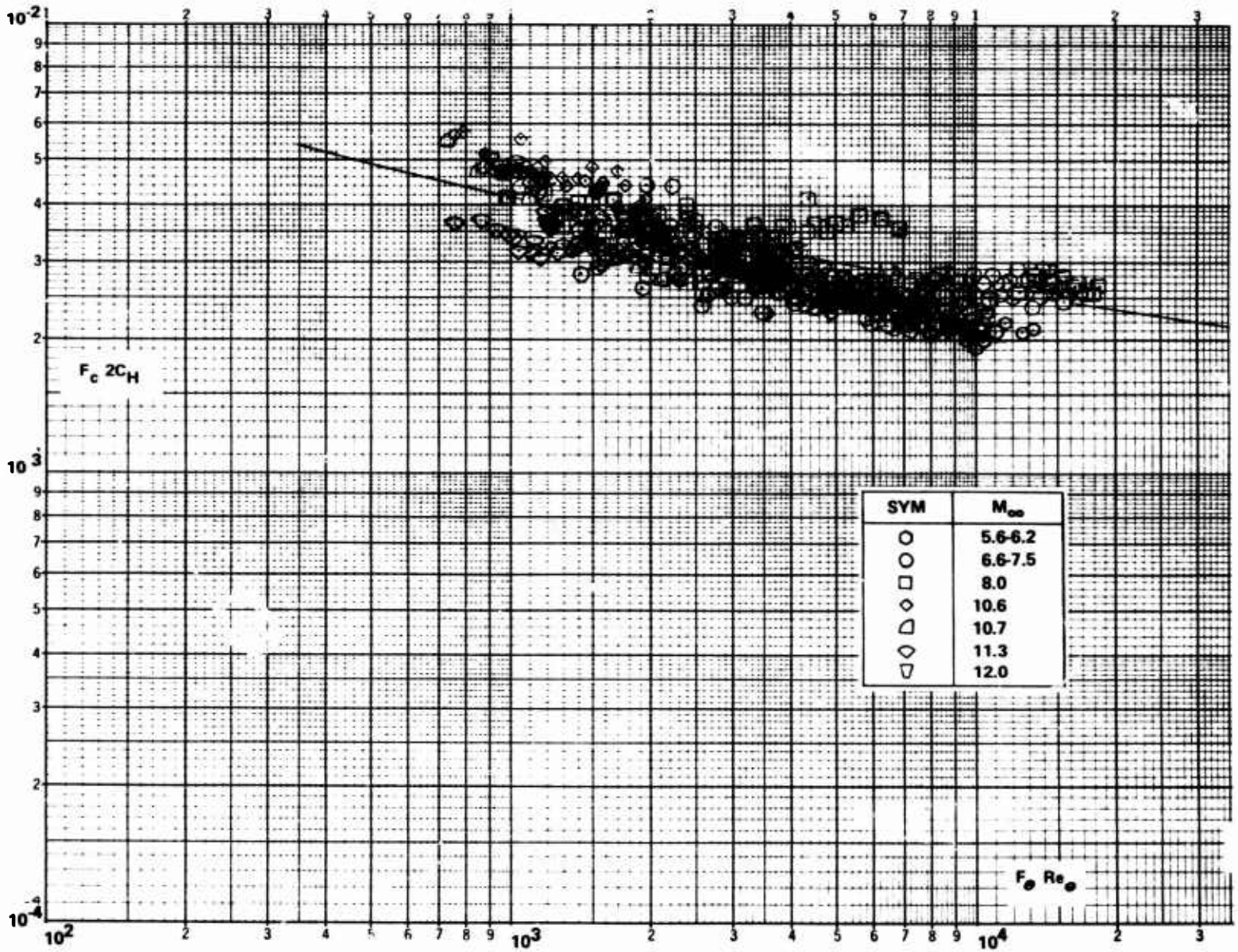


Figure 19c. COMPARISON BETWEEN THE MEASURED HEAT TRANSFER AND THE THEORY OF VAN DRIEST ON SHARP FLAT PLATES

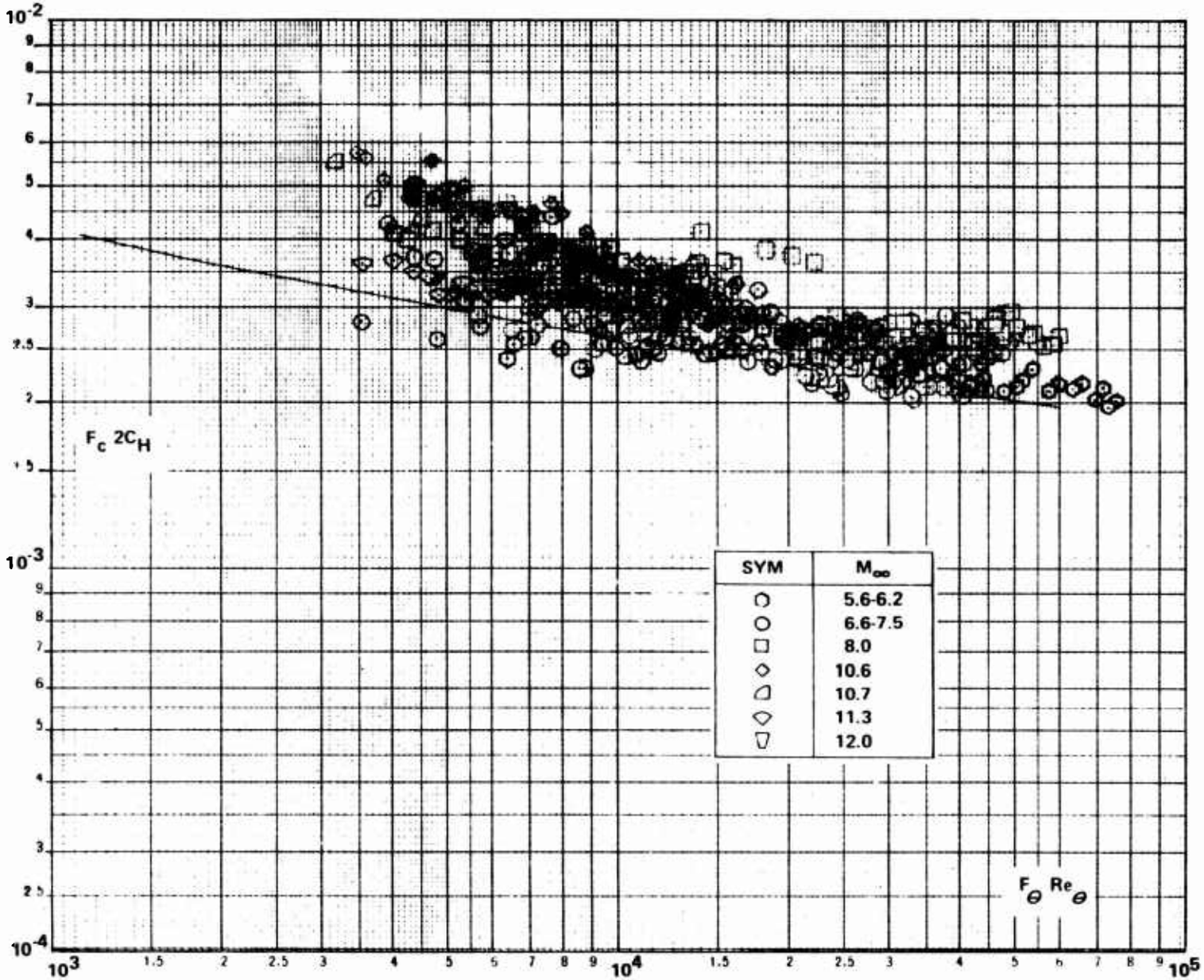


Figure 19d. COMPARISON BETWEEN THE MEASURED HEAT TRANSFER AND THE SPALDING-CHI THEORY ON SHARP FLAT PLATES

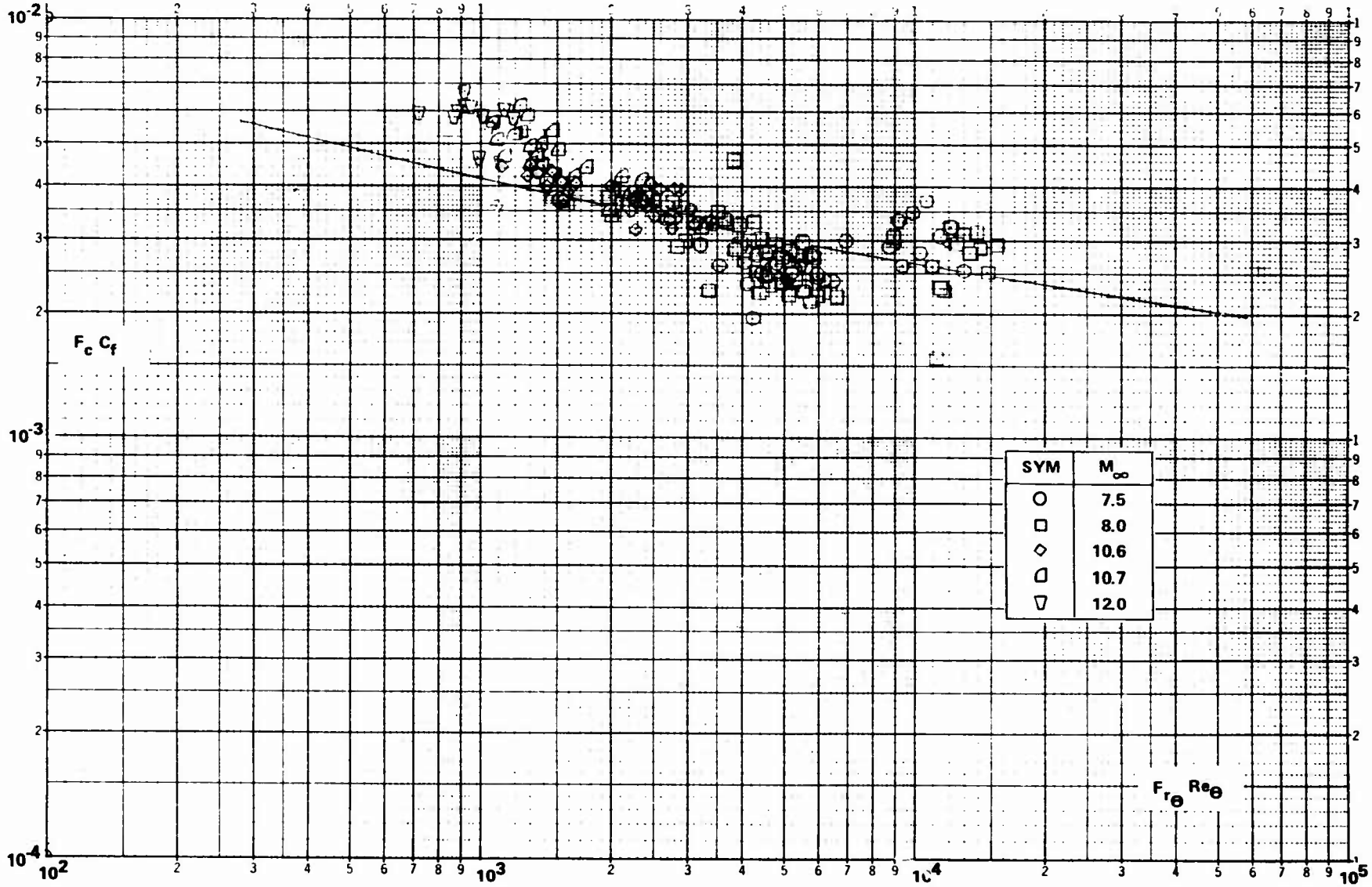


Figure 20a. COMPARISON BETWEEN THE MEASURED SKIN FRICTION AND THE THEORY OF ECKERT (T_A*)

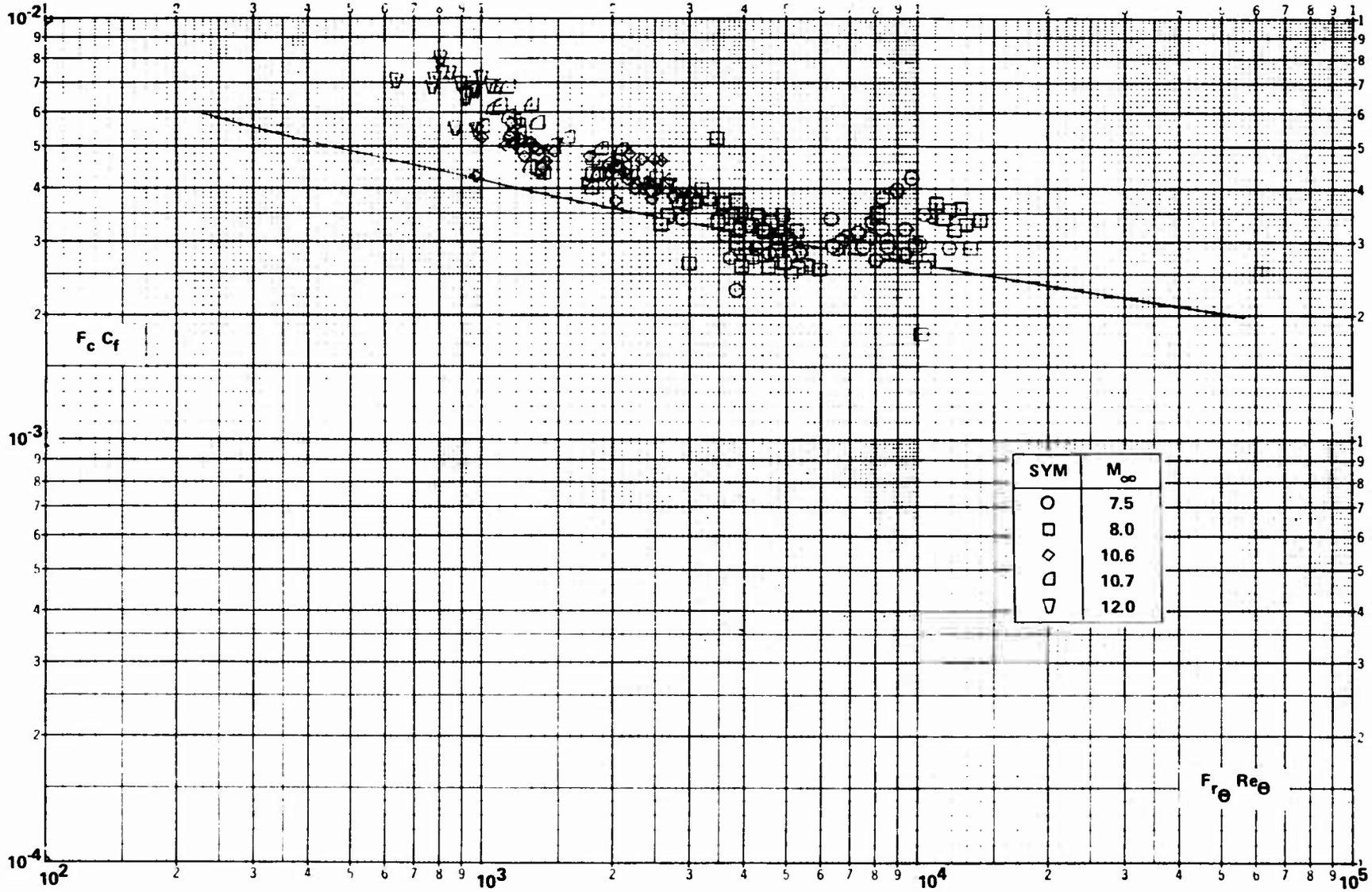


Figure 20b. COMPARISON BETWEEN THE MEASURED SKIN FRICTION AND THE THEORY OF ECKERT (T_E^*)

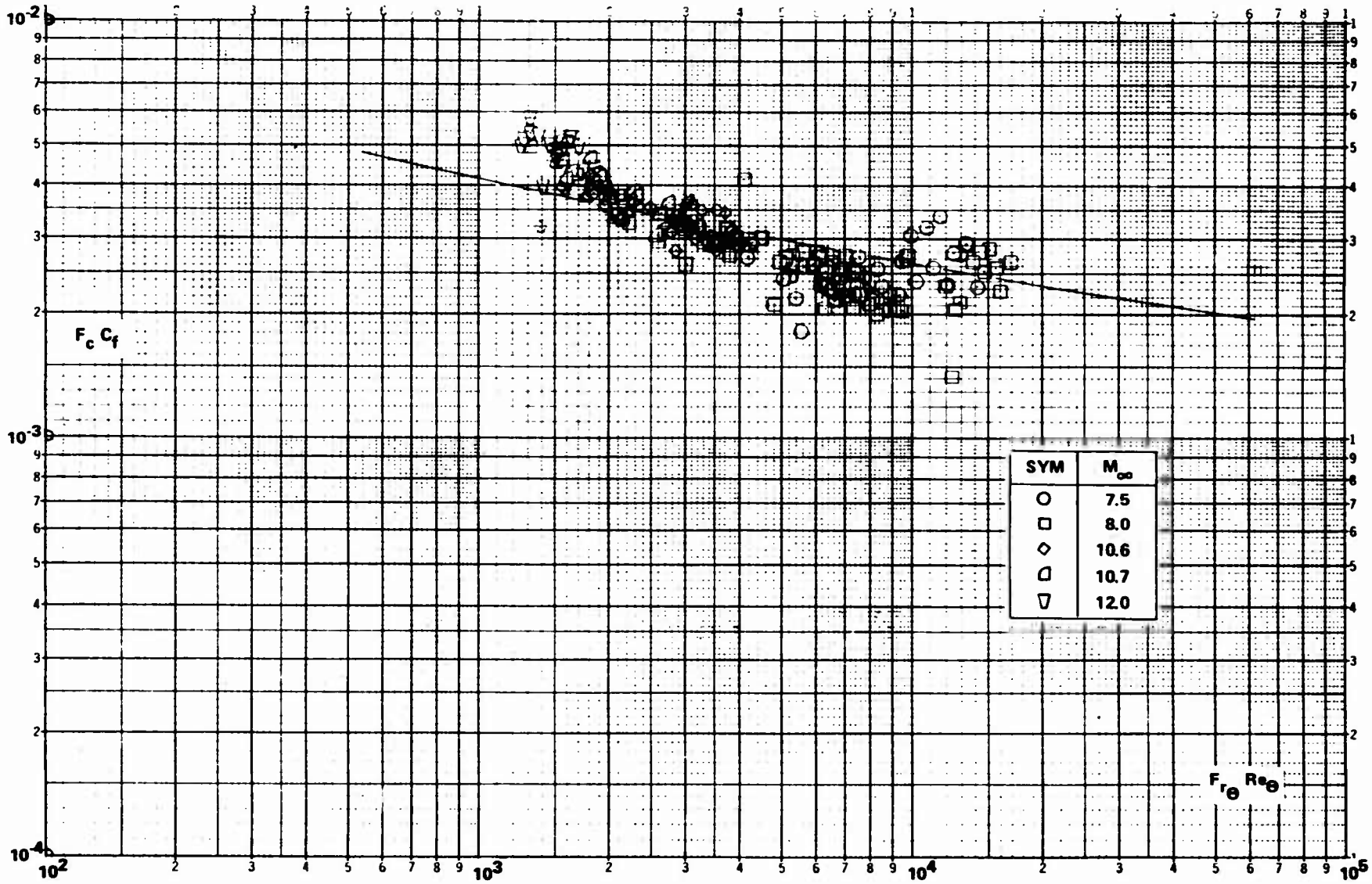


Figure 20c. COMPARISON BETWEEN THE MEASURED SKIN FRICTION AND THE THEORY OF VAN DRIEST

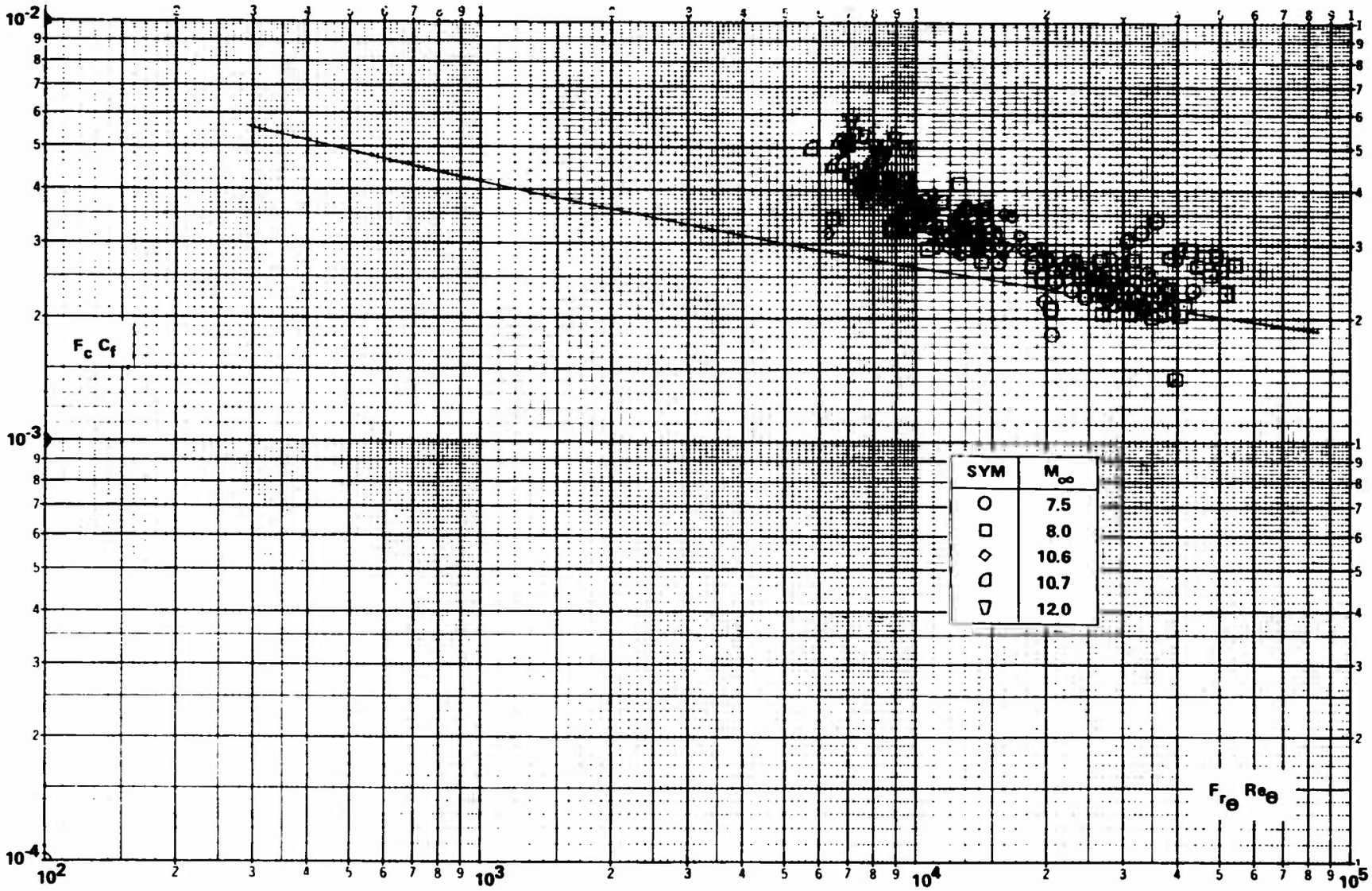


Figure 20d. COMPARISON BETWEEN THE MEASURED SKIN FRICTION AND THE SPALDING-CHI THEORY

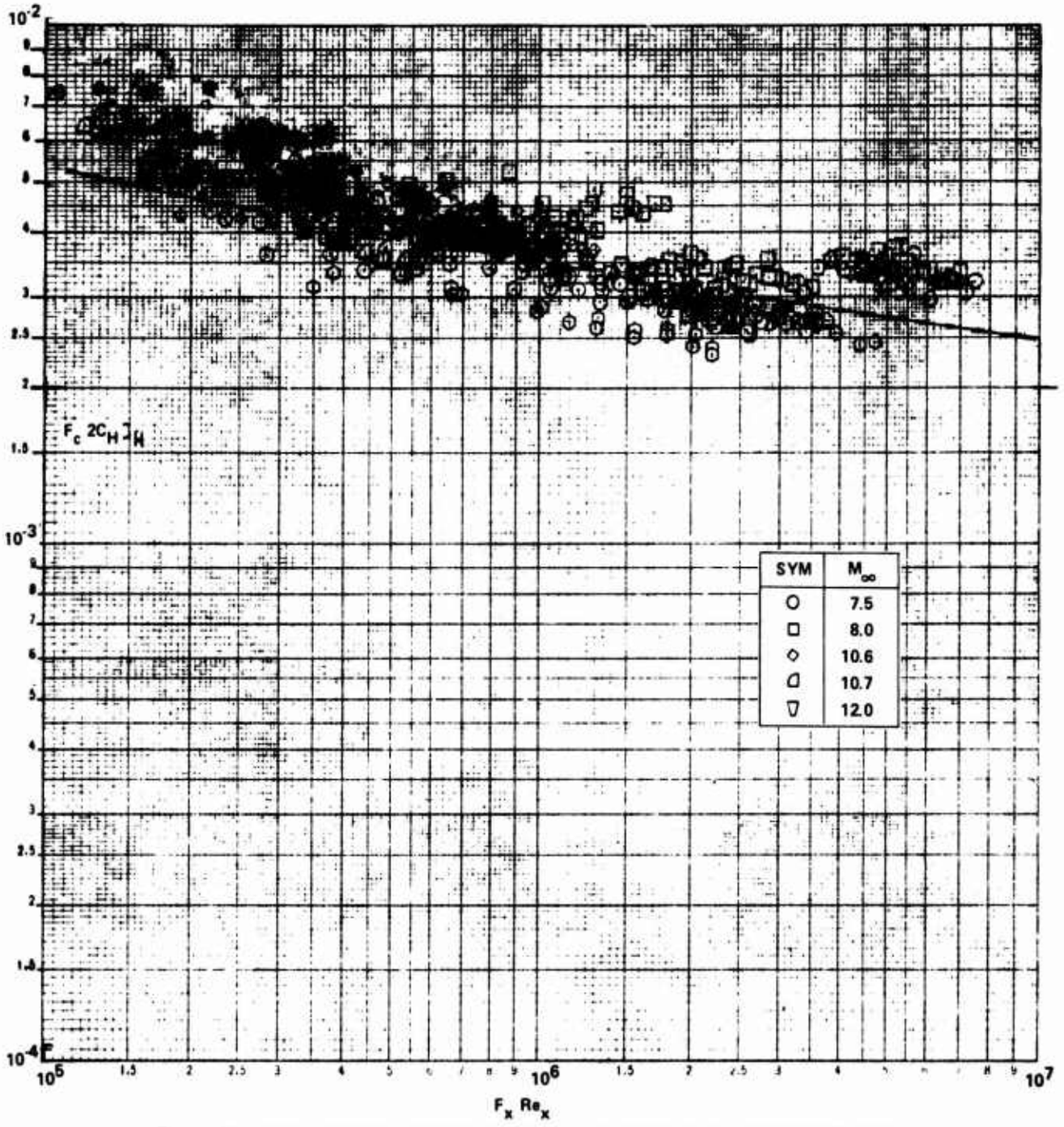


Figure 21a. COMPARISON BETWEEN THE MEASURED HEAT TRANSFER AND THE THEORY OF ECKERT ($\theta_V = \theta_B + \theta_{BE}$)

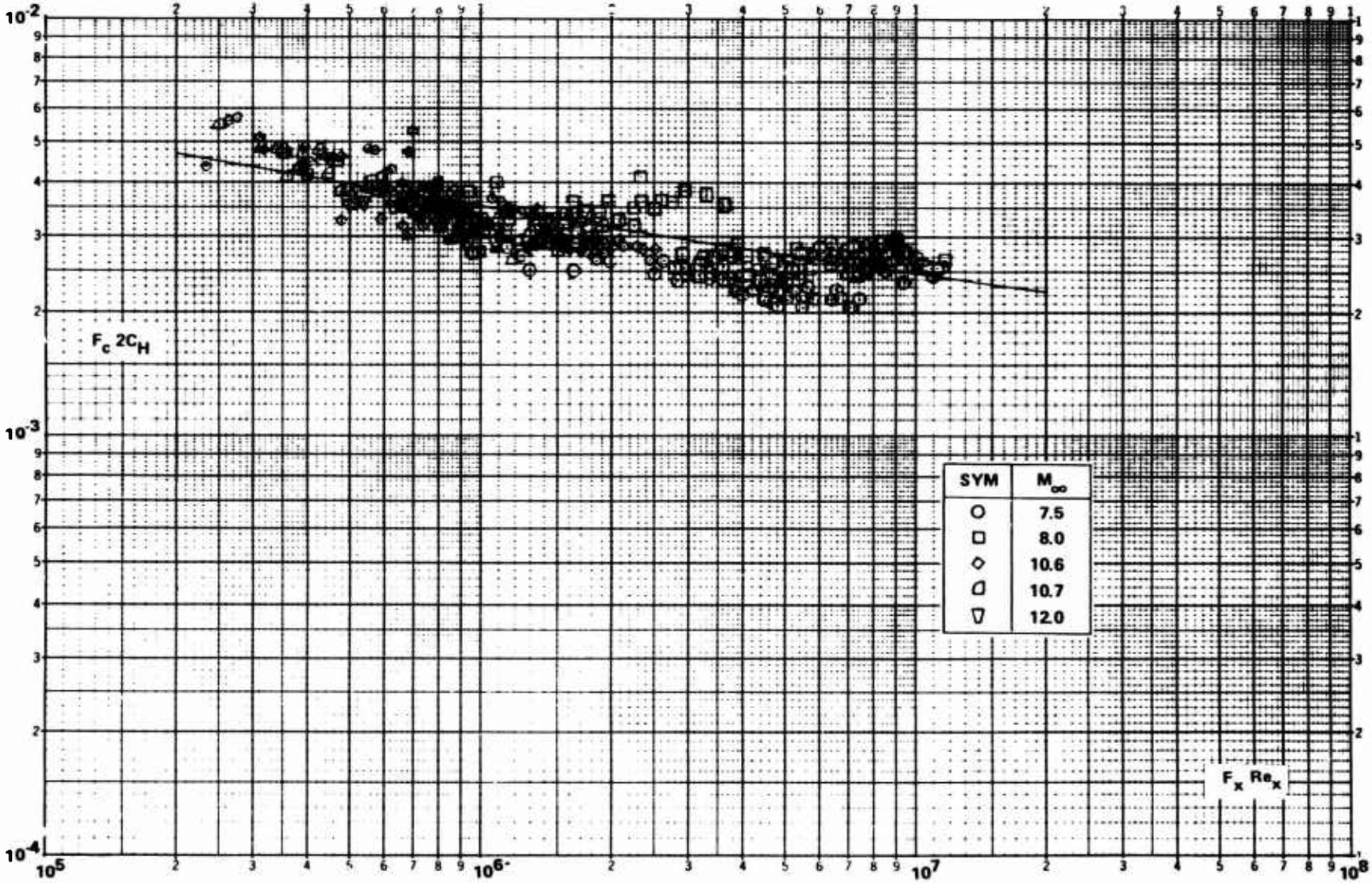


Figure 21b. COMPARISON BETWEEN THE MEASURED HEAT TRANSFER AND THE THEORY OF VAN DRIEST ($\Theta_V = \Theta_B + \Theta_{BE}$)

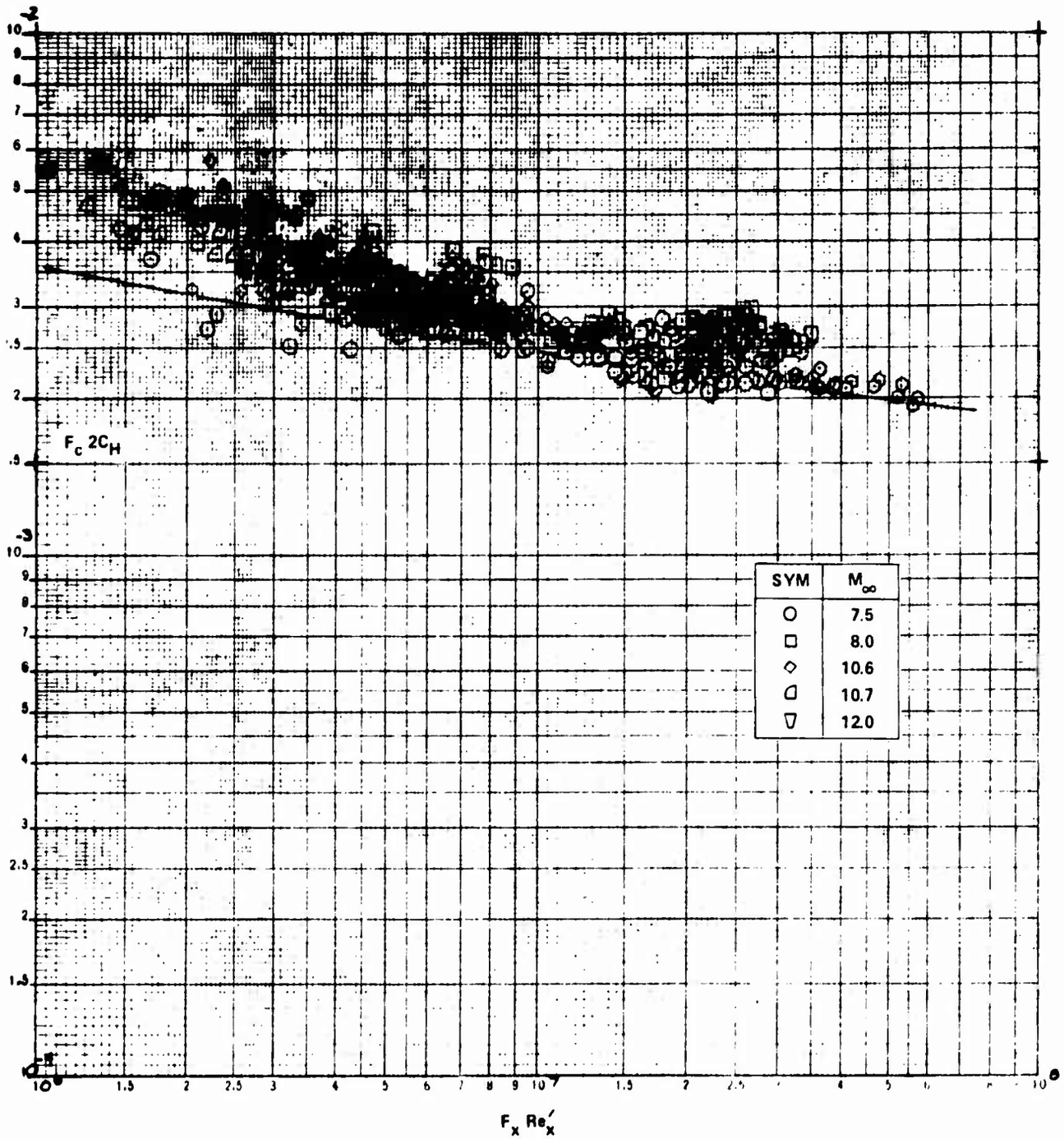


Figure 21c. COMPARISON BETWEEN THE MEASURED HEAT TRANSFER AND THE SPALDING-CHI THEORY ($\theta_V = \theta_B + \theta_{BE}$)

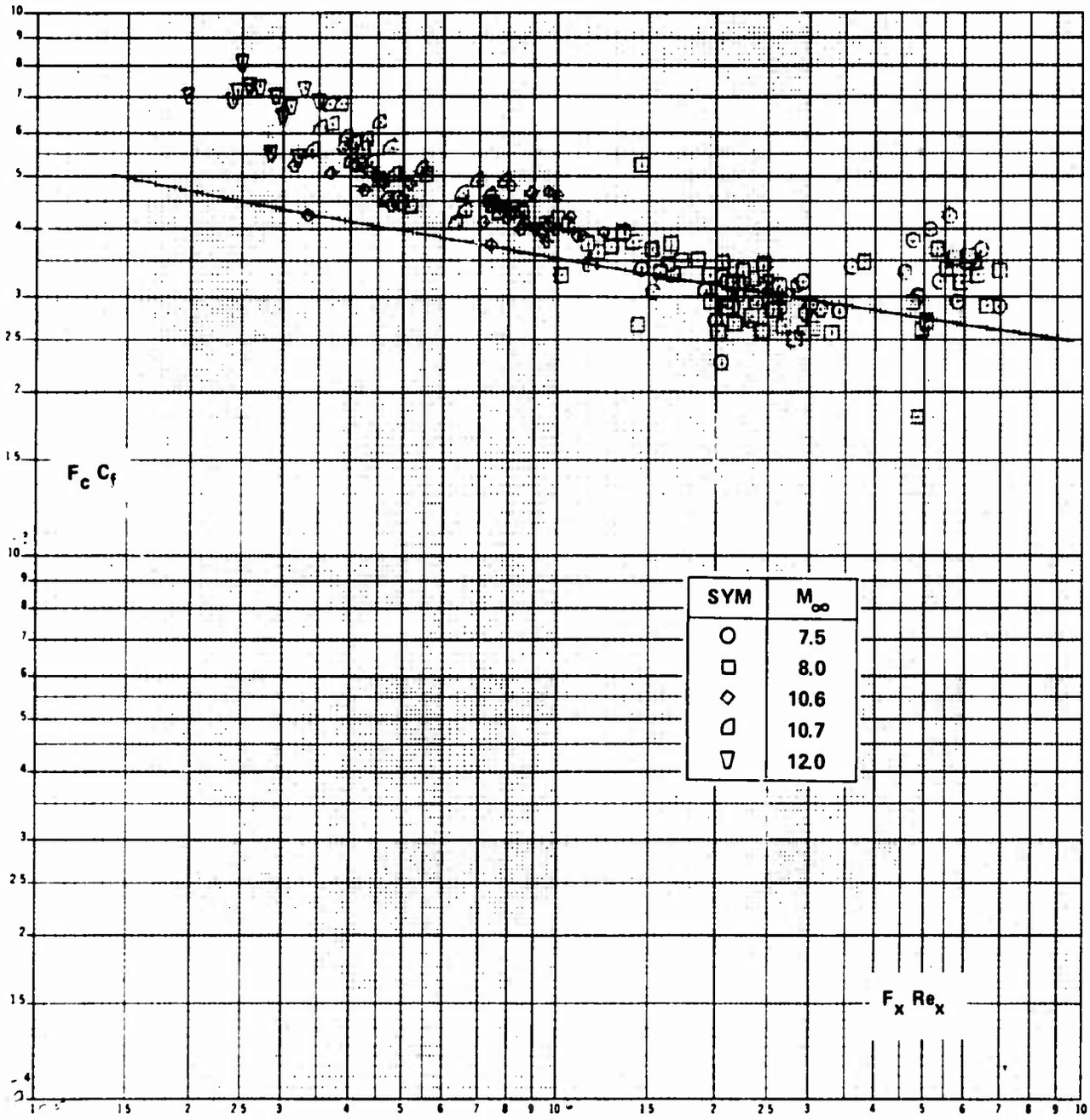


Figure 22a. COMPARISON BETWEEN THE MEASURED SKIN FRICTION AND THE THEORY OF ECKERT ($\theta_V = \theta_B + \theta_{BE}$)

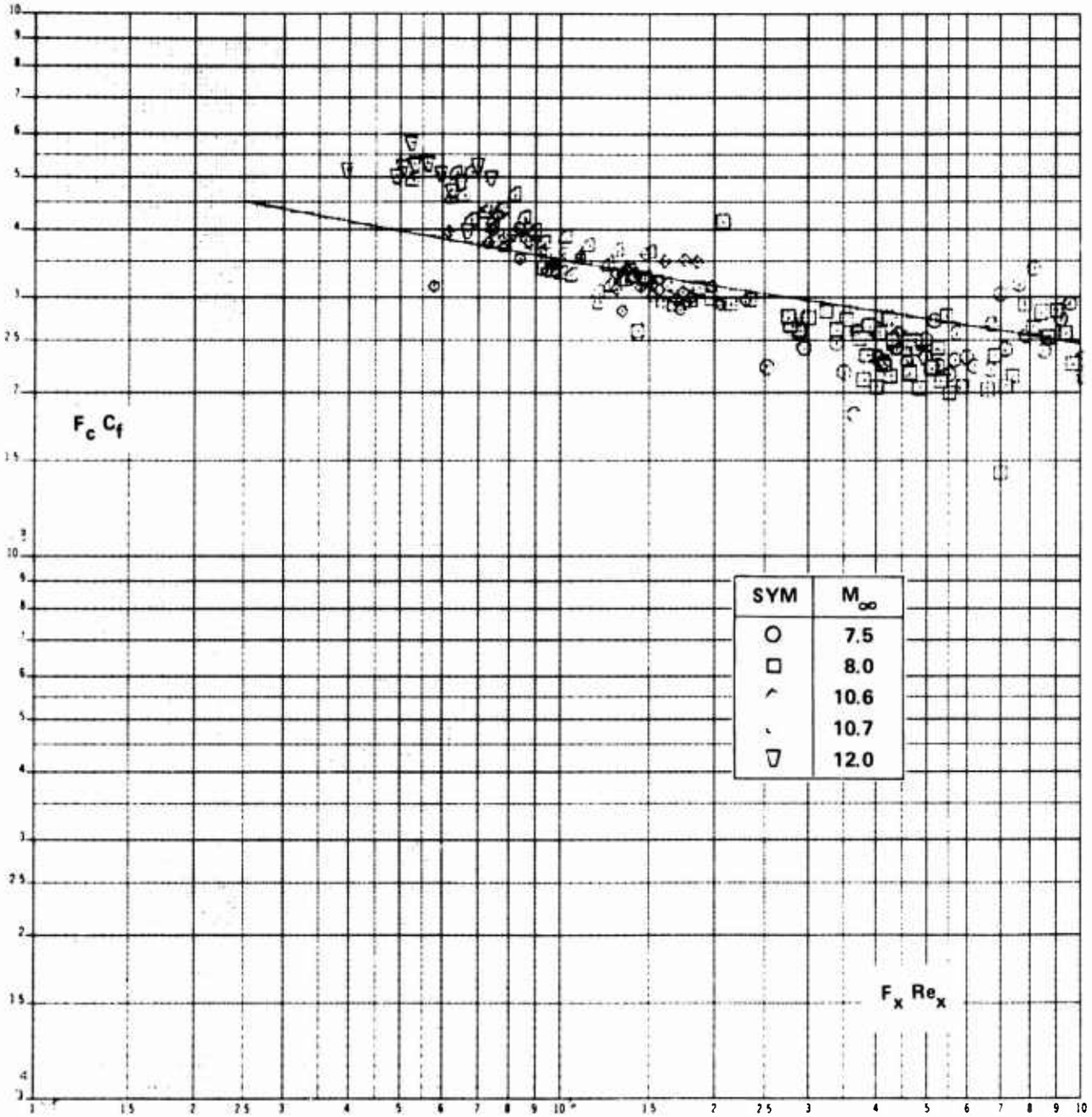


Figure 22b. COMPARISON BETWEEN THE MEASURED SKIN FRICTION AND THE THEORY OF VAN DRIEST ($\Theta_V = \Theta_B + \Theta_{BE}$)

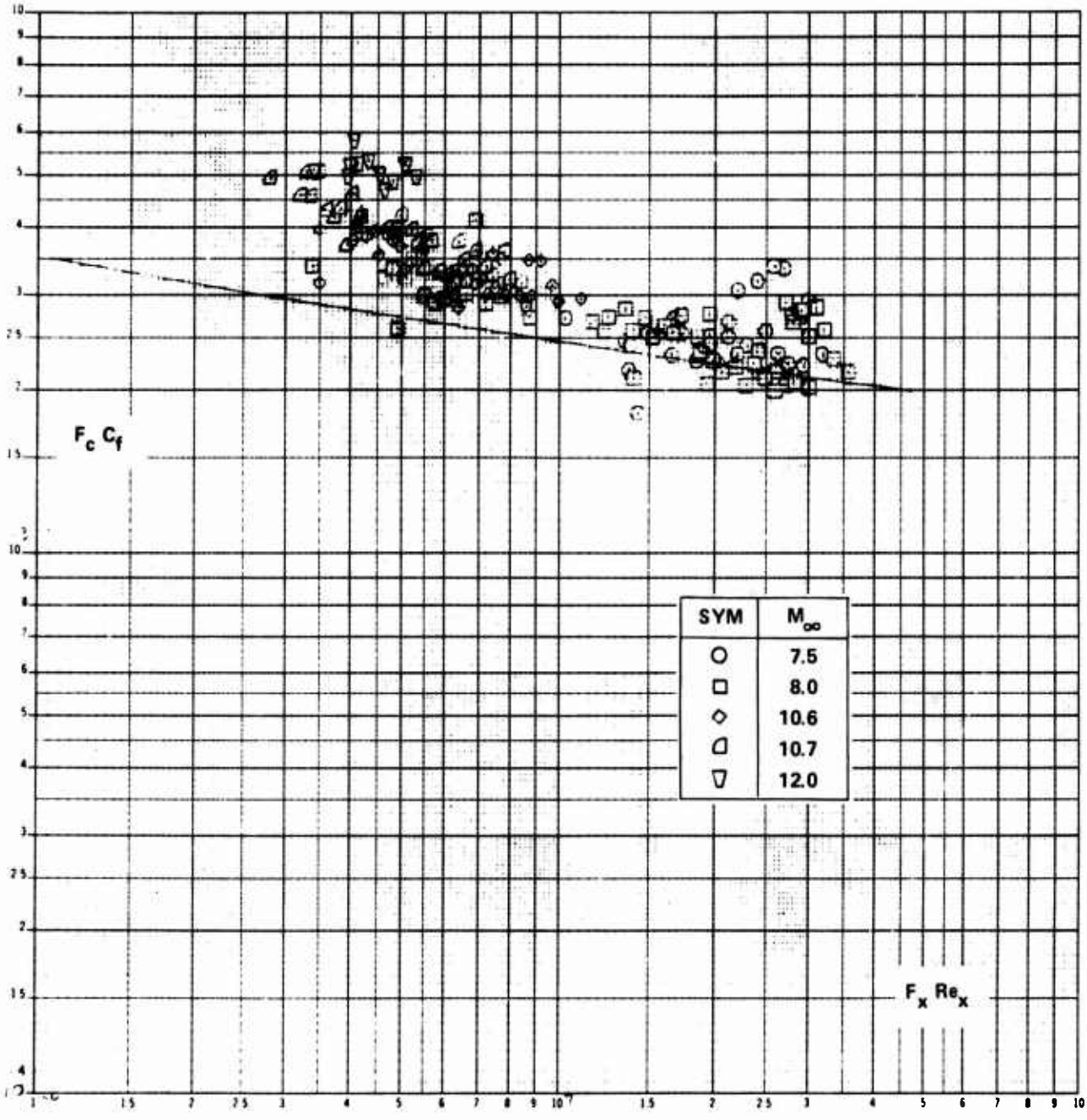


Figure 22c. COMPARISON BETWEEN THE MEASURED SKIN FRICTION AND THE SPALDING-CHI THEORY ($\Theta_V = \Theta_B + \Theta_{BE}$)

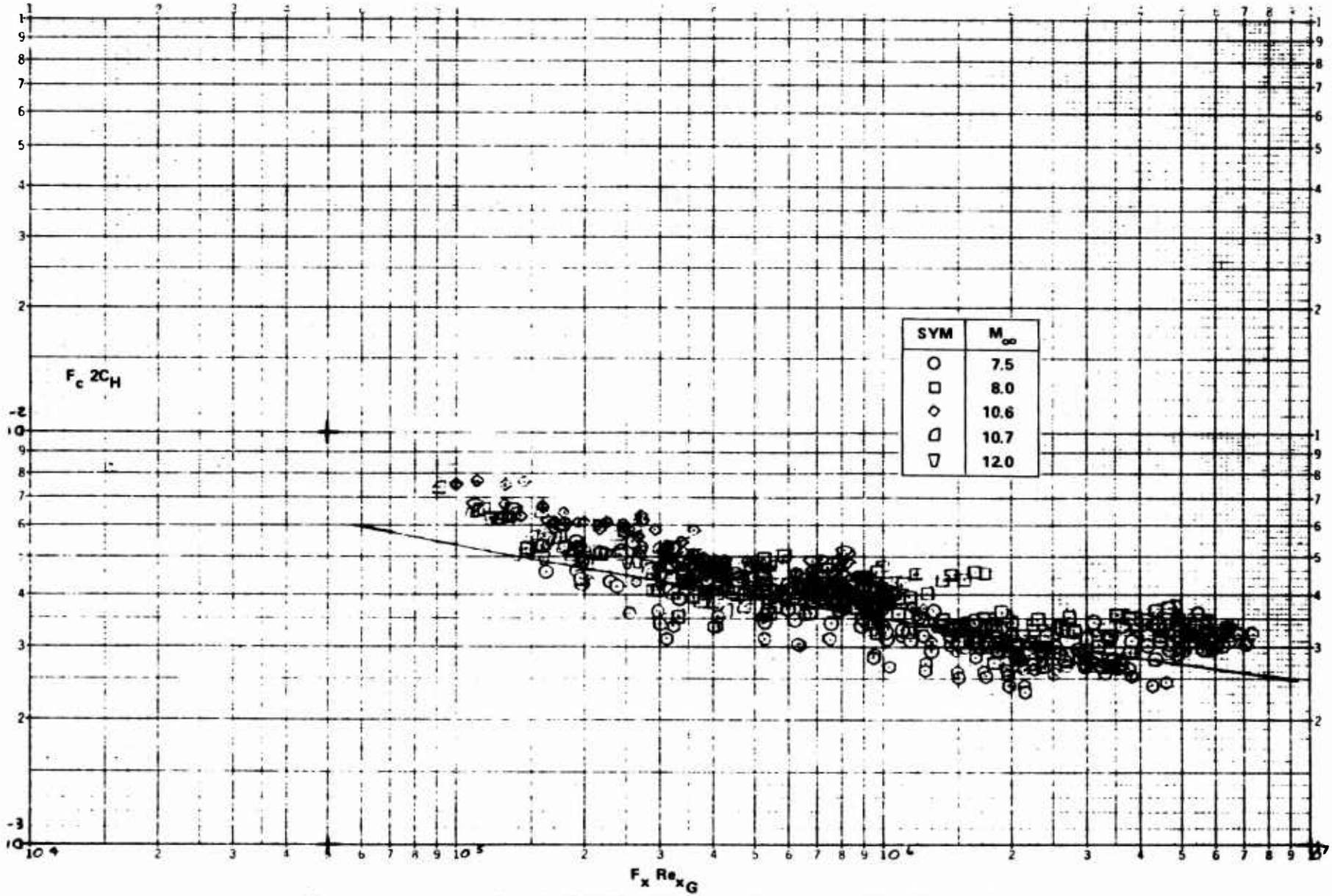


Figure 23a. COMPARISON BETWEEN THE MEASURED HEAT TRANSFER AND THE THEORY OF ECKERT ($\Theta_V = \Theta_B + \Theta_{BE/2}$)

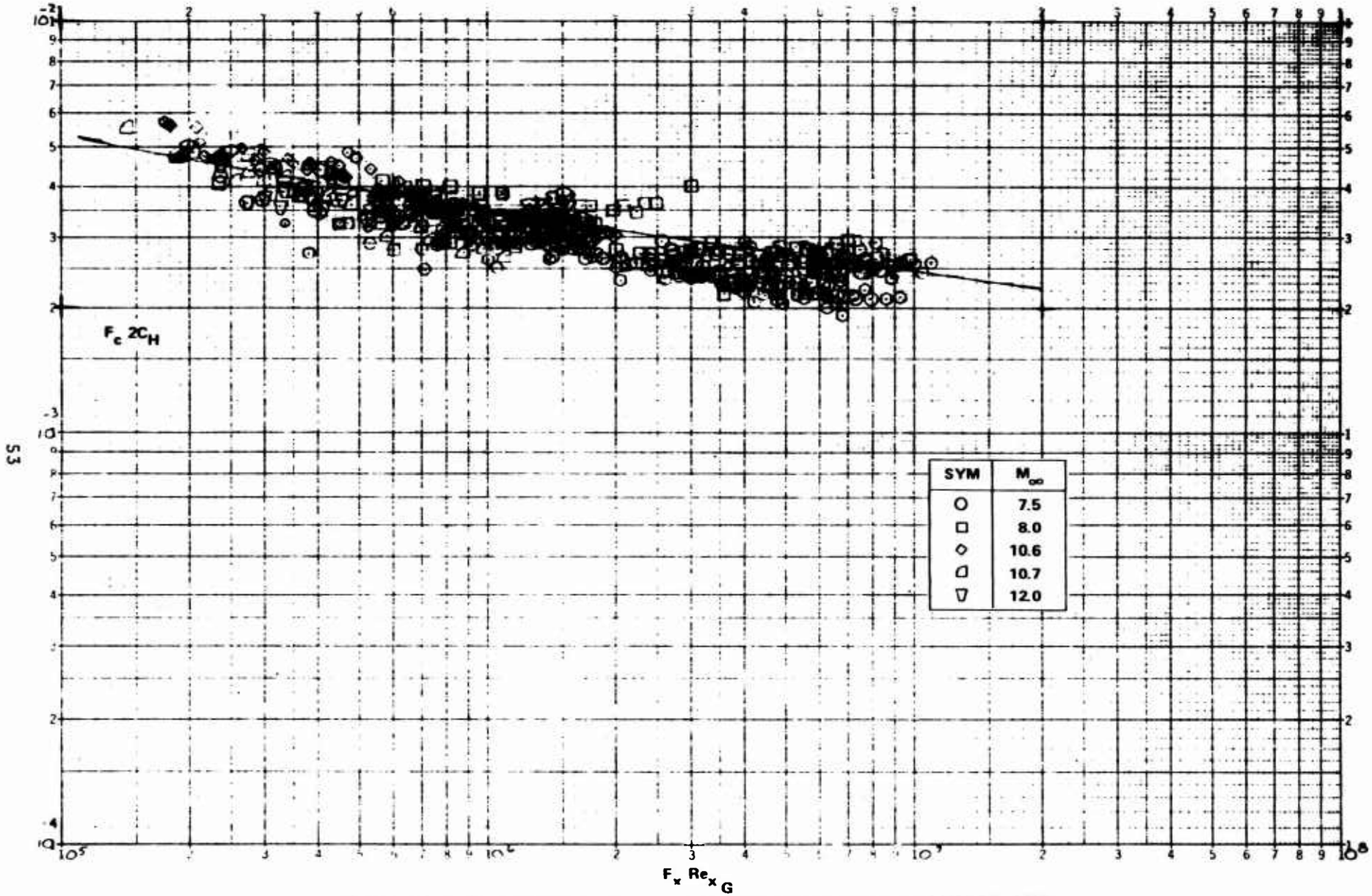


Figure 23b. COMPARISON BETWEEN THE MEASURED HEAT TRANSFER AND THE THEORY OF VAN DRIEST $(\theta_V = \theta_B + \theta_{BE/2})$

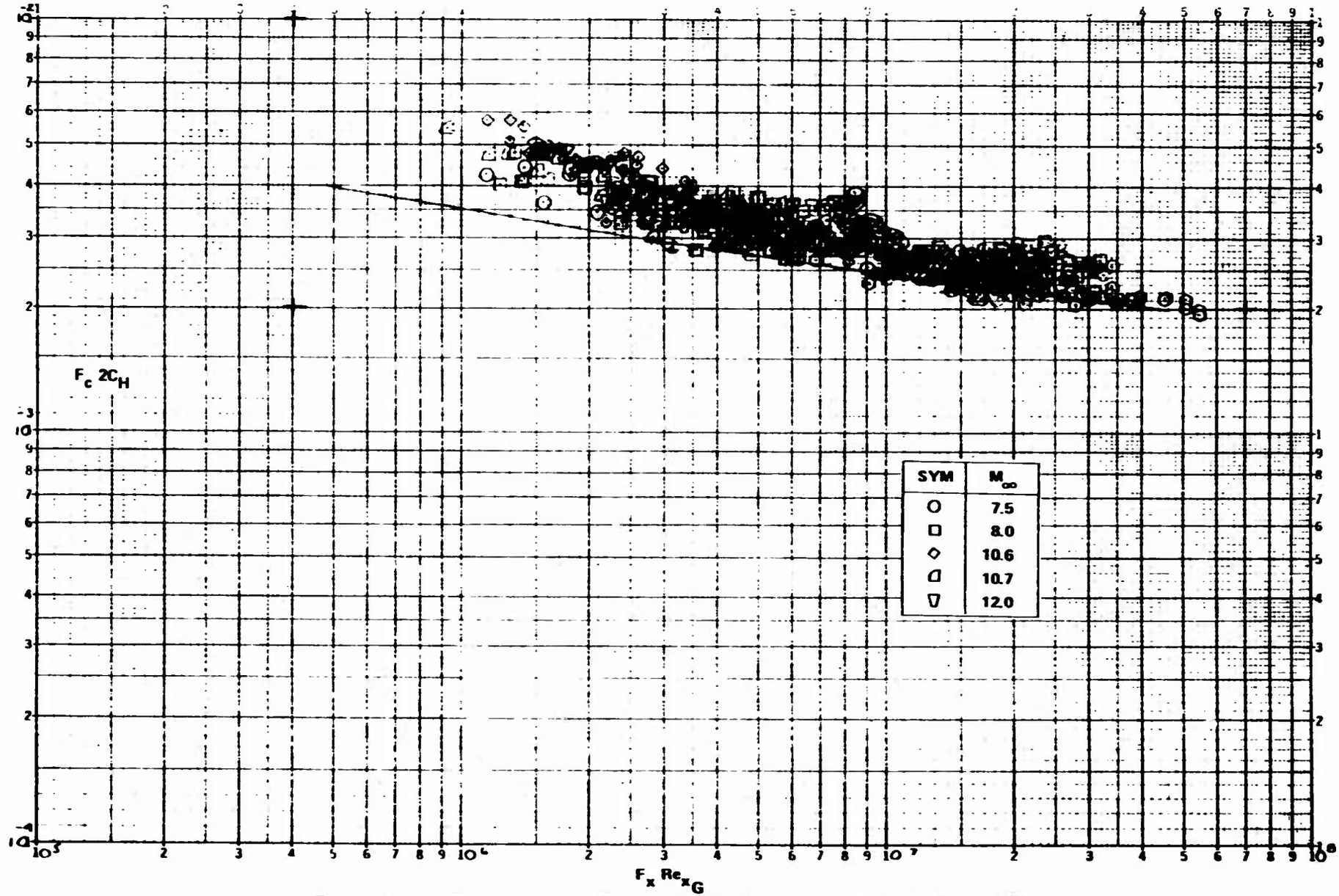


Figure 23c. COMPARISON BETWEEN THE MEASURED HEAT TRANSFER AND THE SPALDING-CHI THEORY ($\Theta_V = \Theta_B + \Theta_{BE/2}$)

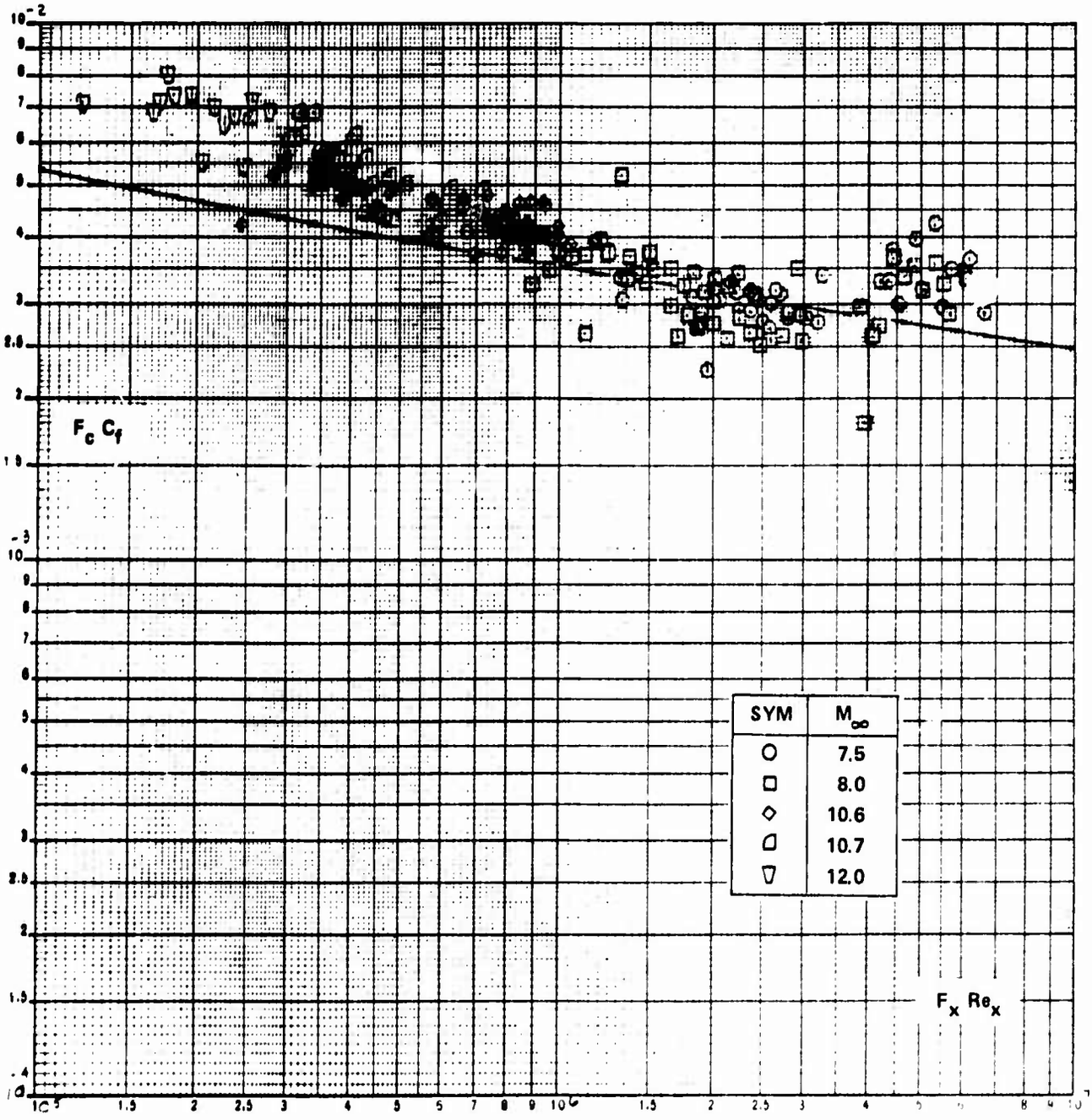


Figure 24a. COMPARISON BETWEEN THE MEASURED SKIN FRICTION AND THE THEORY OF ECKERT $(\theta_V = \theta_B + \theta_{BE/2})$

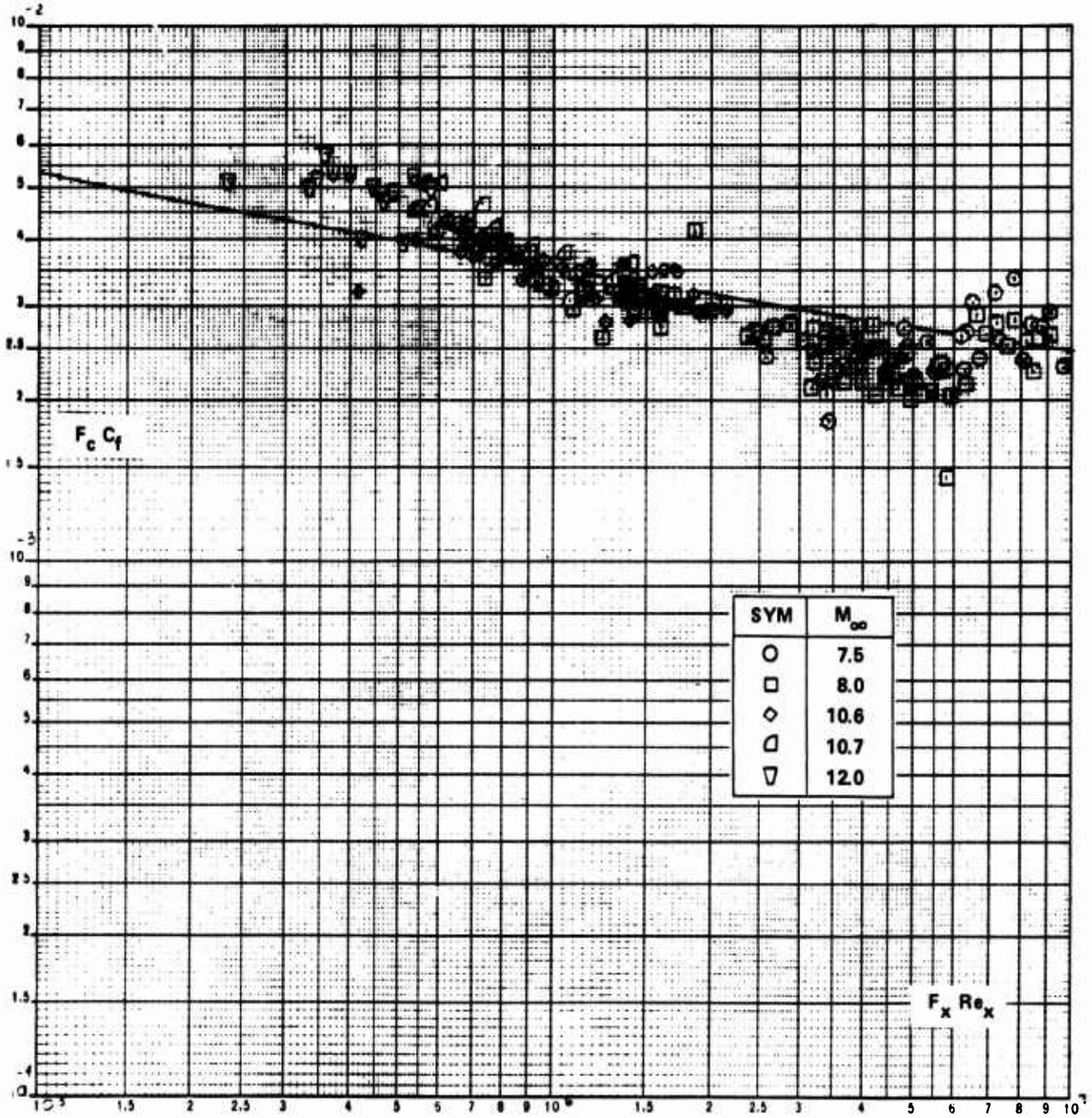


Figure 24b. COMPARISON BETWEEN THE MEASURED SKIN FRICTION AND THE THEORY OF VAN DRIEST ($\Theta_V = \Theta_B + \Theta_{BE/2}$)

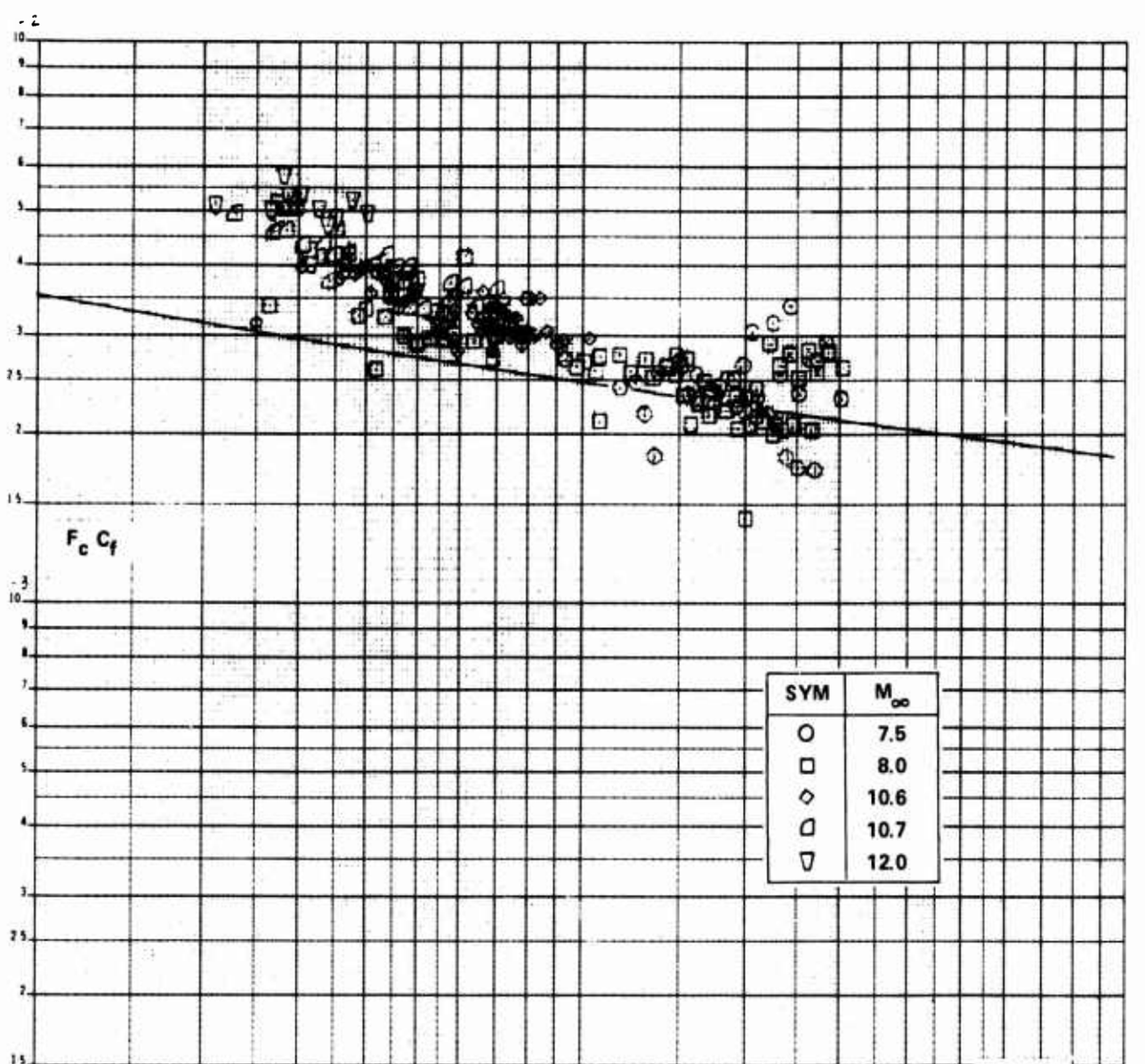


Figure 24c. COMPARISON BETWEEN THE MEASURED SKIN FRICTION AND THE SPALDING-CHI THEORY ($\Theta_V = \Theta_B + \Theta_{BE/2}$)

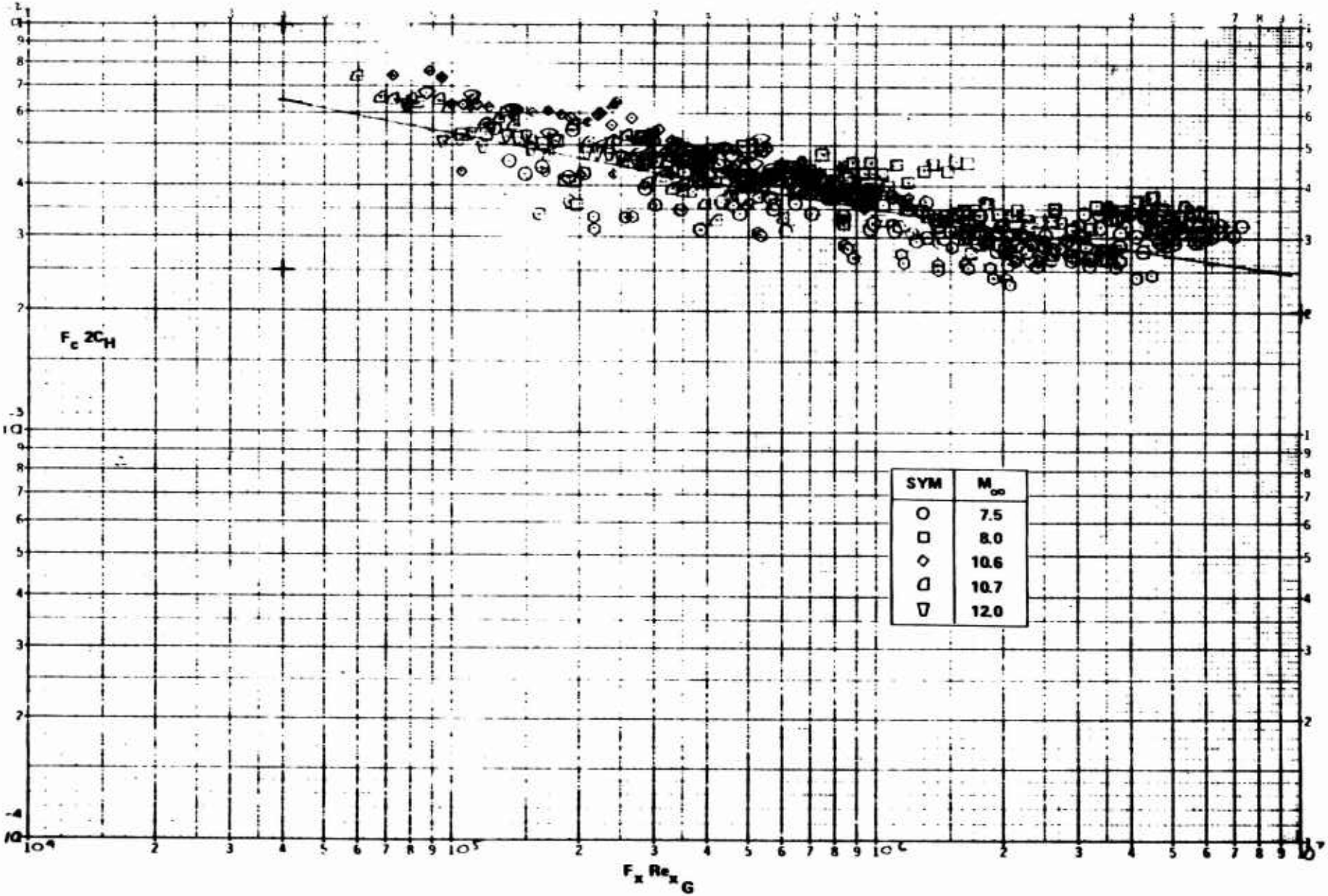


Figure 25a. COMPARISON BETWEEN THE MEASURED HEAT TRANSFER AND THE THEORY OF ECKERT ($\Theta_V = \Theta_B + \Theta_{BE\ LAMINAR}$)

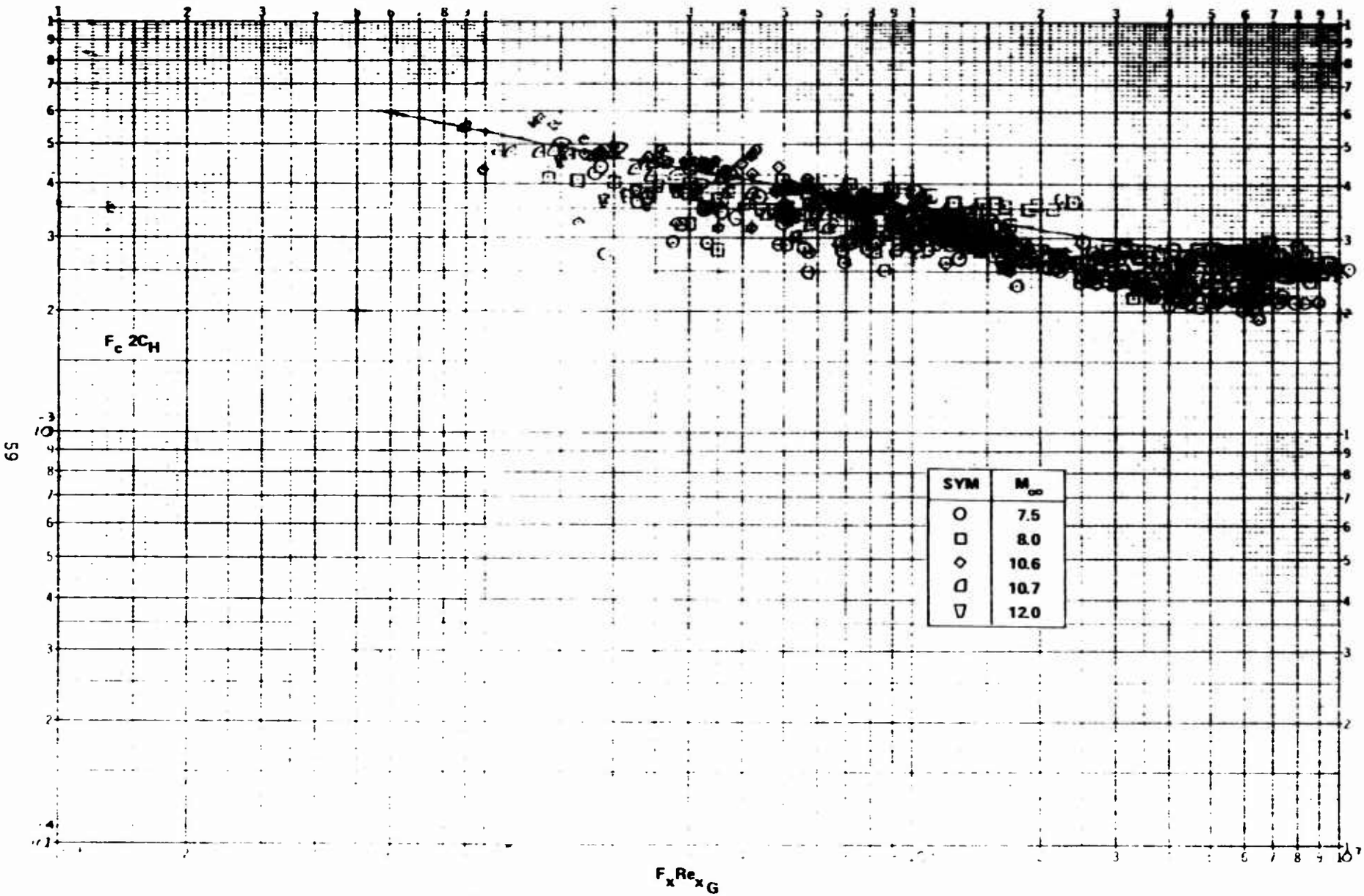


Figure 25b. COMPARISON BETWEEN THE MEASURED HEAT TRANSFER AND THE THEORY OF VAN DRIEST ($\Theta_V = \Theta_B + \Theta_{BE\ LAMINAR}$)

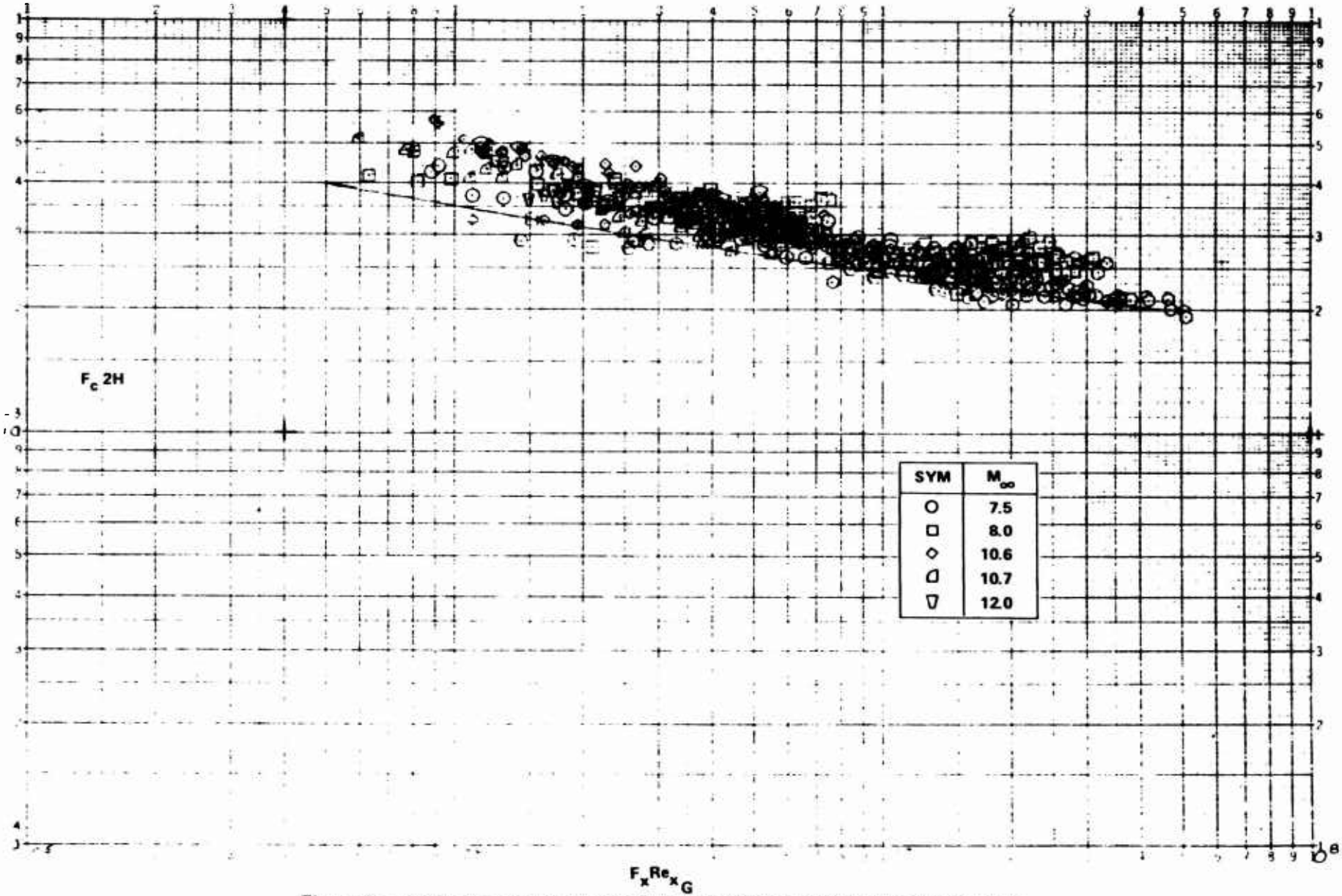


Figure 25c. COMPARISON BETWEEN THE MEASURED HEAT TRANSFER AND THE SPALDING-CHI THEORY ($\Theta_V = \Theta_B + \Theta_{BE\ LAMINAR}$)

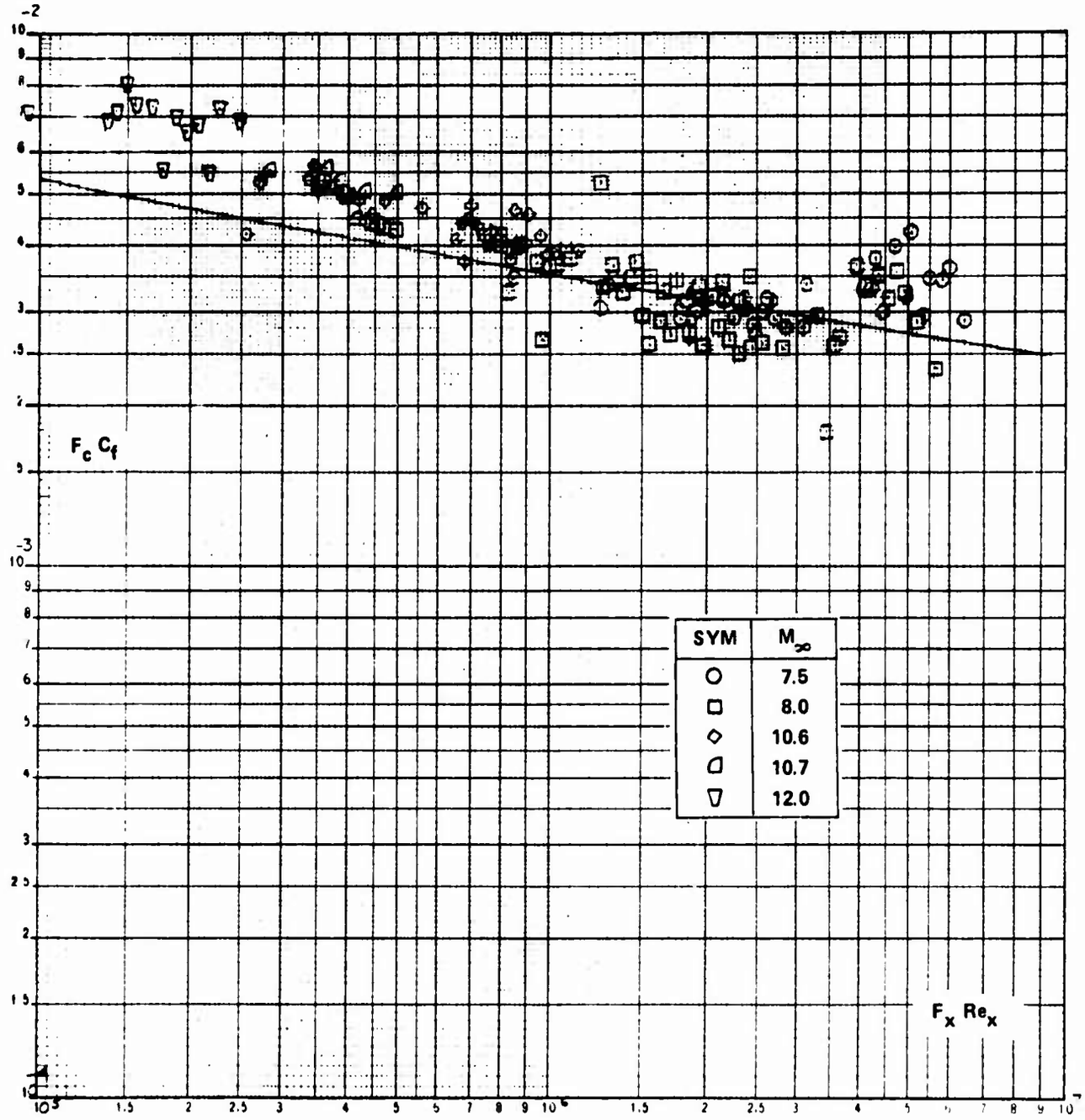


Figure 26a. COMPARISON BETWEEN THE MEASURED SKIN FRICTION AND THE THEORY OF ECKERT ($\theta_V = \theta_B + \theta_{BE\ LAMINAR}$)

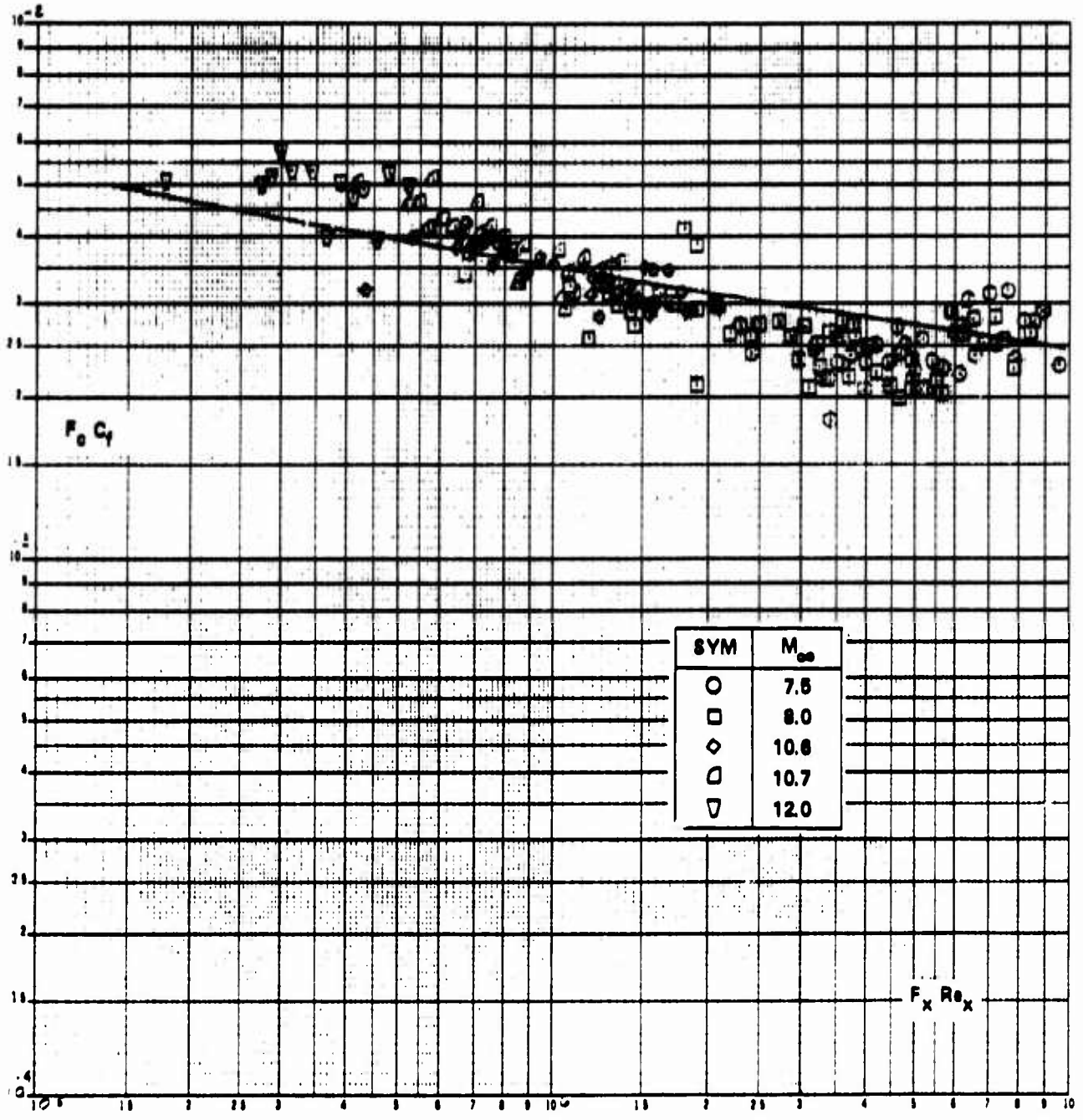


Figure 26b. COMPARISON BETWEEN THE MEASURED SKIN FRICTION AND THE THEORY OF VAN DRIEST ($\theta_V = \theta_B + \theta_{BE\ LAMINAR}$).

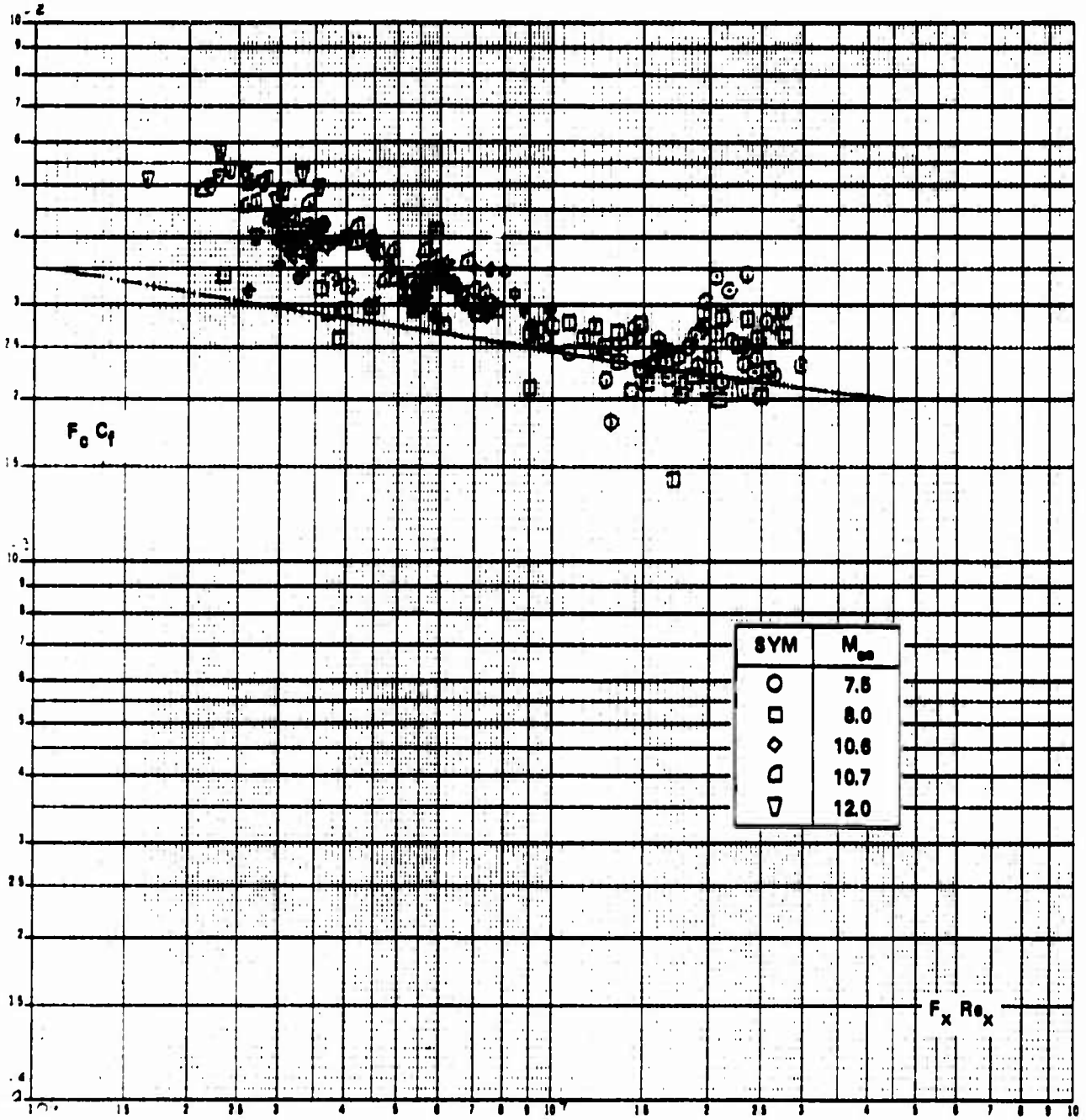


Figure 26c. COMPARISON BETWEEN THE MEASURED SKIN FRICTION AND THE SPALDING-CHI THEORY ($\theta_V = \theta_B + \theta_{BE\ LAMINAR}$)

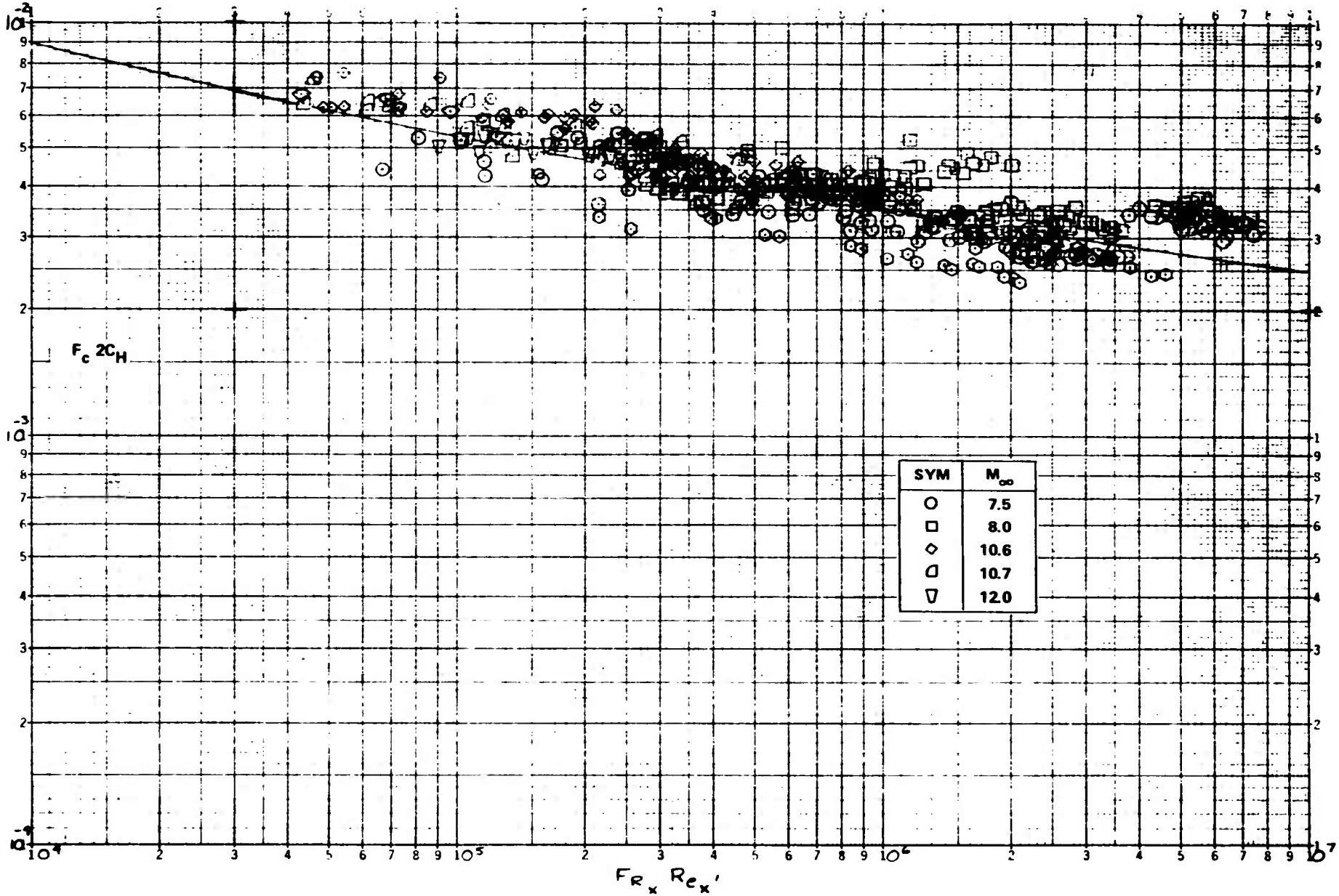


Figure 27a. COMPARISON BETWEEN THE MEASURED HEAT TRANSFER AND THE THEORY OF ECKERT ($\theta_V = \theta_B$)

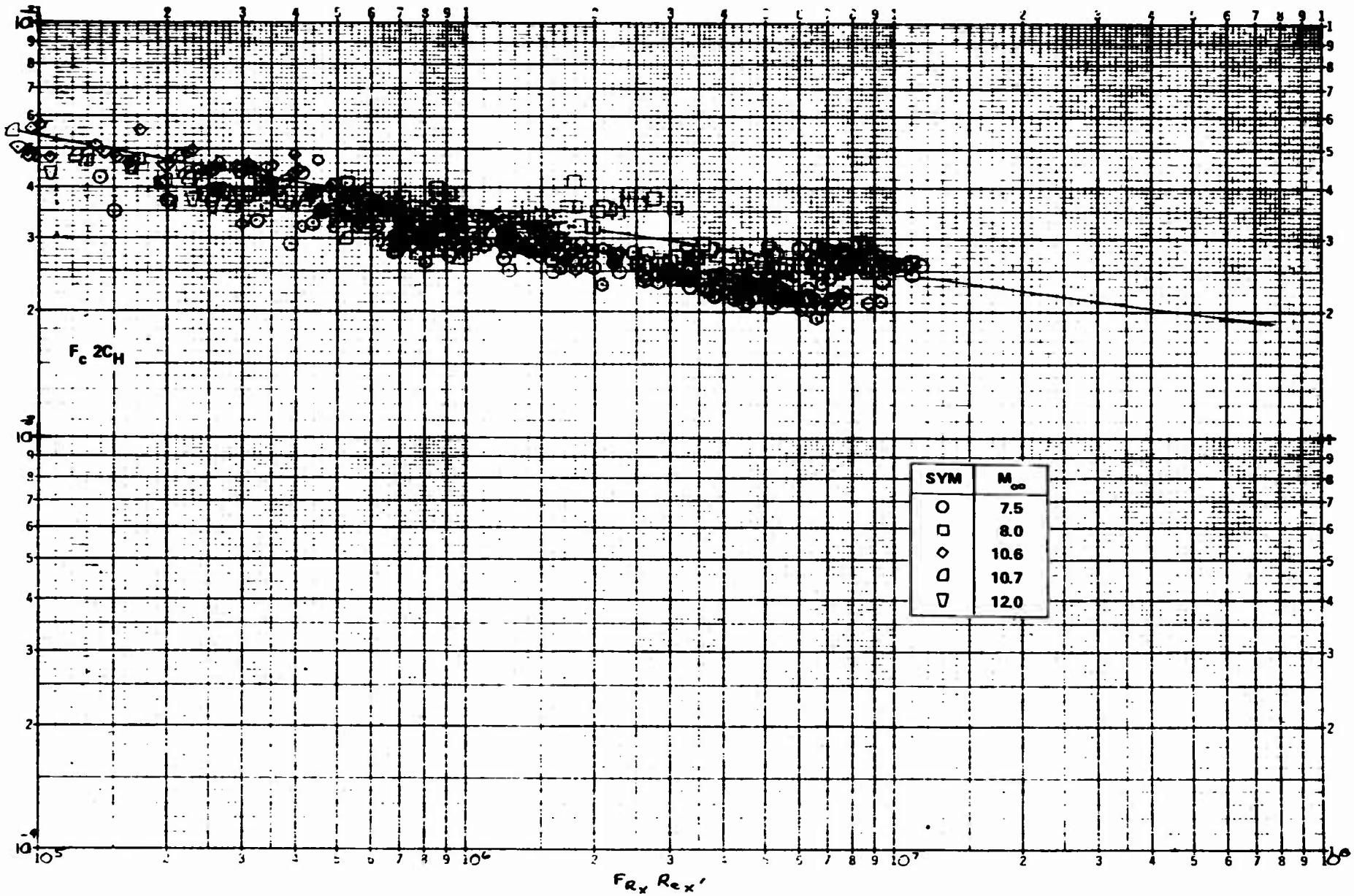


Figure 27b. COMPARISON BETWEEN THE MEASURED HEAT TRANSFER AND THE THEORY OF VAN DRIEST ($\theta_V = \theta_B$)

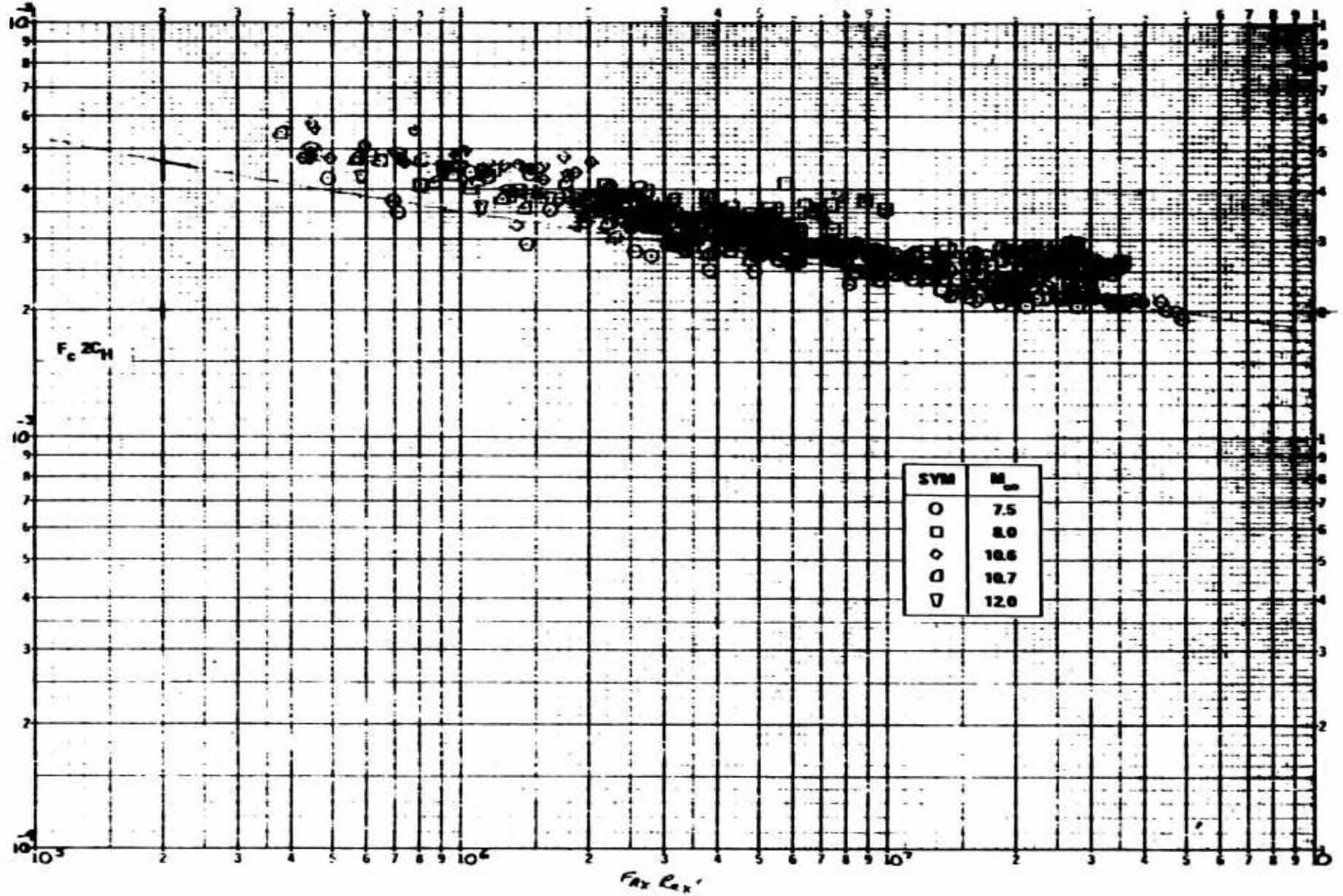


Figure 27c. COMPARISON BETWEEN THE MEASURED HEAT TRANSFER AND THE SPALDING-CHI THEORY ($\theta_V = \theta_B$)

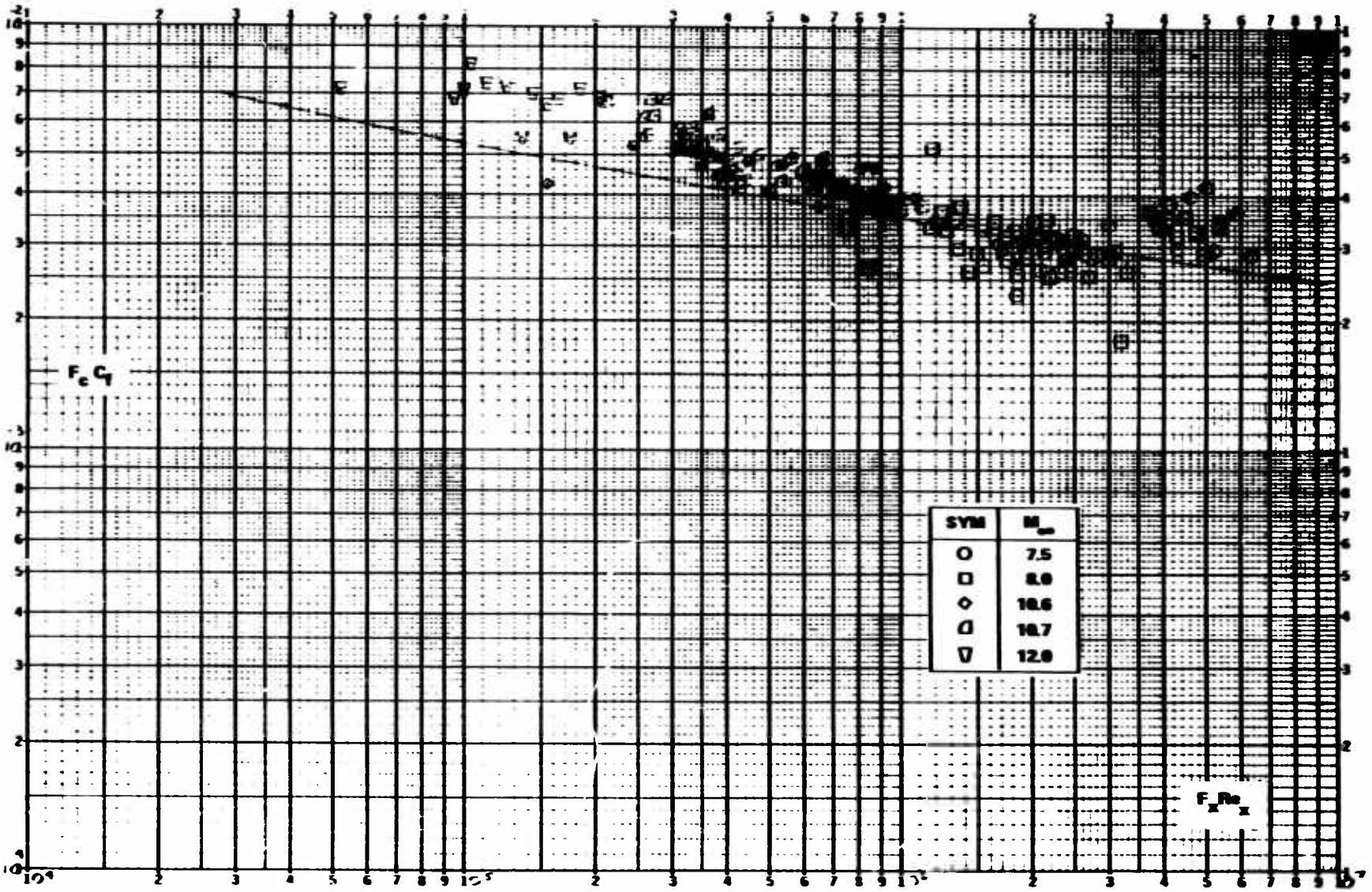


Figure 28a. COMPARISON BETWEEN THE MEASURED SKIN FRICTION AND THE THEORY OF ECKERT ($\theta_V = \theta_B$)

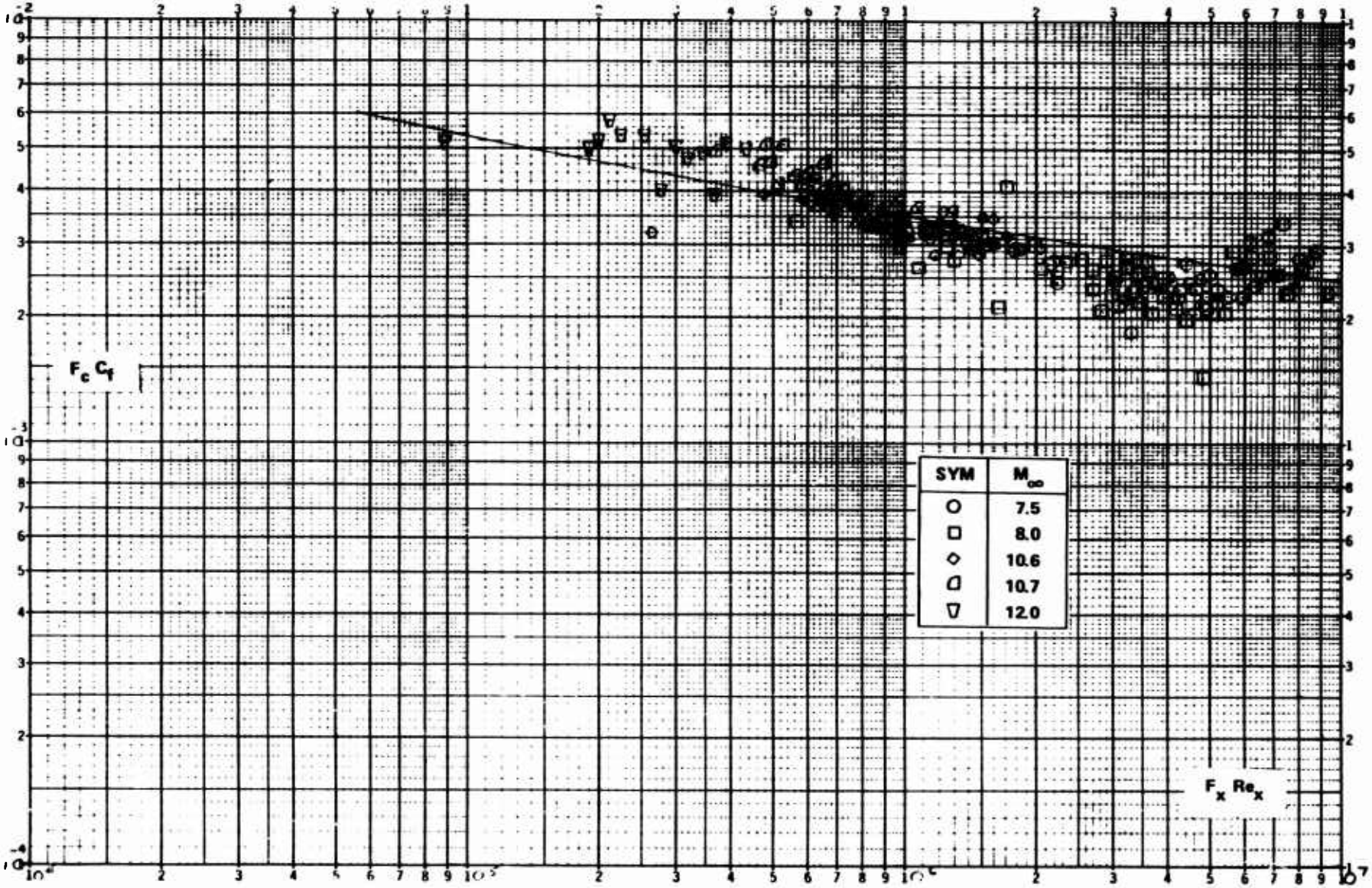


Figure 28b. COMPARISON BETWEEN THE MEASURED SKIN FRICTION AND THE THEORY OF VAN DRIEST ($\Theta_V = \Theta_B$)

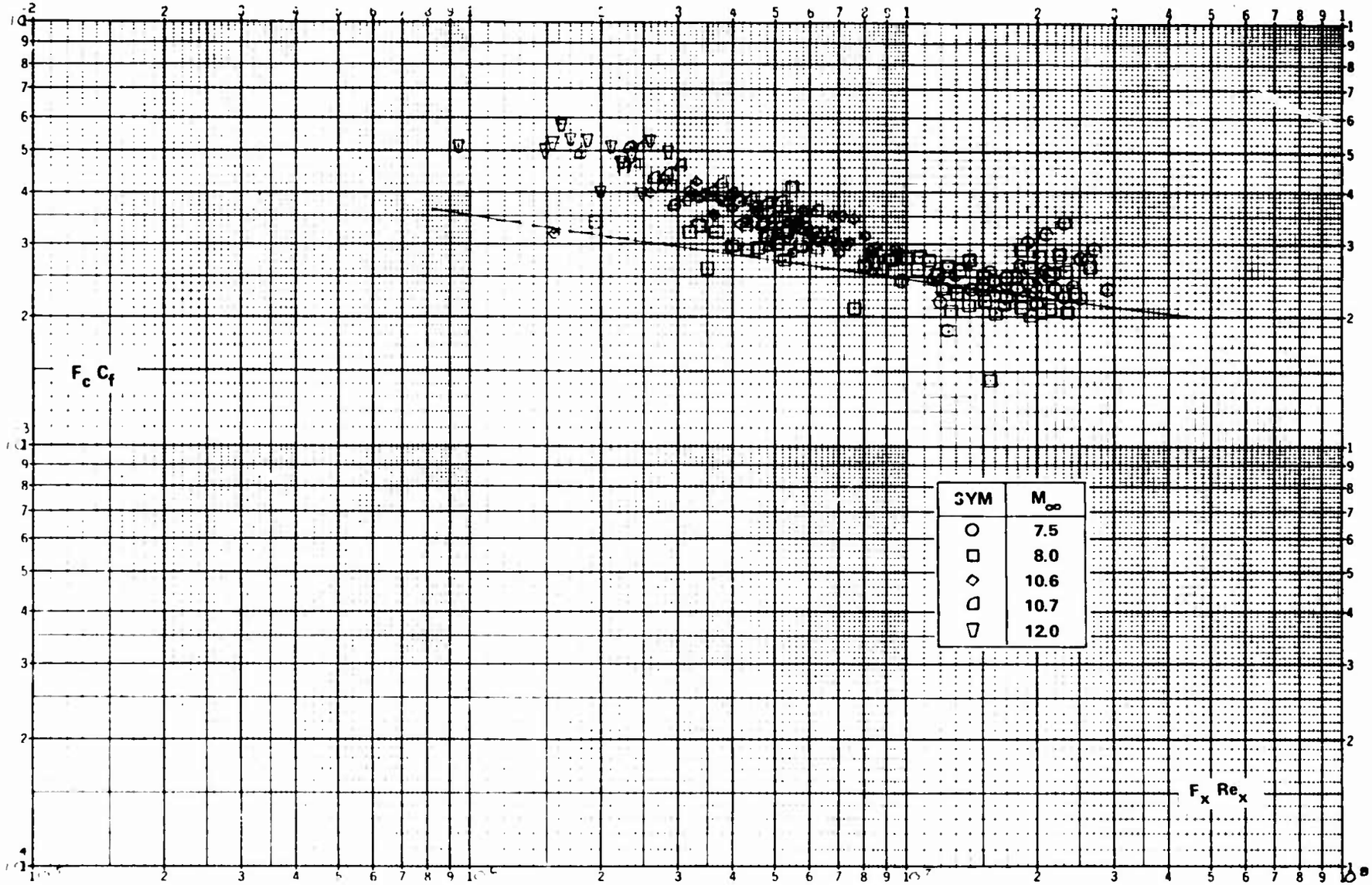


Figure 28c. COMPARISON BETWEEN THE MEASURED SKIN FRICTION AND THE SPALDING-CHI THEORY ($\Theta_V = \Theta_B$)

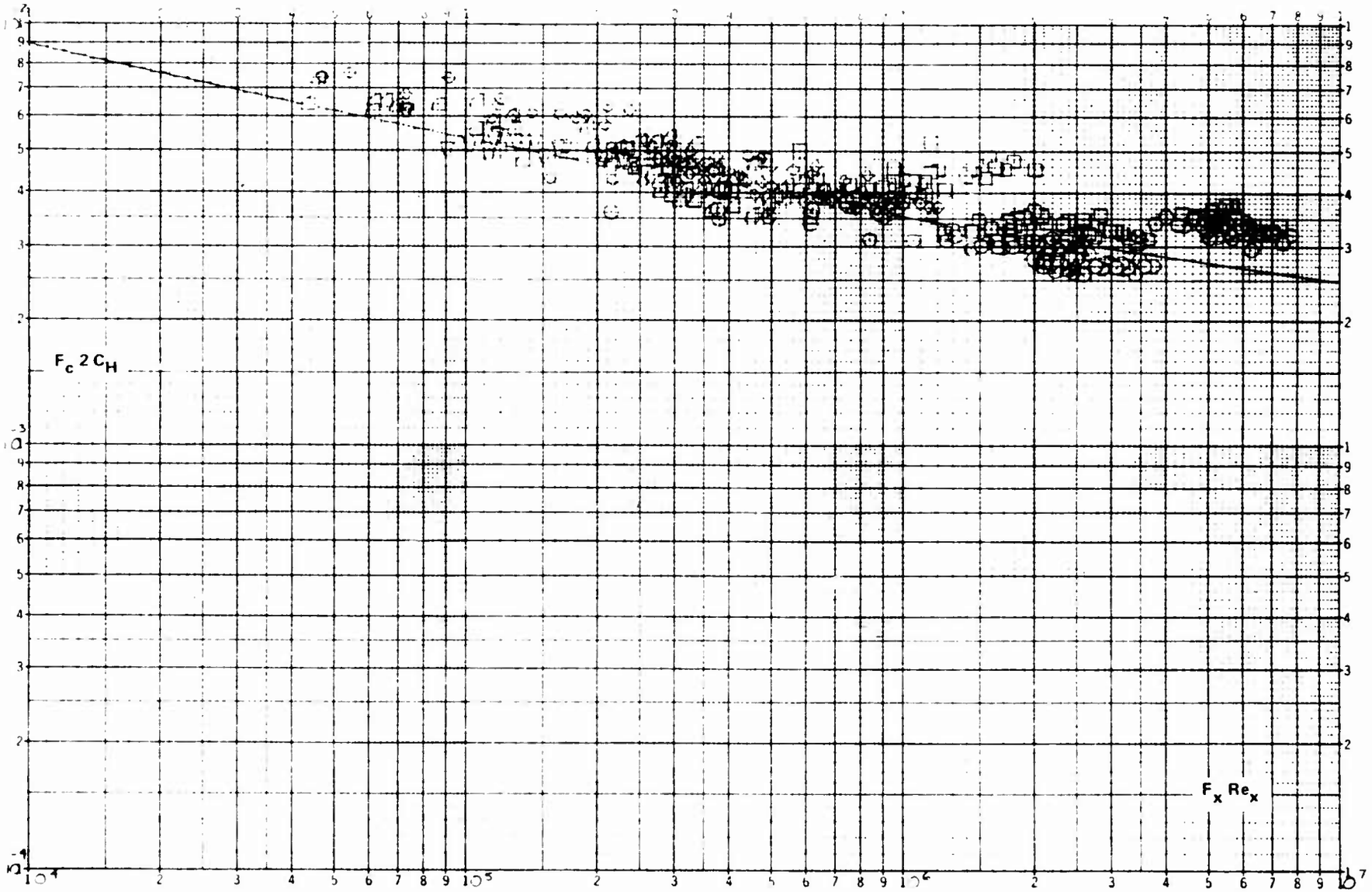


Figure 29a. COMPARISON BETWEEN THE MEASURED HEAT TRANSFER AND THE THEORY OF ECKERT (X_V = 0 AT $\Theta_B + \Theta_{BE/2}$)

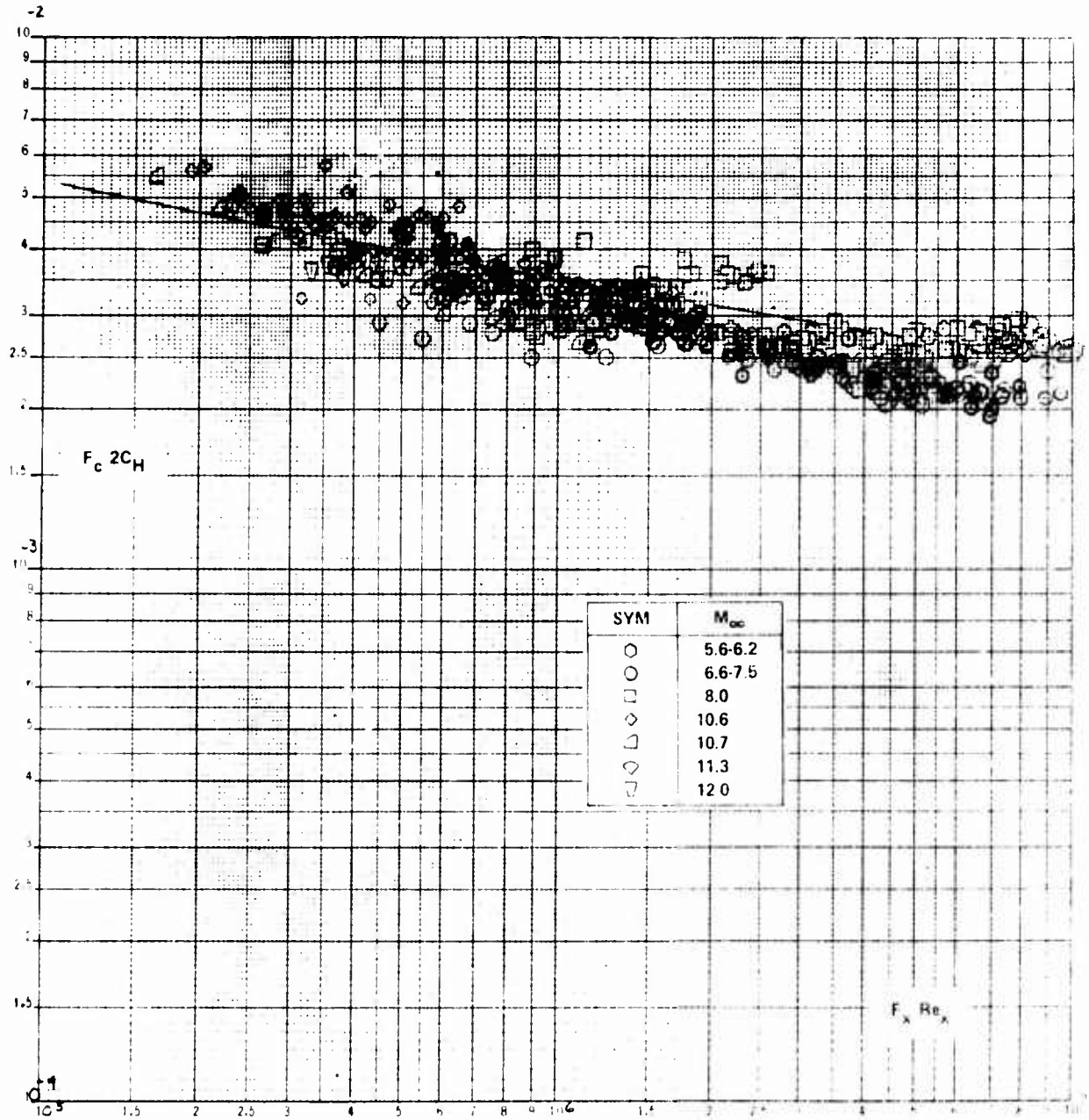


Figure 29b. COMPARISON BETWEEN THE MEASURED HEAT TRANSFER AND THE THEORY OF VAN DRIEST ON SHARP FLAT PLATES ($\Theta_V = \Theta_B + \Theta_{BE/2}$)

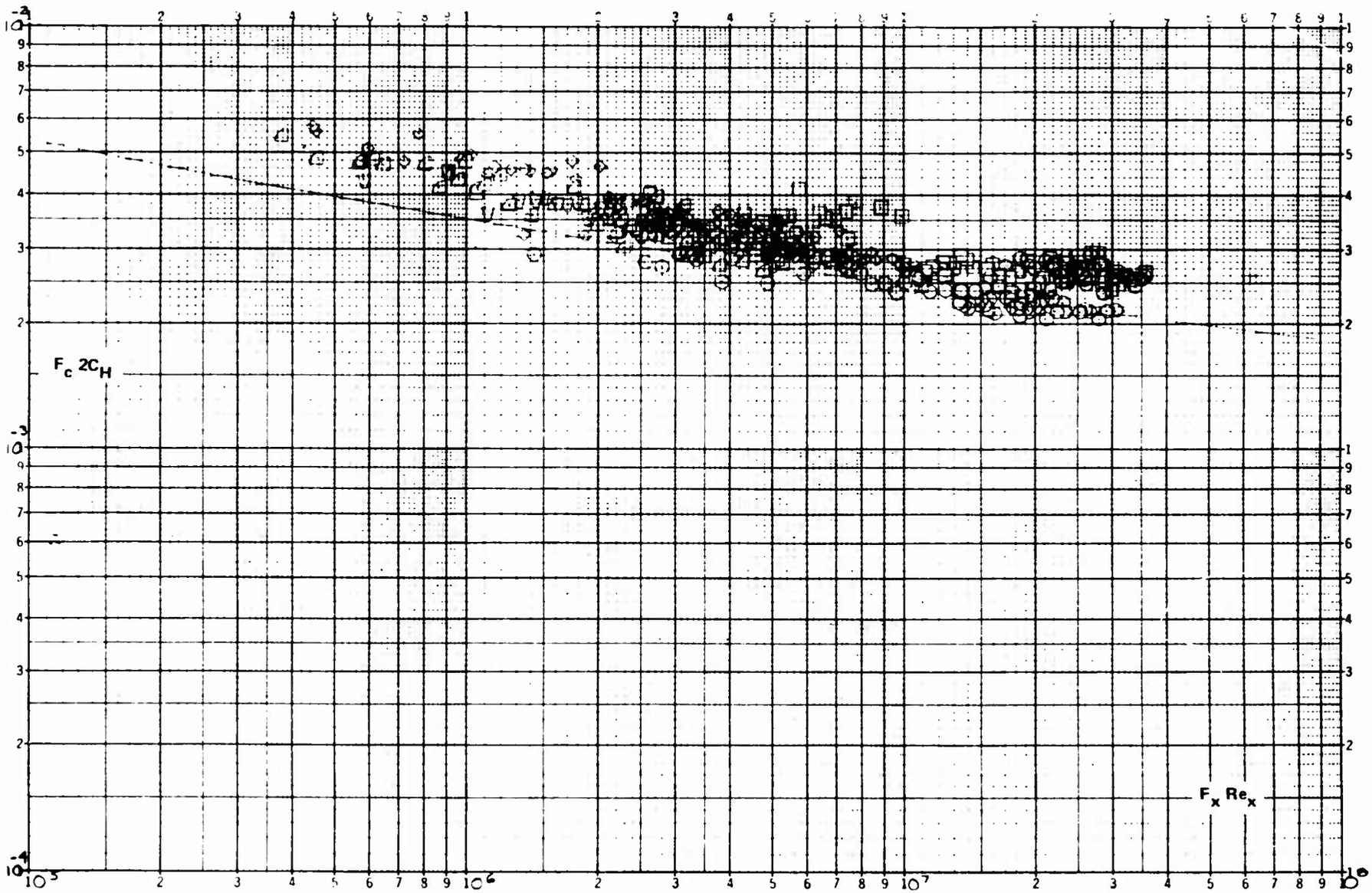


Figure 29c. COMPARISON BETWEEN THE MEASURED HEAT TRANSFER AND THE THEORY OF SPAULDING-CHI (X_V = 0 AT $\Theta_B + \Theta_{BE/2}$)

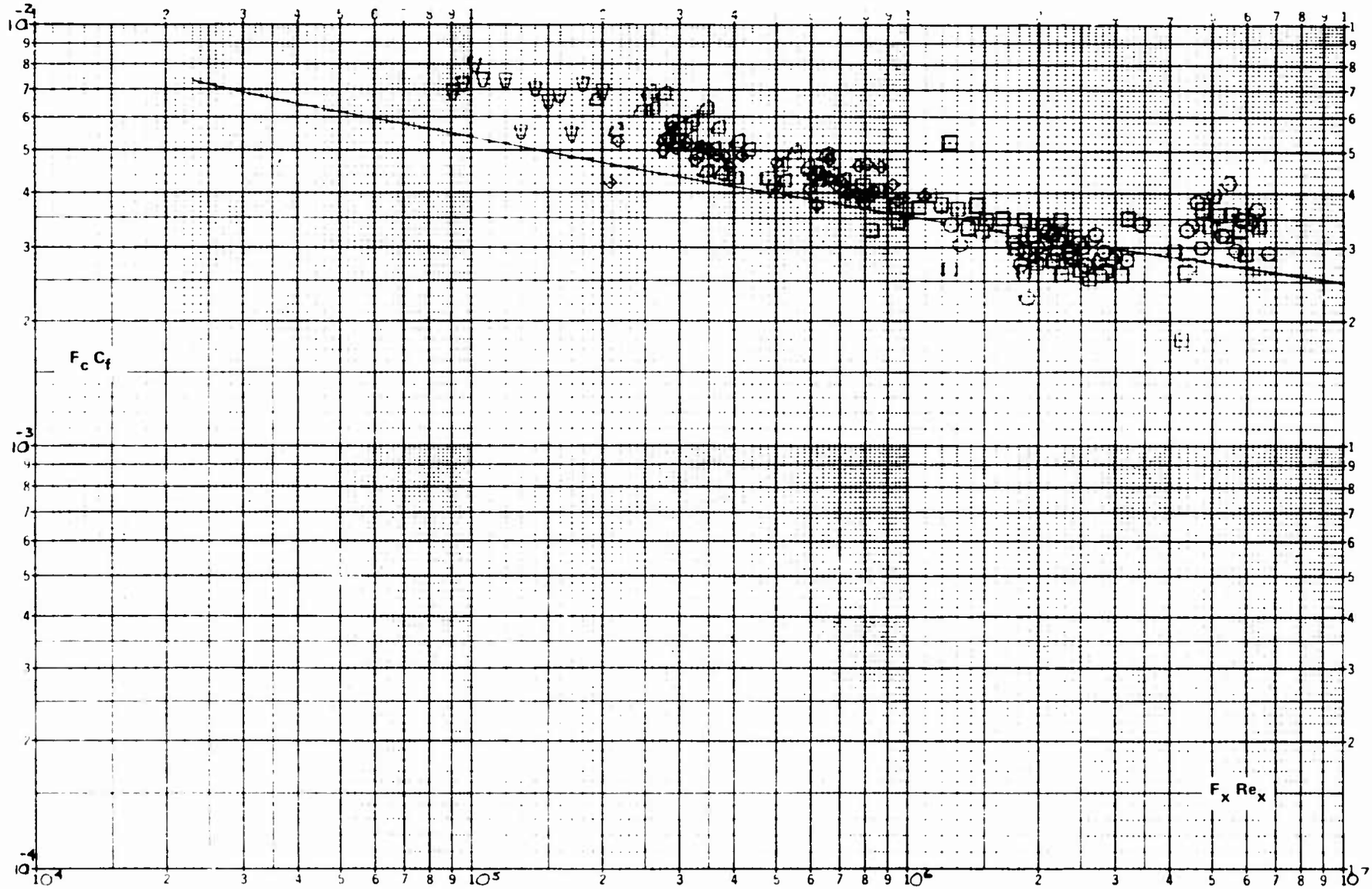


Figure 30a. COMPARISON BETWEEN THE MEASURED SKIN FRICTION AND THE THEORY OF ECKERT ($X_V = 0$ AT $\Theta_B + \Theta_{BE/2}$)

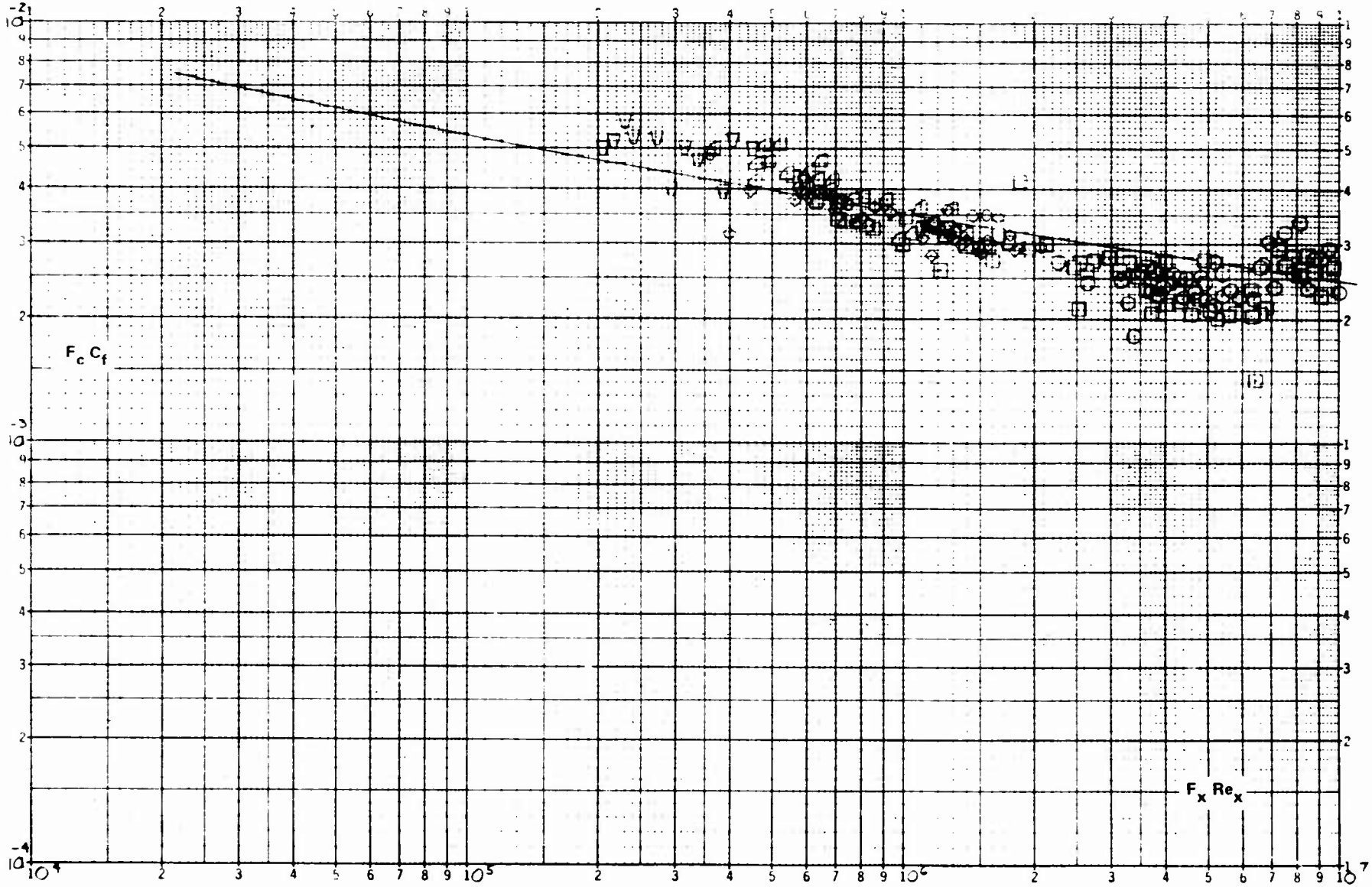


Figure 30b. COMPARISON BETWEEN THE MEASURED SKIN FRICTION AND THE THEORY OF VAN DRIEST (X_V = 0 AT $\Theta_B + \Theta_{BE/2}$)

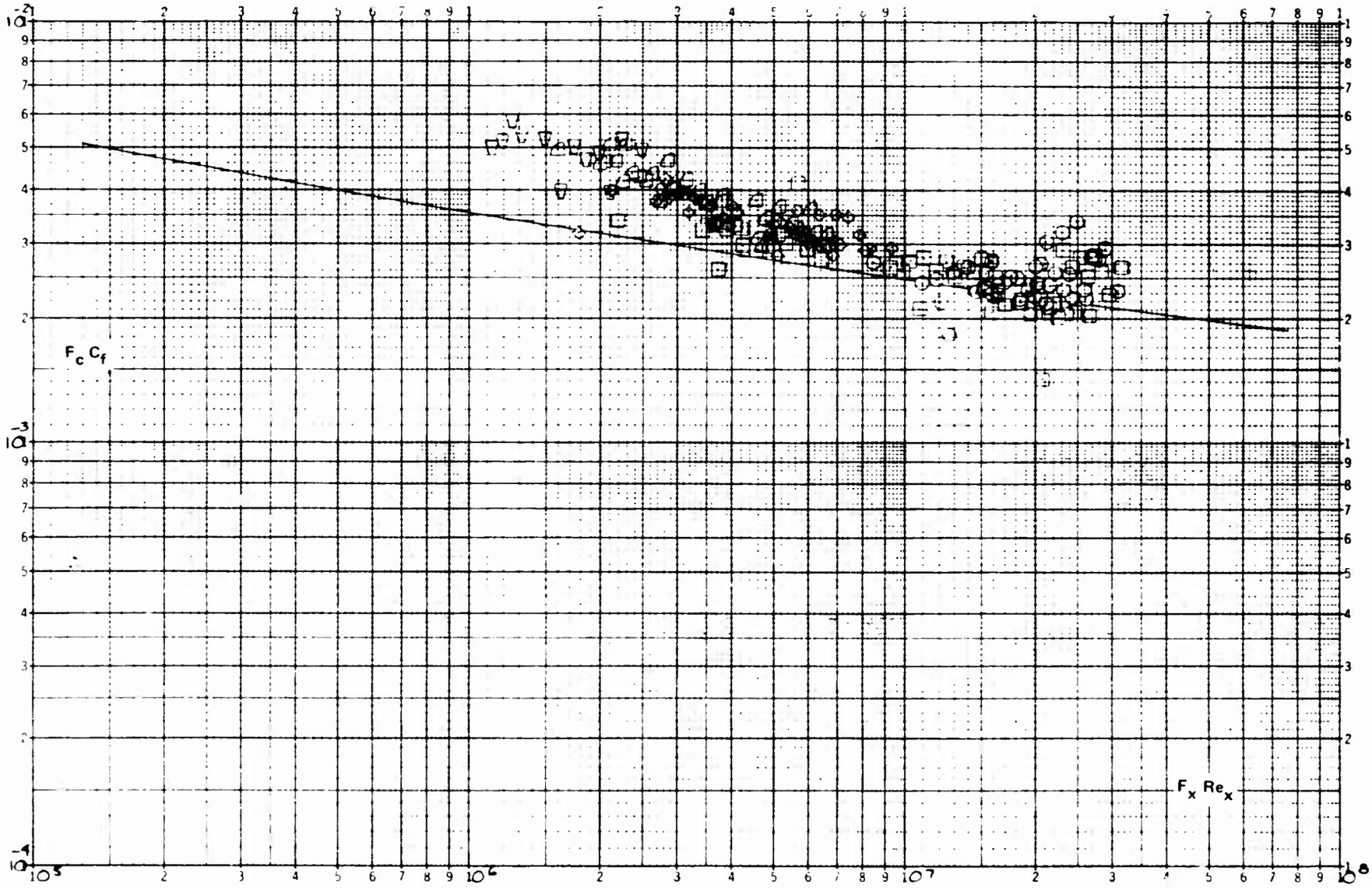


Figure 30c. COMPARISON BETWEEN THE MEASURED SKIN FRICTION AND THE THEORY OF SPAULDING-CHI ($X_V = 0$ AT $\Theta_B + \Theta_{BE/2}$)

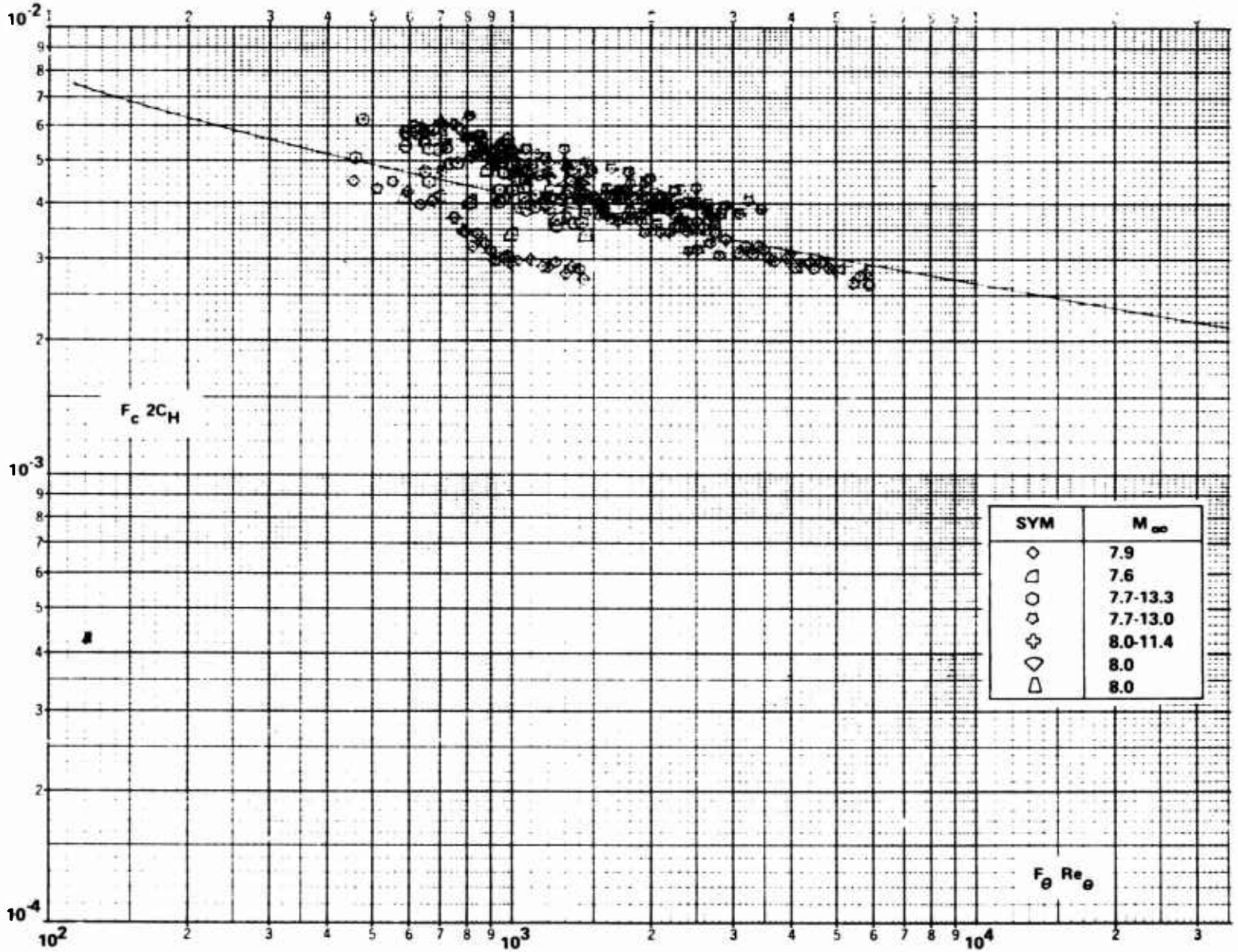


Figure 31a COMPARISON BETWEEN THE MEASURED HEAT TRANSFER AND THE THEORY OF ECKERT (T_A*) ON SHARP CONES

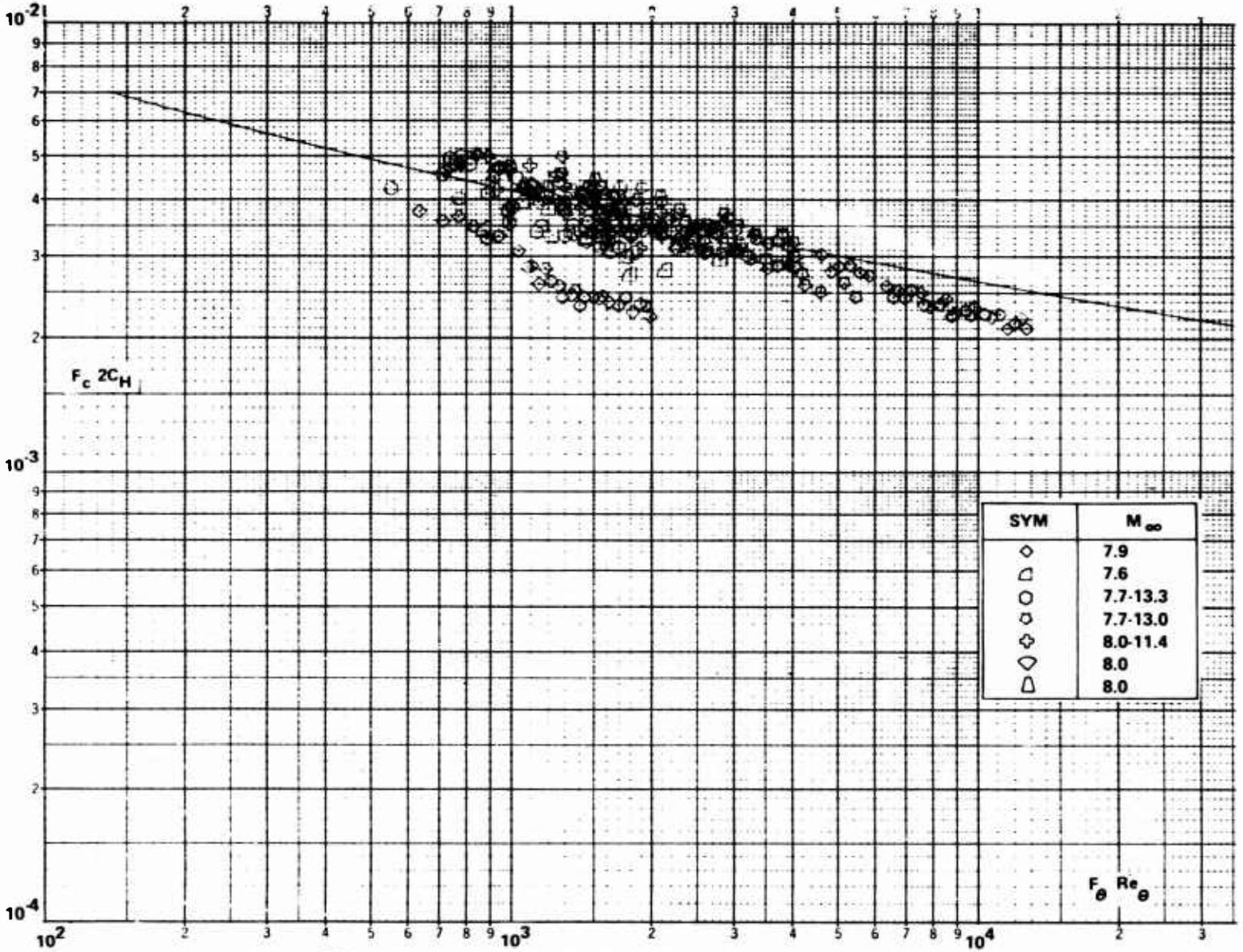


Figure 31b COMPARISON BETWEEN THE MEASURED HEAT TRANSFER AND THE THEORY OF VAN DRIEST (T_E*) ON SHARP CONES

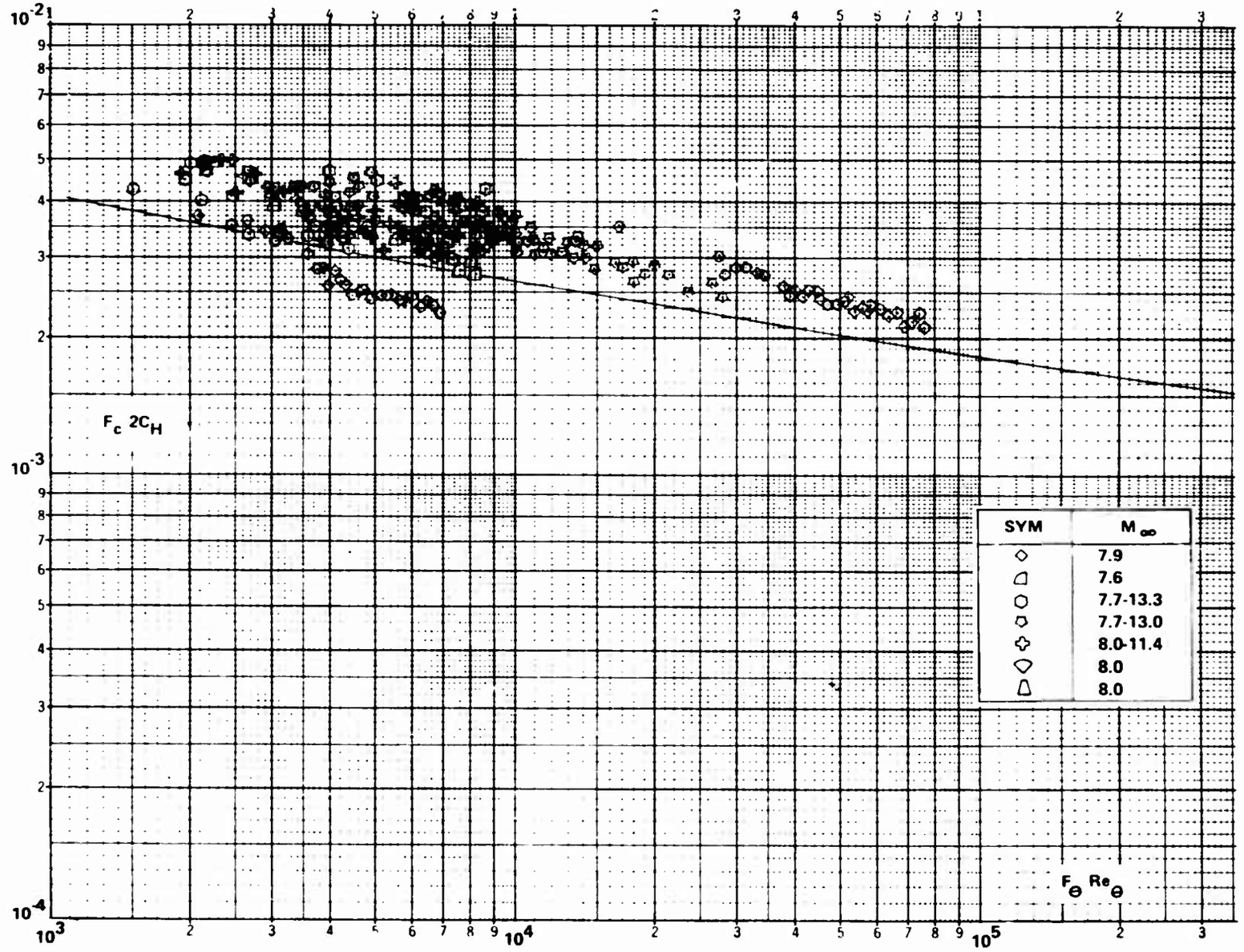


Figure 31c COMPARISON BETWEEN THE MEASURED HEAT TRANSFER AND THE THEORY OF SPALDING-CHI ON SHARP CONES

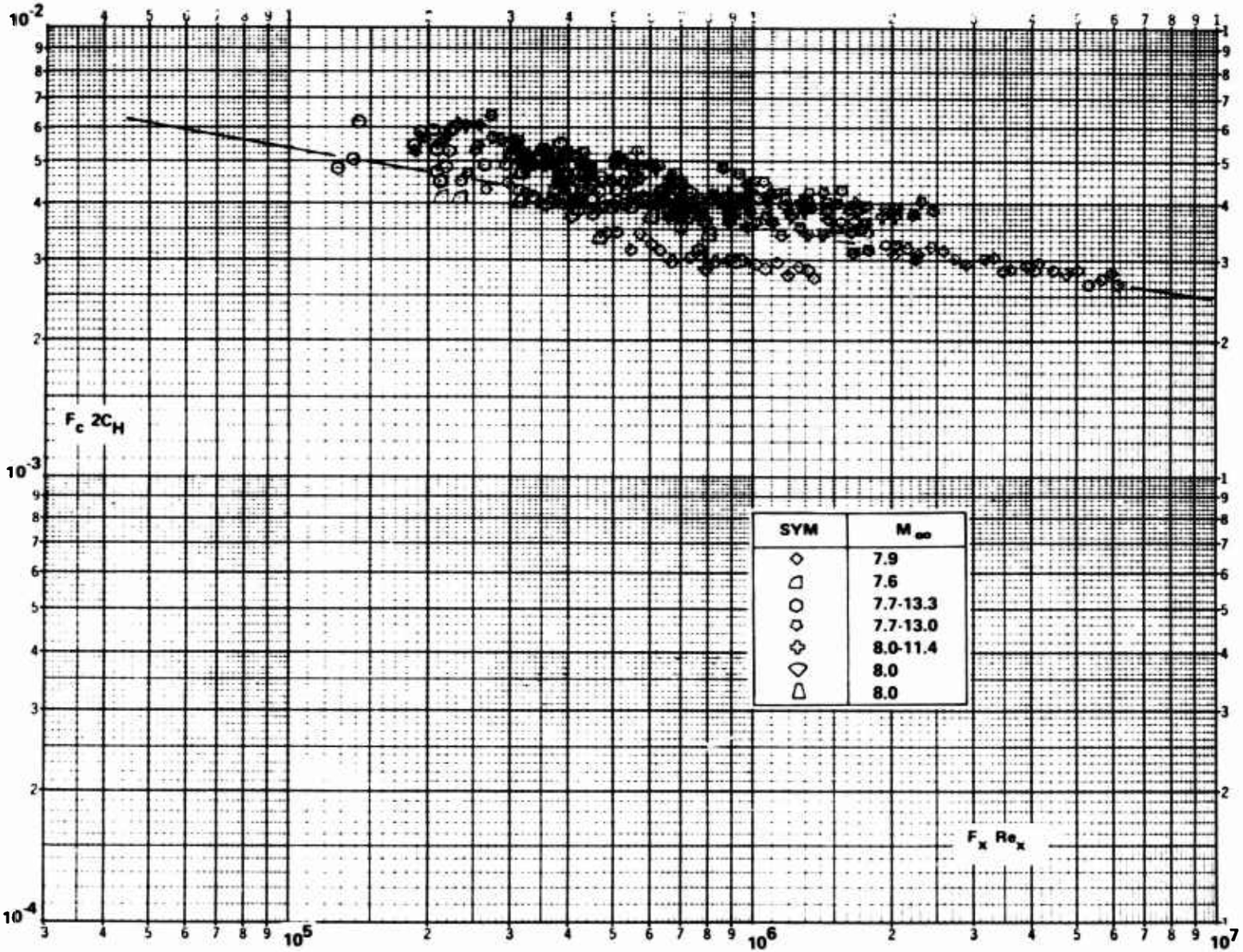


Figure 32a COMPARISON BETWEEN THE MEASURED HEAT TRANSFER AND THE THEORY OF ECKERT ON SHARP CONES ($\theta_V = \theta_B + \theta_{BE}$)

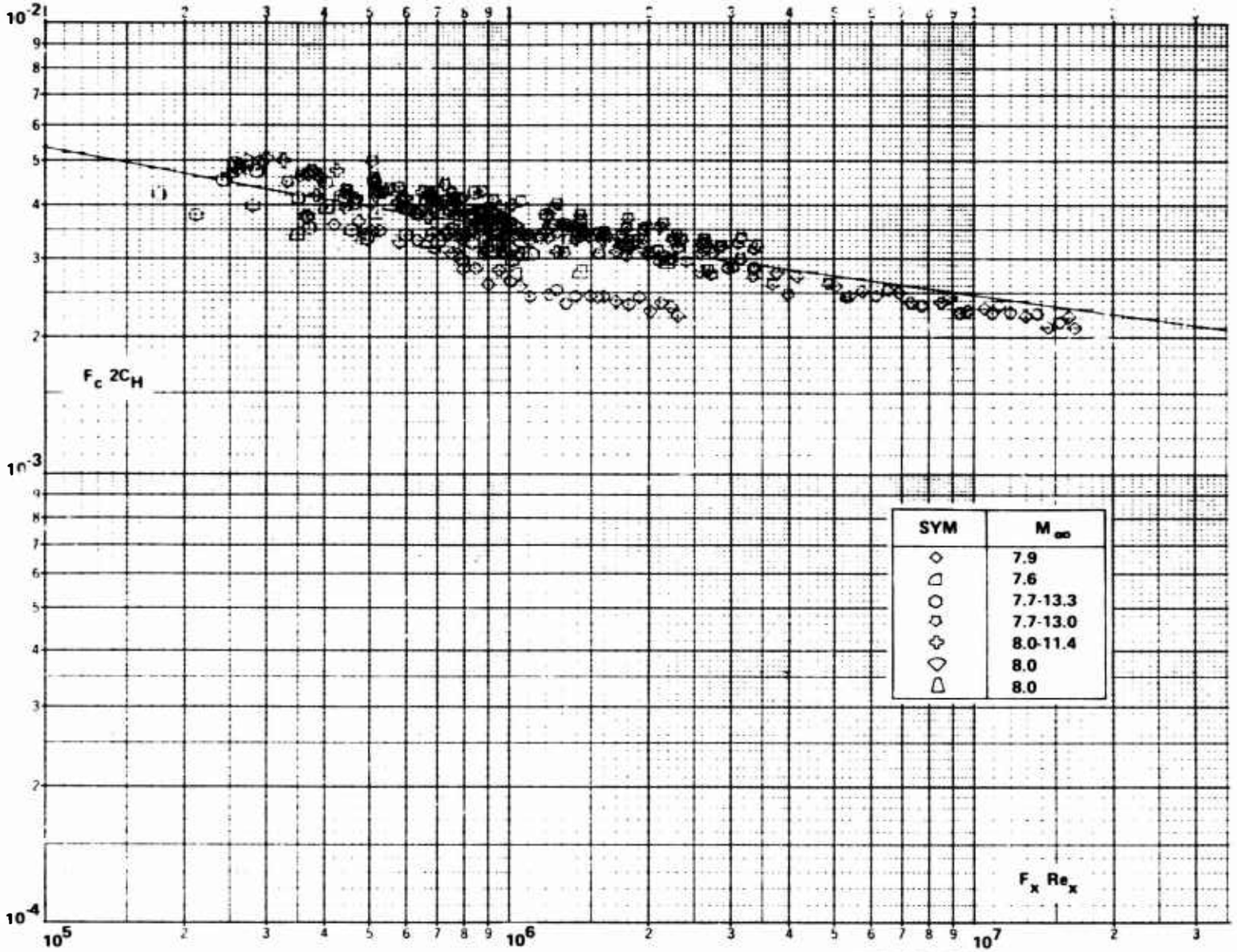


Figure 32b COMPARISON BETWEEN THE MEASURED HEAT TRANSFER AND THE THEORY OF VAN DRIEST ON SHARP CONES ($\theta_V = \theta_B + \theta_{BE}$)

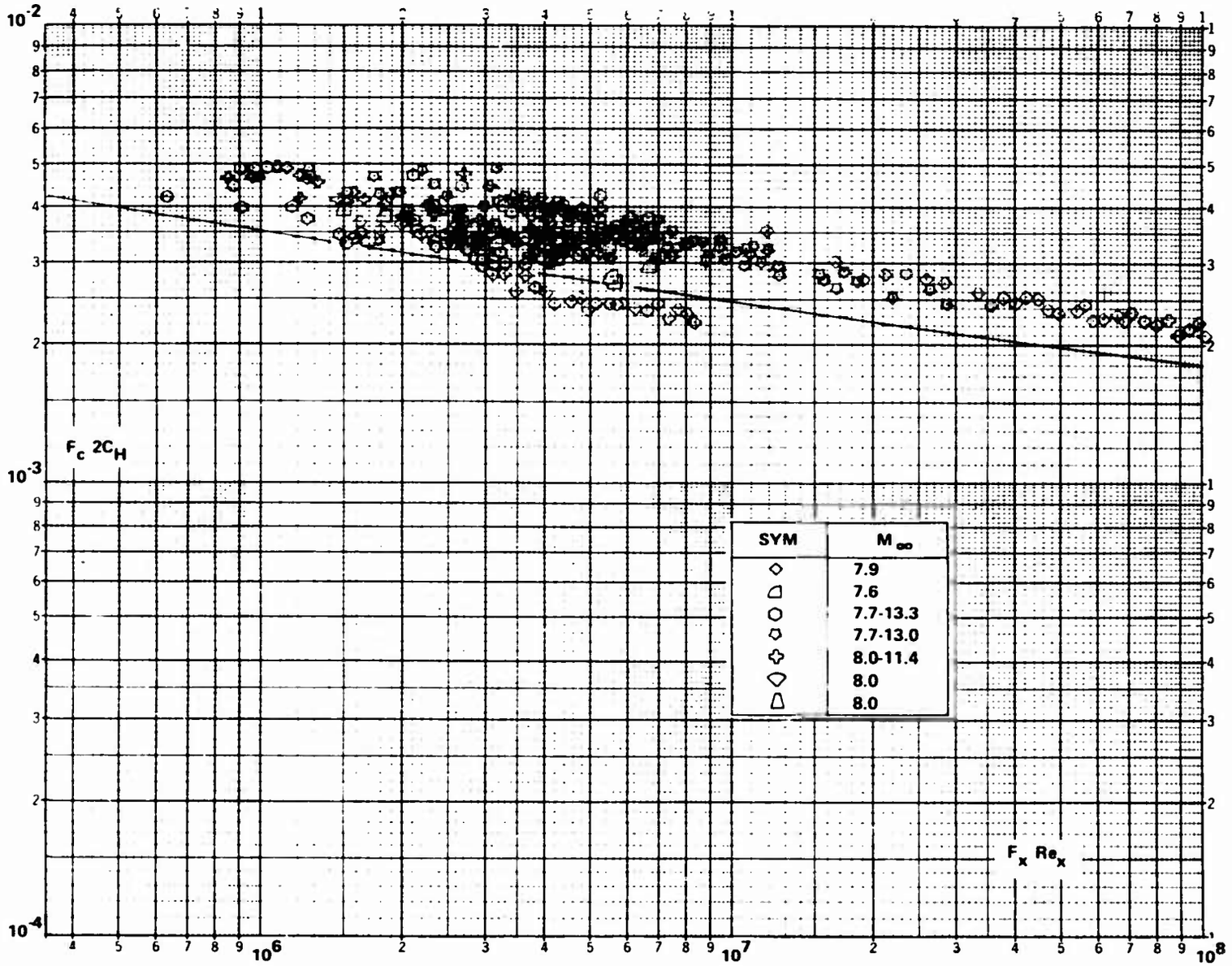


Figure 32c COMPARISON BETWEEN THE MEASURED HEAT TRANSFER AND THE SPALDING-CHI THEORY ON SHARP CONES ($\Theta_V = \Theta_B + \Theta_{BE}$)

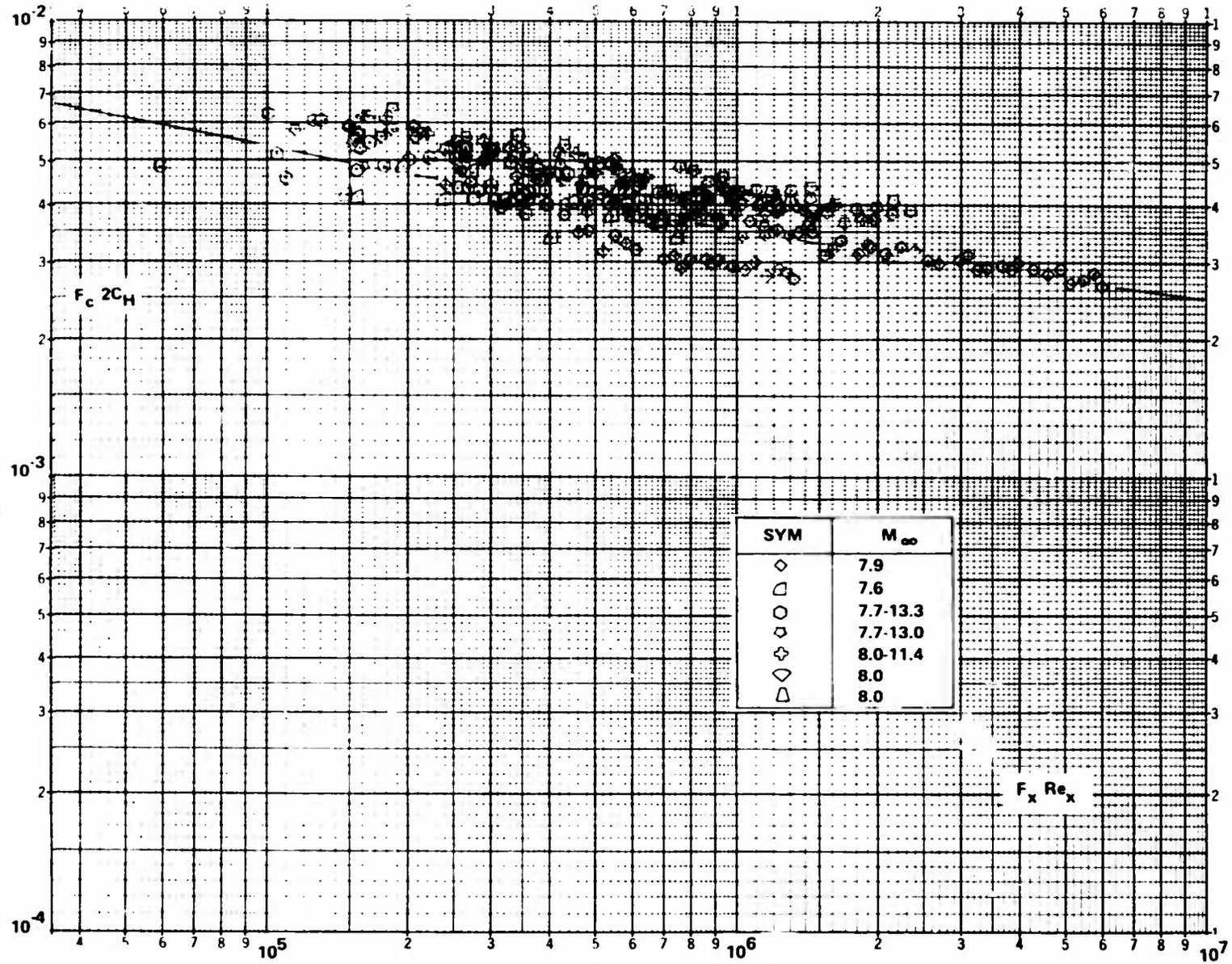


Figure 33a COMPARISON BETWEEN THE MEASURED HEAT TRANSFER AND THE THEORY OF ECKERT ON SHARP CONES ($\Theta_V = \Theta_B + \Theta_{BE/2}$)

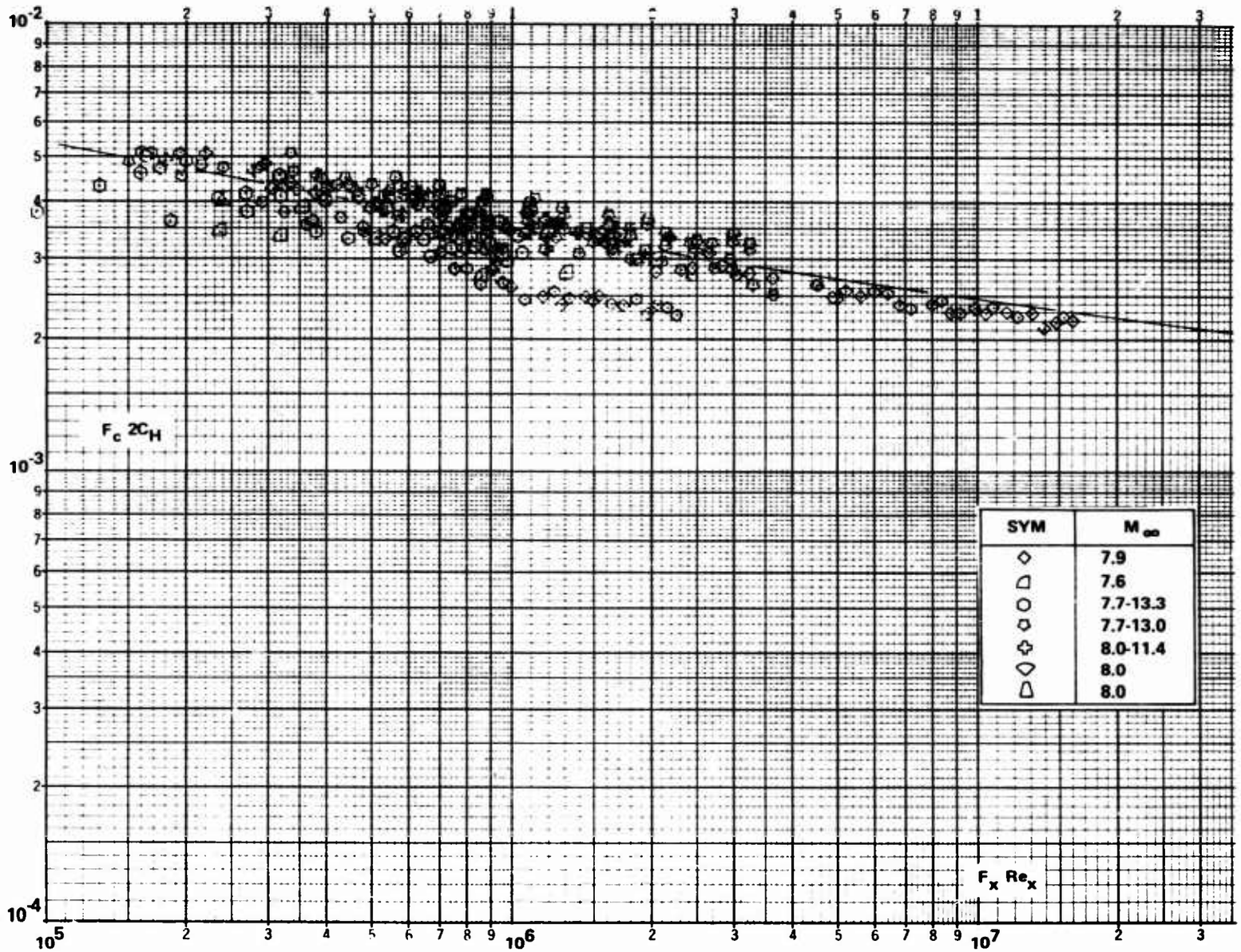


Figure 33b COMPARISON BETWEEN THE MEASURED HEAT TRANSFER AND THE THEORY OF VAN DRIEST ON SHARP CONES ($\Theta_V = \Theta_B + \Theta_{BE/2}$)

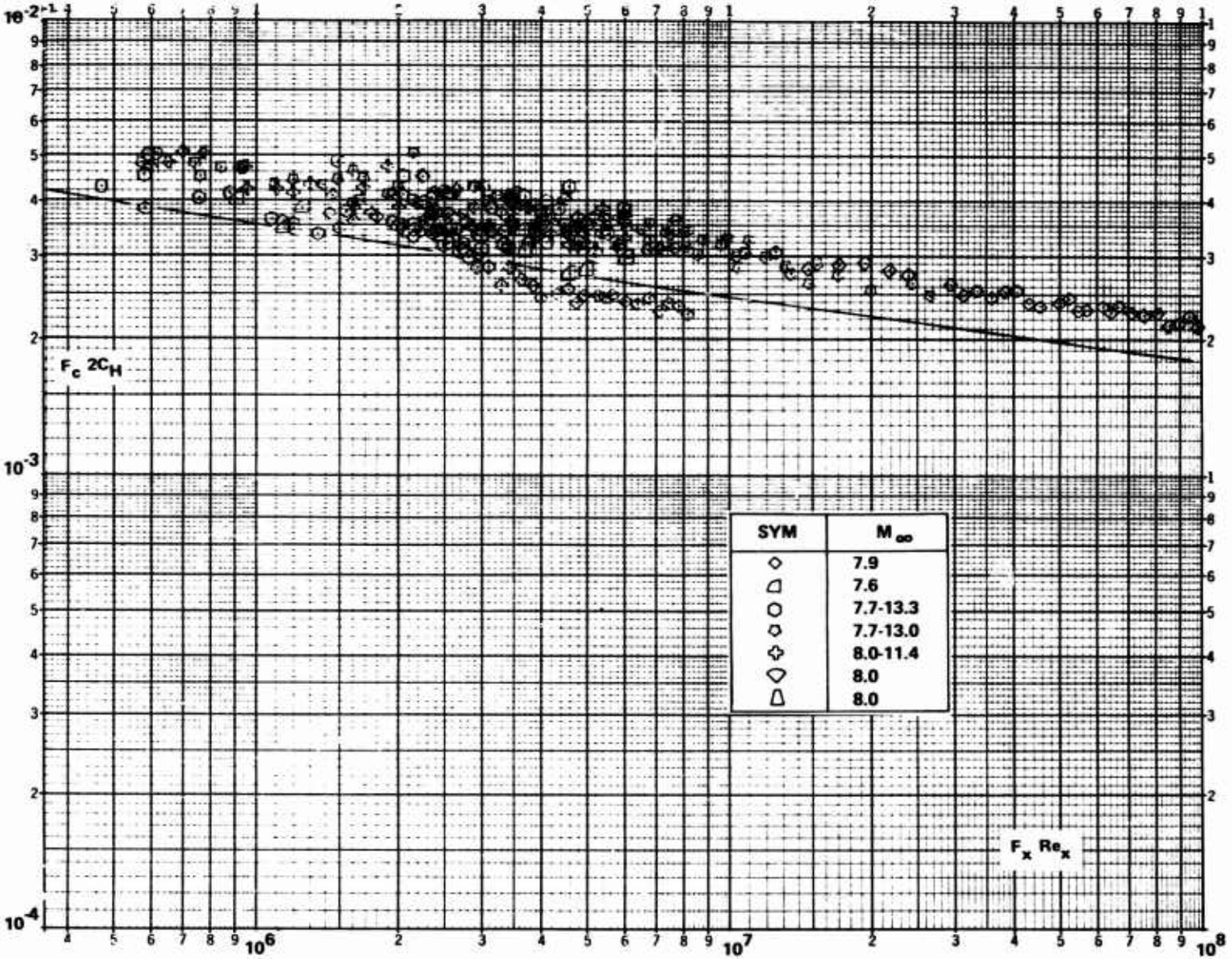


Figure 33c COMPARISON BETWEEN THE MEASURED HEAT TRANSFER AND THE SPALDING-CHI THEORY ON SHARP CONES ($\theta_V = \theta_B + \theta_{BE/2}$)

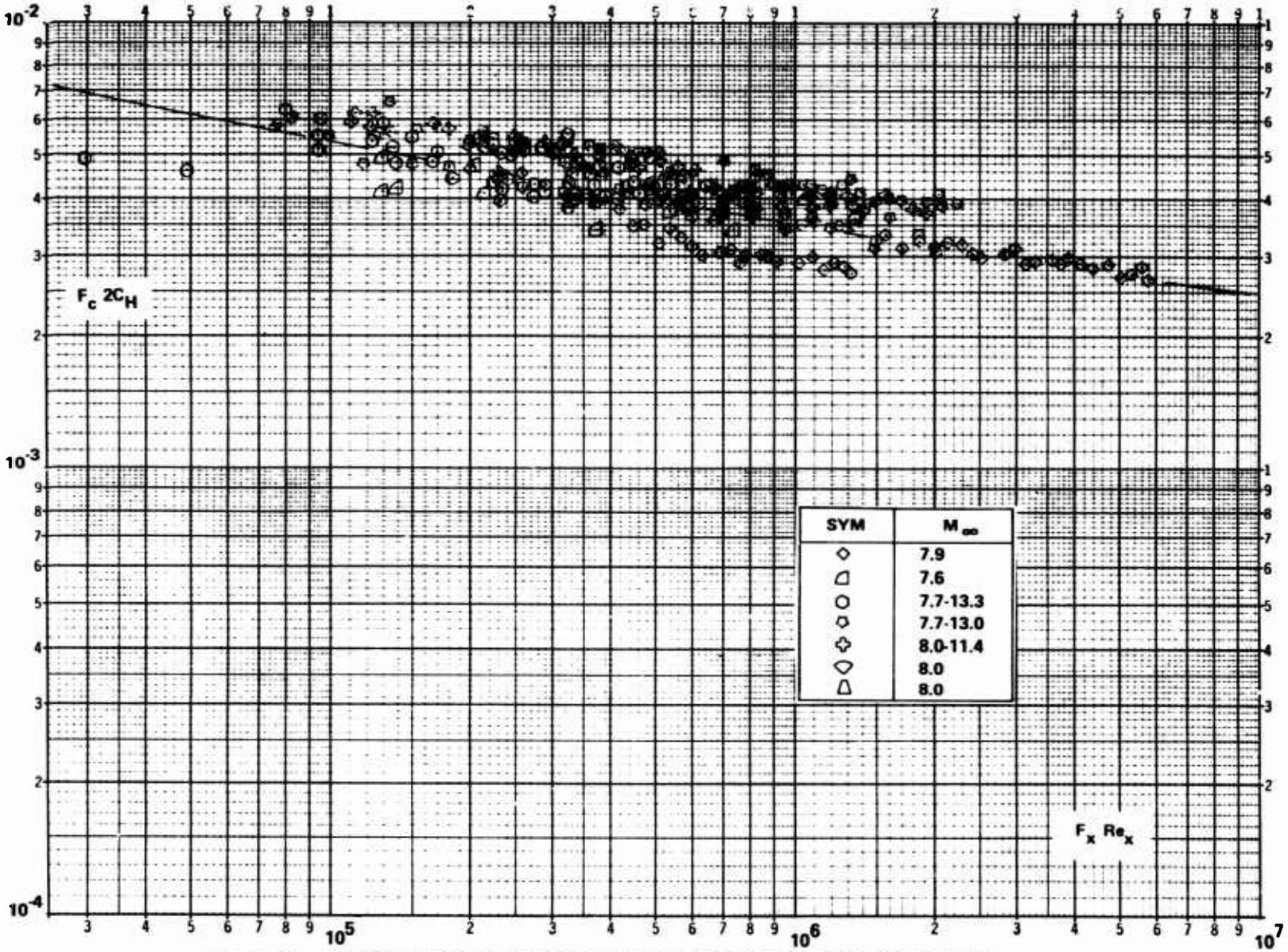


Figure 34a COMPARISON BETWEEN THE MEASURED HEAT TRANSFER AND THE THEORY OF ECKERT ON SHARP CONES ($\theta_V = \theta_B + \theta_{BE\ LAMINAR}$)

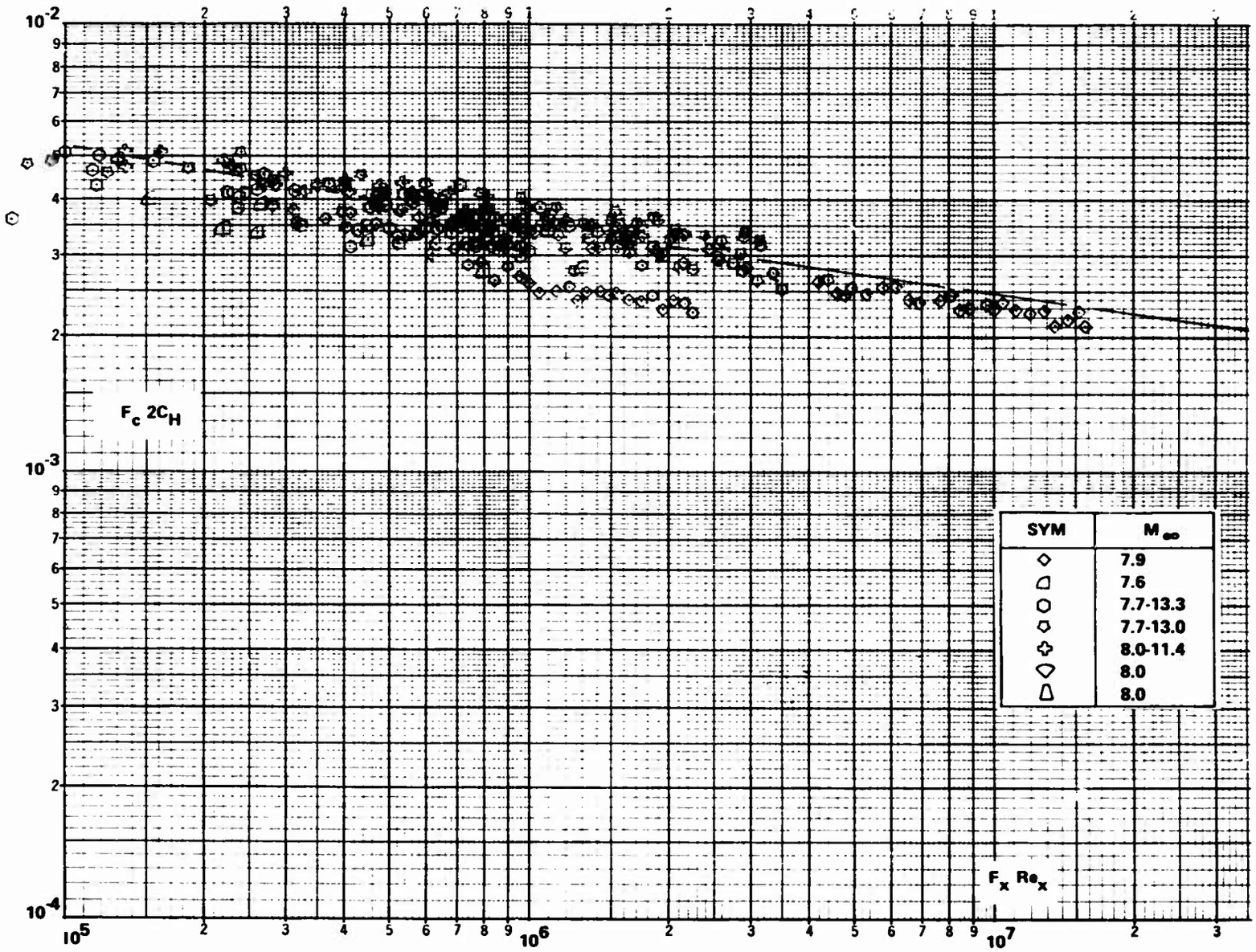


Figure 34b COMPARISON BETWEEN THE MEASURED HEAT TRANSFER AND THE THEORY OF VAN DRIEST ON SHARP CONES ($\Theta_V = \Theta_B + \Theta_{BE\ LAMINAR}$)

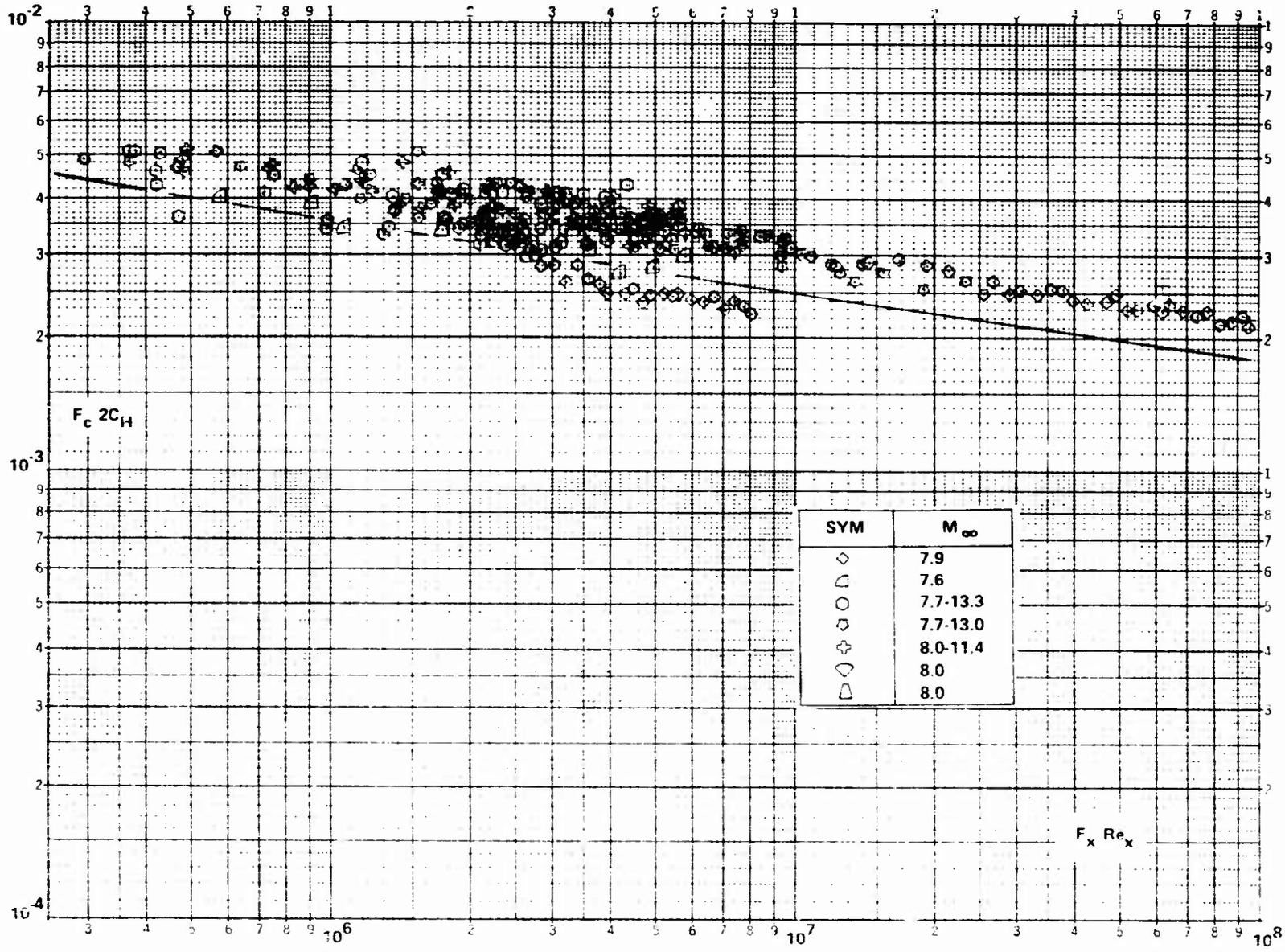


Figure 34c COMPARISON BETWEEN THE MEASURED HEAT TRANSFER AND THE SPALDING-CHI THEORY ON SHARP CONES ($\Theta_V = \Theta_B + \Theta_{BE\ LAMINAR}$)

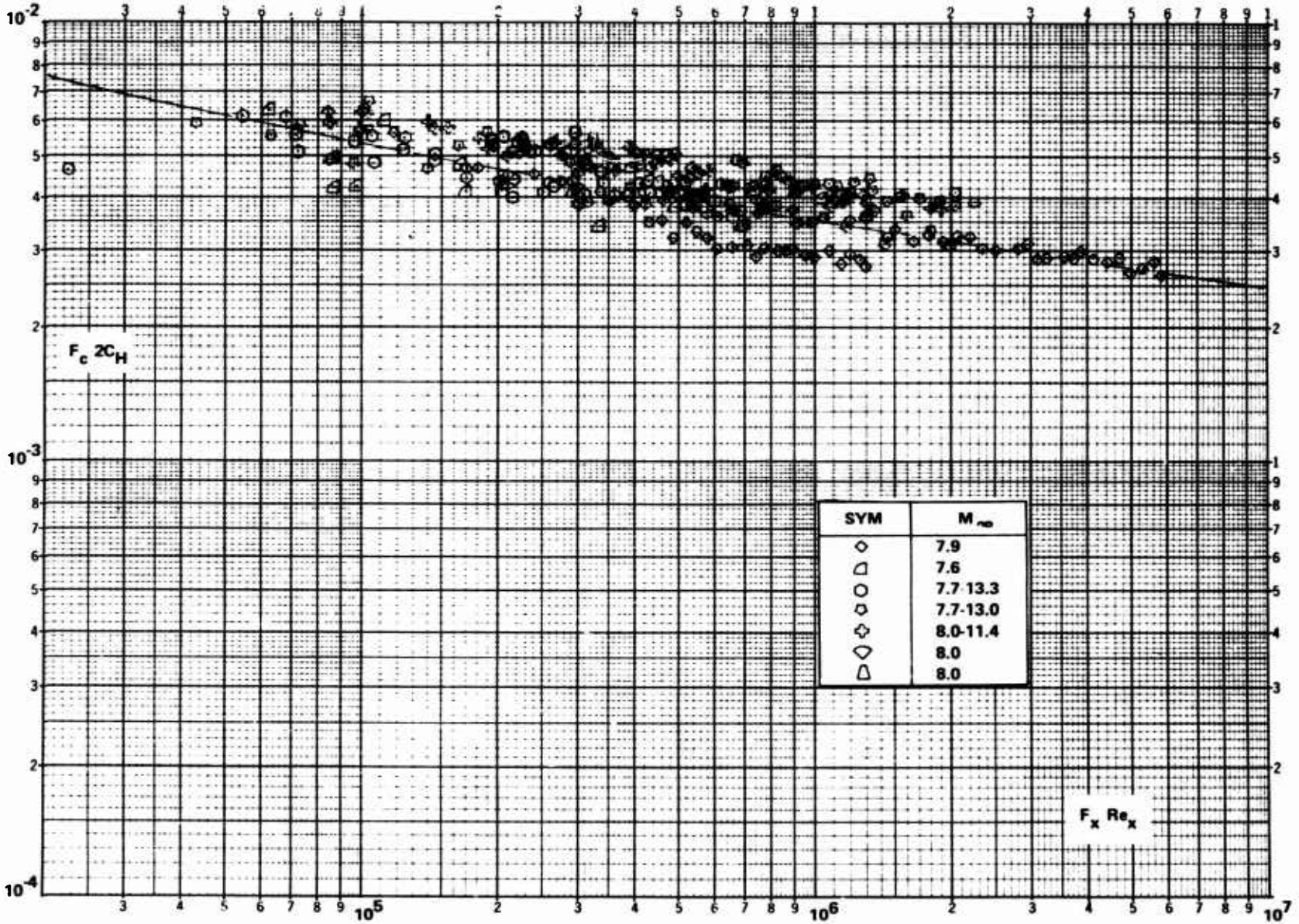


Figure 35a COMPARISON BETWEEN THE MEASURED HEAT TRANSFER AND THE THEORY OF ECKERT ON SHARP CONES ($\theta_V = \theta_B$)

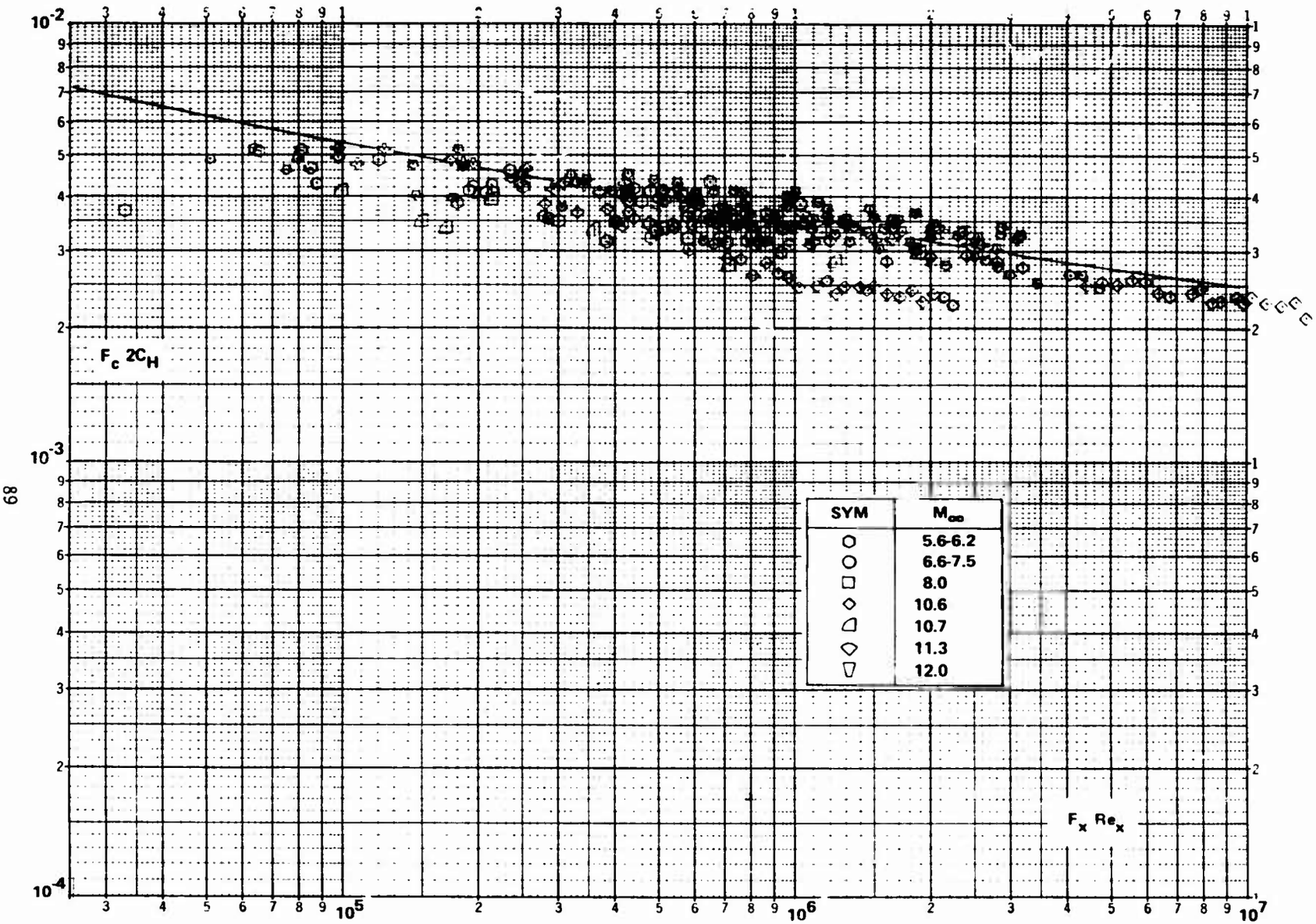


Figure 35b COMPARISON BETWEEN THE MEASURED HEAT TRANSFER AND THE THEORY OF VAN DRIEST ON SHARP CONES ($\Theta_V = \Theta_B$)

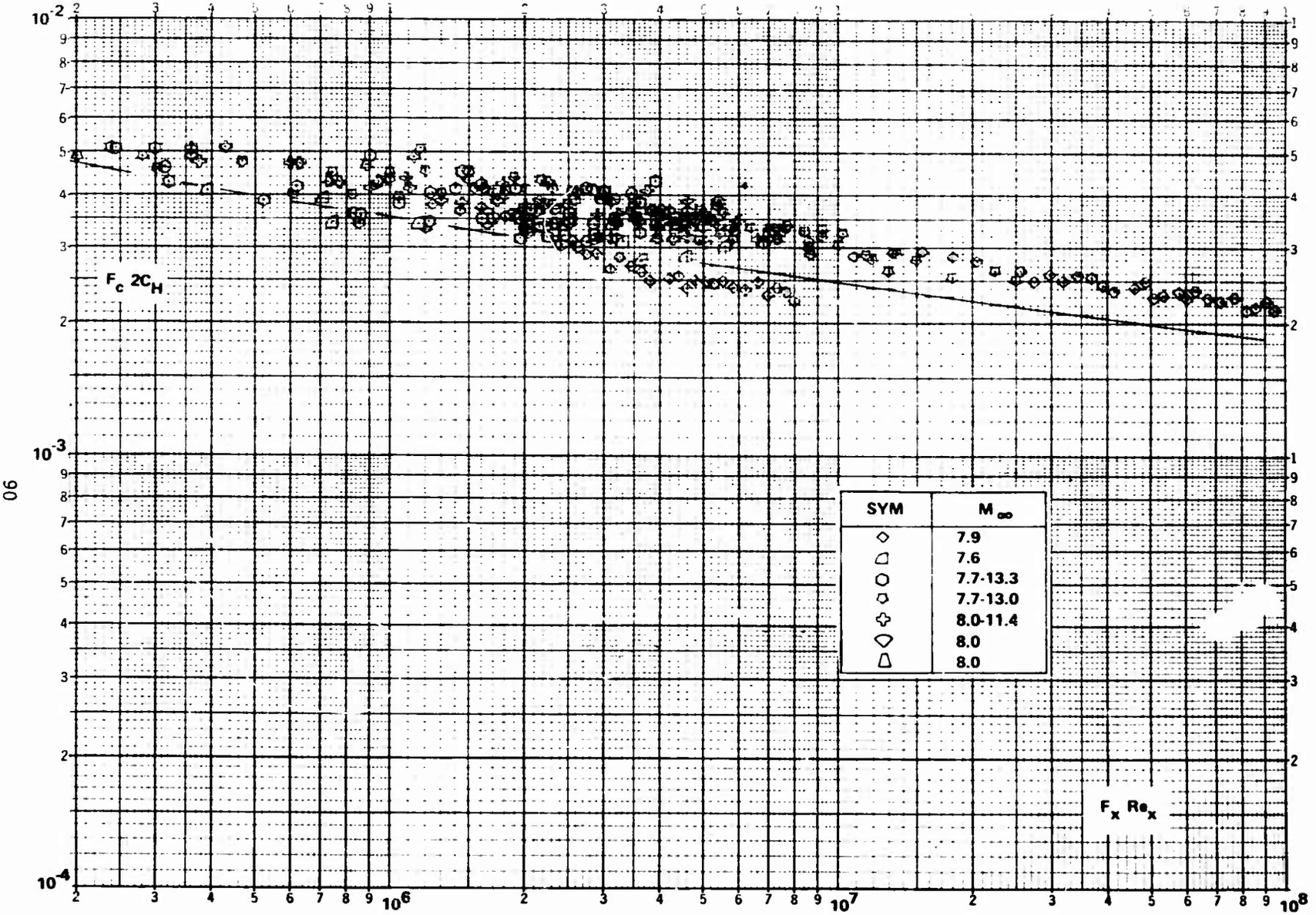


Figure 35c COMPARISON BETWEEN THE MEASURED HEAT TRANSFER AND THE SPALDING-CHI THEORY ON SHARP CONES ($\Theta_V = \Theta_B$)

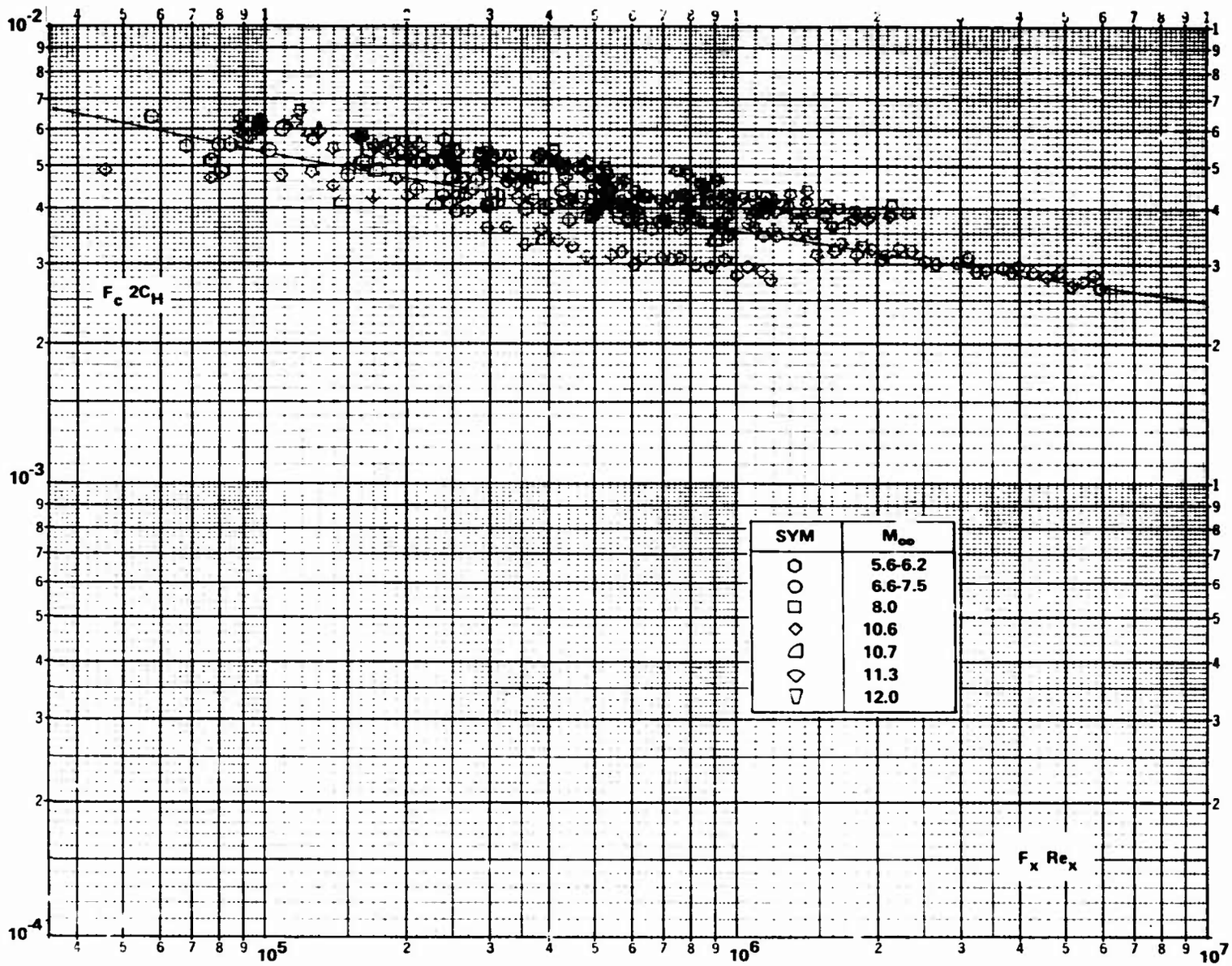


Figure 36a COMPARISON BETWEEN THE MEASURED HEAT TRANSFER AND THE THEORY OF ECKERT ON SHARP CONES ($X_V = 0$ AT $\Theta_B + \Theta_{BE/2}$)

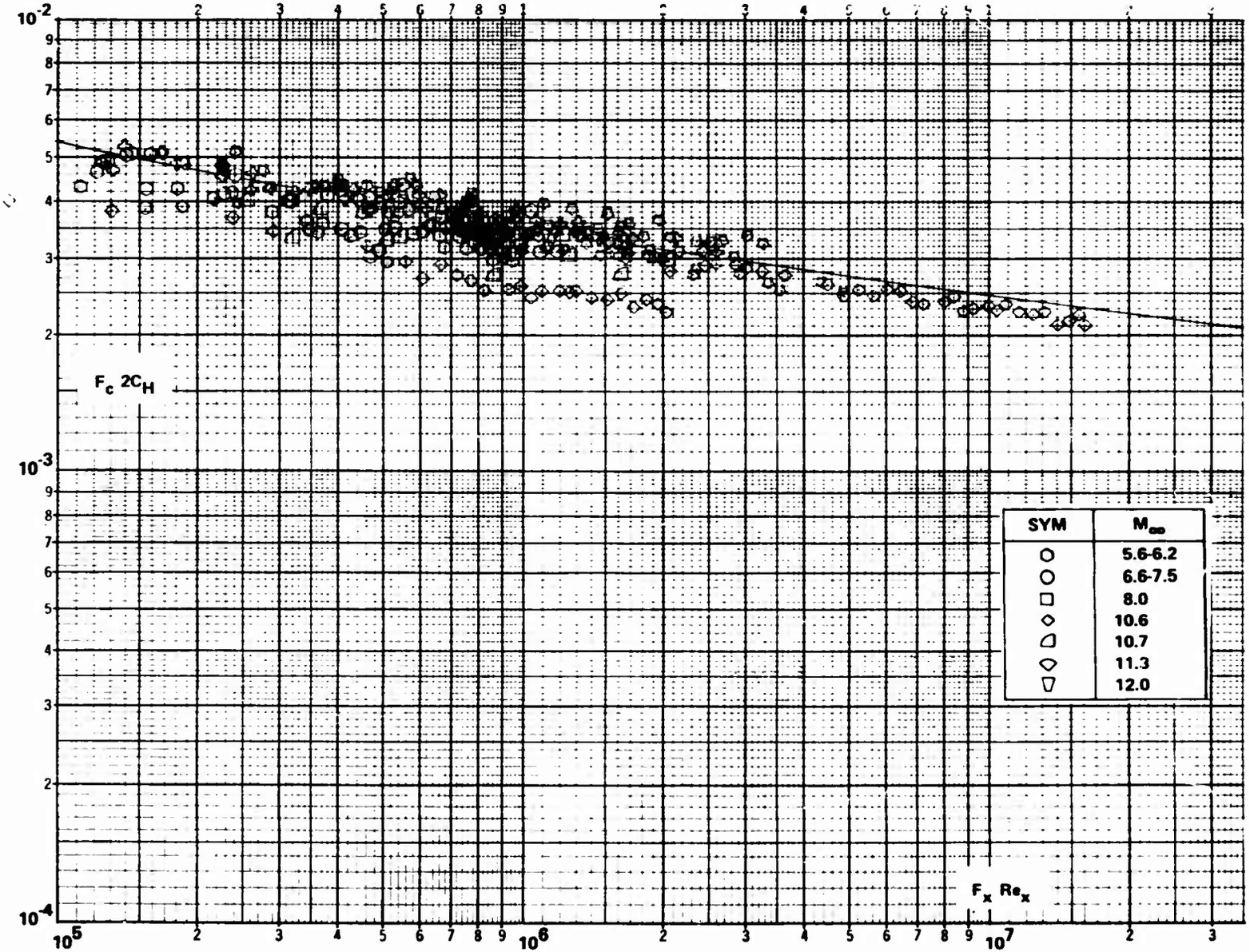


Figure 36b COMPARISON BETWEEN THE MEASURED HEAT TRANSFER AND THE THEORY OF VAN DRIEST ON SHARP CONES (X_V = 0 AT $\Theta_B + \Theta_{BE/2}$)

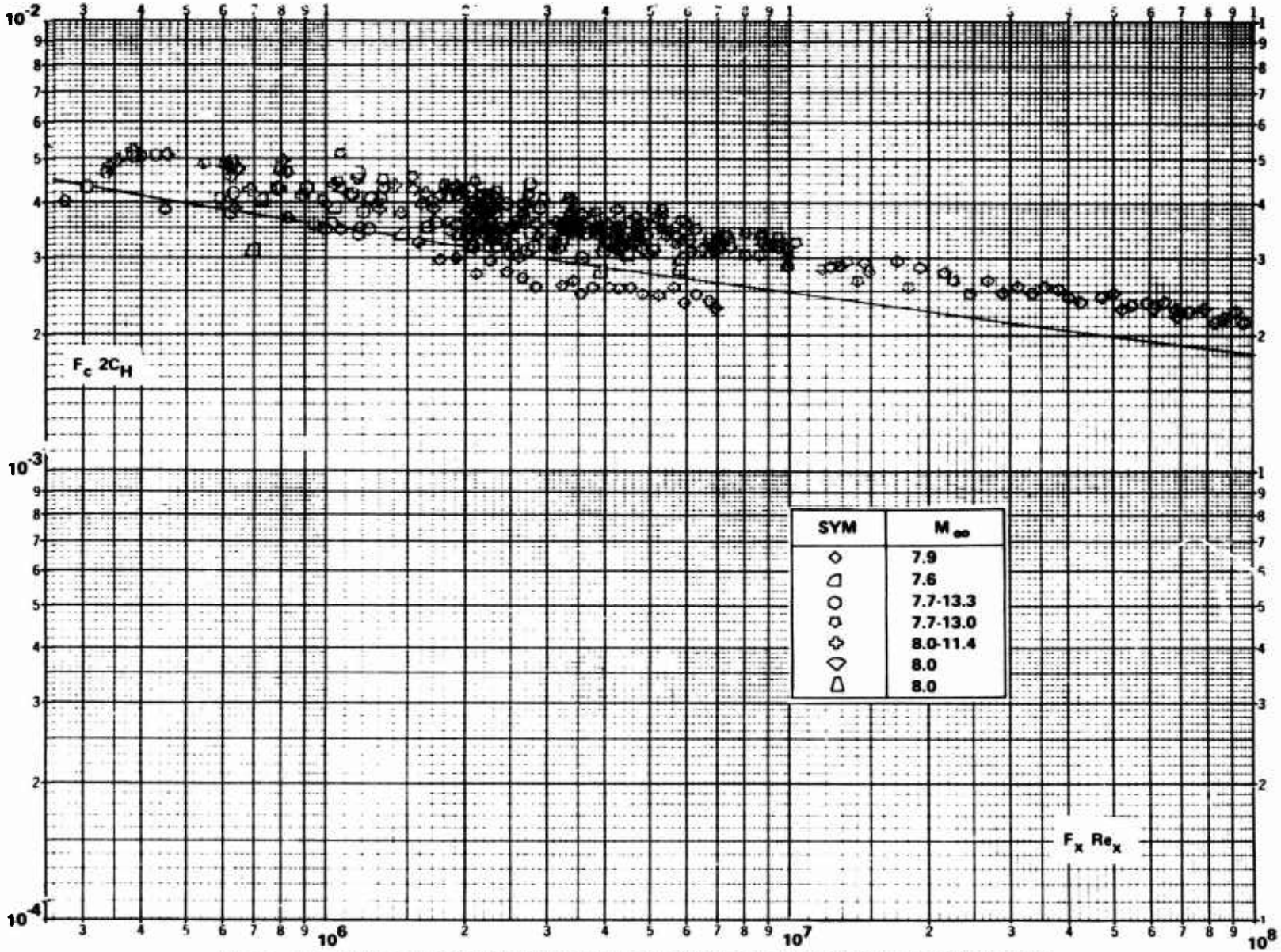


Figure 36c COMPARISON BETWEEN THE MEASURED HEAT TRANSFER AND THE THEORY OF SPALDING-CHI ON SHARP CONES ($X_V = 0$ AT $\theta_B + \theta_{BE/2}$)

SECTION V

EXPERIMENTAL STUDIES OF SHOCK WAVE-TURBULENT BOUNDARY LAYER INTERACTION

1. INTRODUCTION

The complexity of regions of shock wave-turbulent boundary layer interaction makes it essential that information from experimental observations and measurements be used to construct realistic models of the basic interaction and the turbulent transport mechanisms, which control the detailed structure of these flows. A feature of turbulent interaction regions which presents particular difficulties for both theoreticians and experiments arises because of the inherent bi-model structure of the boundary layer. The laminar sublayer in regions of shock wave-turbulent boundary layer interaction in high speed flow is of particular significance because it is within this region disturbances are first propagated upstream, and in this region, a region of reverse flow is first established. Clearly, the importance of this region is a function of the sublayer thickness, and for a given Mach number and Reynolds number is largest under adiabatic wall conditions. To construct simple models of turbulent interaction regions, the theoretician first needs to determine the mechanism of upstream influence through the boundary layer. Here a central issue revolves about whether a boundary layer subjected to a distrubance, responds upstream of the disturbance in such a way that a mutual and self-sustaining interaction between the viscous and inviscid flow takes place. If such a mechanism occurs, is it independent of the nature of the downstream disturbance, does the disturbance trigger a free interaction process? While for laminar interactions in supersonic flows experiments have verified analytical techniques based on free-interaction models for turbulent flows, the situation is not as well defined. While the measurements of Bogdonoff and Kepler in shock-induced and step-induced turbulent separated flows indicate that the pressure distribution in the separation region is independent of the agency-promoting separation, the result was not confirmed in extensive studies by Chapman, Kuehn and Larson. In more recent studies of both shock- and wedge-induced separated regions in hypersonic flows, Holden

found that these flows exhibit free interaction phenomena at the low end of the Mach number range. However, at Mach numbers greater than 10, where the length of the interactions were small compared with the initial thickness of the boundary layer, the forms of the pressure, skin friction and heat transfer distributions in shocks and wedge-induced interaction regions with equal pressure rises exhibit measureable differences.

While basic models of the turbulent interaction process must be sought by theoreticians who use some form of the first or second order boundary layer equations to describe the development of the viscous layer, this problem does not confront those who attempt to solve the time dependent Navier Stokes equations. Rather these problems are replaced by problems involving the numerical technique and mesh size used in the computation. However, the common element to all approaches which attempt to describe, in some detail, attached and separated regions resulting from shock wave-turbulent boundary layer interaction is the necessity to model turbulence. A key problem in modelling and interpreting measurements made in such regions revolves about an understanding of how the properties of turbulence develop through and downstream of transition, and in regions of strong pressure gradients and flow separation. While these problems are difficult enough at low Mach numbers, at Mach numbers above 5 we are confronted with new questions which center about phenomena which might be classed under the collective title "turbulent compressibility effects". The development and relaxation of turbulence through the transition region may also be strongly influenced by compressibility effects because strong pressure disturbances are generated in this region.

In this program, we have performed experimental studies designed to examine in detail some of the phenomena discussed above so that we may more accurately describe and understand the characteristics of attached and separated turbulent interaction regions. Here we sought not only to obtain information which we can use to better model such flows, but also planned to generate sets of measurements of sufficient detail that they can be used to evaluate theoretical models of these flows, for example solutions to the time-dependent form of the Navier Stokes equations. While this latter

technique does not require a specific flow model, the numerical codes and, of course, the turbulence modelling remain a subject for research.

One approach which can be taken to examine whether the free interaction modelling is a valid concept is to compare the distribution of properties and salient features of attached and separated interactions promoted by widely different disturbances. In this study we have compared the distributions of skin friction, heat transfer and pressure in the separation, plateau pressure and reattachment regions of shock and wedge-induced flows. The pressure rise to separation, the plateau pressure, the reattachment pressure and heat transfer are distinctive features of shock- and wedge-induced flow which can be readily compared. In addition to providing information against, which to test the flow models, empirical correlations of such measurements provide an important guide to the designer where numerical solutions are unavailable, too costly or unnecessary.

In laminar two-dimensional flows, incipient separation is defined as a condition where the interaction strength is sufficient to induce a condition where skin friction is zero at one point only in the interaction region. Turbulent interaction regions are more complex and our studies reveal that the time wise variation of skin friction at conditions close to incipient separation is a significant feature. Thus, we have defined incipient separation in our studies as the condition when the time-average of the skin friction is zero. A discussion of the definition of incipient separation in terms of properties used to define it is given together with comparisons between measurements made in earlier studies in Section 5.5. The influence of Reynolds number on the occurrence and scale of a turbulent interactions has been a subject of controversy within the past several years because of conflicting results from researchers where experiments closely resembled one another. A discussion of the Reynolds number effects is given in Section 5.4. A characteristic feature of shock- or wedge-induced turbulent separated regions in hypersonic flow is an unsteadiness which stems, it is believed, from the shock-turbulence interaction. While the magnitude of the pressure fluctuations are of such proportions that they warrant detailed investigation from a

structural engineering viewpoint, the gross unsteadiness of the turbulent separated regions poses serious questions on the validity of modelling those flows without including these unsteady characteristics. Finally, measurements of heat transfer, pressure and skin friction obtained in our studies are compared with solutions to the time-dependent Navier Stokes equations obtained by Baldwin using the MacCormack formulation.

2. DISTRIBUTIONS OF PROPERTIES IN WEDGE AND SHOCK-INDUCED INTERACTION REGIONS

A major purpose of this experimental program was to investigate whether there is a reversal in the variation of the length of a separated interaction region, as well as pressure rise to induce incipient separation, with Reynolds number (Re_δ) in the range $10^5 \leq Re_\delta \leq 10^7$. Earlier experimental studies of boundary layer separation on tunnel walls and models mounted within the test core show conflicting trends with Reynolds number. While measurements on models mounted in the test core indicated that increasing Reynolds number increased the size of a separated region or made the boundary layer easier to separate (a trend similar to that observed for laminar boundary layers), the reverse trend was noted for turbulent separated regions on tunnel walls. In general the experiments performed on tunnel walls were at larger Reynolds numbers (based on the local boundary layer thickness) than those for models mounted within the test core. This suggests that the absolute Reynolds number may be an important parameter. However, comparisons between measurements in separated regions induced on walls of different facilities by the same strength of interaction differed in structure. This suggests some influence of three-dimensional effects on these interaction regions. Three-dimensional effects should be at a minimum at incipient separation. Since a reverse in the trend of the variation of incipient separation with Reynolds number is also observed in these studies, we are inclined to believe this reversal is connected with changes in the structure of the turbulent boundary layer upstream of the interaction region or with the viscous-inviscid interaction mechanism. Theoretical and experimental studies by Bushnell et al.[42] have indicated that turbulent boundary layers on tunnel walls can be far out of fluid dynamic equilibrium close to the exit plane of the nozzle.

In fact their studies show that one must travel at least one thousand boundary layer thicknesses downstream of this point before remnants of the boundary layer on the nozzle wall are dissipated and the boundary layer approaches local self-similarity. Few experiments performed on tunnel walls fall within 1000 δ's from the exit plane, and thus precise effects of the distortion of the velocity profile resulting from nonsimilarity on turbulent separation remain to be determined.

In our test program in the Calspan 96-inch Shock Tunnel, regions of shock- and wedge-induced attached and turbulent separated regions have been studied. Figure 37 is a photograph of the model in the flat plate configuration installed in this tunnel. This model is similar to that used in our earlier studies of turbulent flows, but was completely redesigned with almost an order of magnitude increase in the density of instrumentation in the interaction regions. The model contained over 200 pieces of instrumentation distributed between three leading edge plates, a center section of the model, and a flap or wedge section. Figure 38 shows the installation of the instrumentation in the wedge and center section of the model. Because loads of several tons are imposed impulsively upon the model during starting and stopping of the tunnel, the skin friction gages are shock-mounted, and extensive measures are taken to prevent extraneous signals from acceleration or cable movements. Because of the severity of the fluctuating flow field in the reattachment region under some conditions the skin friction gages there were torn apart, again underscoring the importance of the reattachment region in both the thermal and mechanical design of hypersonic re-entry vehicles.

Wedge-Induced Separated Flows--The development of a turbulent separated region with increasing interaction strength is shown with the aid of Schlieren photographs and pressure distributions in Figures 39a and b. Figures 40, 41 and 42 show in detail the development of the heat transfer and pressure distributions with interaction strength, for three values of the Reynolds number at beginning of the interaction. Here, as in our earlier studies,[43] there is almost no upstream influence ahead of the compression surface before separation is induced in the interaction region. The separation bubble



Figure 37. FLAT PLATE - WEDGE MODEL

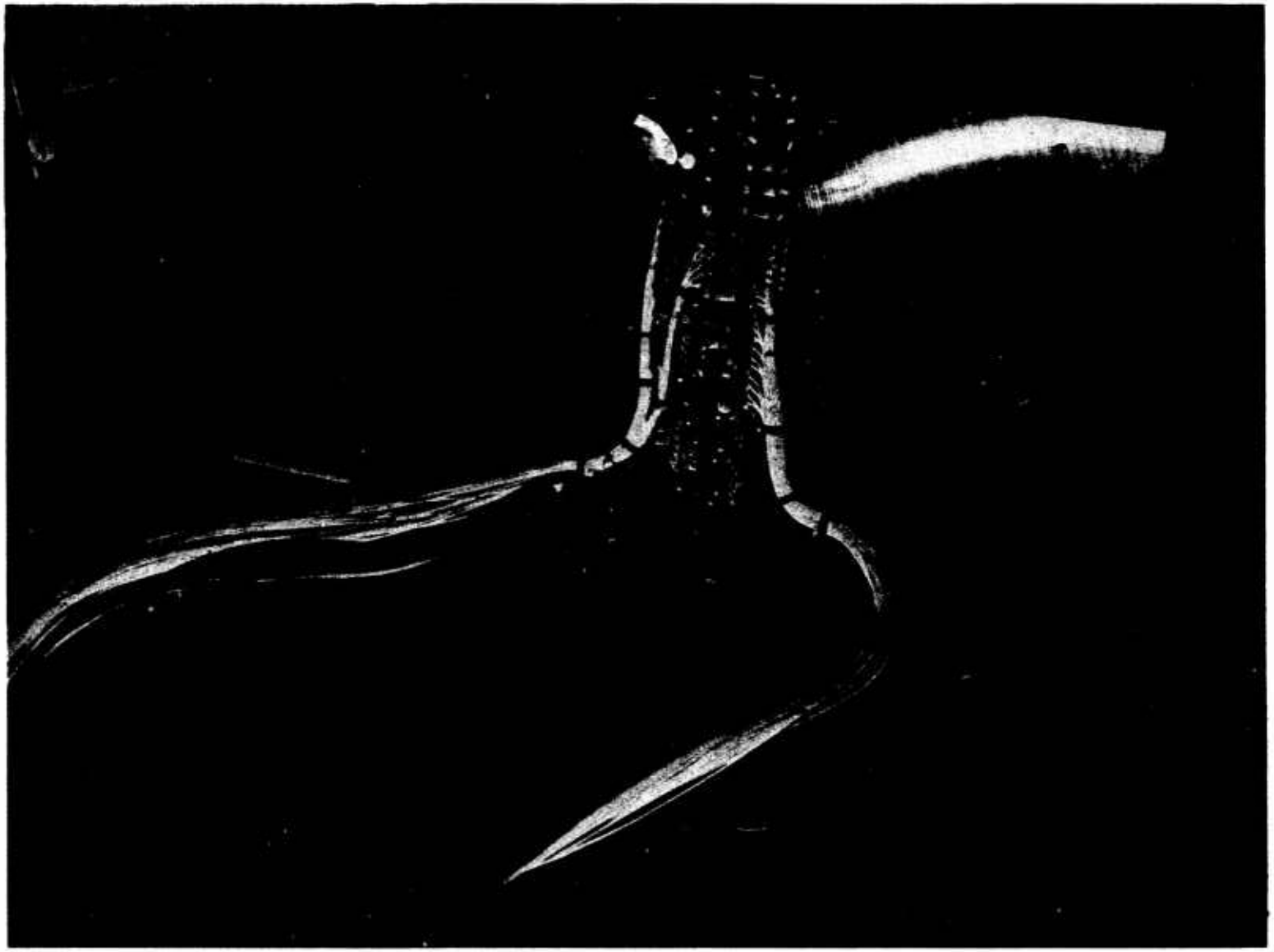


Figure 38a. FLAT PLATE MODEL INSTRUMENTATION

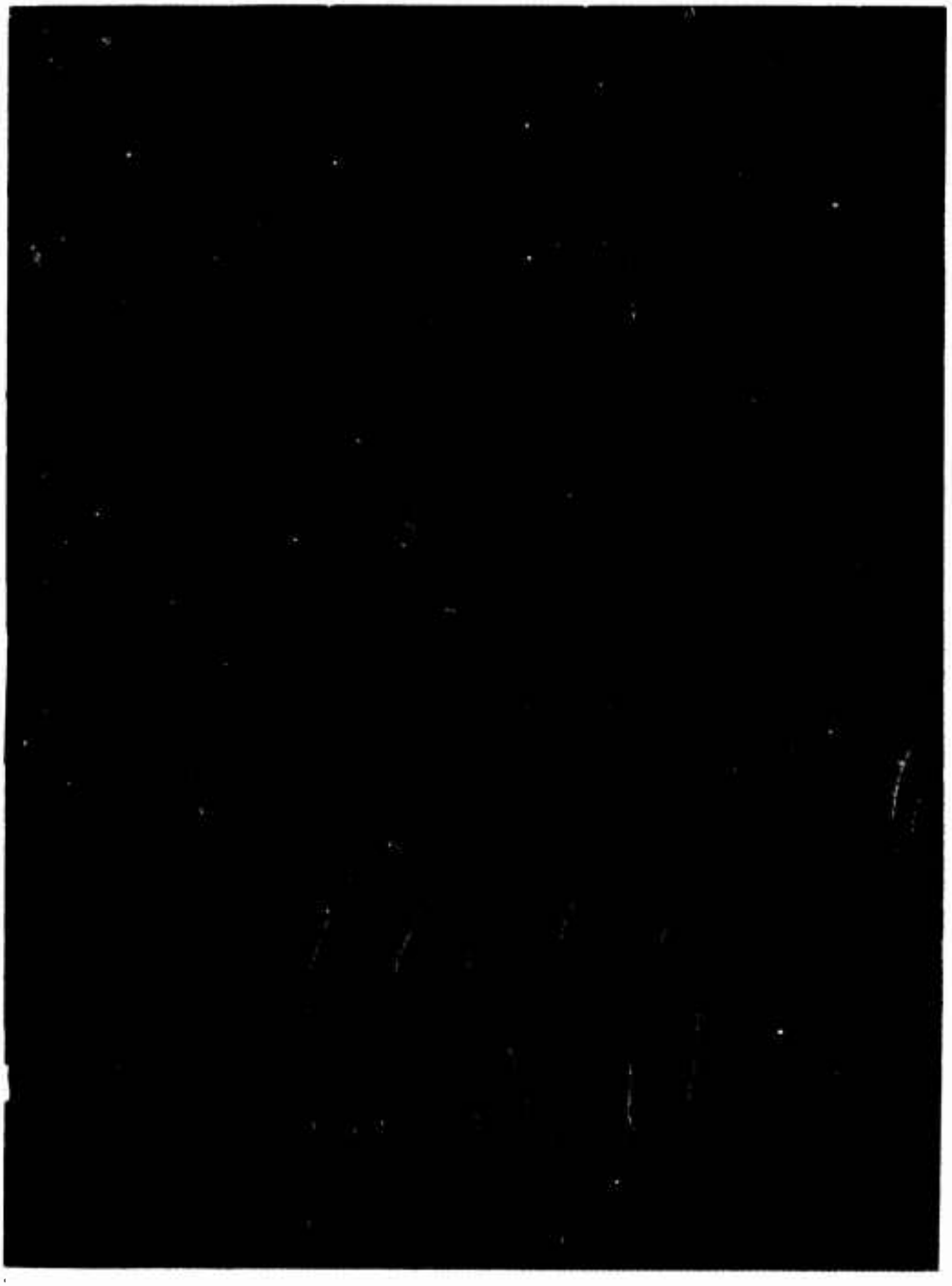
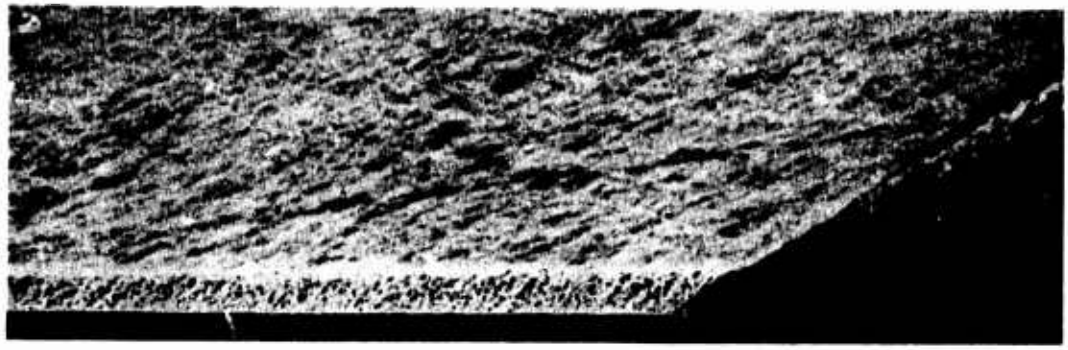


Figure 38b. FLAT PLATE MODEL - INSTRUMENTATION



RUN 10
$\theta_w = 27^o$



RUN 13
$\theta_w = 30^o$



RUN 17
$\theta_w = 33^o$



RUN 23
$\theta_w = 36^o$

Figure 39a. VARIATION OF THE SIZE OF THE INTERACTION REGION WITH STRENGTH OF INTERACTION ($M_\infty = 8.6$; $Re_\delta = 1.4 \times 10^6$)

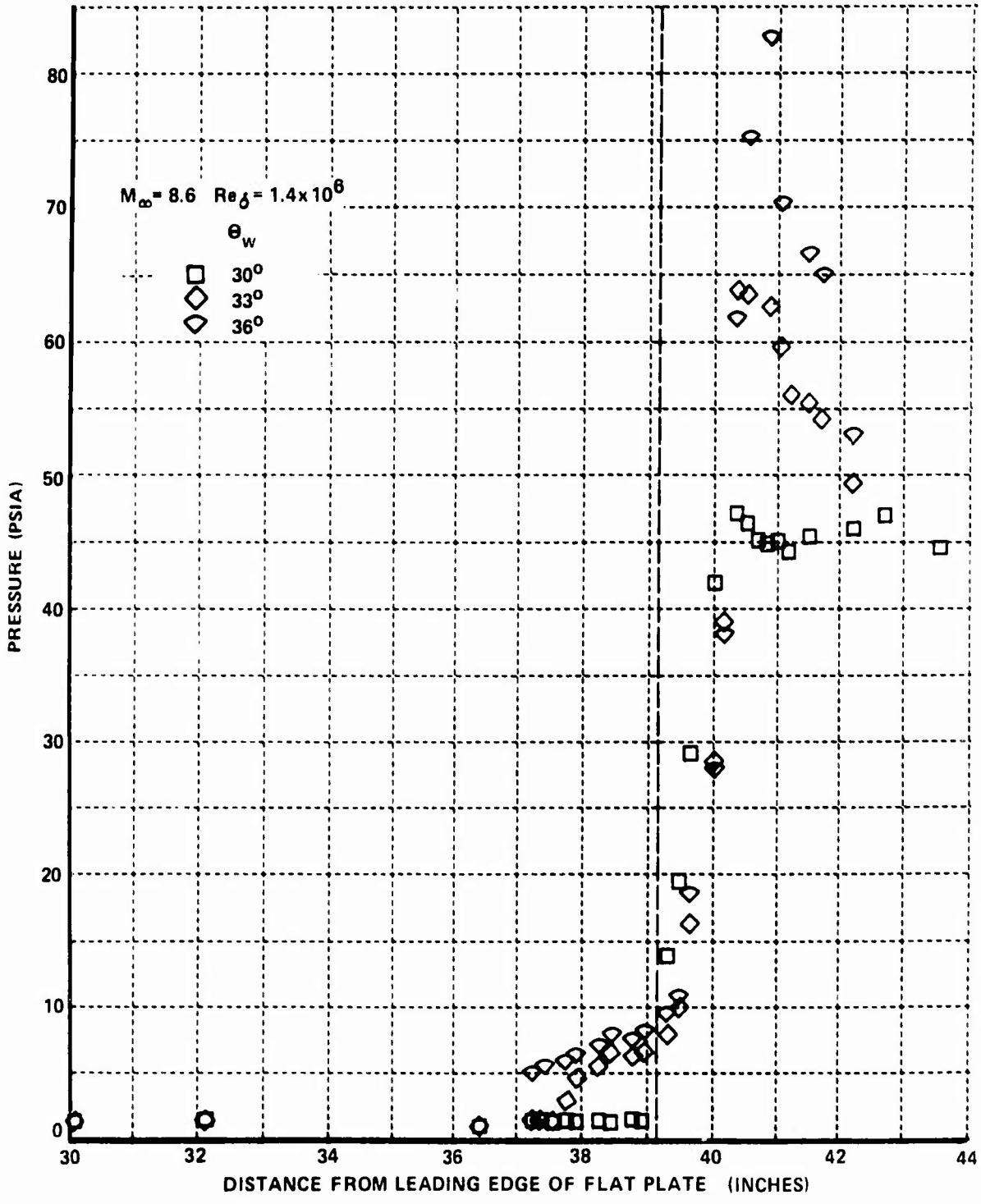


Figure 39b. VARIATION OF PRESSURE DISTRIBUTION WITH INTERACTION STRENGTH

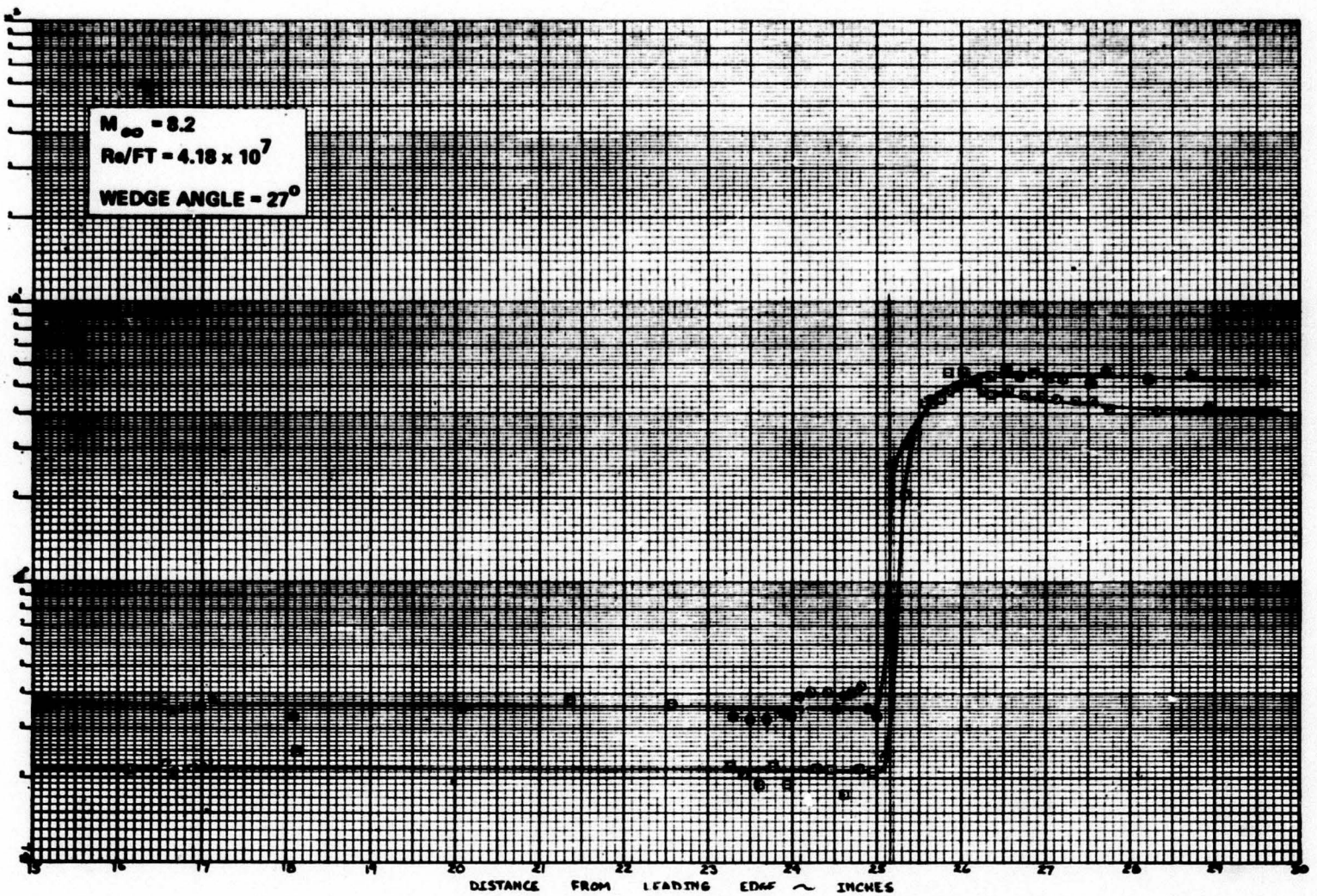


Figure 40a. DISTRIBUTION OF HEAT TRANSFER AND PRESSURE FOR AN ATTACHED WEDGE-INDUCED INTERACTION REGION

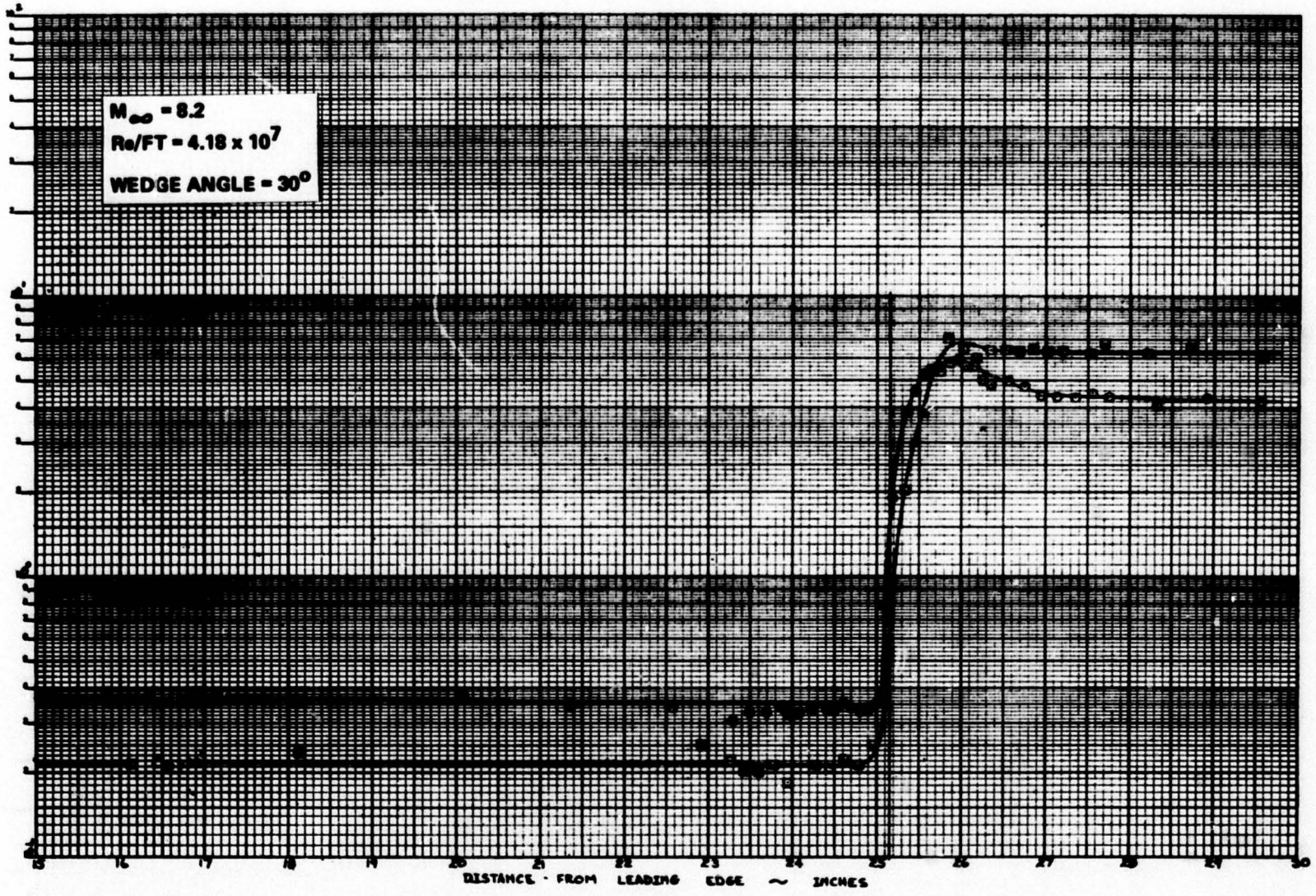


Figure 40b. DISTRIBUTION OF HEAT TRANSFER AND PRESSURE FOR AN ATTACHED WEDGE-INDUCED INTERACTION REGION

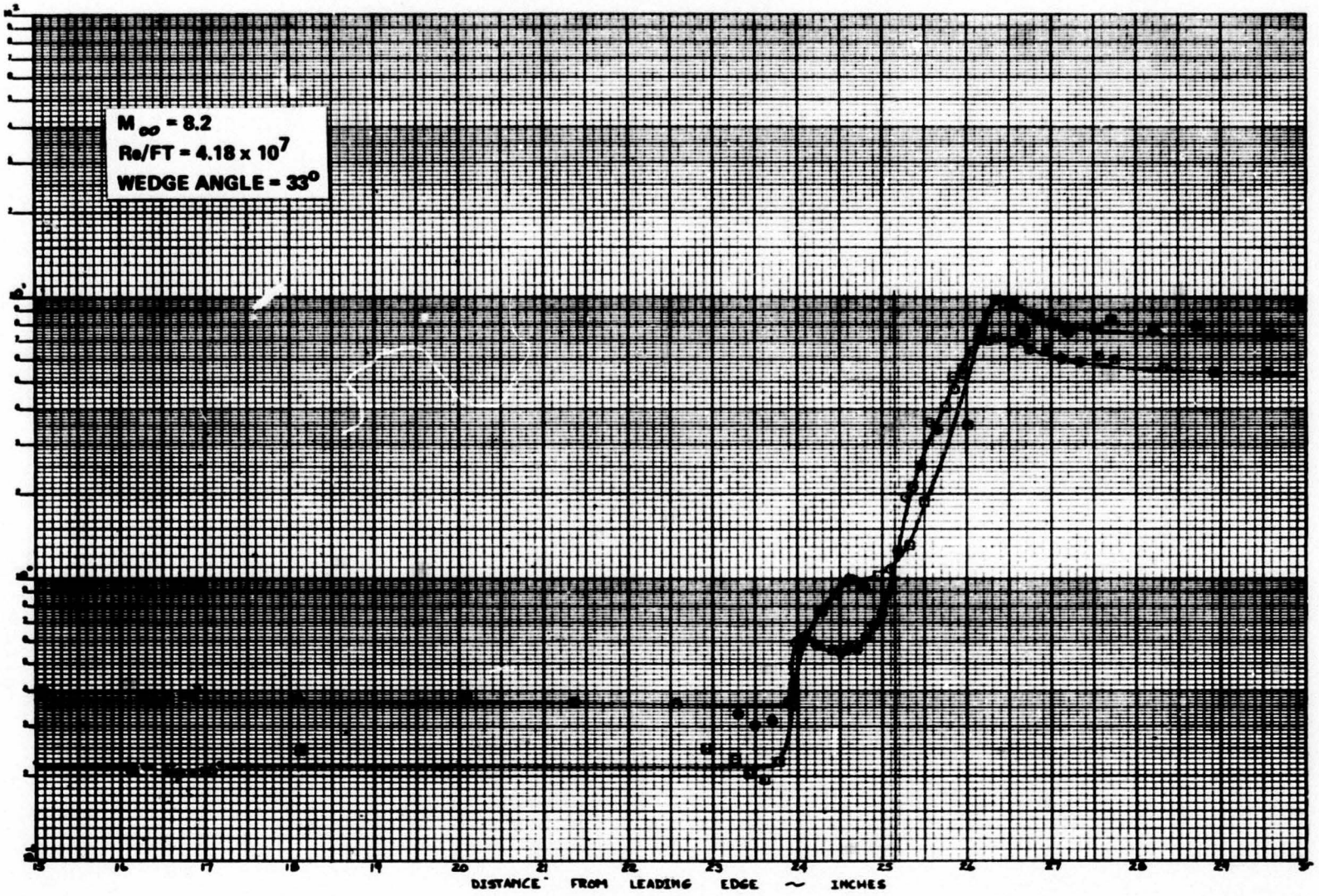


Figure 40c. DISTRIBUTION OF HEAT TRANSFER AND PRESSURE IN A SMALL SEPARATED REGION IN WEDGE-INDUCED FLOW

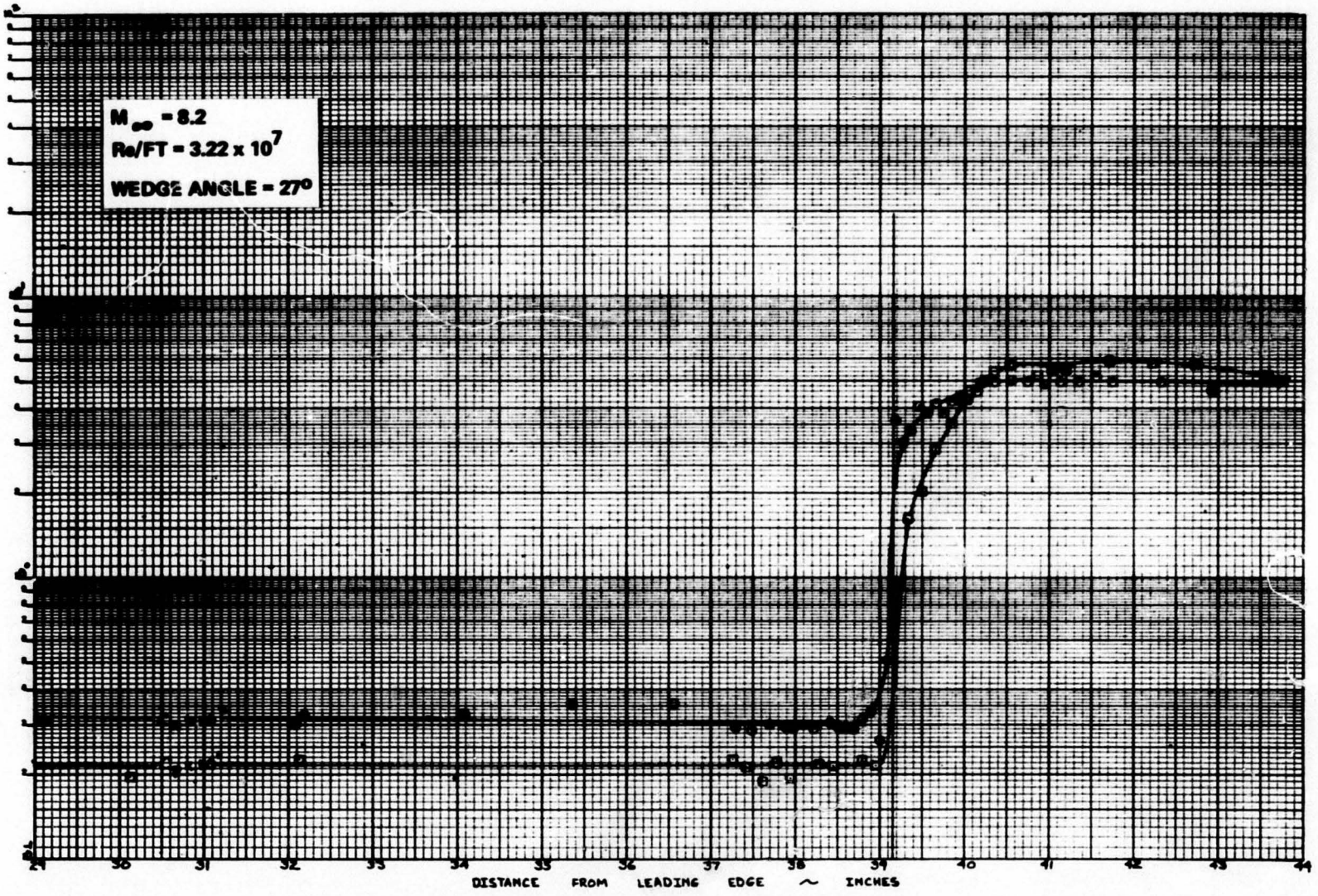


Figure 41a. DISTRIBUTION OF HEAT TRANSFER AND PRESSURE IN AN ATTACHED WEDGED INDUCED INTERACTION REGION

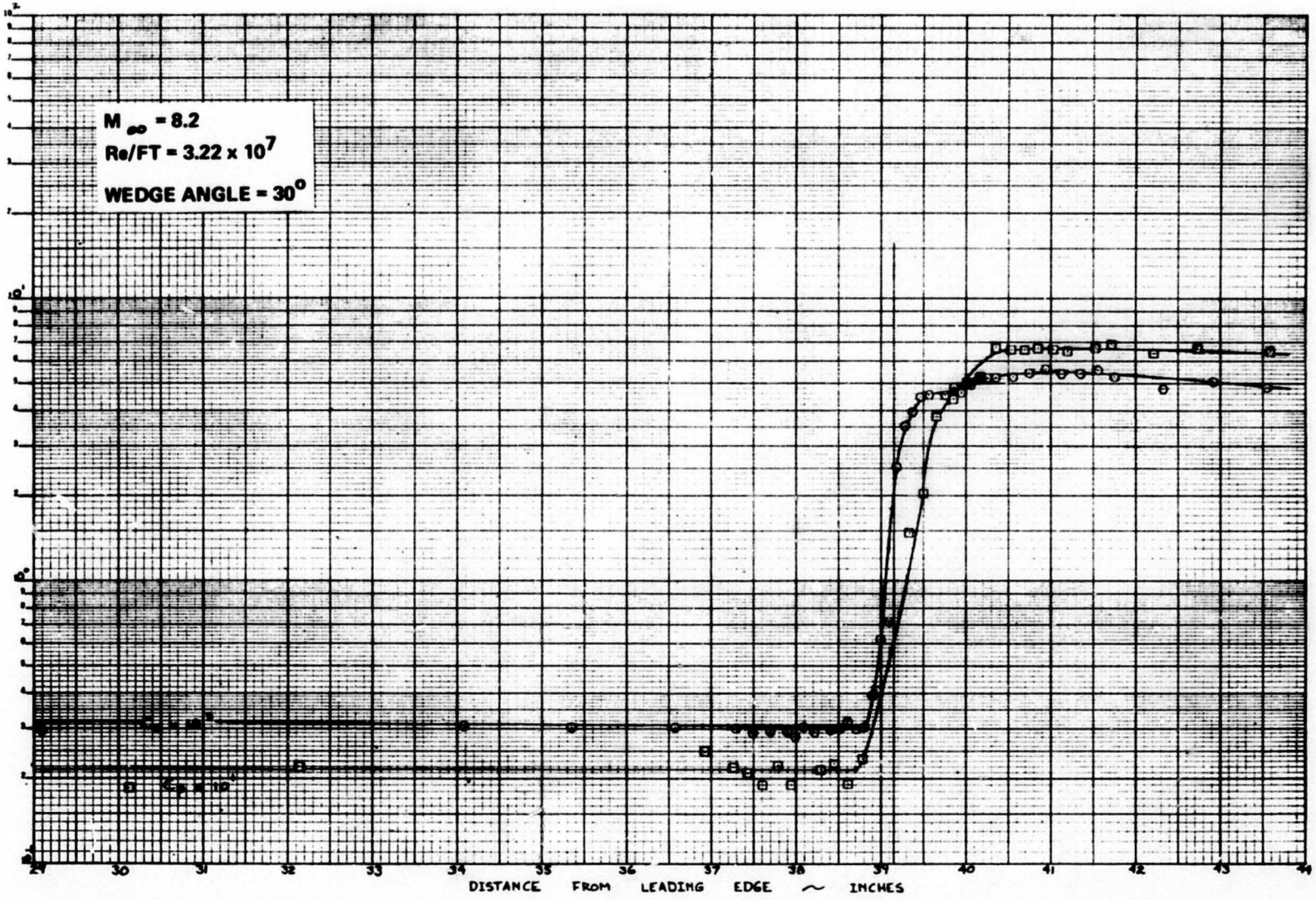


Figure 41b. DISTRIBUTION OF HEAT TRANSFER AND PRESSURE IN AN ATTACHED WEDGE - INDUCED INTERACTION REGION

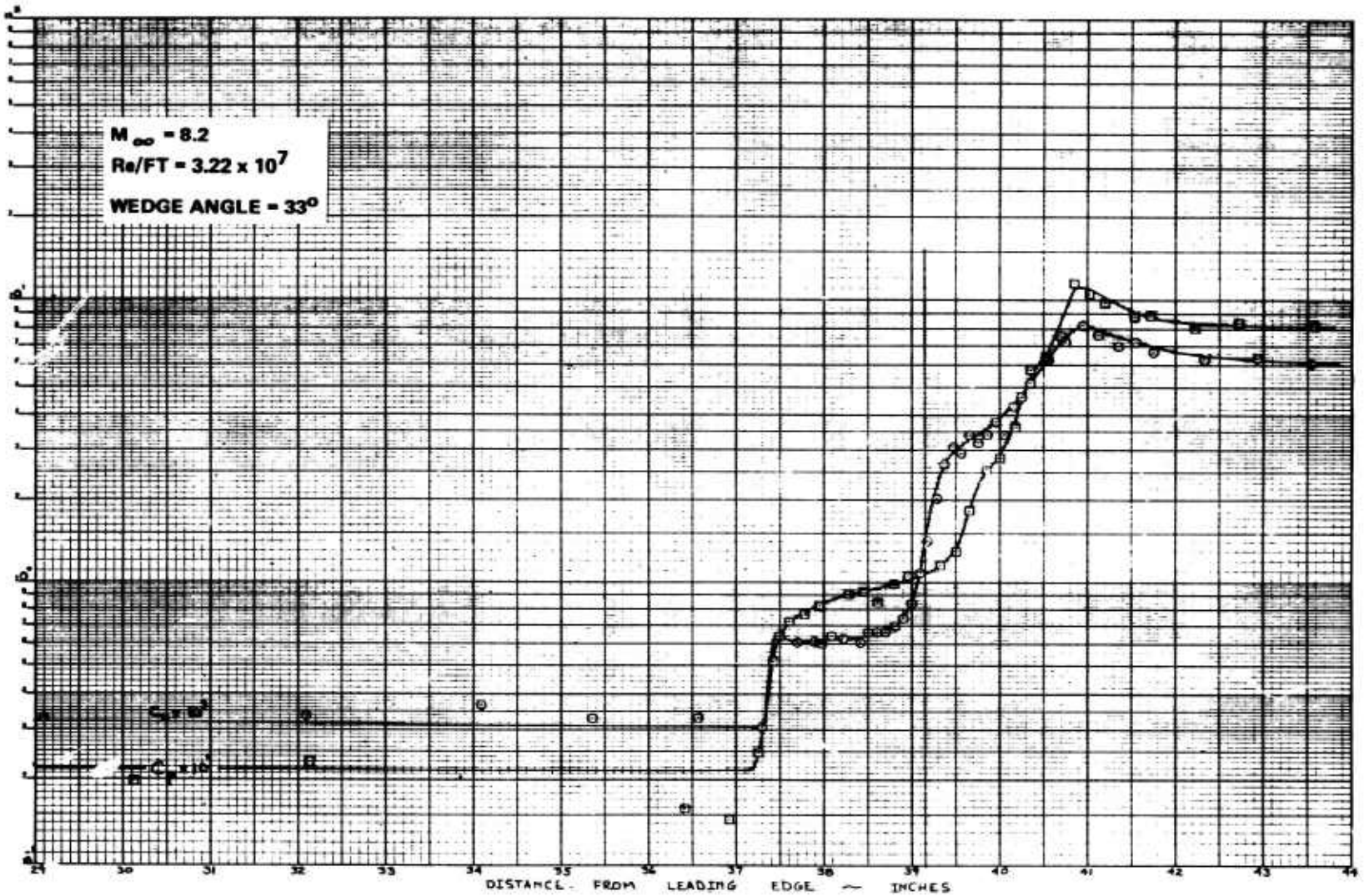


Figure 41c. DISTRIBUTION OF HEAT TRANSFER AND PRESSURE IN A SEPARATED WEDGE-INDUCED INTERACTION REGION

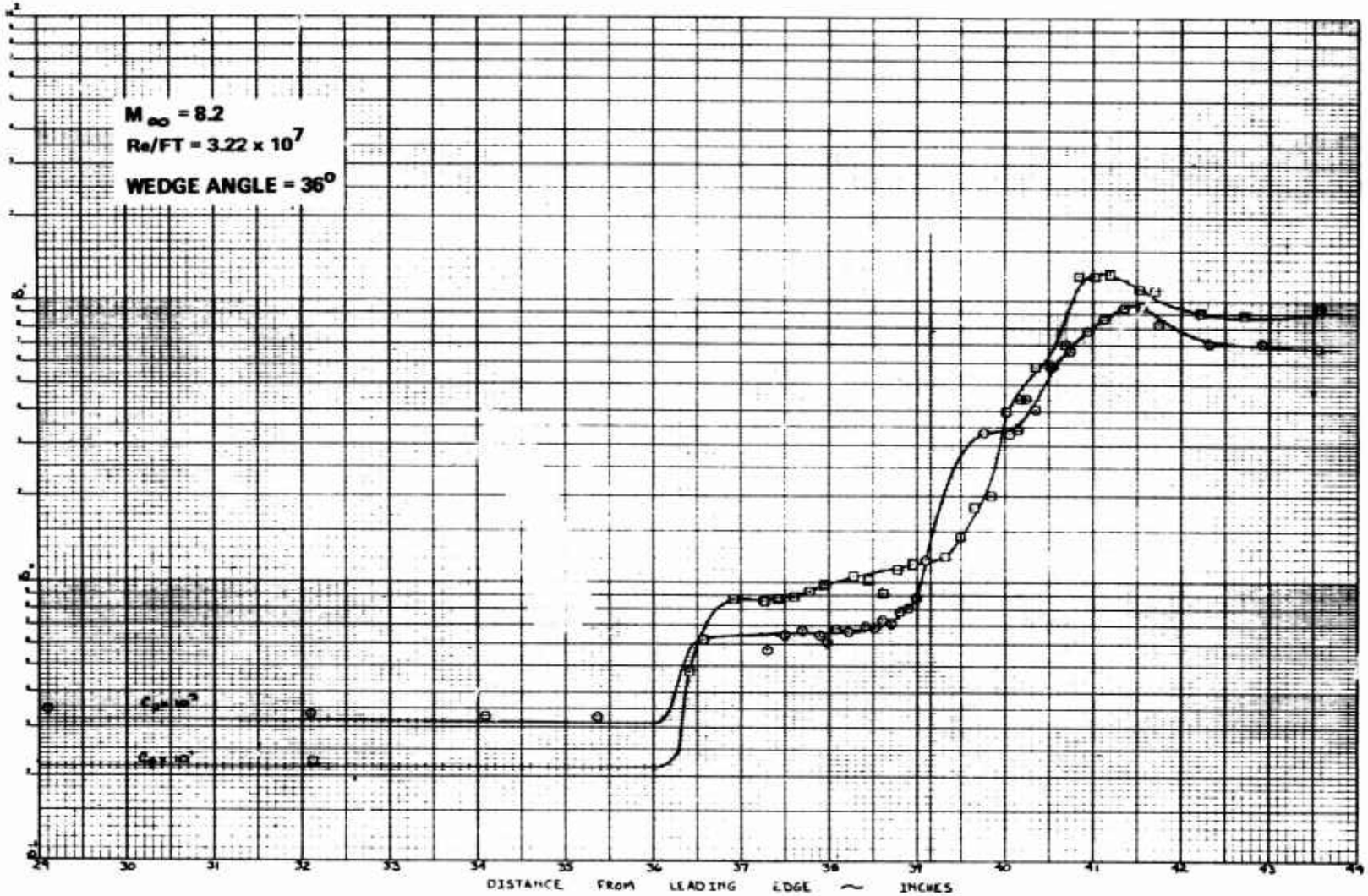


Figure 41d. DISTRIBUTION OF HEAT TRANSFER AND PRESSURE IN A WELL SEPARATED WEDGE-INDUCED INTERACTION REGION

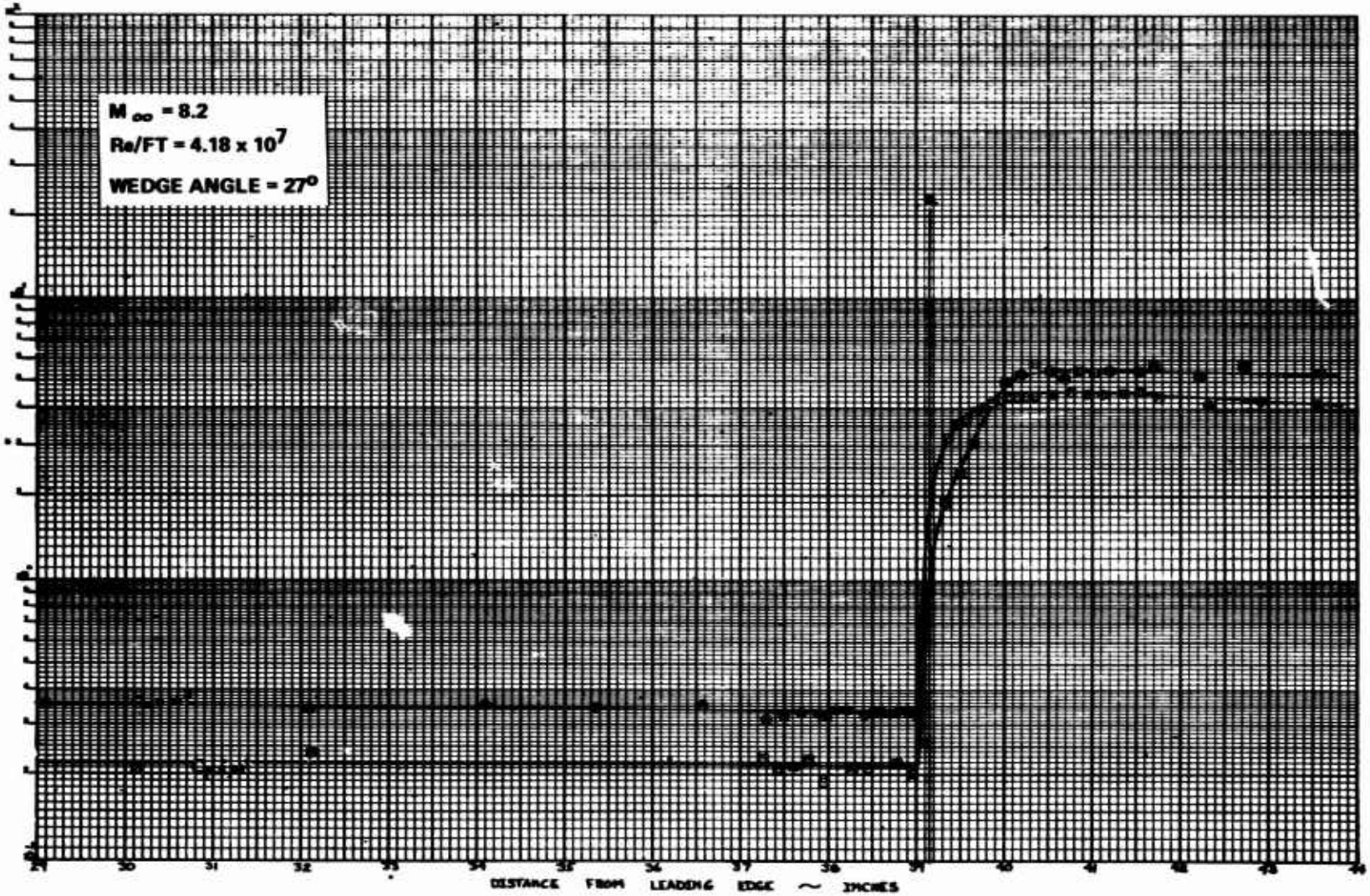


Figure 42a. VARIATION OF THE HEAT TRANSFER AND PRESSURE DISTRIBUTION WITH THE STRENGTH OF THE INTERACTION

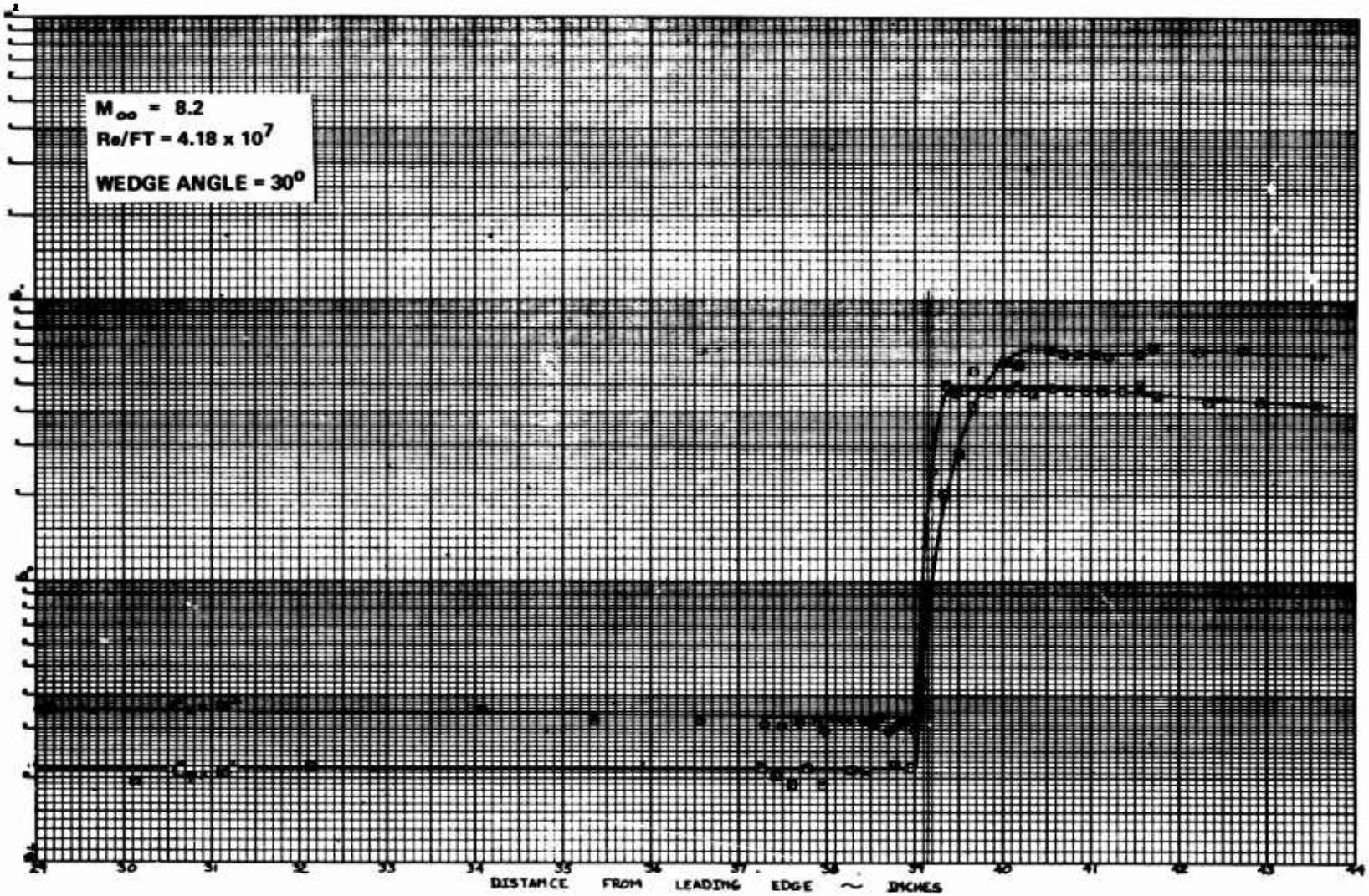


Figure 42b. VARIATION OF THE HEAT TRANSFER AND PRESSURE DISTRIBUTION WITH THE STRENGTH OF THE INTERACTION

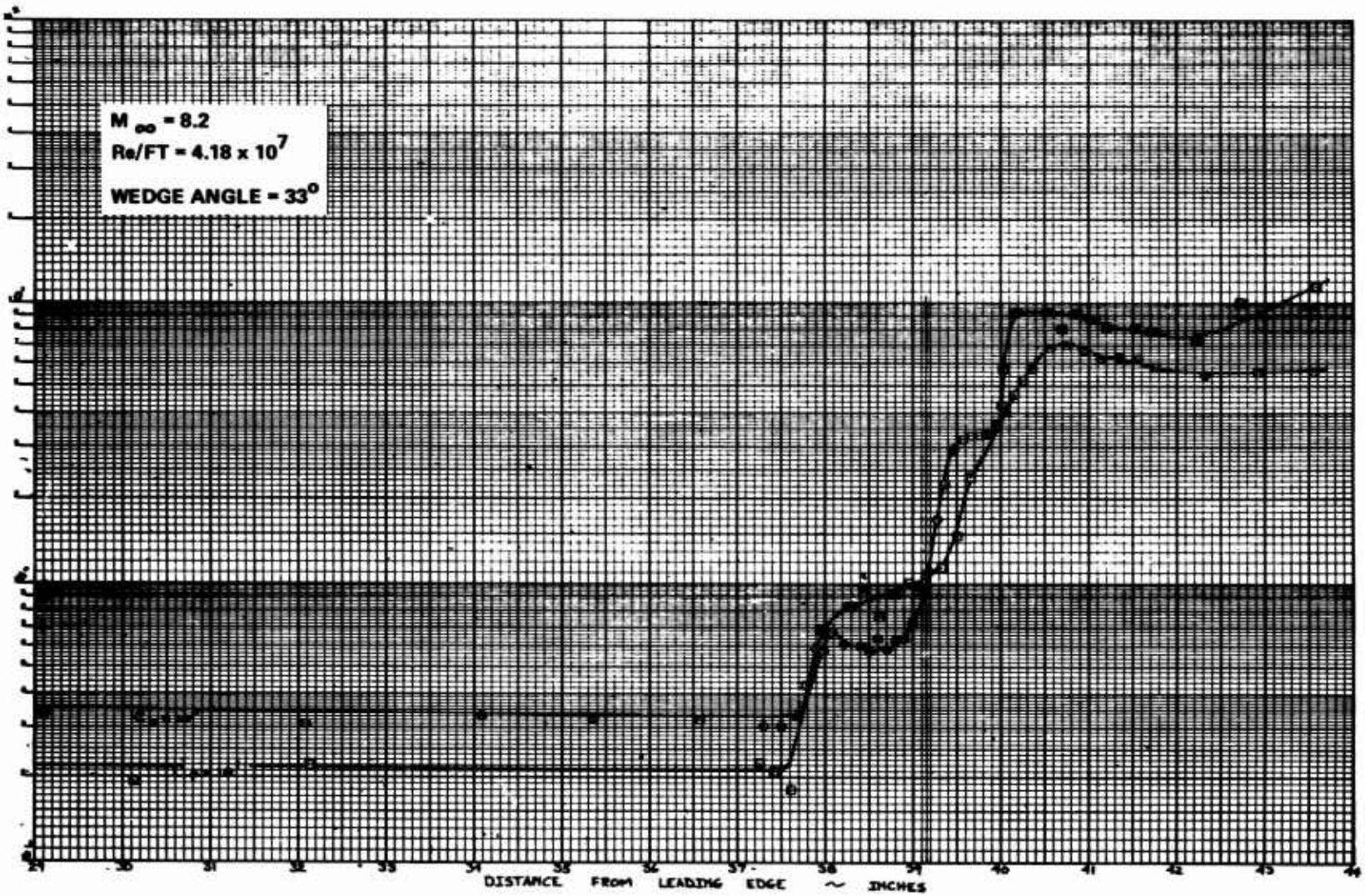


Figure 42c. VARIATION OF THE HEAT TRANSFER AND PRESSURE DISTRIBUTION WITH THE STRENGTH OF THE INTERACTION

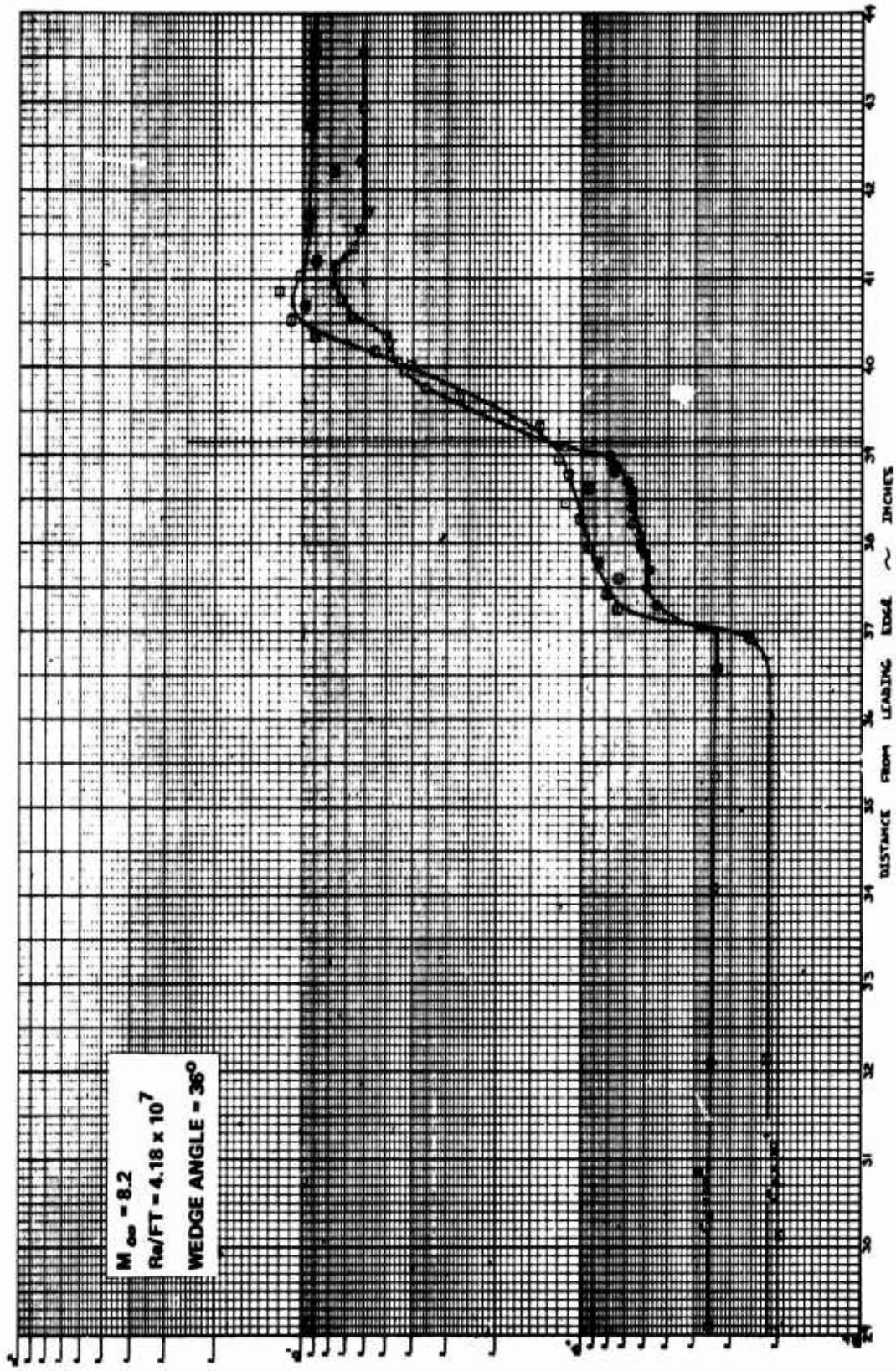


Figure 42d. VARIATION OF THE HEAT TRANSFER AND PRESSURE DISTRIBUTION WITH THE STRENGTH OF THE INTERACTION

is formed at the bottom of the boundary layer and spreads forward rapidly with increasing wedge angle. A well-defined plateau region is evident in the heat transfer and pressure distributions for large separated regions. In these flows the separation and reattachment regions occupy a length comparable with the initial thickness of the boundary layer, and thus the flows in these regions cannot be accurately described by the boundary layer equations. We found large fluctuations of pressure and skin friction in the reattachment region, and the measurements there and close to separation indicate that the separation bubble is highly unsteady.

The most important result from the present study is the reversal shown in the Reynolds number trend. Specifically, if a sufficiently large Reynolds number (based on boundary layer thickness) is reached, the R_e number trend for incipient separation and length of separated region is reversed. The variation of the length of separated region with Reynolds number based on boundary layer thickness is shown in Schlieren photographs and pressure measurements given in Figures 43a and b. Here we se that with δ approximately constant, increasing R_{e_δ} causes the separated region to decrease in size in contrast to the measurements reported in Holden[43] and earlier studies, where an increase in unit Reynolds number caused an increase in the size of a separated region. Figures 44, 45 and 46 show the effect of Reynolds number on the size of the interaction region for a range of interaction strengths. We see that at large Reynolds numbers increases Reynold number decreases the length of the interaction. This is the first time such a reversal in trend has been observed in a single experiment, though the trends we observe at high R_{e_δ}'s are in agreement with measurements on tunnel walls by Roshko and Thomke.[45] Whether this reversal results from changes in the properties of the initial boundary layer or from changes in the mechanics of the viscous-inviscid interaction process remains to be determined. However, this result has far-reaching implications from both wind tunnel simulation and theoretical modeling viewpoints.

Externally Generated, Shock-Induced Separated Flows--The previous section included Schlieren photographs and distributions of heat transfer, skin friction, and pressure for wedge-induced separated regions over a Reynolds

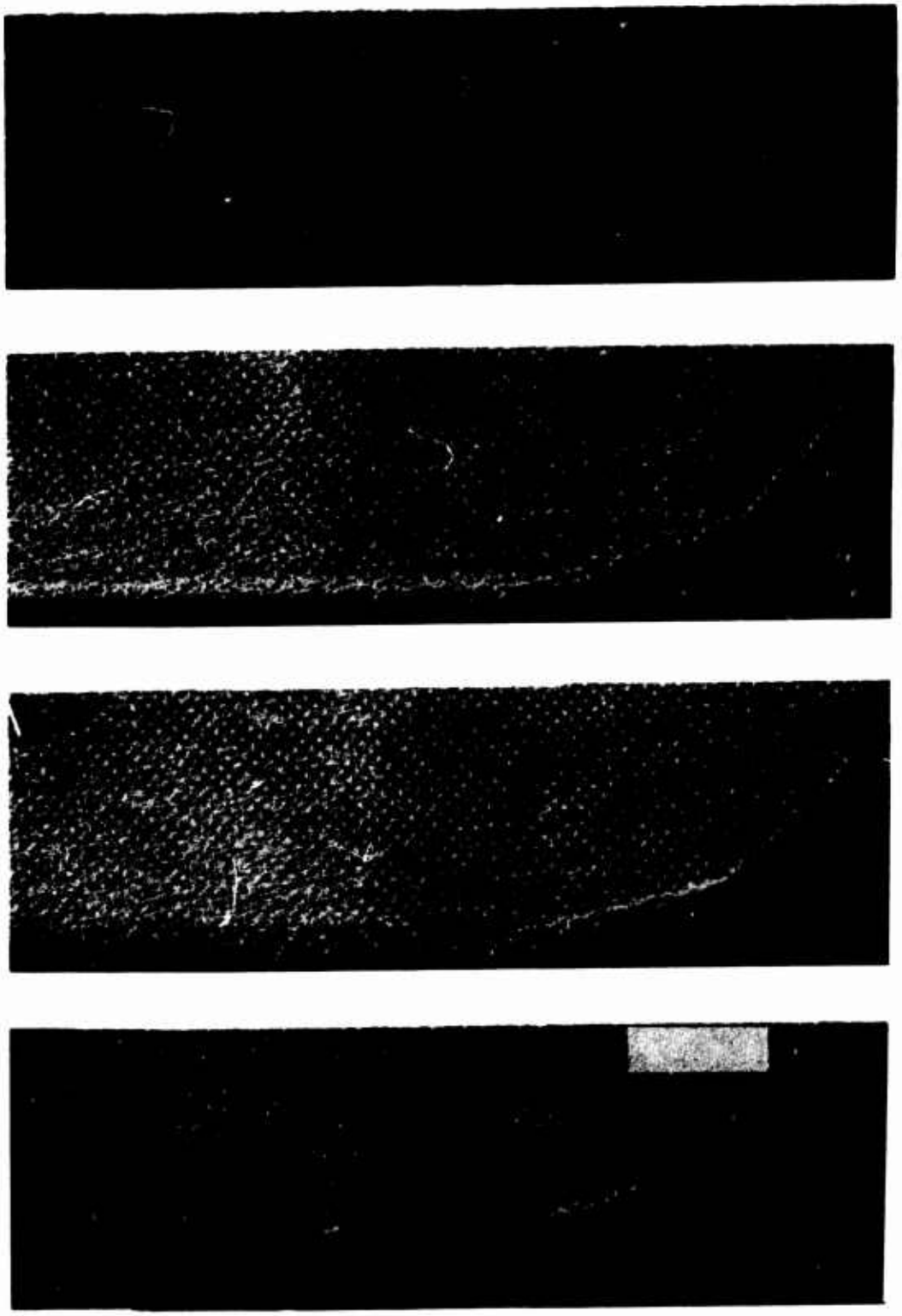


Figure 43a. VARIATION OF SIZE OF SEPARATED REGION WITH REYNOLDS NUMBER ($M_\infty = 8.6$ $\Theta_W = 33^O$)

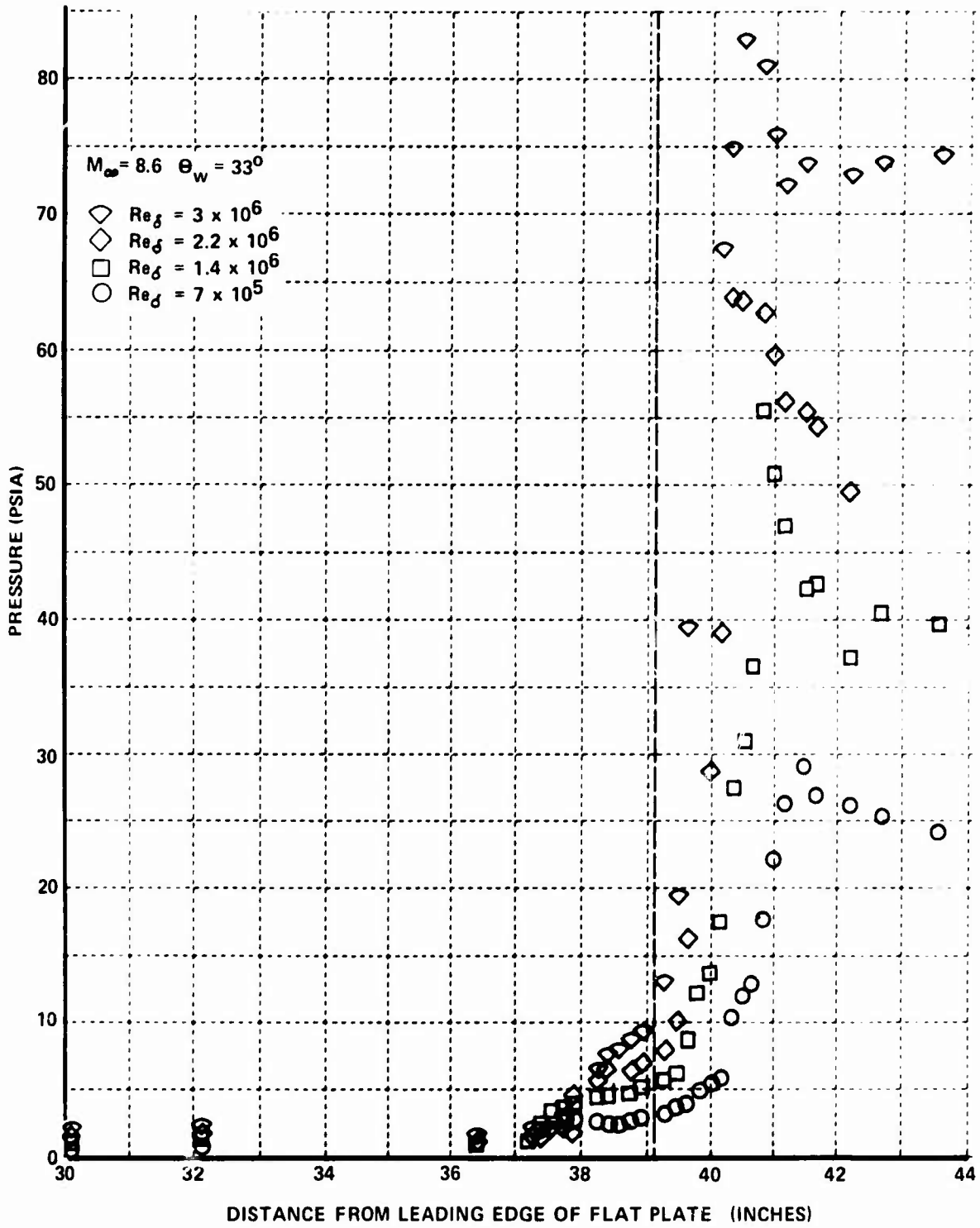


Figure 43b. VARIATION OF PRESSURE DISTRIBUTION WITH UNIT REYNOLDS NUMBER

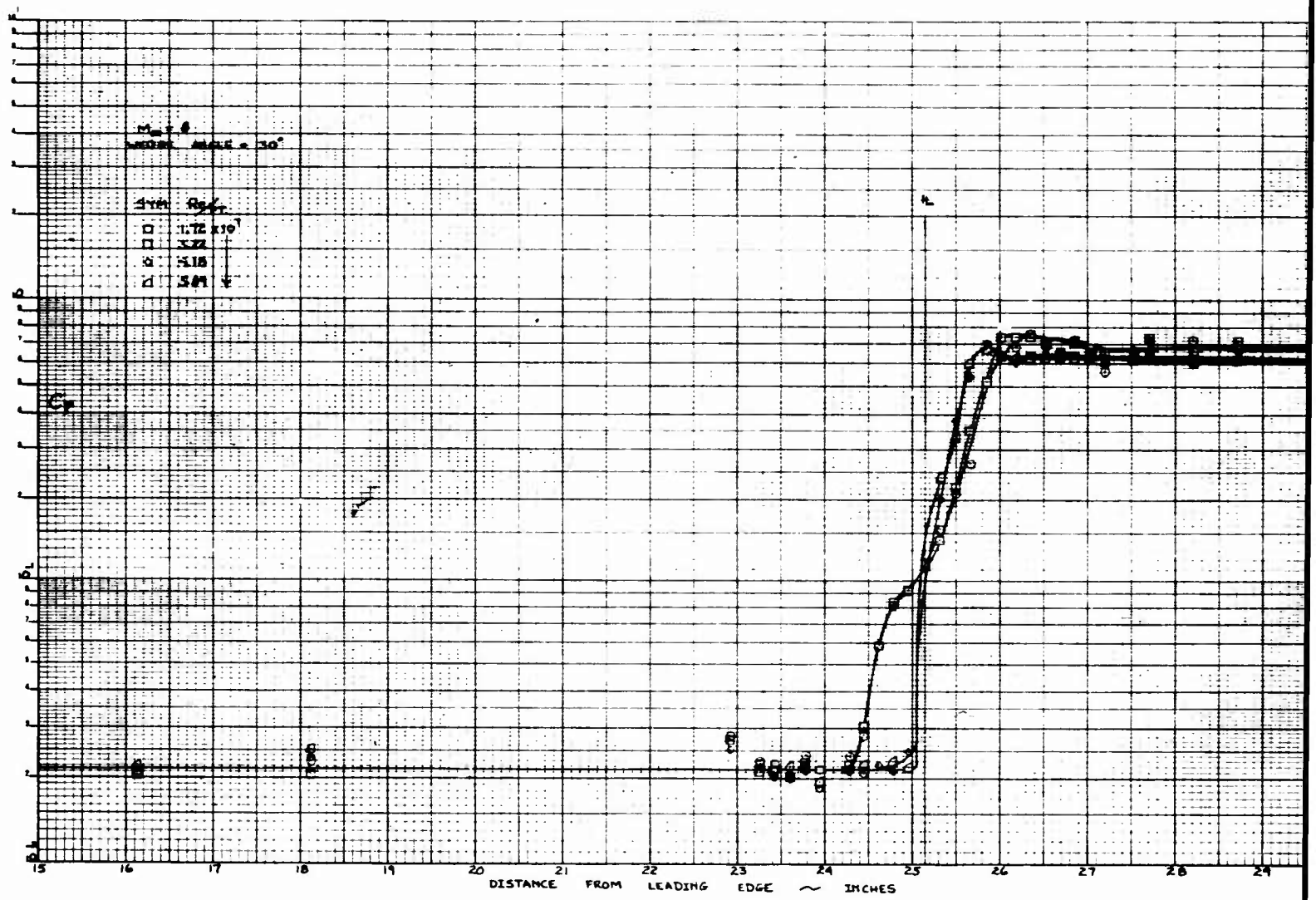


Figure 44a. VARIATION OF PRESSURE DISTRIBUTION WITH REYNOLDS NUMBER

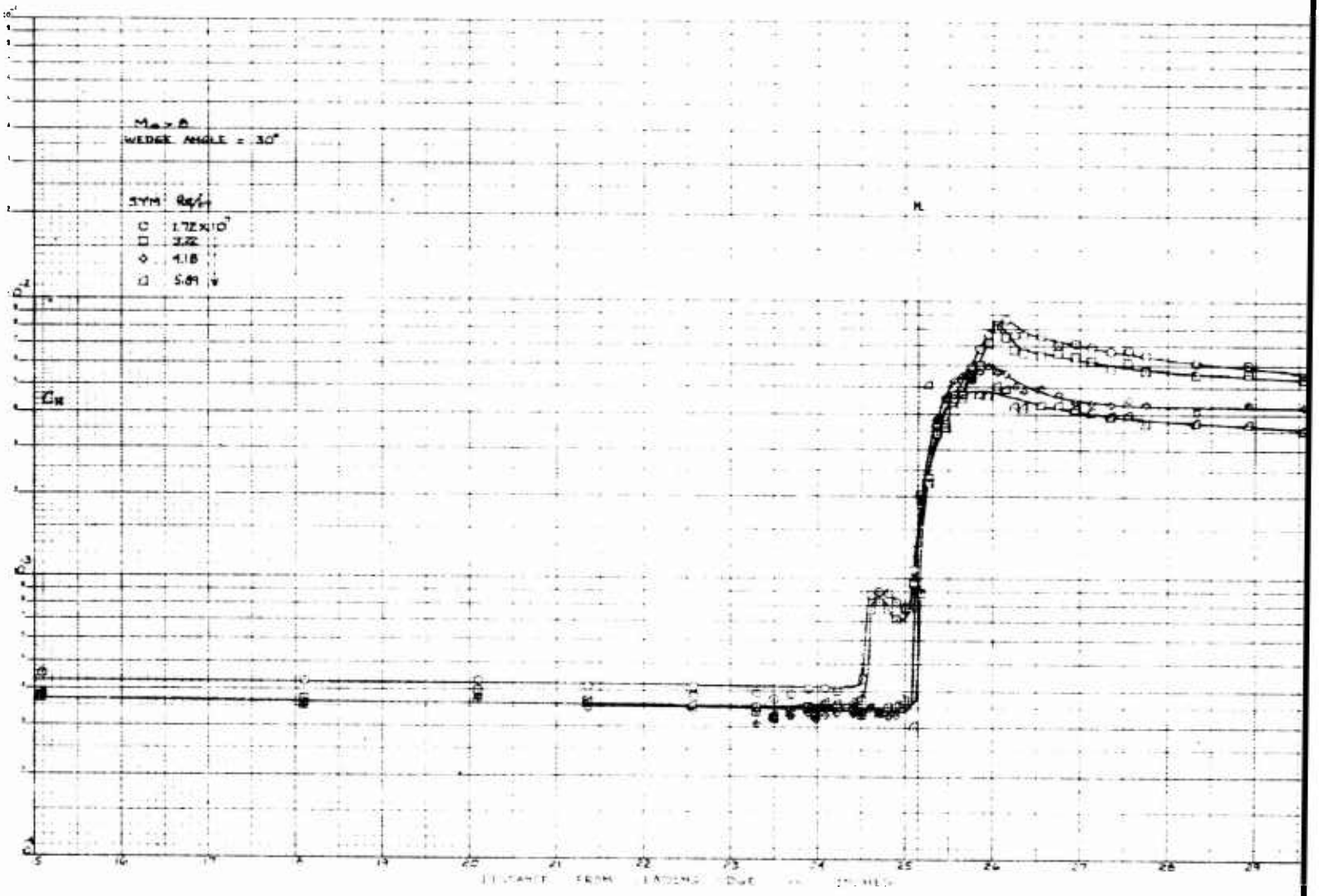


Figure 44b. VARIATION OF HEAT TRANSFER DISTRIBUTION WITH REYNOLDS NUMBER FOR A WEDGE-INDUCED INTERACTION REGION

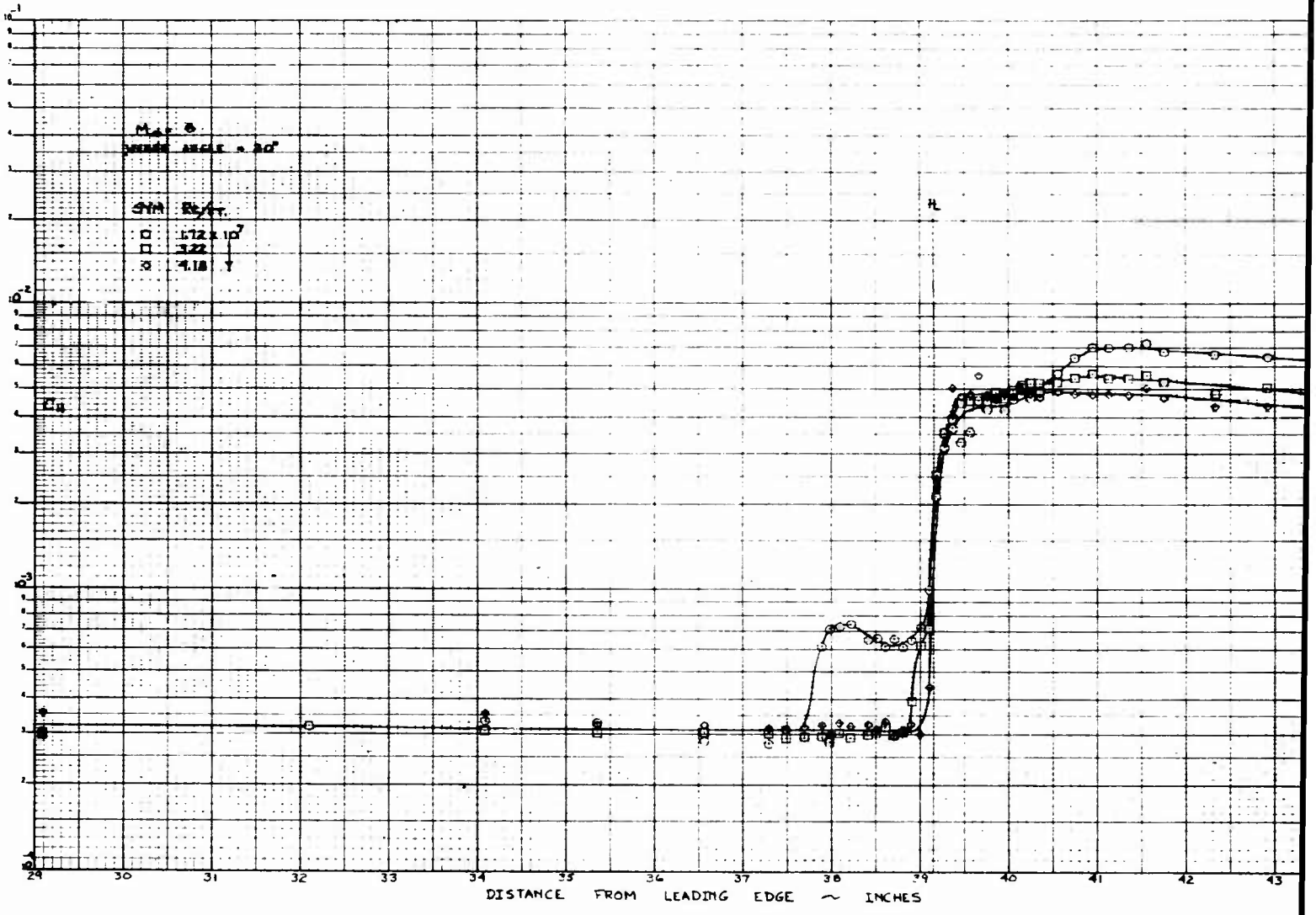


Figure 45a. VARIATION OF HEAT TRANSFER DISTRIBUTION WITH REYNOLDS NUMBER

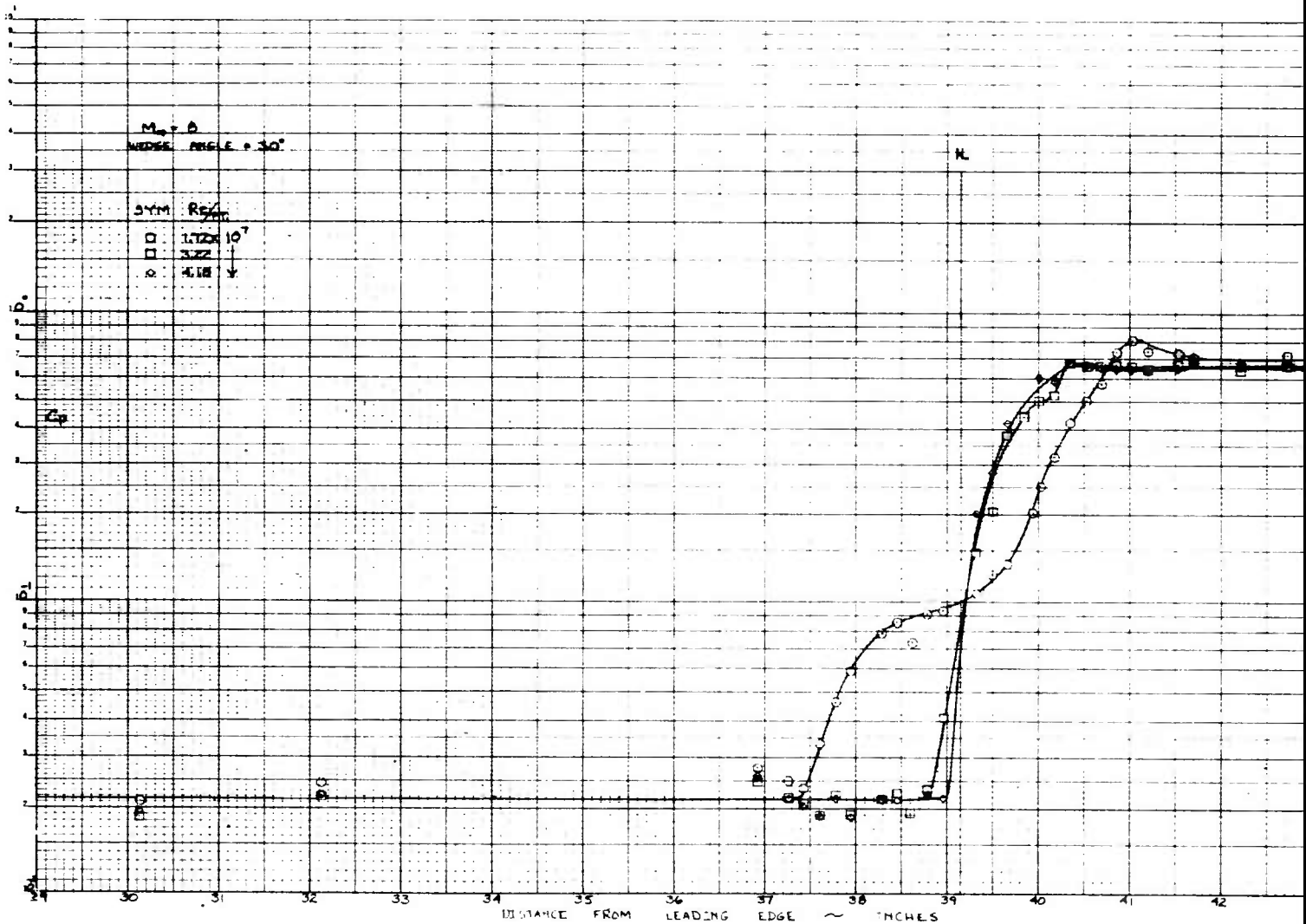


Figure 45b. VARIATION OF PRESSURE DISTRIBUTION WITH REYNOLDS NUMBER

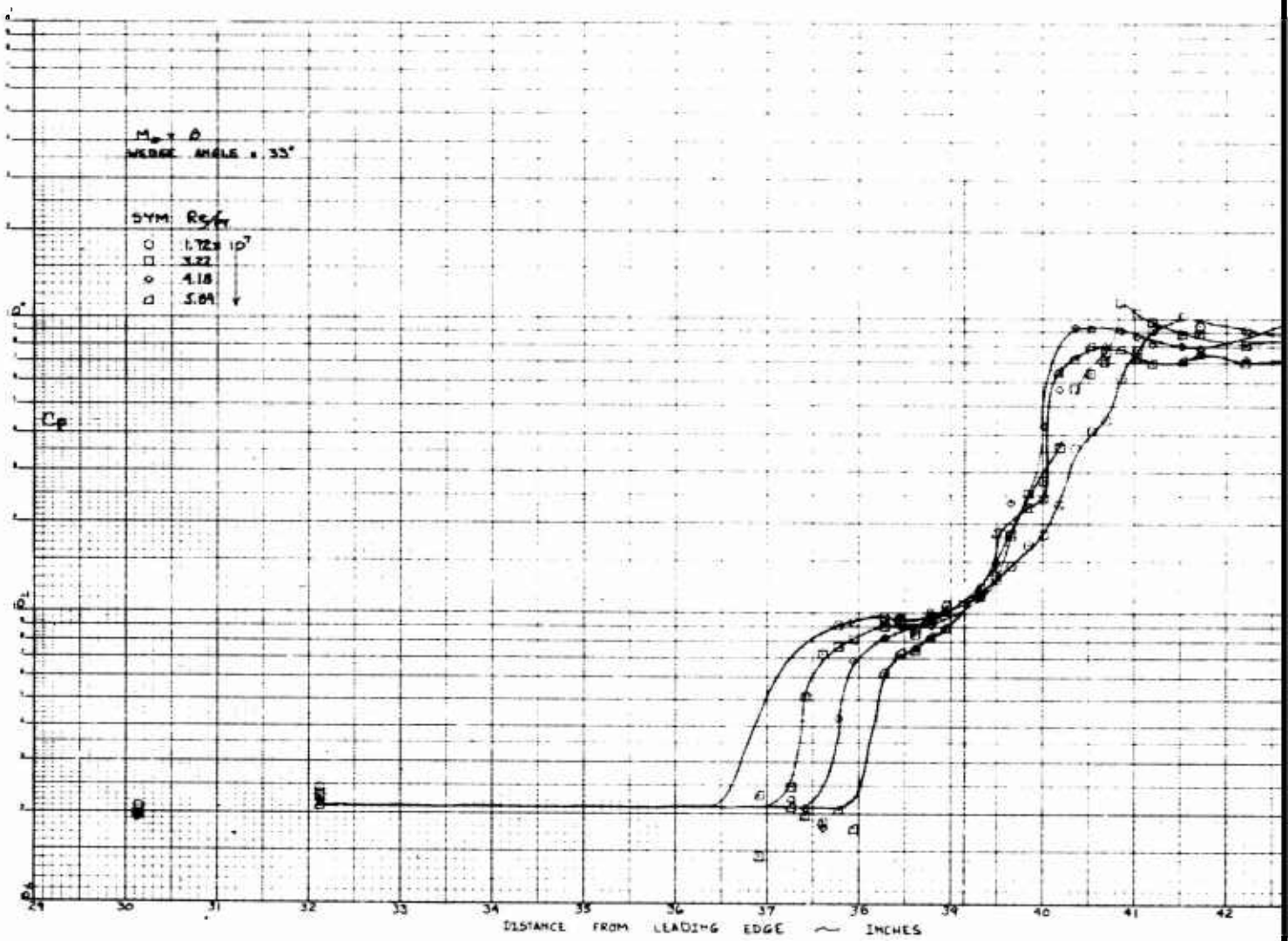


Figure 46a. VARIATION OF PRESSURE DISTRIBUTION WITH REYNOLDS NUMBER

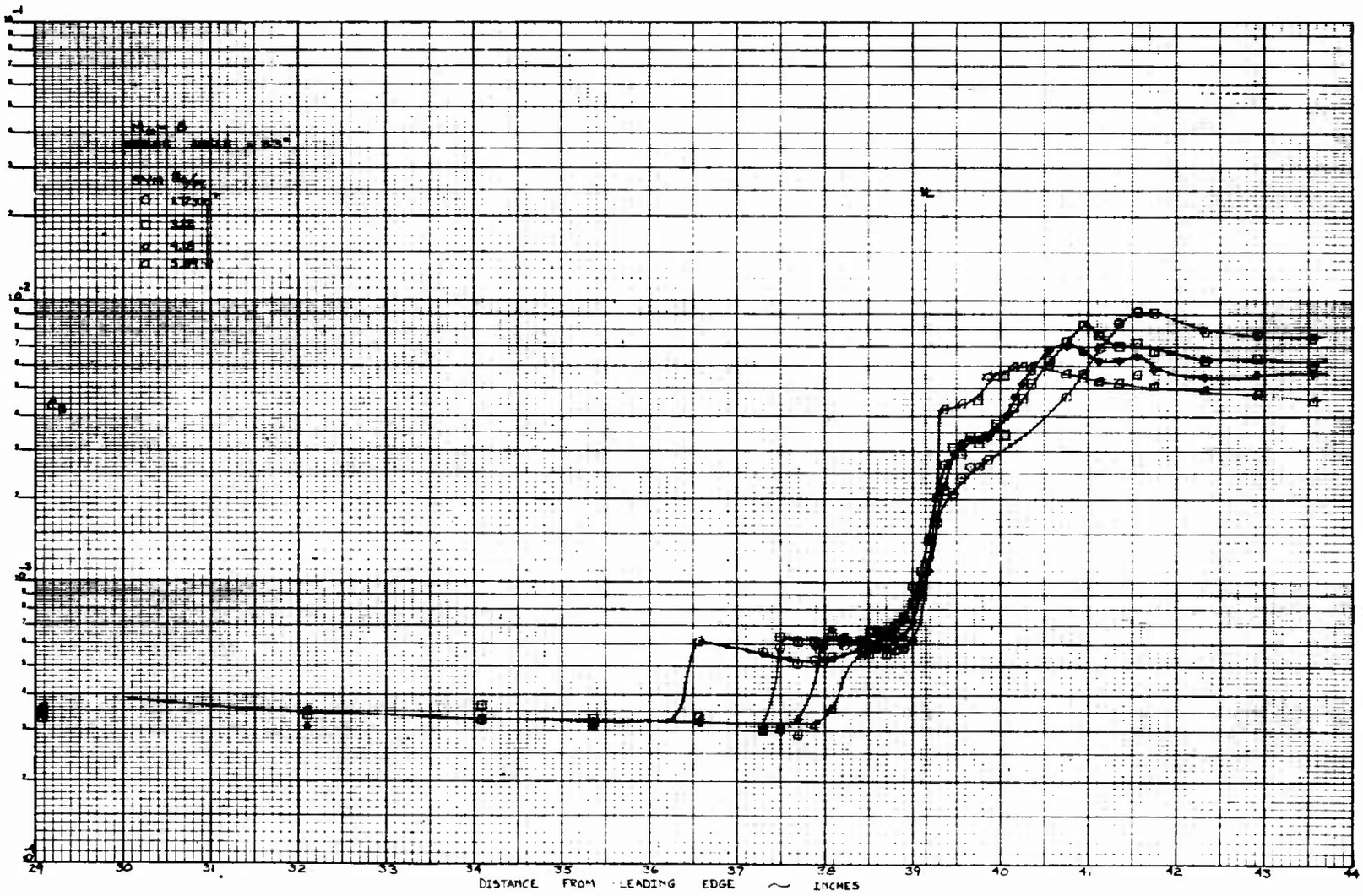


Figure 46b. VARIATION OF HEAT TRANSFER DISTRIBUTION WITH REYNOLDS NUMBER

number R_{e_δ} range from 10^4 to 3×10^6. The effects of both unit and absolute Reynolds number on incipient separation and the scale of a separated interaction region were studied for shock-induced interaction regions over the same range of Reynolds number and Mach number conditions. Figure 47 shows the development of the interaction with increasing strength of incident shock. It is almost impossible to determine whether separation has occurred by examining the Schlieren photographs or the static pressure distribution. However, the fluctuating component of both heat transfer and pressure increases dramatically when separation occurred from the skin friction distribution. In fact, observing the fluctuating component of pressure, or output from thin-film or hot-wire gages, may be one of the best ways of detecting separation. With increasing strength of interaction, the separation shock moves upstream of its initial position at the base of the incident shock. Interestingly, there are strong visual similarities between shock-wave-laminar and shock-wave-turbulent boundary layer interactions at high hypersonic Mach numbers (M_∞ 16→19). Possibly the similarities are the result of similar positions of the sonic line.

The distribution of properties through the interaction regions is shown in Figures 48 and 49. As in the wedge-induced separated flow studies, a well-defined plateau region is evident in the pressure and heat transfer distribution for large separated regions. Contrary to the most recent predictions by Reeves,[24] the plateau pressure is not strongly dependent on the scale of the interaction. This discrepancy is illustrated in Figures 50a and b, where the Reeves method can be seen to overpredict the observed plateau pressure. Perhaps one of the most important features of these shock-induced interaction regions is the large degree of unsteadiness in the separation and reattachment regions, which may be of considerable practical importance.

The results of the measurements of incipient separation induced by an externally generated shock are in agreement with measurements for wedge-induced interactions with respect to the pressure rise to cause separation. Perhaps as important, there is also a reversal in the Reynolds number trend for incipient separation once a sufficiently large Reynolds number is reached. The

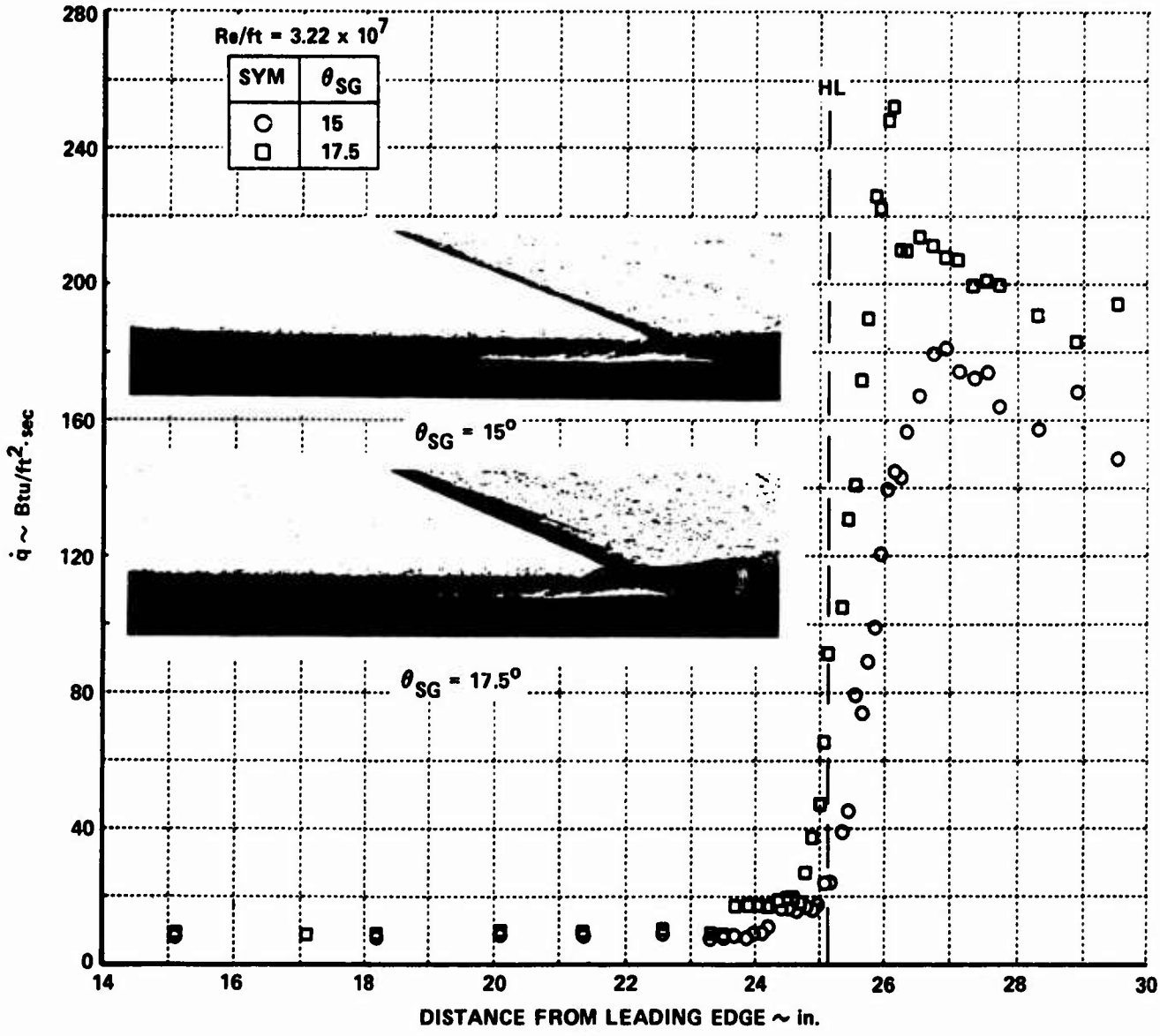


Figure 47. VARIATION OF HEAT TRANSFER WITH SHOCK STRENGTH

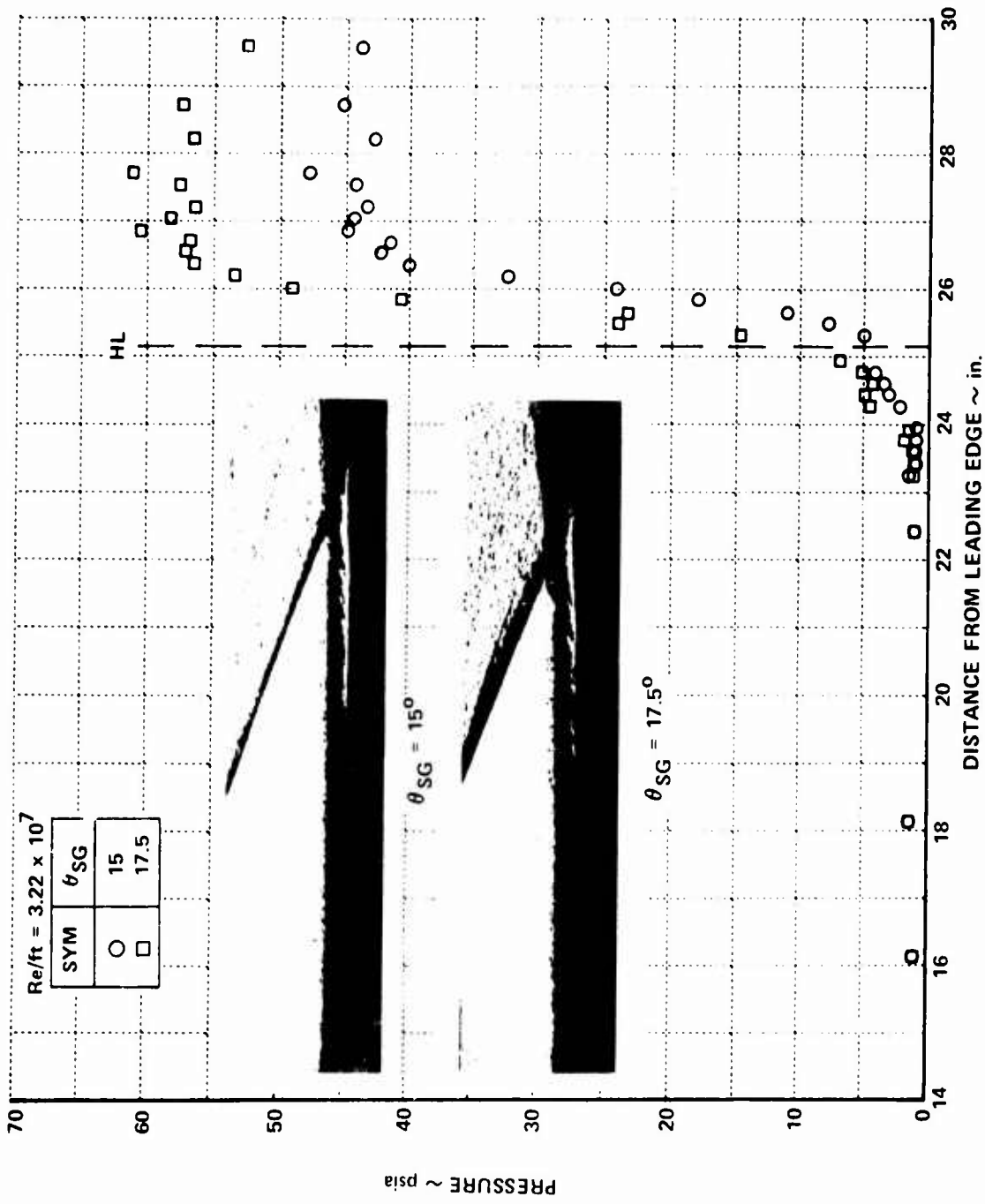


Figure 48. VARIATION OF PRESSURE DISTRIBUTION WITH SHOCK STRENGTH

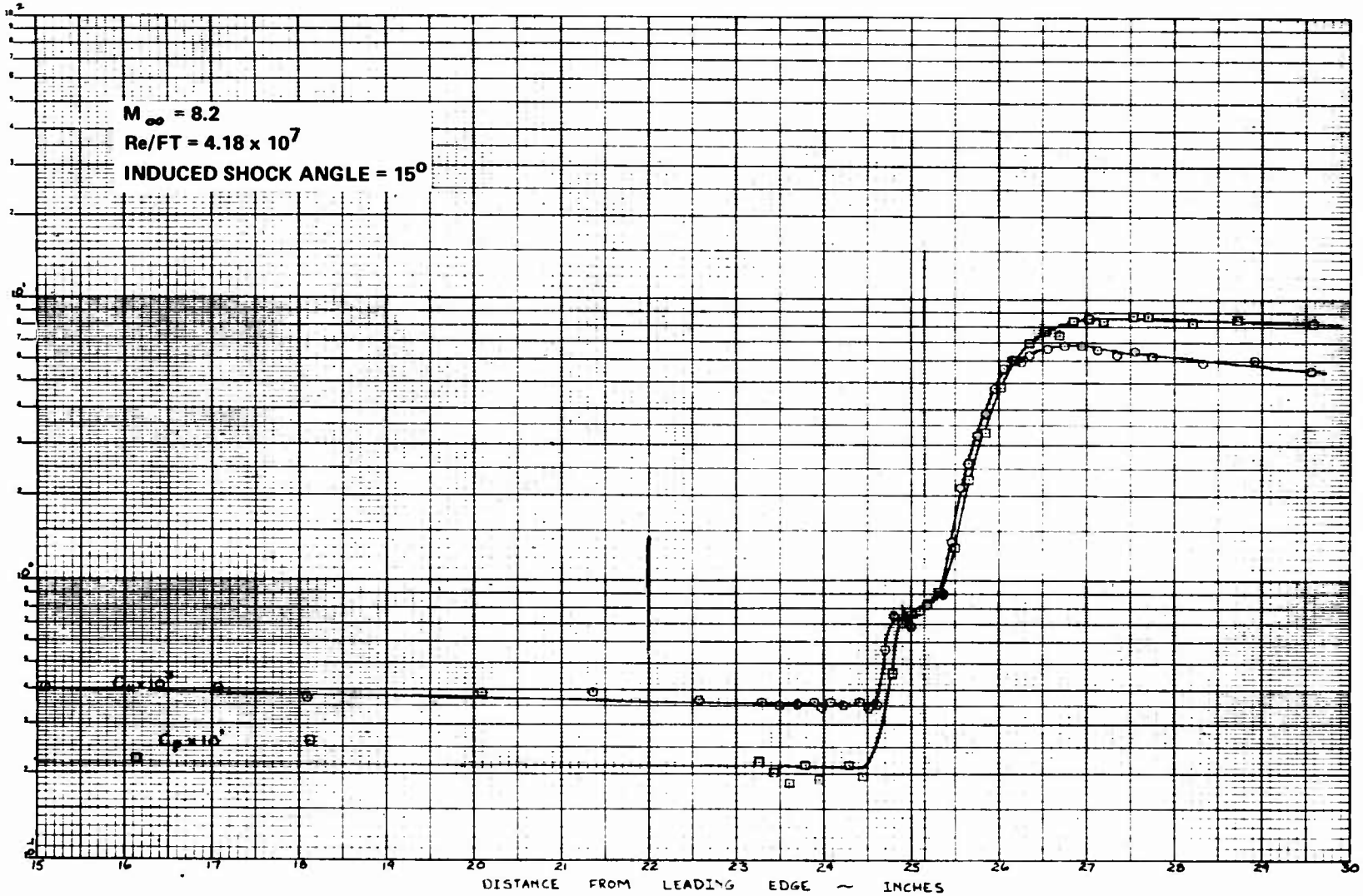


Figure 49a. DISTRIBUTION OF PRESSURE AND HEAT TRANSFER IN SHOCK-INDUCED SEPARATED FLOW

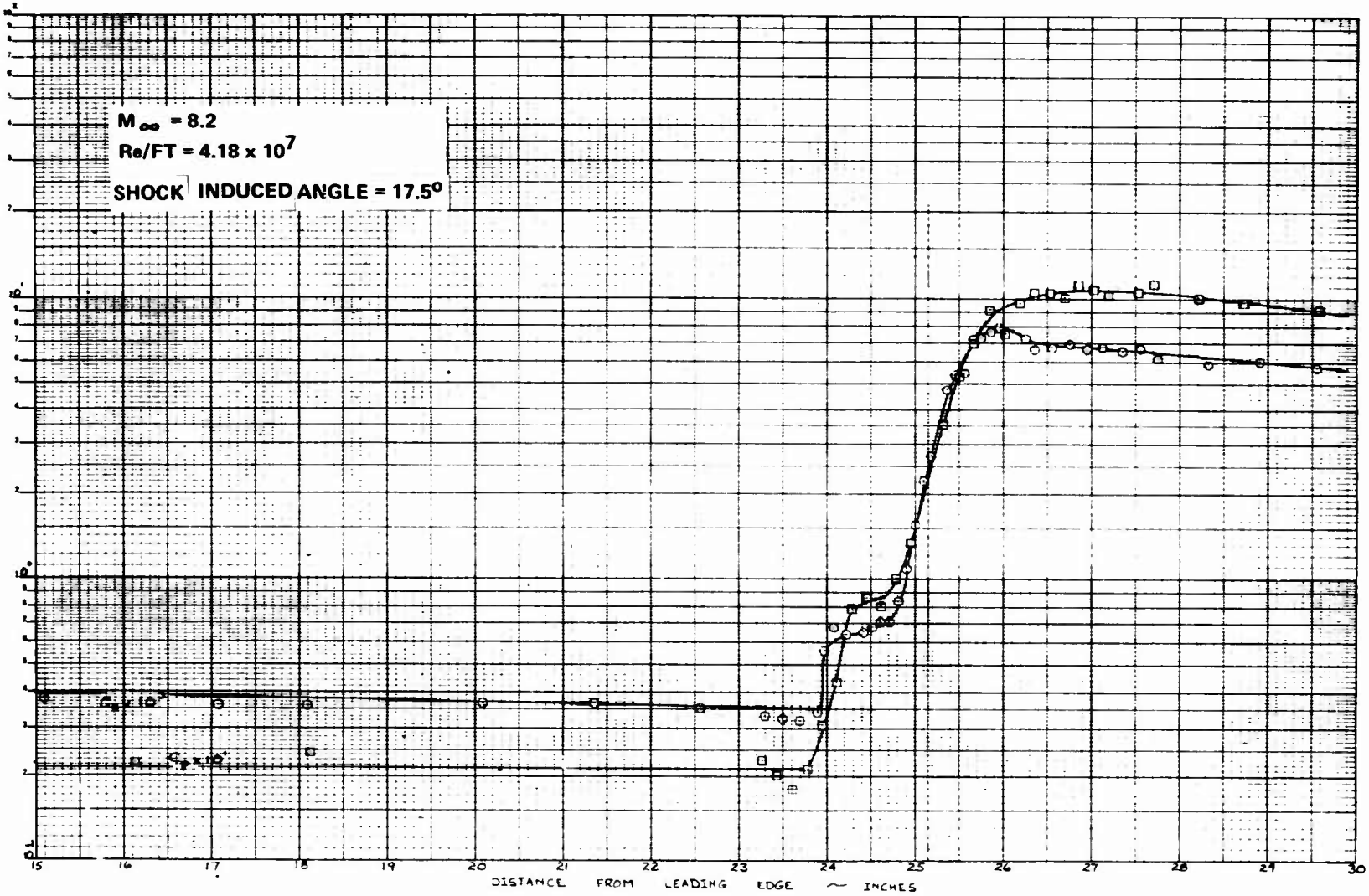


Figure 49b. **DISTRIBUTION OF HEAT TRANSFER AND PRESSURE IN A SHOCK-INDUCED SEPARATED FLOW**

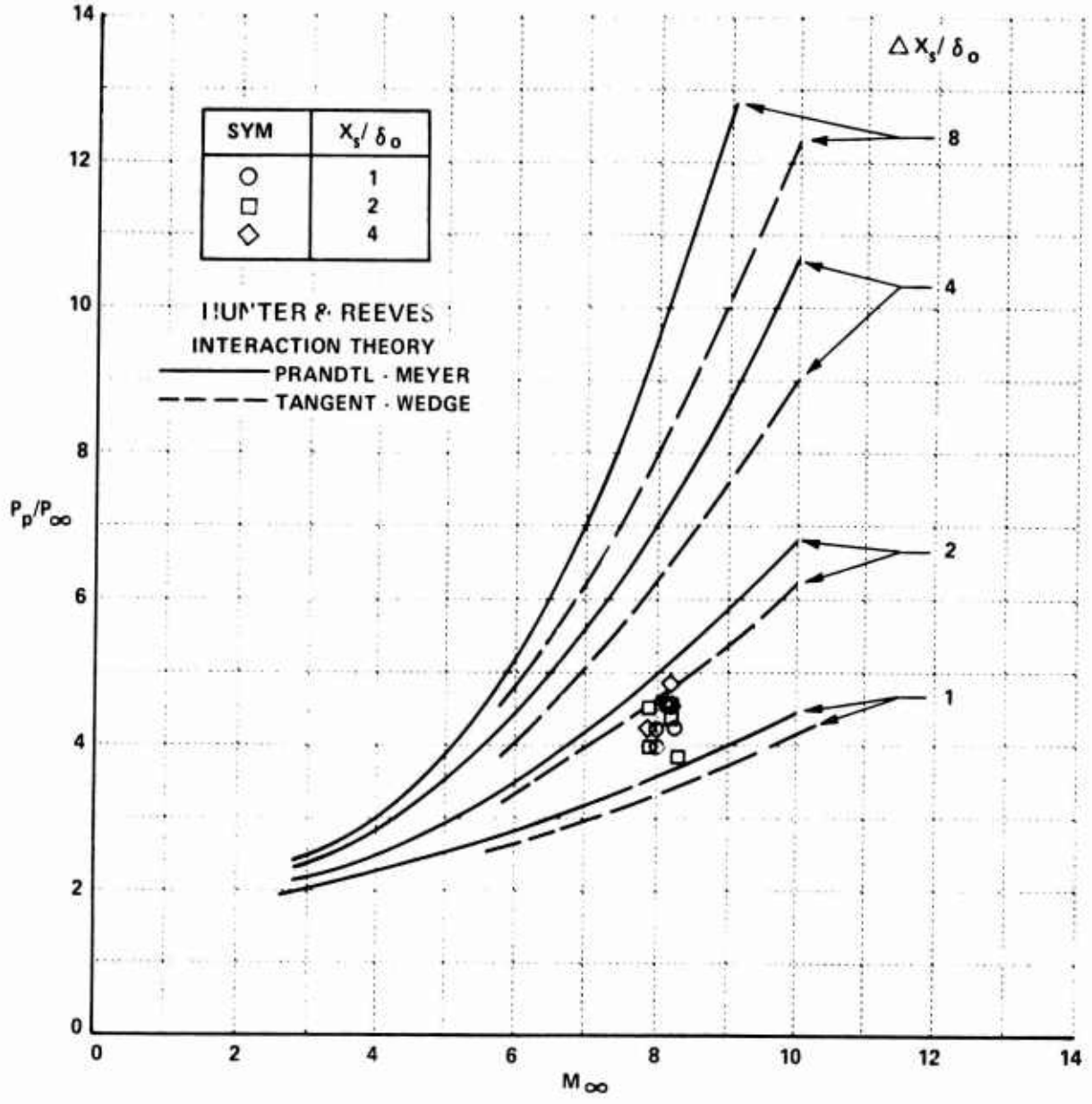


Figure 50a. VARIATION OF PLATEAU PRESSURE WITH MACH NUMBER

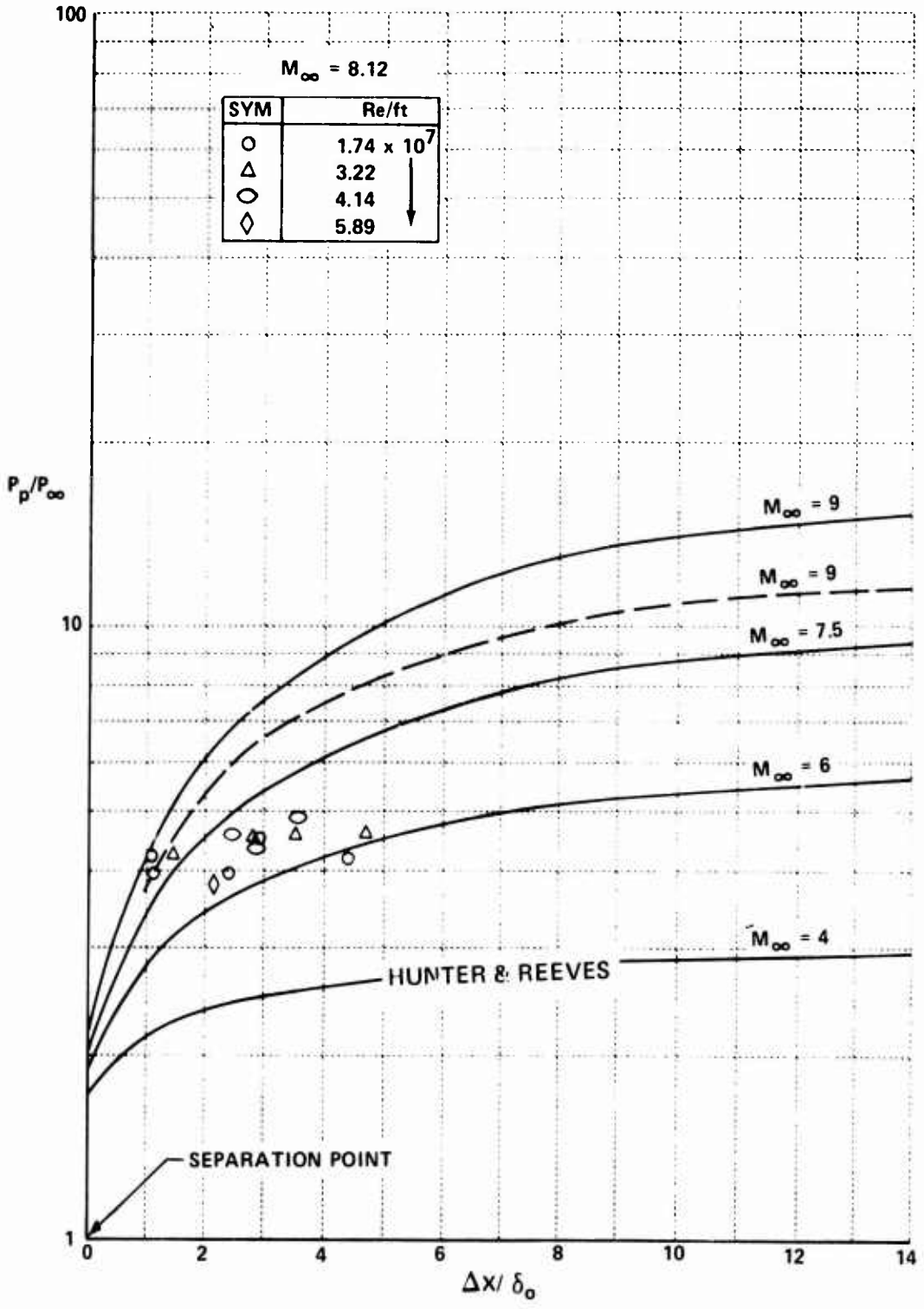


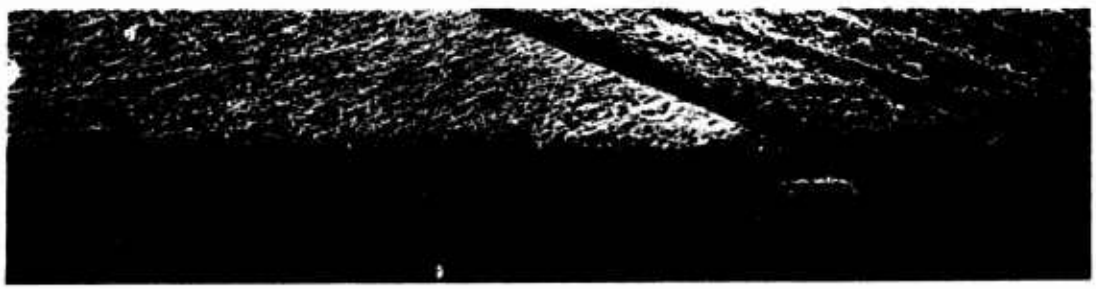
Figure 50b. VARIATION OF PLATEAU PRESSURE WITH SIZE OF SEPARATED REGION



(1) Re/ft = 1.74×10^7



(2) Re/ft = 3.22×10^7



(3) Re/ft = 4.14×10^7

Figure 51a. REYNOLDS NUMBER EFFECT ON LENGTH OF SEPARATION
$M_\infty = 8.1$, $\theta_{SG} = 17.5^o$

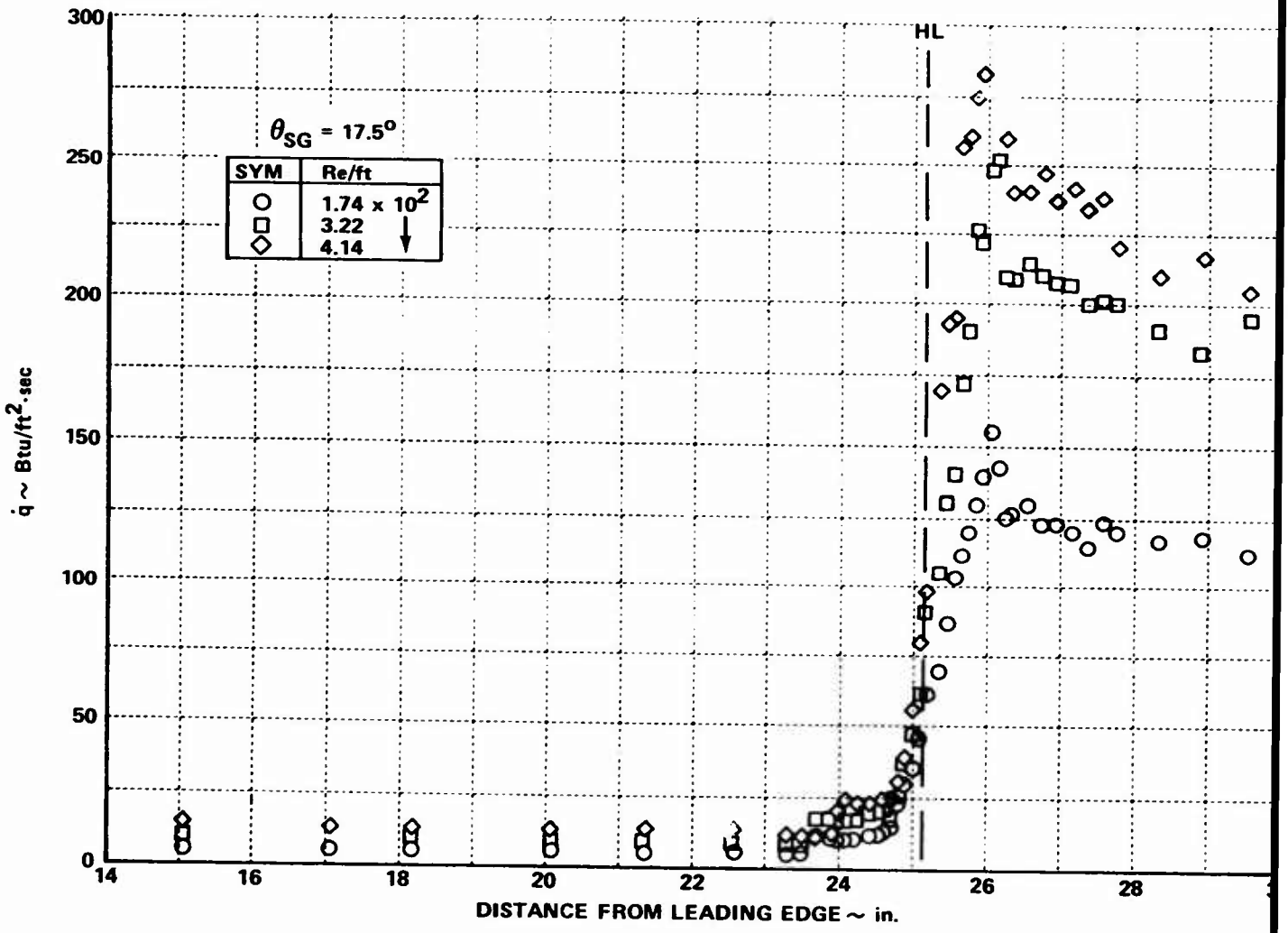


Figure 51b. REYNOLDS NUMBER EFFECT ON LENGTH OF SEPARATION

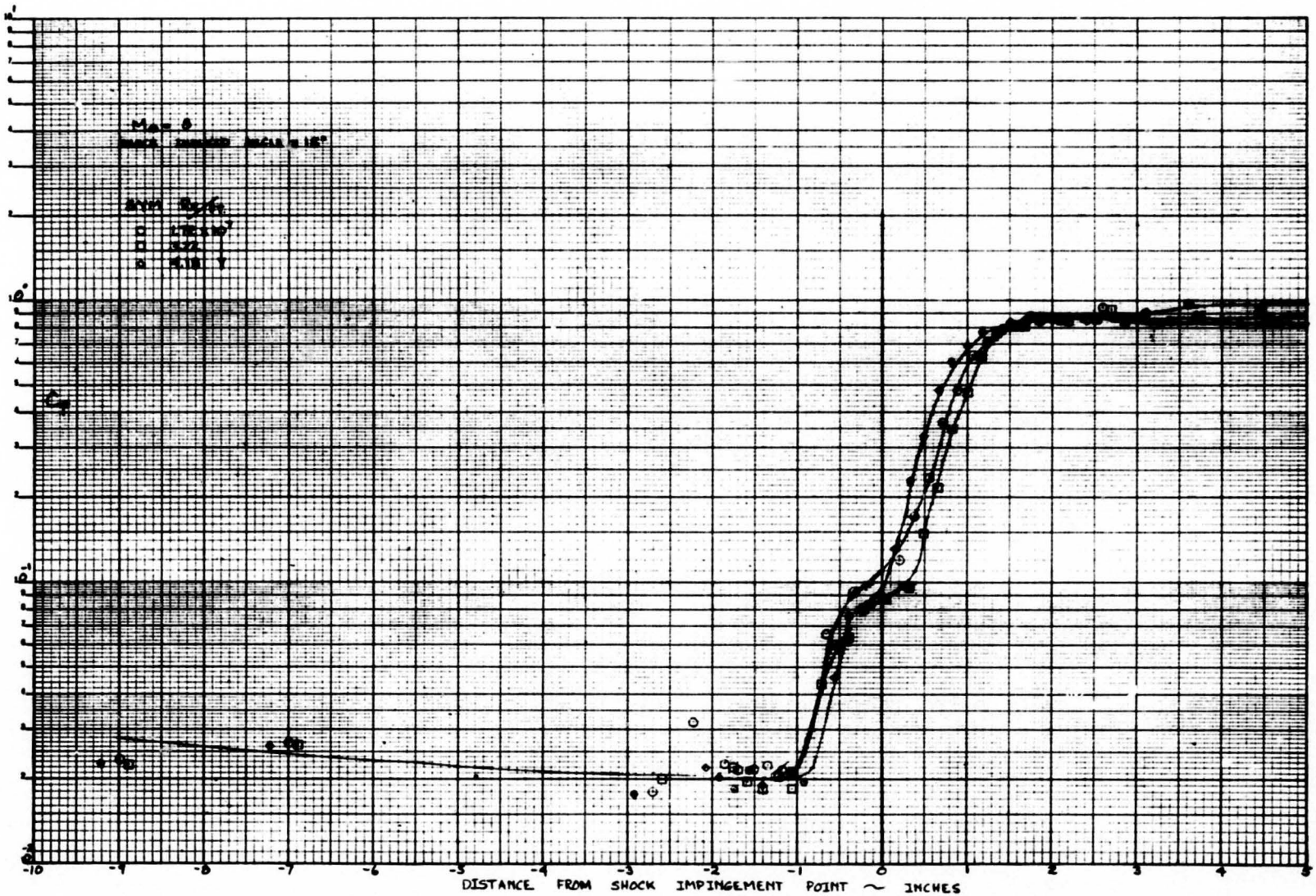


Figure 52a. VARIATION OF THE PRESSURE DISTRIBUTION WITH REYNOLDS NUMBER FOR SHOCK-INDUCED SEPARATED FLOW

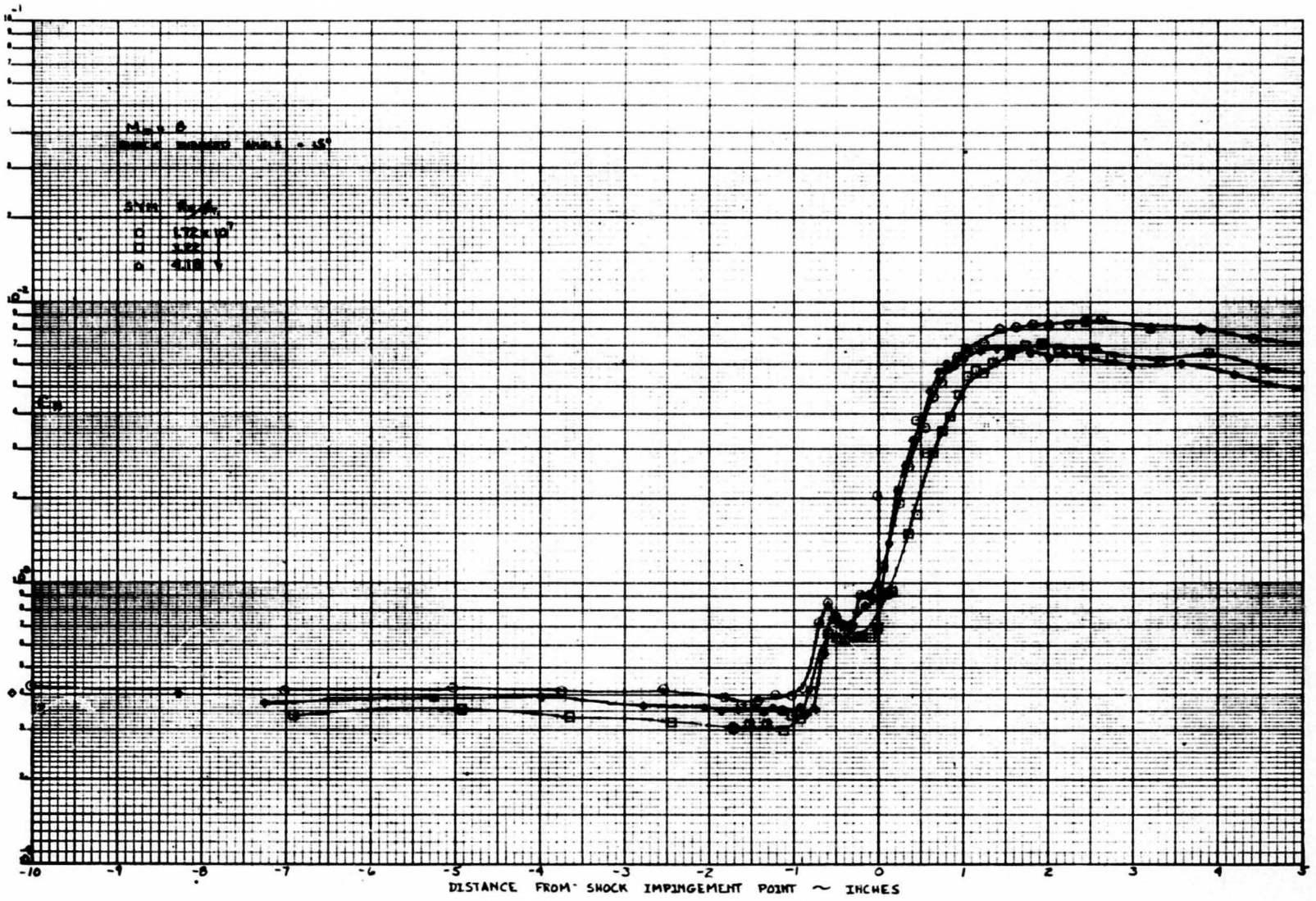


Figure 52b. VARIATION OF HEAT TRANSFER DISTRIBUTION WITH REYNOLDS NUMBER IN SHOCK-INDUCED SEPARATED FLOW

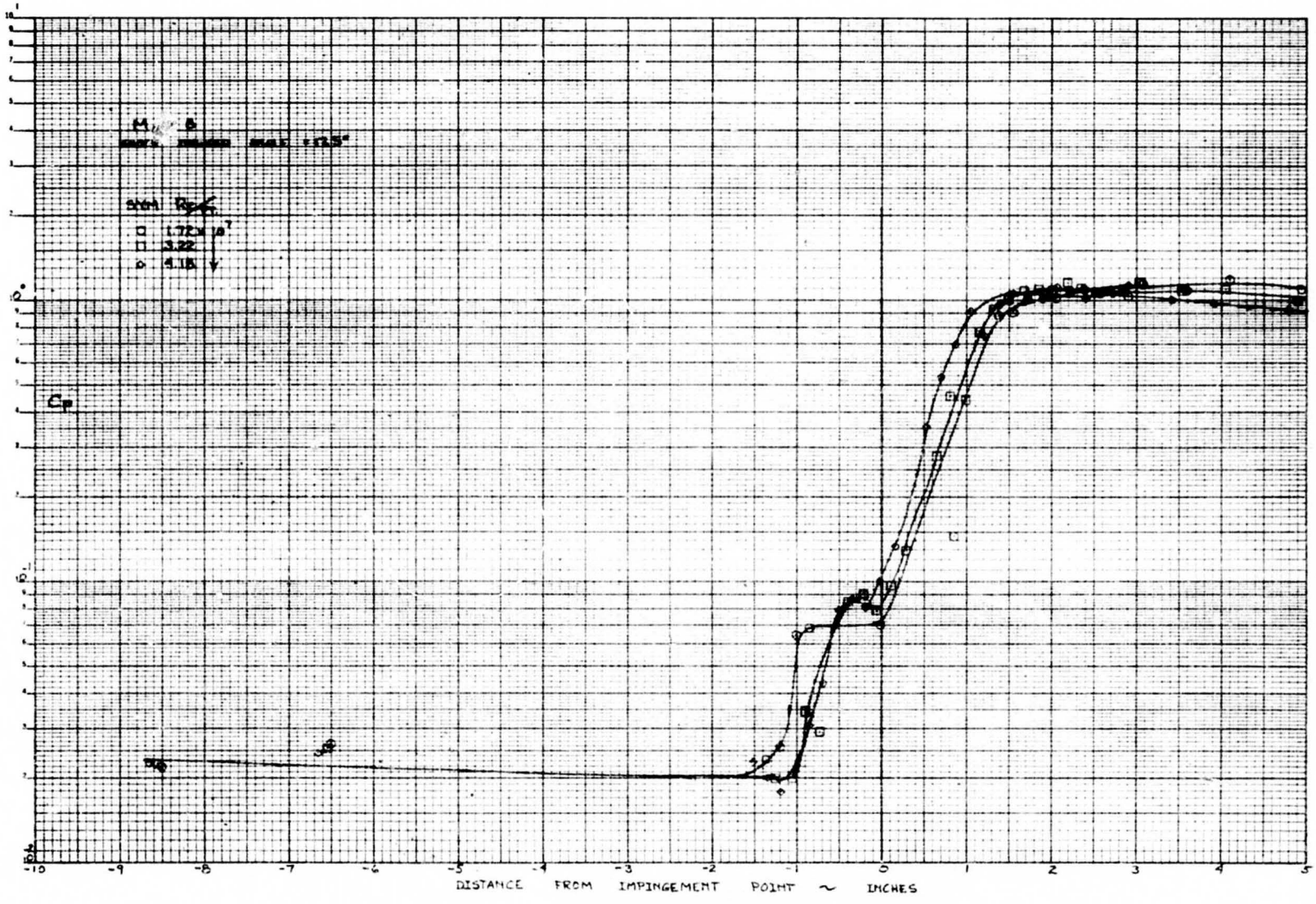


Figure 53a. VARIATION OF PRESSURE DISTRIBUTION WITH REYNOLDS NUMBER IN SHOCK-INDUCED SEPARATED FLOW

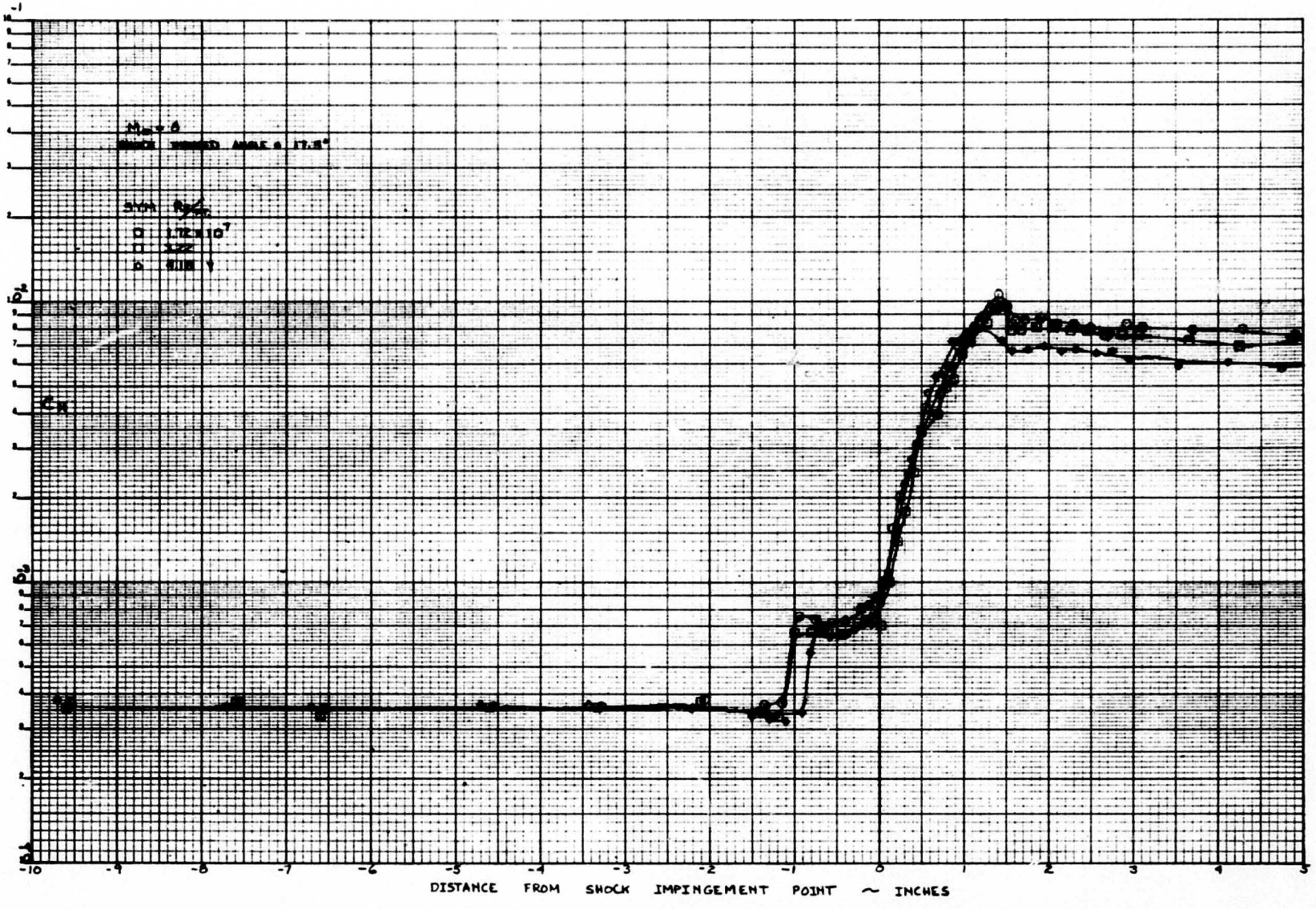
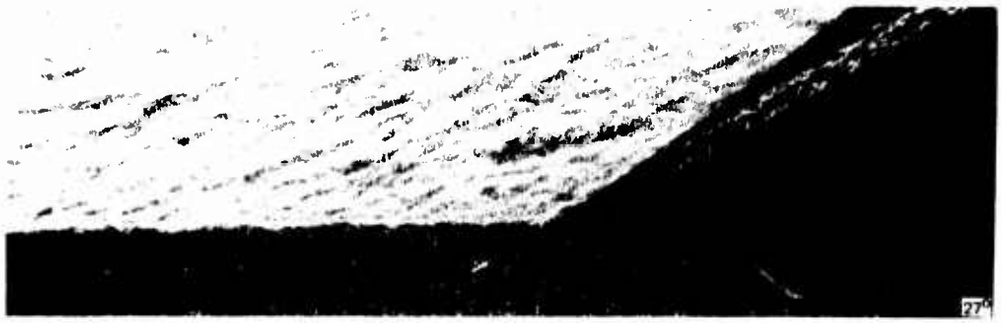


Figure 53b. VARIATION OF HEAT TRANSFER DISTRIBUTION WITH REYNOLDS NUMBER IN SHOCK-INDUCED SEPARATED FLOW

3. CHARACTERISTICS OF SEPARATED TURBULENT INTERACTION REGIONS

A major object of both theoretical and experimental studies is to determine the size, development and properties of turbulent regions, in terms of the strength and nature of the disturbance, the Mach number and Reynolds number in the local inviscid flow, and the character of the undisturbed boundary layer upstream of the interaction. Of course, turbulent separated regions can be promoted in numerous physical situations; however, from the viewpoint of understanding the scaling parameters and developing theoretical models to describe these regions from the beginning of the interaction to downstream of the neck region, experimental measurements in regions of shock wave-boundary layer interaction resulting from an oblique shock incident on a turbulent boundary layer over a flat plate, or in a compression corner where neither separation of reattachment is fixed by the model geometry, are of most value. Almost without exception the measurements made in studies to determine the characteristic and scaling laws of turbulent viscous interactions regions were obtained with instrumentation with zero or very limited frequency response. Our recent measurements in hypersonic flows indicate that the fluctuating component of the separated flow field is also of great importance. However, we will defer a discussion of this aspect of the subject until the next section, and concentrate on observations on the mean properties of these flows.

The development of separated regions, induced in a compression corner and at the base of an incident shock, with increase in interaction strength in hypersonic flow are illustrated in Figures 39 to 53, respectively. Separation is first observed in the laminar sublayer and a well-defined separation bubble is clearly visible in Figure 54. The initial development of the separation region takes place by an elongation into the laminar sublayer, with the separation and reattachment shocks combining within the boundary layer to form a single shock. Only when the separation point has fed well forward of the junction is a well-defined plateau region formed. Then, in contrast to laminar interaction regions, the separation shock originates at the bottom of the boundary layer and is contained within the boundary layer until it coalesces with the reattachment compression process.



(a) WEDGE ANGLE = 27°



(b) WEDGE ANGLE = 30°



(c) WEDGE ANGLE = 33°



(d) WEDGE ANGLE = 36°

Figure 54. THE DEVELOPMENT OF A WEDGE-INDUCED SEPERATED FLOW ($M_\infty = 8.6$, $Re_L = 22.5 \times 10^6$)

In separated regions induced by externally generated shock, separation first takes place in the region where the incident shock strikes the laminar sublayer. The separation point moves forward with increasing strength of the incident shock until the separation shock becomes visible in the inviscid flow downstream of the incident shock; as yet separation is still downstream of the point where the incident shock passes through the edge of the boundary layer. For large incident shock strengths, the separation point feeds well forward of the incident shock and boundary thickening occurs ahead of the incident shock in an analogous fashion to laminar flow separation. However, as in wedge-induced separated regions, viscous-inviscid interaction takes place almost entirely within the original boundary layer. The structure wedge and shock-induced turbulent interaction regions at Mach 13 are very similar to those at Mach 8; however, as we might anticipate, the viscous interaction region and the associated shocks are even more firmly embedded within the original boundary layer.

The surface measurements indicated that turbulent separated regions were highly unsteady and typically the separation point would oscillate in a streamwise direction with an amplitude of approximately one-quarter to one-third of the local boundary layer thickness, at frequencies in the range from 1 to 10 kHz. The unsteady character of the records from transducers in the recirculation region indicated it would be unrealistic to assume that a laminar sublayer model, in the conventional sense, could be used to describe the lower part of the recirculating region as is done, for example, in Rose's[26] theoretical model. The mean distribution of skin friction, heat transfer and pressure to the wall's bounding, both shock- and wedge-induced interaction regions were similar for well separated flows with identical total pressure rises. Figure shows such distributions for a shock-induced interaction at Mach 8.6. Both the pressure and heat transfer distributions are characterized by well-defined plateaus in the recirculation region and large gradients in the separation and reattachment regions. The maximum heat transfer rates generated in the reattachment regions of these flows is, of course, of considerable importance. We found that for separated interaction regions the maximum pressure and heat

transfer measurements over the Mach number range from 6.5 to 13 could be correlated in the form:

$$\frac{q_{MAX}}{q_o} = \left(\frac{p_{MAX}}{p_o}\right)^{0.85}$$

as shown in Figure 55, with data from other sources.

The effects of Reynolds number, Mach number, and wall-to-free stream stagnation temperature ratio on the scale of the interaction region has been a source of controversy since the time experimental studies of these regions began. Dealing first with the less controversial aspects, our studies at Mach numbers from 6 to 13 showed that the length of the separated region decreased with increasing Mach number and decreasing wall-to-free stream temperature ratio, though the latter trend was weak. The weak effect of wall-to-free stream temperature ratio is in marked contrast to the behavior of laminar interaction regions but is again consistent with the results of studies in supersonic flow and those of Gulbran[53] et al. at hypersonic speeds.

The influence of Reynolds number on the length of the separated regions remains unresolved. Most of the early studies of shock wave-turbulent boundary layer interaction were made in the turbulent boundary layer over a tunnel wall. Major discrepancies were found between experiments conducted under the same nominal conditions in different experimental facilities and, for example, the measurements of Bogdonoff and Kepler[54] differed considerably from those of Gadd[17] for identical free stream Mach numbers and interaction strength, when both experimenters had indicated that there was little effect of free stream Reynolds number on the length of the separated region. Hammitt and Hight[55] found that the separated length was influenced by Reynolds number; however, their results were not in quantitative agreement with earlier measurements with identical free stream conditions and interaction strengths but in different facilities. It was concluded at that time that both the model and tunnel geometry were important factors in the absolute scale size of the interaction and there appeared to be little object in obtaining correlation of scale size in terms of the initial boundary layer thickness and properties of the free stream. However, the measurements of Green,[44] Roshko and Thomke,[45] Law[46]

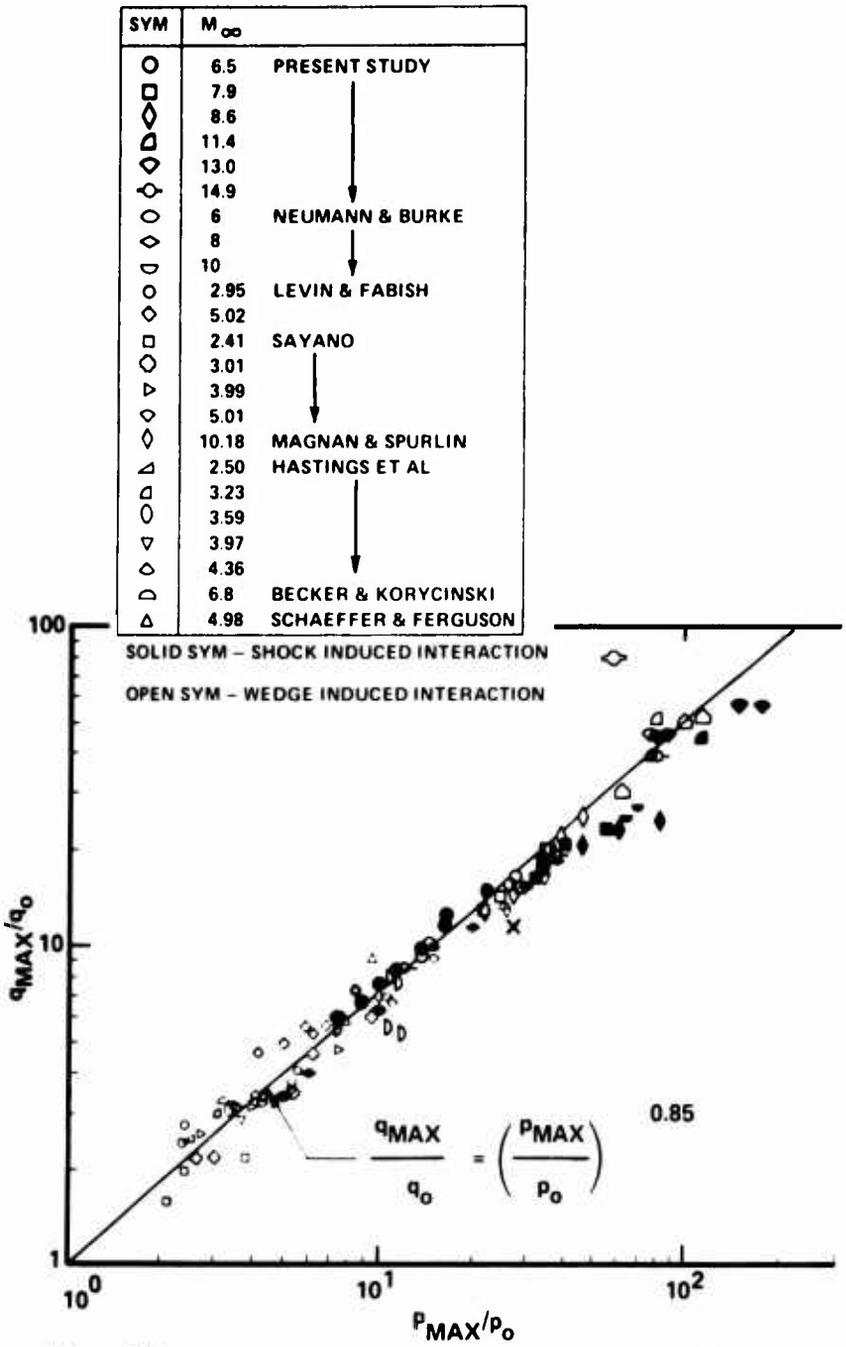
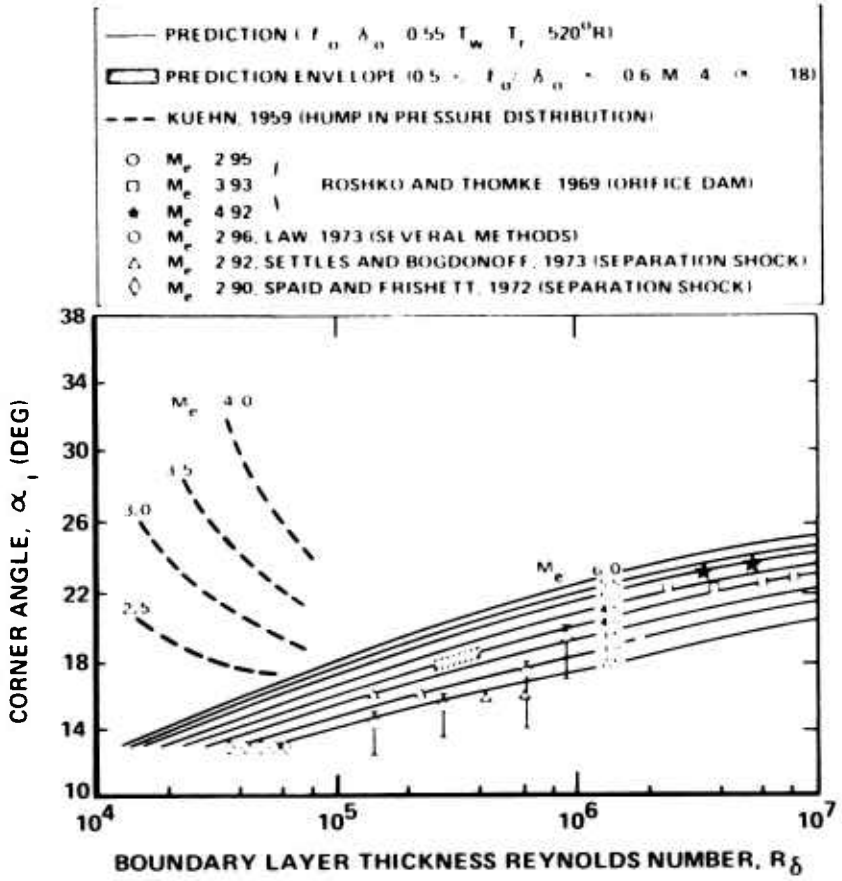


Figure 55. CORRELATION OF MAXIMUM HEATING RATE IN WEDGE - AND EXTERNALLY-GENERATED SHOCK-INDUCED TURBULENT SEPARATED FLOWS

Settles, Bogdonoff and Vas,[47] and Appels,[48] all made under adiabatic wall conditions, indicate that increasing Reynolds number decreases the size of a turbulent separated region. In contrast, the studies of Chapman, Kuehn and Larson,[15], Kuehn[49] and more recently Holden,[50] Elfstrom[56] and Appels[52] at hypersonic speeds, all conducted on "highly cooled" models mounted in the test section, have shown the opposite trend. As in the case of incipient separation the answer may lie in changes in the equilibrium structure of a turbulent boundary layer with Reynolds number. This hypothesis is supported by present measurements of shock- and wedge-induced separated flows at Re_δ's of up to $3 \times 10^{+7}$ by Holden. For Re_δ's 7×10^5, Holden found the same trend observed by Roshko as illustrated in Figures 56 and 60. Again, further studies are required to completely resolve this issue.

The plateau pressure of a turbulent separated region is an important characteristic, which from free interaction theory should not depend upon the way in which separation is promoted. The correlation of experimental measurements shown in Figure 57 suggests that this is the case, and the method of Reshotko and Tucker[65] presents a simple way of calculating this quantity. In contrast, the more sophisticated method of Reeves[24] predicts far larger plateau pressures at high Mach numbers than are observed in experiment. Reeves suggests that the plateau pressure is strongly influenced by the length of the separated region, which again is not supported by experimental measurements as shown in Figures 50a and b. Although the time-dependent Navier Stokes equations have been used with some success to describe turbulent separated flows, the development of simple methods, such as the integral technique are still required for engineering calculations of these flows.



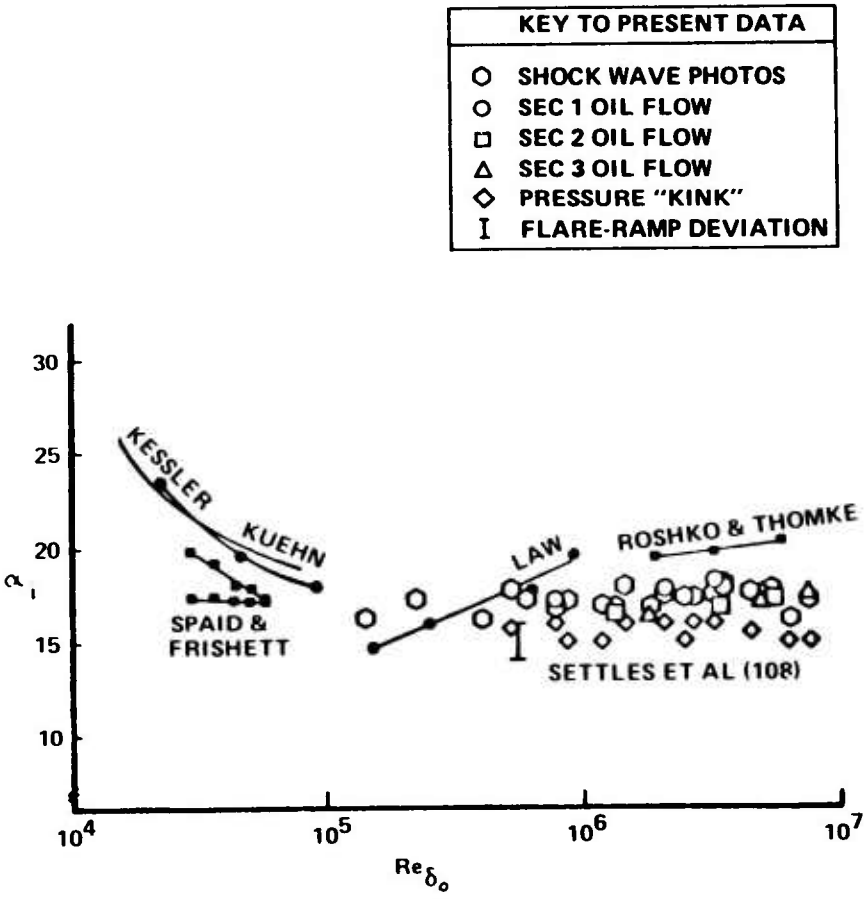


Figure 56a. CONDITIONS FOR INCIPIENT SEPARATION

ROSHKO & THOMKE(1975

Figure 56b. SUMMARY OF REYNOLDS NUMBER EFFECT ON COMPRESSION CORNER ANGLE FOR INCIPIENT SEPARATION AT ABOUT MACH 2.9

SETTLES ET AL (1975)

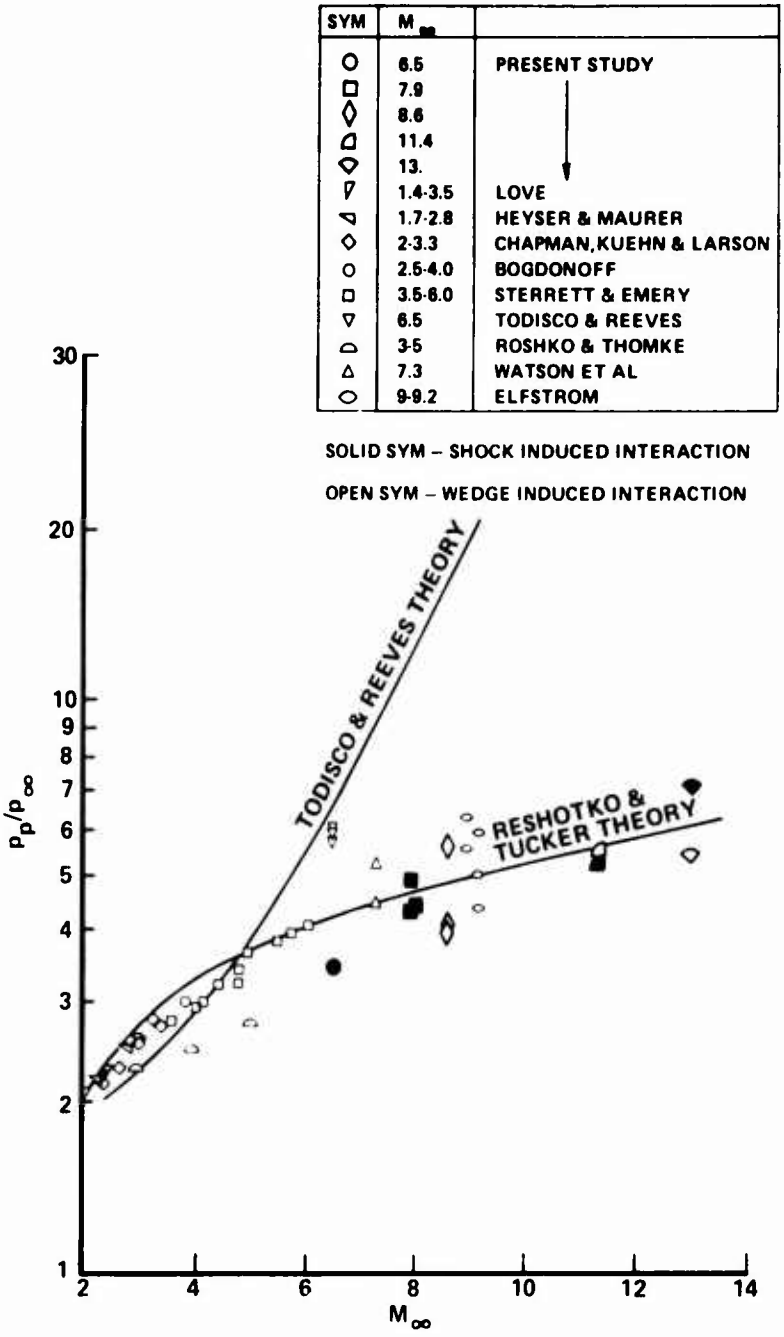


Figure 57. CORRELATION OF PLATEAU PRESSURE MEASUREMENTS IN WEDGE- AND SHOCK-INDUCED TURBULENT SEPARATED REGION

4. INCIPIENT SEPARATION

The first appearance of a region of reverse flow adjacent to the wall or a condition where there is a vanishingly small separated region, is referred to as incipient separation. A knowledge of incipient separation is important from a designer's viewpoint because it is at this point that sudden and generally unpredictable changes occur in the fluid dynamics of the system under study. However, it is even more important to a theoretician for it allows him to check a theoretical description of a viscous interaction region for a limit where a separation profile is formed, and yet a recirculation region has not yet developed.

From both the theoretician's and the experimentalist's viewpoint, it is important to establish whether the incipient separation phenomenon is independent of how the interaction is induced. If incipient separation can be induced on a flat plate-wedge compression surface for the same total pressure rise that it takes to separate an identical boundary layer with an externally generated oblique shock, then this has far reaching implications for the theoretical modelling of the flow. The variation of the incipient separation condition with Mach number and Reynolds number of the free stream, also provides a method for cross checking theoretical models and experimental measurements. It would be hoped that the identical incipient separation condition could be approached by either increasing the disturbance, tending to promote the separation of an attached boundary layer, or reducing the strength of the interaction for a separated flow. While our studies indicate this appears to hold true for externally generated shock-induced and wedge-induced interaction regions, the studies of turbulent interaction regions by Kuehn[49] indicate that a significant hysteresis effect can take place on curved surfaces in a dynamic situation. He found that the deflection angle required to promote a separated region when flow was initially attached was larger than the wedge angle for incipient separation when separation was already established, and the deflection angle was lowered to produce incipient separation.

From the recent experimental studies of turbulent separation, there appears to be an emerging picture of turbulent separation as a two-stage process. First, separation occurs in the laminar sublayer, with a laminar recirculation region forming at the base of the turbulent boundary layer. As the strength of the interaction is increased, a turbulent recirculation region is formed and the size of this region increases rapidly with interaction strength. Based on this model of the turbulent separation process, the occurrence of separation must depend upon the method chosen to detect it and the relative thickness of the laminar sublayer. For example, the relatively small thickness of the laminar sublayer in high Reynolds number, highly cooled flow should make the laminar separation harder to detect and of less importance than in slightly supersonic flows over adiabatic surfaces. The studies of Holden,[43] Elfstrom[56] and Appels[48] in hypersonic flows over highly cooled walls have demonstrated an abrupt change in the characteristics of upstream influence when a turbulent boundary layer "separates." In contrast, measurements by Spaid and Frishett,[57] Appels,[48] Roshko and Thomke,[45] and Settles et al.,[47] made under conditions where the laminar sublayer exerts a fargreater influence on the development of separation, demonstrate a less definitive separation process.

Although it is difficult to define incipient separation for the general case of three-dimensional turbulent separated regions, for two-dimensional steady flow we can define incipient separation the condition where the skin friction is positive everywhere in the interaction region but at one point is vanishingly small. Unfortunately, turbulent interaction regions in hypersonic flow are far from steady and the problem in these regions becomes how to define incipient separation in an unsteady flow. In the experimental studies by Holden,[43] where dynamic measurements of the skin friction in turbulent interaction regions were made, the separation conditions were defined when the time average of surface shear at one point only on the surface was zero.

Most experimentalists do not have access to small skin friction transducers and thus a number of alternative techniques have been devised as separation criteria. One of the most widely used separation criteria was proposed by Kuehn, which equates the first appearance of an inflection point in the

pressure distribution in the interaction region with separation. Green[44] found that in shock-induced turbulent separated regions a distribution with an inflection point was developed only when a relatively large separated region has been formed. Holden also showed this criteria is seriously in error when applied to externally generated shock-induced interactions in hypersonic flow; separation was found to take place well downstream of the point where the incident shock entered the boundary layer. A Schlieren photograph of the incipient separation condition at Mach 6.5 is shown in Figure 58. We must, as pointed out earlier, distinguish between techniques to detect the first appearance of reverse flow and ones suggested to determine when the size of separated regions are of significant proportions. Oil flow measurements, measurements of surface shear with skin friction gates, or surface pitot's, orifice dam and heat transfer measurements have been used to detect the presence of separation in the sublayer. Observing an inflection in the pressure distribution, plotting the upstream influence with interaction strength and observing the first appearance of a separation shock wave served as pragmatic indicators of boundary layer separation. The studies of Green, Spaid and Frishett, Appels and Settles, Bogdonoff and Vas have demonstrated that incipient separation measurements using the liquid line method give incipient separation angles significantly less than those determined from the pragmatic methods, because each detects a different phenomena. The relative difference between the methods depends on the structure of the boundary layer and the size of the instrumentation. However, there is relatively good agreement between measurements of incipient separation where a specific criteria is uniformly applied. Figure 56 shows a comparison between measurements made at approximately Mach 3 on models with adiabatic wall conditions. These measurements are seen to be in relatively good agreement despite the differences in Reynolds number trend, which will be discussed later. Roshko and Thomke[45] have recently suggested the correlations of incipient separation in terms of α_i, l_o, δ_o, and C_{f_i} shown in Figure 59. They suggest that $l_o/\delta_o = 0.55$ is the upstream influence when the pragmatic separation criteria are used, whereas $l_o/\delta_o = 0.05$ characterizes the upstream influence when oil flow measurements are used. Roshko and Thomke note that the results of other investigators' measurements at higher Mach numbers and under cooled wall conditions do not agree with the later correlation, presumably because the relative structure of the laminar sublayer is different.



Figure 58. INCIPIENT SEPARATION AT MACH 6.5 AND $RE_L = 27 \times 10^6$

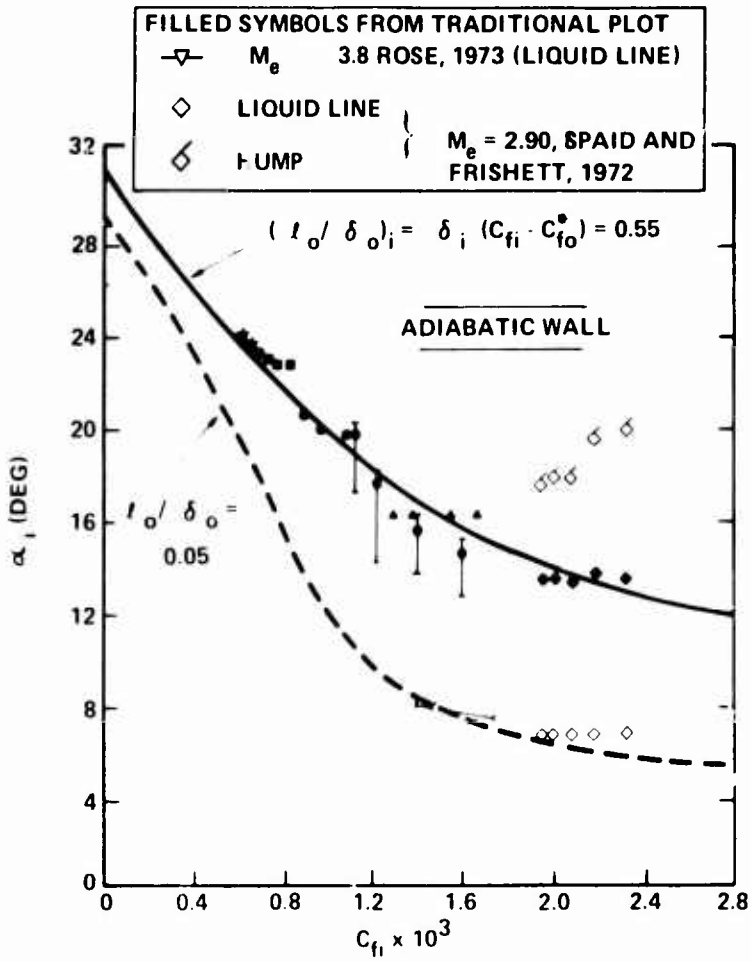


Figure 59. CONDITIONS FOR INCIPIENT SEPARATION, $2.5 \leq M_e \leq 5$
(ROSHKO AND THOMKE 1975)

Measurements made by Holden,[43] Elfstrom[56] and Appels[52] under high Mach number highly cooled wall conditions are compared with adiabatic wall data discussed above in Figure 60. These measurements clearly indicate that increasing the Mach number increases the strength of the interaction required to induce separation. Holden found, by studying both shock- and wedge-induced separated flows, from Mach 6.5 to 13 that the pressure rise to induce incipient separation was independent of the disturbance promoting the interaction. In view of the vastly different flow geometries in these two experiments, this is perhaps a surprising and important result. However, this allows us, with some justification, to view the separation mechanism as a gross balance between inertial and viscous forces at the wall. We can write, in the spirit of Chapman's analysis

$$\frac{\partial \tau}{\partial y} = \frac{\partial p}{\partial x} \qquad \frac{\tau_{w_o}}{\delta_o} \qquad \frac{p_{incip} - p_o}{L}$$

where we suggest $L = M_o \delta$, thus

$$\frac{p_{incip} - p_o}{\frac{\gamma}{2} M^3 p_o} \sim \frac{\tau_w}{\frac{1}{2} \rho_o u_o^2} \qquad \frac{p_{incip} - p_o}{p_o} \propto C_{f_o} M_o^3$$

Figure 61 shows a correlation of incipient separation conditions determined in the studies at hypersonic speeds together with the measurements on adiabatic walls at supersonic speeds. With the exception of Kuehn's measurements, the effect of Reynolds number is weak. However, the studies of Kuehn,[49] Sterrett and Emery,[58] Holden,[43] Elfstrom[56] and Appels[52] indicate that for $Re_\delta = 7 \times 10^5$ increasing the Reynolds number decreases the angle to promote separation or decreases the length of a separated region. Roshko and Thomke,[45] Law,[46] and Appels[48] find that increased Reynolds number increases the angle to promote separation or decreases the length of a separated region. However, Settles, et al.[47] finds incipient separation remains uninfluenced by Reynolds number, while the scale of a separated interaction region decreases with increased Reynolds number. It remains to be determined how the method used to define incipient separation can be influenced by the trend observed. The reader is referred to the original papers by Roshko and Thomke,[45] Law,[46] Settles,

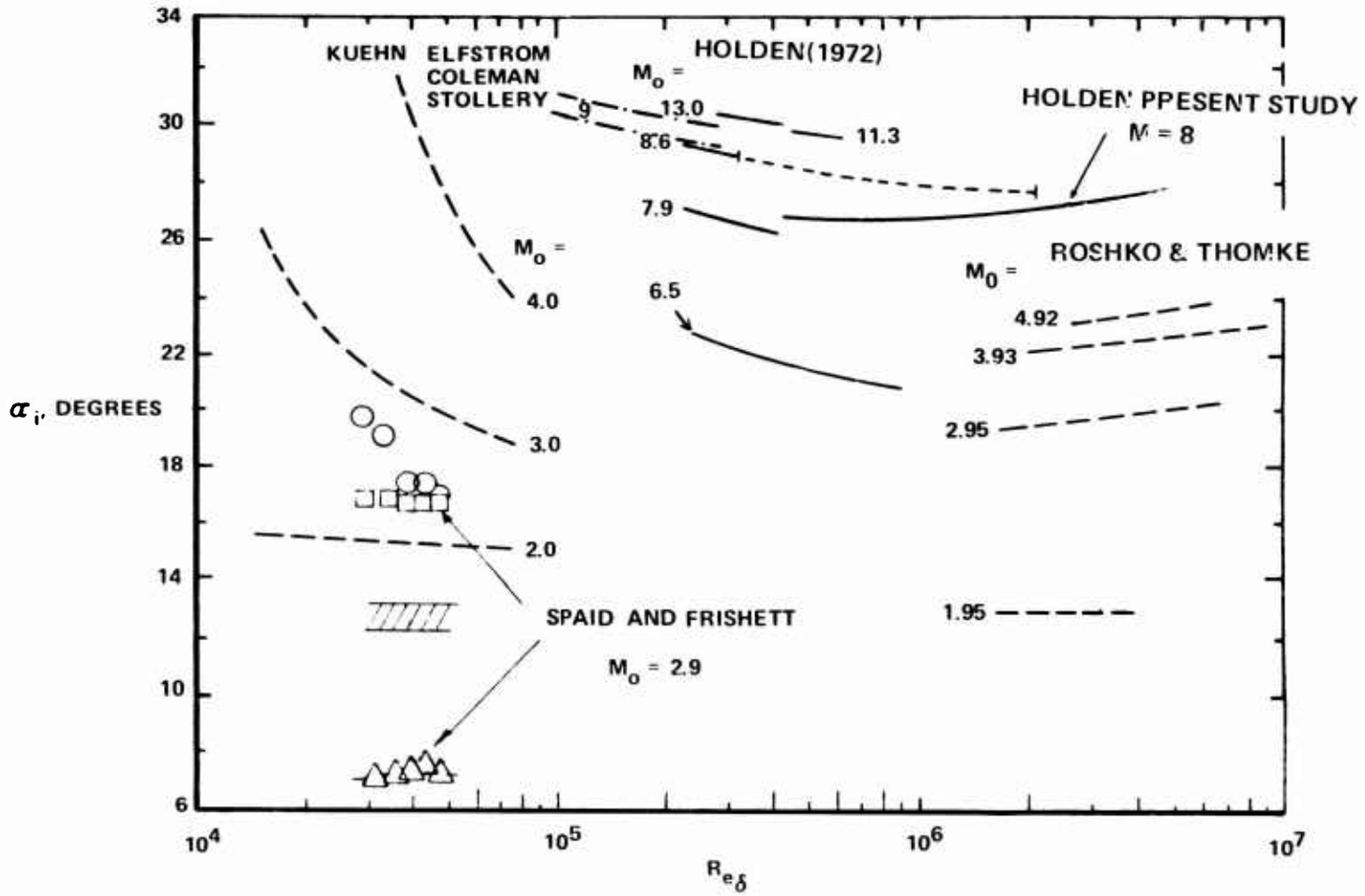


Figure 60. WEDGE ANGLE TO INDUCE INCIPIENT SEPARATION

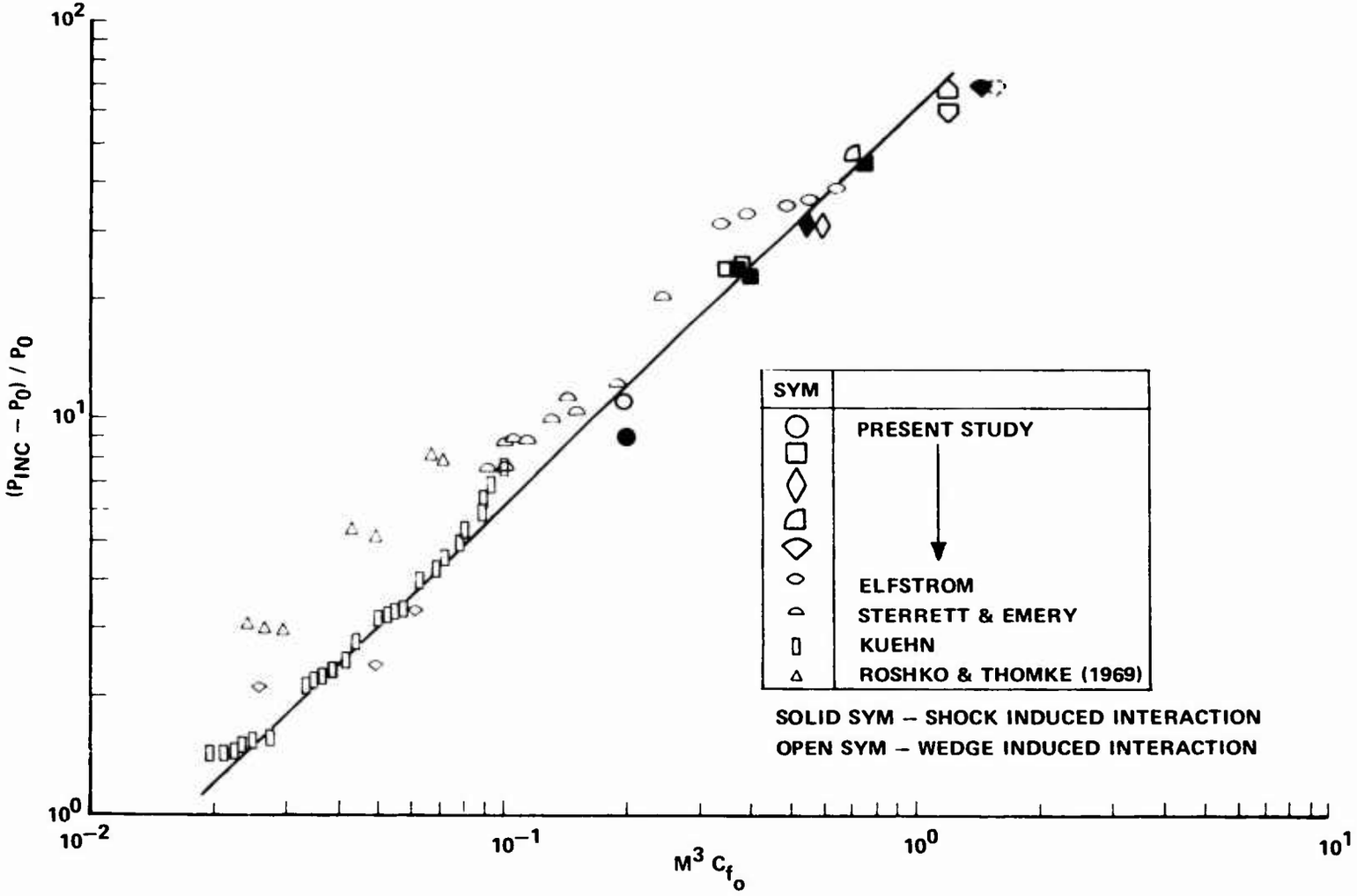


Figure 61. CORRELATION OF INCIPIENT SEPARATION CONDITIONS FOR WEDGE- AND SHOCK-INDUCED TURBULENT INTERACTION REGIONS

Bogdonoff and Vas[47] for a detailed debate on the validity of each other's techniques and data interpretation. We should, however, briefly discuss the difference in the Reynolds number trends observed when a similar criteria was used to detect incipient separation.

Most of the arguments advanced to explain the difference in Reynolds number trends observed, center about the nonequilibrium development of a turbulent boundary layer downstream of a transition region or downstream of an expansion to which a nozzle wall boundary layer is subjected. Studies by Johnson and Bushnell[51] have demonstrated that the power law exponent $[n]$ in the relationship, $\frac{u}{u_\infty} = \left(\frac{y}{\delta}\right)^{1/n}$ decreases from a local maximum downstream of transition, with increasing Reynolds number until the boundary layer becomes fully developed (see Figure 60). Beyond this point $[n]$ increases with Reynolds number. From this viewpoint, Kuehn's[49] measurements show a decreased resistance to separation with Reynolds number because the velocity profile becomes less full as a result of relaxation of the boundary layer. The measurements of Roshko and Thomke[45] exhibit the opposite trend because they were performed at Reynolds numbers where $[n]$ was increasing with Re_δ. It should be mentioned that the measurements made on tunnel walls are also influenced by similar nonequilibrium effects. Studies by Wallace,[59] Bushnell[60] and Fiore[61] have demonstrated that the structure of a turbulent boundary layer on a tunnel wall differs significantly from the boundary layer over a flat plate. The nonequilibrium effects introduced by the favorable pressure gradient on the tunnel walls can persist as far as 100 boundary layer thicknesses downstream of the end of the nozzle. This effect causes a relatively fuller turbulent boundary layer profile, which would be more difficult to separate. However, both Roshko and Thomke,[45] and Settles, Bogdonoff, and Vas[47] find the same variations with Reynolds number whether the experiments were conducted on tunnel walls or with axisymmetric models. We found in the present study a change in the Reynolds number dependence from a decrease to an increase in the resistance to separation, as the length or unit Reynolds number increased. See Figure 61. Again, this result can be explained in terms of a change in the variation of skin friction coefficient with Reynolds number, because of nonequilibrium effects through the relatio ship $C_f \propto \frac{1}{(Re_L)^{1/n}}$ where $n = n(Re_\theta)$. The

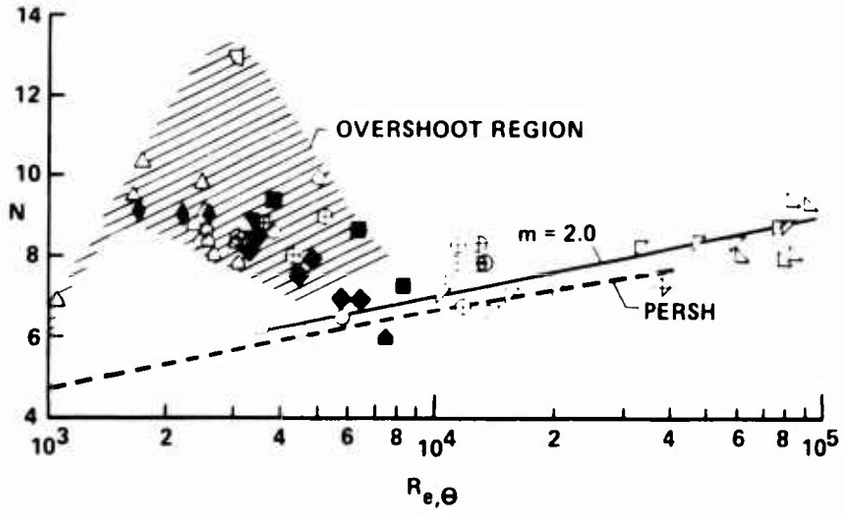


Figure 62. VARIATION OF N WITH $R_{e,\Theta}$ FOR FLAT PLATES, CONES, AND HOLLOW CYLINDERS
(JOHNSON AND BUSHNELL, NASA TN D-5753)

measurements on flat plates and cones combined with the present separation study strongly support this explanation. Our measurements suggest that between 50 to 100 boundary layer thickness downstream of the point of maximum heating for the turbulent boundary layer to exhibit the characteristics of an equilibrium turbulent boundary layer. Beyond this point the boundary layer exhibits an increase in N with Reynolds number, and becomes more difficult to separate. An alternative explanation is offered by Elfstrom[56] who equates the change in Reynolds number trend to detailed changes in the wake component of the boundary layer. Clearly, further experimental and theoretical studies are required to fully understand the mechanism of turbulent boundary layer separation.

5. COMPARISON BETWEEN EXPERIMENT AND NAVIER-STOKES SOLUTIONS

The experiments performed in the present study revealed, for the first time, that both trends can be observed on models mounted within the test core if a sufficiently large Reynolds number range can be generated. In addition, it was demonstrated that this behavior was not sensitive to whether the Reynolds number at the interaction was generated by a long model with a moderate unit Reynolds number, or a short model under high Reynolds number conditions. Studies of the heat transfer and skin friction distributions in and downstream of the transition region on the flat plates suggest that the boundary layer approaches an equilibrium turbulent condition well upstream of the basic interactions under study. However, the exact reason for this reversal in trend has yet to be explained. It has been suggested that the reversal observed in the experiments results from the variation of n with Reynolds number in the power law relationship $U/U_\infty = (y/\delta)^n$ in that n exhibits first a decrease and then subsequently an increase as the local Reynolds number increases. However, this explanation does not advanced the understanding of the viscous-inviscid interaction by which turbulent separation takes place. Because the length of the separation region is of the same magnitude as the boundary layer thickness, we are concerned that <u>any</u> explanations or scaling laws derived from the boundary layer equations will prove satisfactory. To circumvent these and other problems resulting from the elliptic nature of the recirculating flow, attempts have been made by Baldwin and McCormack at NASA Ames Research Center to solve the Navier-Stokes equations.

The explicit finite-difference method used in the calculations are described in Baldwin[29] and MacCormack.[28] This theory has been compared with experiments performed in the present study for shock-induced separations ($M = 8.47$, $R_{e_L} = 22.5 \times 10^6$, $\theta_{shock} = 19.8°$). The computational field was confined to the neighborhood of the interaction, a region extending between 23 and 28 inches from the leasing edge of the flat plate. The initial boundary-layer profiles at x = 23 were computed according to Marvin[62] with variations that will be described. Preliminary results have been obtained at two levels of approximation: a simple mixing length model,[63] and the Saffman two-equation transport model of turbulence.[64]

Figure 62 shows variations in the initial velocity profile that have been considered in calculations based on the mixing length model of turbulence. The computed streamlines resulting from the assumed velocity defect are shown in Figure 63. The extent of the separation bubble both along the plate and normal to the plate is about twice as large as from the computations based on the Marvin-Sheaffer profile.

Figure 64 contains comparisons of computed pressure, skin friction and heat transfer with the measurements. The results from the Saffman model are in better agreement with the experiment than those from the mixing-length model except for possibly the pressure distribution. However, a slight variation of the assumed velocity defect could easily alter the pressure distribution. The higher values of skin friction and heat transfer aft of reattachment from the Saffman model are due to time lags in turbulent energy and scale of turbulence, not accounted for in the mixing length model. A high level of turbulence generated over the bubble persists downstream and diffuses toward the wall. Significantly larger values of eddy viscosity occure in the viscous sublayer than indicated by the mixing length model.

An interesting result from these solutions was a calculation of the real time that it took for a steady solution to be reached. Figure 65 contains a plot of C_F (28 inches from the leading edge) versus time according to a Saffman model calculation. The starting solution at time zero was taken to be the converged solution from a mixing length calculation. An equilibrium condition of the Saffman equations (turbulent energy production equal to dissipation) was used to obtain the starting values of pseudovorticity and turbulent energy corresponding to the local values of eddy viscosity from the mixing length model. Experiments indicate that steady turbulent separated flows are established within 1 millisecond after the initiation of the flow over the model.

Although the Saffman two-equation transport model of turbulence gives better agreement with the measurements than does the mixing length model, we are still faced with the problem of how best to evaluate the model of turbulence.

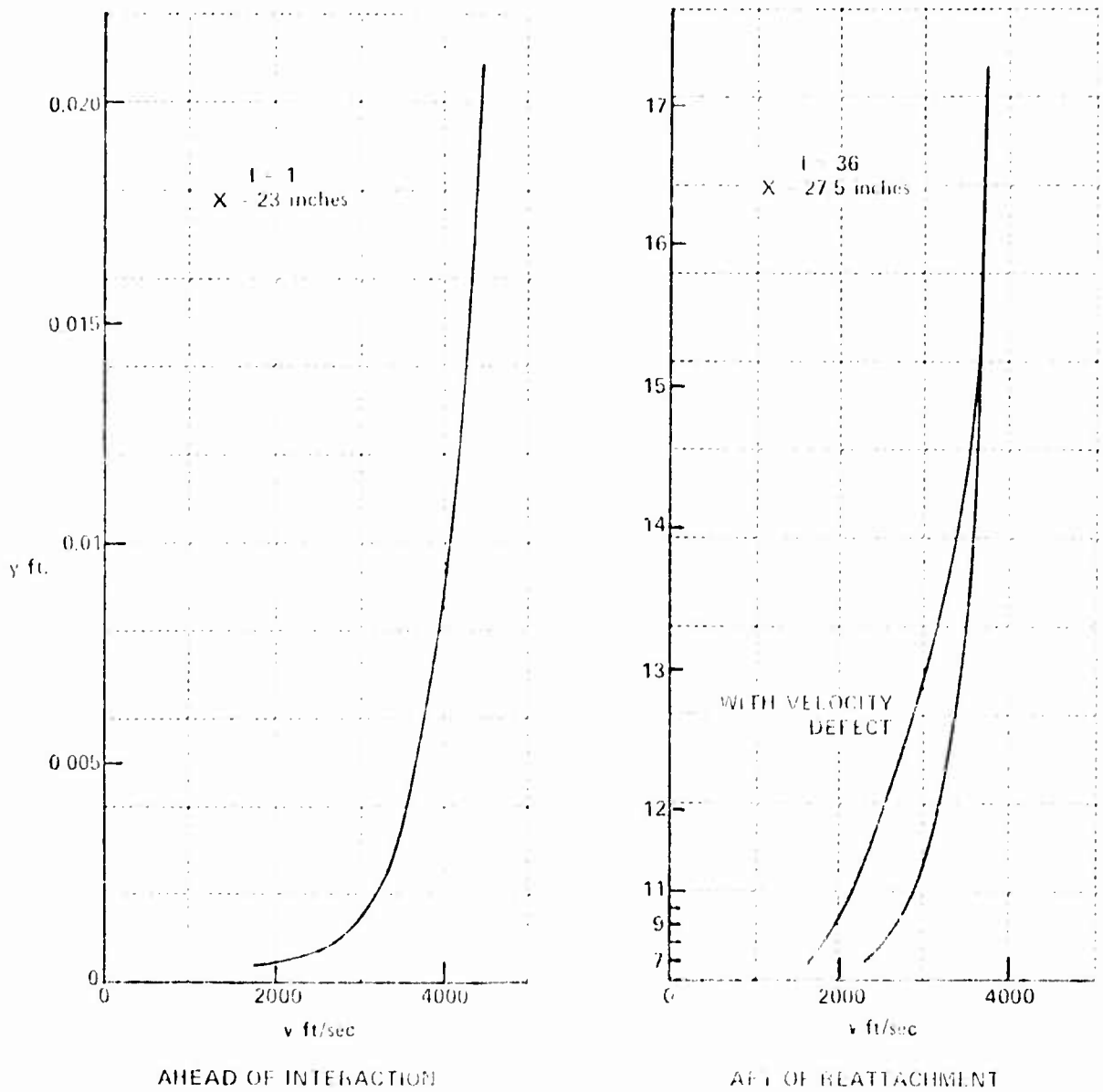


Figure 63. VELOCITY PROFILES AHEAD AND DOWNSTREAM OF THE INTERACTION

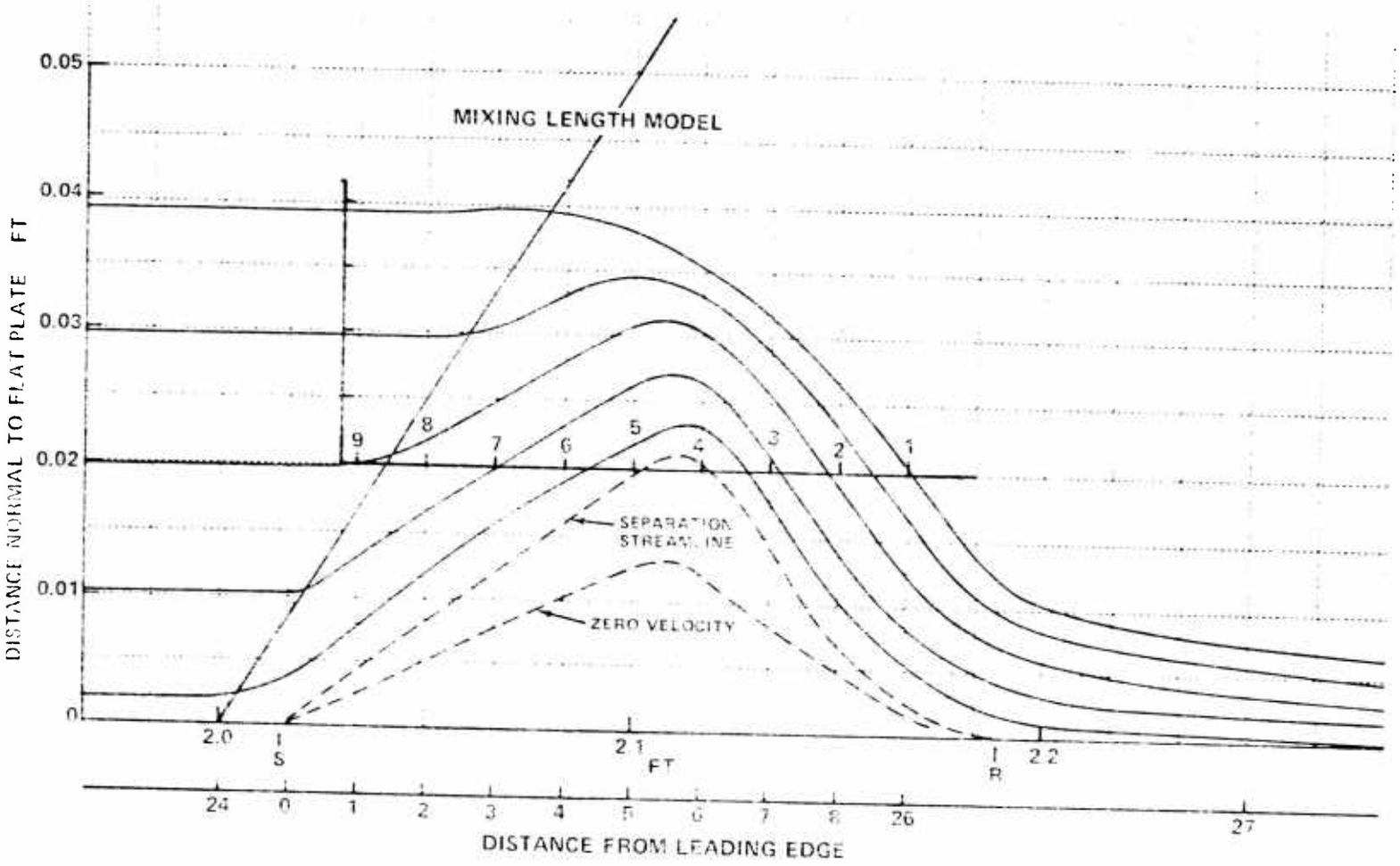


Figure 64. CALCULATED STREAM LINES WITH VELOCITY DEFECT (in.)

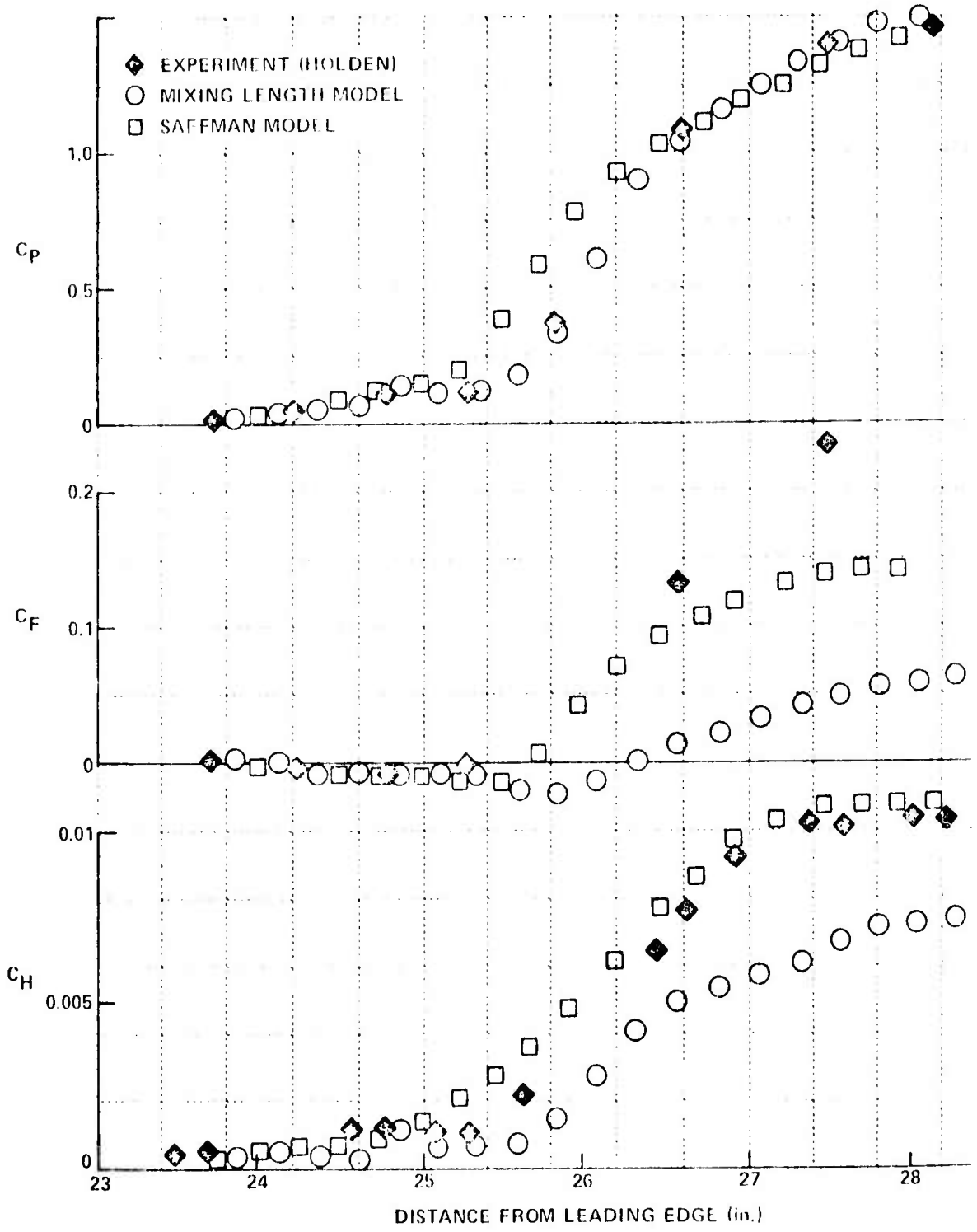


Figure 65. COMPARISON BETWEEN NAVIER-STOKES SOLUTIONS AND EXPERIMENT

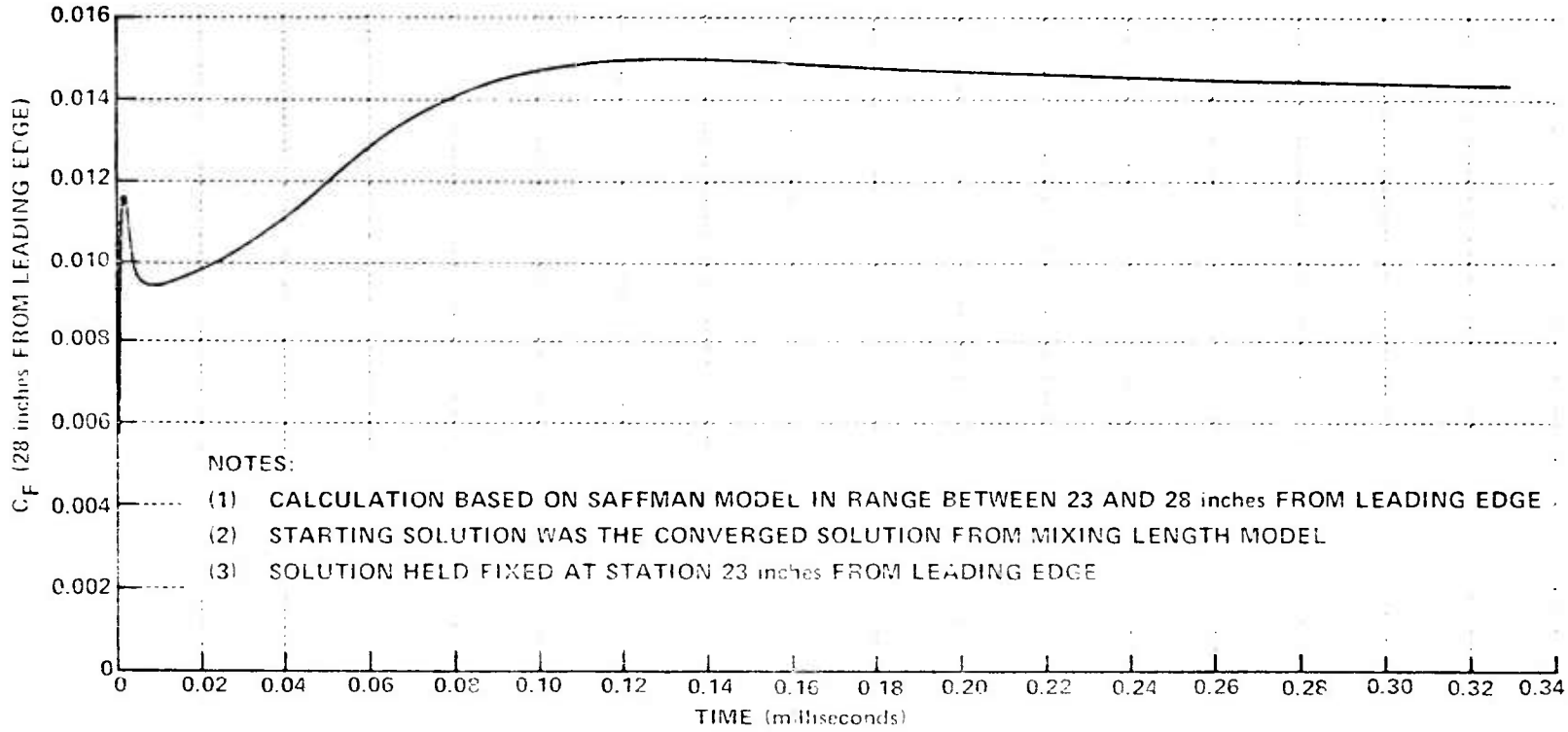


Figure 66. TIME FOR CONVERGENCE TO STEADY STATE

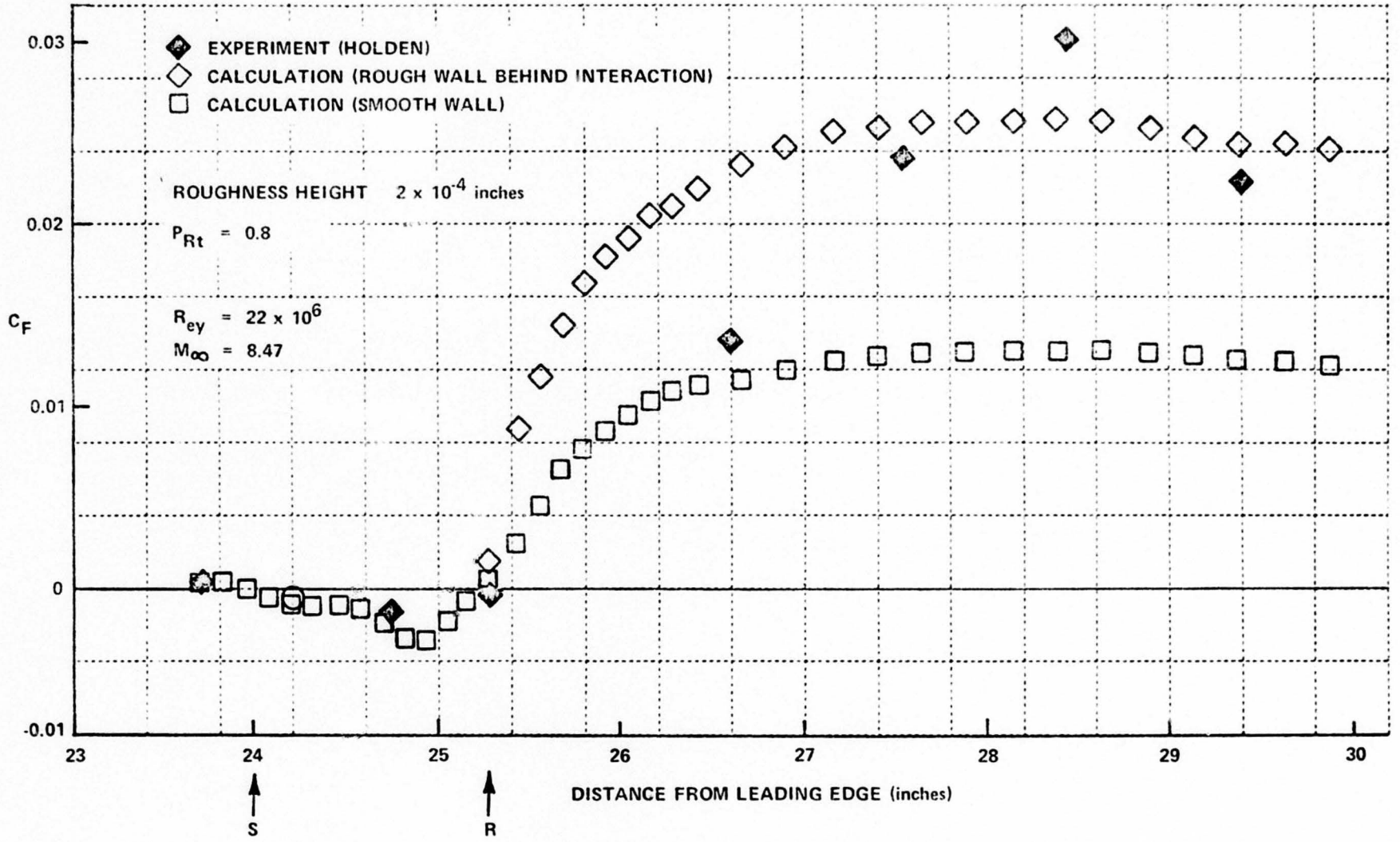


Figure 67. CALCULATIONS OF THE EFFECT OF ROUGHNESS ON SKIN FRICTION

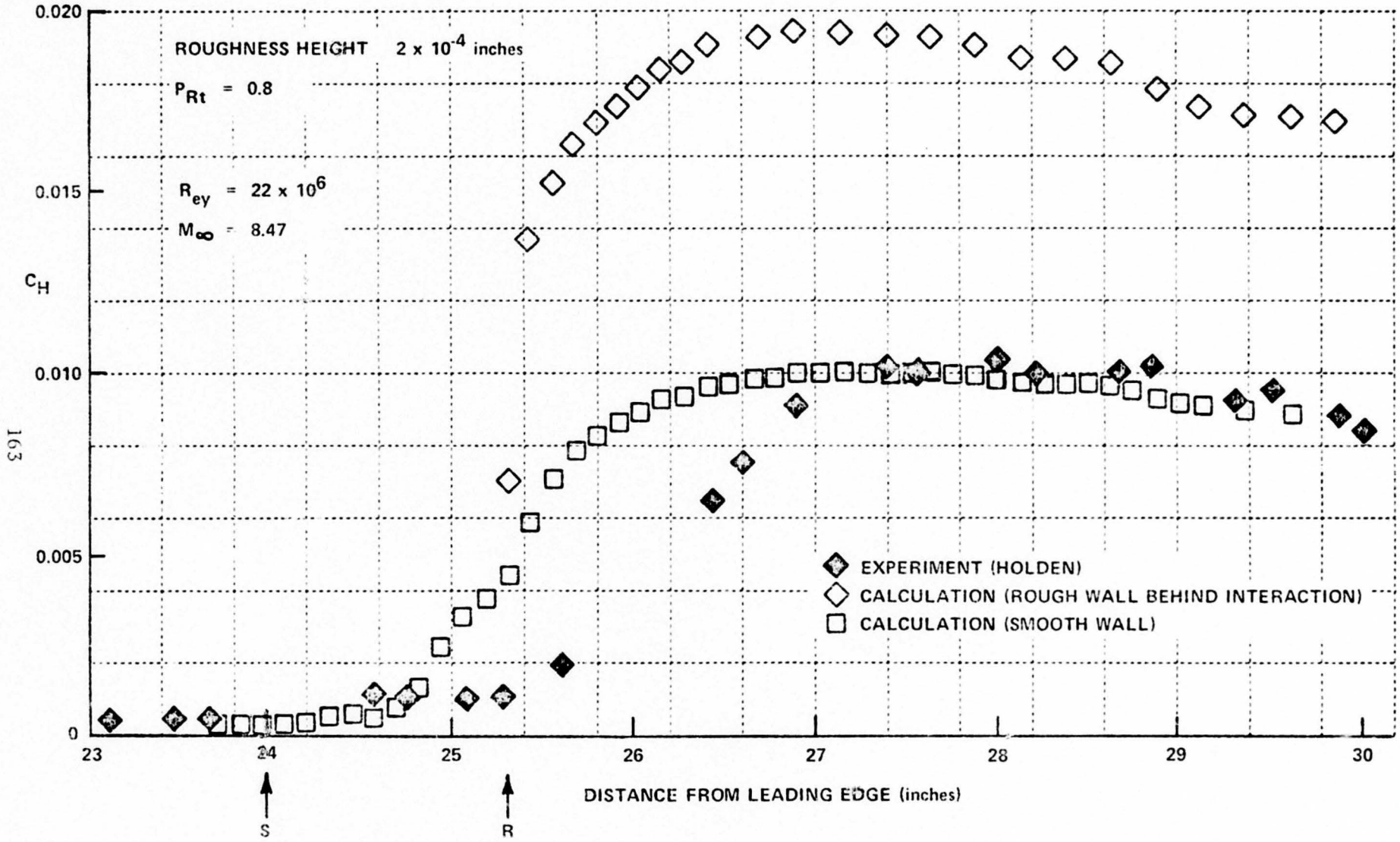


Figure 68. CALCULATIONS OF THE EFFECT OF ROUGHNESS ON HEAT TRANSFER

Indeed, one can achieve a considerable change in the computer solution for heat transfer and skin friction distribution by incorporating surface roughness into mixing length theory. Figures 66 and 67 show comparisons of calculated values of skin friction and heat transfer with and without a roughness height of 0.0002 inch behind the interaction. In these calculations, Baldwin incorporated roughness into the calculations by increasing the argument of the exponential in the Van Driest factor to 26 times the recommended value for smooth walls. The extreme sensitivity of the surface solutions to roughness makes it important to obtain definitive data in the interacting flow field.

6. CONCLUSIONS

Correlations are presented of the properties of transitional and turbulent boundary layers in high Reynolds number hypersonic flow over flat plates and cones. Measurements of transition have been correlated in terms of Re_θ, Re_λ and M as well as the parameters suggested by Pate and Schueler. The measurements did not correlate well in the latter format. Heat transfer measurements through the transition region could be expressed in terms of the intermittency relationship $C_F = \gamma\ C_{F\ TURB} + (\gamma - 1)\ C_{F\ LAM}$ where the intermittency factor γ is expressed by the relationship $\gamma = (1 - e^{-A\beta})/(1 - e^{-A})$. The skin friction and heat transfer measurements made on flat plates and cones have been compared with the theories of Van Driest II, Spalding and Chi, and Eckert. The Van Driest II method is in best overall agreement with the measurements in the $F_c\, c_f - F_{R\theta}\, Re\theta$ plane. Our measurements suggest that it take from 50 to 100 boundary layer thicknesses downstream of the point of maximum heating in the transition region before the boundary layer attains "equilibrium".

Detailed measurements have been made in regions of shock- and wedge-induced turbulent interaction regions. These measurements have demonstrated a reversal in the trend of incipient separation with Reynolds number postulated previously on the basis of experiments for widely different model configurations and test conditions. We believe that this trend reversal results directly from changes which occur in the velocity profile downstream of transition such that N (in the relationship $N = N(Re_\theta)$) decreased downstream of transition until an equilibrium boundary layer is established, when N increases slowly with Reynolds number. Correlations of the characteristics of these interaction regions are presented in terms of model configuration and free stream conditions. The solutions to the Navier-Stokes equations were found to be in surprisingly good agreement with the measurements considering the problems involved in describing the development of turbulence through these interaction regions. However, further detailed profile measurements are required to assist in the development of accurate models to describe turbulence in regions of shock wave-turbulent boundary layer interaction.

REFERENCES

1. Howarth, L., The Propagation of Steady Disturbances in a Supersonic Stream Bounded on One Side by a Parallel Subsonic Stream, Proc. Camb. Phil. Soc. 1947, 44, Part 3.

2. Tsien, H.S. and Finston, M., Interaction Between Parallel Streams of Subsonic and Supersonic Velocities, J. Aero. Sci., 1949, 16, 515.

3. Lighthill, M.J., Reflection at a Laminar Boundary-Layer of a Weak Steady Disturbance to a Supersonic Stream Neglecting Viscosity and Heat Conduction, Quart. J. Mech. and Appl. Maths, 1950, 3, 303.

4. Oswatitsch, K. and Wieghardt, K., Theoretical Analysis of Stationary Potential Flows and Boundary-Layers at High Speed, German Wartime Report, 1941. Translated as N.A.C.A. TM. 1189.

5. Crocco, L. and Lees, L., A Mising Theory for the Interaction Between Dissipative Flows and Nearly Isentropic Streams, J. Aero. Sci., 1952, 19, No. 10.

6. Lighthill, M.J., On Boundary-Layers and Upstream Influence. Part II. Supersonic Flows Without Separation, P.R.S.A., 1953, 217, 478.

7. Stewartson, K. and Williams, P.G. (1969), Self-Induced Separation, Proc. Roy. Soc. (London), Vol. A-312, pp. 181-206.

8. Glick, H.S., Modified Crocco-Lees Mixing Theory for Supersonic Separated and Reattaching Flows, J. Aero. Sci., Vol 29 No. 10, pp. 1238-1244 (October 1962).

9. Honda, M., A Theoretical Investigation of the Interation Between Shock Waves and Boundary Layers, J. Aero/Space Sci. 25, pp. 667-678, November 1958, Japan Tokyo Univ. Rep. Inst. High Speed Mech. 8, 1957, pp. 109-130.

10. Crocco, L., Conisderations on the Shock-Boundary Layer interaction, Proceedings Conference on High-Speed Aeronautics, Polytechnic Institute of Brooklyn, pp. 75-112, January 20-22, 1955.

11. Lees, L. and Reeves, B.L., Supersonic Separated and Reattaching Laminar Flows: I. General Theory and Application to Adiabatic Boundary Layer-Shock Wave Interactions, GALCIT Tech. Report No. 3 (October 1963).

12. Cohen, C.B. and Reshotko, E., Similar Solutions for the Compressible Laminar Boundary Layer with Heat Transfer and Pressure Gradient, NACA Report No. 1293 (1956).

13. Bray, K.N.C., Gadd, G.E. and Woodger, M., Some Calculations by the Crocco-Lees and Other Methods of Interactions Between Shock Waves and Laminar Boundary Layer, Including Effects of Heat Transfer and Suction, A.R.C. Report No. C.P. 556 (1960).

14. Savage, S.B., The Effect of Heat Transfer on Separation of Laminar Compressible Boundary Layers, GALCIT, Separated Flows Research Project, Report No. 2, (June 1962).

15. Chapman, D.R., Kuehn, D.M. and Larson, H.G., The Investigation of Separated Flows in Supersonic and Subsonic Streams with Emphasis on the Effects of Transition, NACA Report No. 1356 (1958).

16. Holden, M.S., An Analytical Study of Separated Flow Induced Shock Wave-Boundary Layer Interaction, Calspan Report No. AI-1972-A-3 (December 1965).

17. Klineberg, J. and Lees, L., Theory of Laminar Viscous-Inviscid Interactions in Supersonic Flow, AIAA Paper No. 69-7 (January 1969).

18. Gautier, B.G. and Ginoux, J.J., A Theoretical of Wall Cooling Effects Upon Shock Wave-Laminar Boundary Layer Interaction by the Method of Lees-Reeves - Klineberg, von Karman Institute Technical Note 71, May 1971.

19. Riethmuller, M.L. and Ginoux, J.J., A Parametric Study of Adiabatic Laminar Boundary Layer-Shock Wave Interactions by the Method of Lees-Reeves - Klineberg, von Karman Institute Technical Note 60, June 1970.

20. Bloy, A.W. and Georgeff, M.P., The Hypersonic Laminar Boundary Layer Near Sharp Compression and Expansion Corners, J. Fluid Mech., Vol 63, pp. 431-447, 1974.

21. Holden, M.S. and Moselle, J.R., Theoretical and Experimental Studies of the Shock Wave-Boundary Layer Interaction on Compression Surfaces in Hypersonic Flow, Calspan Report AF-2410-A-1 (October 1969); also ARL 70-0002 (January 1970).

22. Myring, D.F., The Interaction of a Turbulent Boundary Layer and a Shock at Hypersonic Mach Numbers, AGARD CP 30 (1968).

23. Todisco, A. and Reeves, B.L., Turbulent Boundary-Layer Separation and Reattachment at Supersonic and Hypersonic Speeds, Proceedings of the Symposium on Viscous Interaction Phenomena in Supersonic and Hypersonic Flow, Hypersonic Research Laboratory, Aerospace Research Laboratories, 7-8 May 1969.

24. Hunter, L.G., Jr. and Reeves, B.L., Results of a Strong Interaction, Wake-Like Model of Supersonic Separated and Reattaching Turbulent Flows, AIAA Paper No. 71-127, January 1971.

25. Alber, I.E. and Lees, L., Integral Theory for Supersonic Turbulent Base Flow, AIAA Journal, Vol. 6, No. 7, pp. 1343-1351, July 1965.

26. Rose, W.C., A Method for Analyzing the Interaction of an Oblique Shock Wave and a Boundary Layer, NASA SP-228, Symposium on Analytic Methods in Aircraft Aerodynamics, NASA Ames Research Center, pp. 541-567, October 28-30, 1969.

27. Carter, J.E., Numerical Solution of the Supersonic Laminar Flow Over a Two-Dimensional Compression Corner. Lecture notes in Physics, Col. 19 Springer-Verlag, New York, 1973, p. 69.

28. MacCormack, Robert W., Numerical Solution of the Interaction of a Shock Wave with a Laminar Boundary Layer, Lecture Notes in Physics, 1971.

29. Baldwin, Barrett, Calculations on Shock-Induced Turbulent Boundary-Layer Separation, Enclosure in letter from Barrett Baldwin to Dr. Michael S. Holden dated June 12, 1973.

30. Horstman, C.C., Kussoy, M., Coakley, T., Rubesin, M.W. and Marvin, J.G., An Experimental and Numerical Investigation of Shock Wave-Induced Turbulent Boundary Layer Separation at Hypersonic Speeds, AIAA Paper No. 75-4, Presented at AIAA 13th Aerospace Science Meeting, Pasadena, California, January 20-22, 1975.

31. Shang, J.S. and Hankey, W.L., Jr., Two-Dimensional Supersonic Turbulent Separation Over a Compression Ramp, AIAA Paper No. 75-3, Presented at 13th Aerospace Science Meeting, Pasadena, California, January 20-22, 1975.

32. Emmons, H.W., The Laminar-Turbulent Transition in a Boundary Layer, Journal of the Aeronautical Sciences, Vol. 18, No. 7, July 1951, pp. 490-498.

33. Dhawan, S. and Narashima, R., Some Properties of Boundary Layer Flow During the Transition from Laminar to Turbulent Motion, Journal of Fluid Mechanics, Vol. 3, 1958, pp. 418-436.

34. Owen, F.K., A Note on Some Preliminary High Supersonic Transition Results Using Thin Film Heated Gauges, ARC 30 150 - Hyp. 692, April 1968, Aeronautical Research Council.

35. Pate, S.R. and Schueler, C.J., An Investigation of Radiated Aerodynamic Noise Effects on Boundary-Layer Transition in Supersonic and Hypersonic Wind Tunnels, AIAA Paper No. 68-375, April 1968.

36. Stainbeck, P.C., Fischer, M.C. and Wagner, R.D., Effects of Wind-Tunnel Disturbances on Hypersonic Boundary Layer Transition, AIAA 10th Aerospace Sciences Meeting, San Diego, California, 17-19 January 1972.

37. Bradshaw, P., A Note on Reverse Transition, JFM (1969), Vol. 35, Part 2, pp. 387-390.

38. Spalding, D.B. and Chi, S.W., The Drag of a Compressible Turbulent Boundary Layer on a Smooth Flat Plate with and without Heat Transfer, Journal of Fluid Mechanics, January 1964, pp. 117-143.

39. Van Driest, E.R., Turbulent Boundary Layer in Compressible Fluids, J. Aero. Sci., 1951, 18, No. 3, pp. 145-160.

40. Eckert, E.R.G., Engineering Relations for Friction and Heat Transfer to Surfaces in High Velocity Flow, J. Aeronautical Sciences, 1956, 23 (8), pp. 585-587.

41. Bertram, M.H., Cary, A.M., Jr. and Whitehead, A.H., Jr., Experiments with Hypersonic Turbulent Boundary Layers on Flat Plates and Delta Wings, AGARD Specialists Meeting on Hypersonic Boundary Layers and Flow Fields, London, England, May 1-3, 1968.

42. Bushnell, D.M., Johnson, C.B., Harvery, W.D. and Feller, W.V., Comparison of Prediction Methods and Studies of Relaxation in Hypersonic Turbulent Boundary Layers, Turbulent Boundary Layer Conference Proceedings, NASA Langley Research Center, December 1968.

43. Holden, M.S., Shock Wave-Turbulent Boundary Layer Interaction in Hypersonic Flow, AIAA 10th Aerospace Sciences Meeting, San Diego, California, 17-19 January 1972.

44. Green, J.W., Reflection of an Oblique Shock Wave by a Turbulent Boundary Layer, J. Fluid Mech. Vol. 40, Part 1, pp. 81-95 (1970).

45. Roshko, A. and Thomke, G.J., Flare-Induced Separation Lengths in Supersonic, Turbulent Boundary Layers, AIAA Aerospace Sciences Meeting, Paper No. 75-6, 20 January 1975.

46. Law, C.H., Supersonic Turbulent Boundary Layer Separation Measurements at Reynolds Numbers of 10^7 and 10^8, AIAA Journal, Vol. 12, No. 6, June 1974, pp. 794-797.

47. Settles, G.S., Bogdonoff, S.M. and Vas, I.E., Incipient Separation of a Supersonic Turbulent Boundary Layer at Moderate to High Reynolds Numbers, AIAA Aerospace Sciences Meeting, Paper No. 75-7, 20 January 1975.

48. Appels, C., Incipient Separation of a Compressible Turbulent Boundary Layer, von Karman Institute Tech. Note 99, April 1974.

49. Kuehn, D.M., Experimental Investigation of the Pressure Rise Required for the Incipient Separation of Turbulent Boundary Layers in Two-Dimensional Supersonic Flow, NASA Memo 1-21-59A, February 1959.

50. Holden, M.S., Shock Wave-Turbulent Boundary Layer Interaction in Hypersonic Flow, AIAA pre-print No. 72-74.

51. Johnson, C.B., and Bushnell, D.M., "Power-Law Velocity-Profile-Exponent Variations with Reynolds Number Wall Cooling and Mach Number in a Turbulent Boundary Layer", NASA TND 5753, April 1970.

52. Appels, C., Turbulent Boundary Layer Separation at Mach 12, von Karman Institute Technical Note 90, September 1973.

53 Gulbran, C.E., Redeker, E., Miller, D.S. and Strack, S.L., Heating in Regions of Interfering Flow Fields. Part I - Two- and Three-Dimensional Laminar Interactions at Mach 8, AFFDL TR 65-49, Part I, AF Flight Dynamics Laboratory, 1965.

54. Bogdonoff, S.M. and Kepler, C.E., Separation of a Supersonic Turbulent Boundary Layer, J. Aero. Sci, 22, pp. 414-424 (1955).

55. Hammitt, A.G. and Hight, S., Scale Effects in Turbulent Shock Wave Boundary Layer Interactions, USA AFOSR TN 60-82, Procs. 6th Midwestern Conference on Fluid Mech., Texas University, September 1959.

56. Elfstron, G.M., Coleman, G.T. and Stollery, J.L., Turbulent Boundary Layer Studies in a Hypersonic Gun Tunnel, 8th Annual International Shock Tube Symposium, London, England, 5-8 July 1971.

57. Spaid, F.W. and Frishnett, J.C., Incipient Separation of a Supersonic Turbulent Boundary Layer Including the Effects of Heat Transfer, AIAA Paper, November 1971

58. Sterrett, J.R. and Emergy, J.C., Experimental Separation Studies of Two-Dimensional Wedges and Curved Surfaces at Mach Numbers of 4.8 to 6.2, NACA TND-1014.

59. Wallace, J.E., Hypersonic Turbulent Boundary Layer Measurements Using an Electron Beam, Calspan Report No. AN-2112-Y-1, August 1968.

60. Bushnell, D.M., Johnson, C.B., Harvey, W.D. and Feller, W.V., Comparison of Prediction Methods and Studies of Relaxation in Hypersonic Turbulent Boundary Layers, Turbulent Boundary Layer Conference Proceedings, NASA Langley Res. Center, December 1968.

61. Fiore, A., Turbulent Boundary Layer Measurements at Hypersonic Mach Number, ARL Report 70-0166, August 1970.

62. Marvin, Joseph G. and Sheaffer, Yvonne, S., A Method for Solving the Nonsimilar Laminar Boundary-Layer Equations Including Foreign Gas Injection, NASA TN D-5516, November 1969.

63. Cebeci, T. and Smith, A.M.O., A Finite-Difference Solution of the Incompressible Turbulent Boundary Layer Equations by an Eddy Viscosity Concept, Proceedings of 1968 AFOSR-IFR-Standford Conf. on Computation of Turbulent Boundary Layers, Vol. 1, Stanford University, pp. 346-355.

64. Saffman, P.G. and Wilcox, D.C., Turbulence-Model Predictions for Turbulent Boundary Layers, to be published.

65. Reshotko, E. and Tucker, M., "Effect of a Discontinuity on Turbolent Boundary Layer Thickness Parameters With Application to Shock Induced Separation," NACA, TN 3454, 1955.

☆ U. S. GOVERNMENT PRINTING OFFICE 1975—657-630/16